THE RESPONSE OF LOW-LATITUDE CALCAREOUS PHYTOPLANKTON TO GLOBAL CHANGE THROUGH THE EOCENE-OLIGOCENE TRANSITION

Thomas Dunkley Jones
Department of Earth Sciences
UCL

Thesis submitted for the degree of Doctor of Philosophy
December 2007

ProQuest LLC
789 East Eisenhower Parkway
P.O. Box 1346
Ann Arbor, MI 48106-1346

I, Thomas Dunkley Jones, confirm that the work presented in this thesis is my own. Where information has been derived from other sources, I confirm that this has been indicated in the thesis.

Signed:

ABSTRACT

This thesis documents the response of calcareous phytoplankton assemblages to major changes in global climate during the Eocene-Oligocene transition (EOT) at three low-latitude sites; Tanzanian Drilling Project (TDP) Sites 12 & 17 (southern coastal Tanzania), Deep Sea Drilling Site 242 (Mozambique Channel, western Indian Ocean) and St Stephens Quarry (Alabama, USA). High-resolution nannofossil count data from all three study sites clearly indicate a major change in coccolithophore assemblage compositions directly coincident with the first step change in the positive oxygen isotope ($\partial^{18}O$) shift into the early Oligocene Glacial Maximum (EOGM). This is followed by continued shifts in coccolithophore assemblages in the vicinity of the Eocene-Oligocene boundary to reach new "Oligocene" assemblage compositions before the second step in $\partial^{18}O$ and peak glacial conditions of the EOGM. At all sites there is a marked increase in the abundance of *Cyclicargolithus floridanus* (>5μm) and to a lesser extent *Sphenolithus predistentus*, combined with a general loss of warm-water and oligotrophic taxa including *Calcidiscus protoannulus*, discoaster and holococcolith species. This consistent pattern of biotic change, from sites with varying species compositions and preservation states, indicates a large and geographically widespread perturbation in the low-latitude surface water environment and is consistent with new trace metal paleothermometry that indicates a significant, ~2-3°C, cooling of surface waters in the earliest stages of the EOT.

An exceptionally-well preserved and highly diverse nannofossil assemblage from late Eocene-early Oligocene (nannofossil zones NP19/20 to NP21; Martini 1971) sediments of coastal Tanzania is described and its implications for the Cenozoic history of the coccolithophores is discussed. This consists of a total of 114 species-equivalent morphotypes, one new genus (*Pocillithus*), six new species (*Reticulofenestra macmillanii, Blackites culter, Rhabdosphaera suptilis, Orthozygus occultus, Orthozygus arcus, Pocillithus spinulifer*) and a previously unknown Paleogene deep-photic zone assemblage including representatives of the extant genera *Gladiolithus, Algirosphaera* and *Acanthoica.*

ACKNOWLEDGMENTS

Many thanks to many people. To the two Pauls for supervising this project; Paul Bown who first got me into this, kept me at it and has inspired me with the joys of nannofossils for the foreseeable future and Paul Pearson for sharing his enthusiasm for foraminifera, geology and exotic places. To Jackie Lees (gin), Stuart Robinson (career advice), Jim Davy (crisis management) and to all the PhD and MSc students and staff in the UCL, Department of Earth Sciences. To all involved in the Tanzanian Drilling Project; Bridget Wade, Helen Coxall, Carrie Lear, Chris Nicholas, Brian Huber, Luke Handley, Trevor Bailey and Aoife O'Halloran, its been a great privilege working with you; especial thanks to Ian McMillan for sharing spiny fish and tropical cyclones on the Pande Road. To everyone at the Tanzanian Petroleum Development Corporation, Joyce Singano, Amina Karega, Ephraim, Doreen, Michael, Mr K - this project would have been near impossible without your help. To David Dockery and James Starnes (Mississippi DEQ), Ernest Russell (Mississippi State University) and Lewis Dean (Geological Survey of Alabama) for introducing me to the Deep South and its geology. To Jeremy Young - wow! To all those who have funded this research; UCL Graduate School for their Scholarship, NERC for funding Tanzanian Drilling Project and the Palaeontological Association for funding field work in Mississippi and Alabama. To family and friends for all your support. Finally and most of all to Rachel and Isaac.

CONTENTS

Contents

List of figures

Chapter 1. Introduction: low-latitude calcareous phytoplankton and the Eocene-Oligocene transition

Chapter 2. Nannofossil assemblage changes through the Eocene-Oligocene boundary of coastal Tanzania

Chapter 5. Nannofossil assemblage changes through the Eocene-Oligocene boundary at St Stephens Quarry, Alabama

Chapter 6. Discussion: low-latitude calcareous phytoplankton and the Eocene-Oligocene transition

List of plates

Chapter 3. Taxonomy of upper Eocene to lower Oligocene calcareous nannofossils, Pande Formation, Tanzania

List of tables

Chapter 6. Discussion: low-latitude calcareous phytoplankton and the Eocene-Oligocene transition

1. INTRODUCTION: LOW-LATITUDE CALCAREOUS PHYTOPLANKTON AND THE EOCENE-OLIGOCENE TRANSITION

1.1 Overview

The transition between the Eocene and Oligocene epochs is the central point of the most significant climatic change of the Cenozoic, as the earth's climate developed from the ice-free early Paleogene world of global warmth and high atmospheric pCO_2 to the glaciated conditions of the early Oligocene with the appearance, for the first time in the Cenozoic, of continental-scale ice-sheets on Antarctica (Lear *et al.* 2000; Pearson & Palmer 2000; Zachos *et al.* 2001a; Coxall *et al.* 2005; Pagani *et al.* 2005). Marine sedimentary records of the basal Oligocene are characterized by large, ~1.2 to 1.5‰, positive excursions in benthic foraminiferal oxygen isotopes and a rapid deepening of the calcite compensation depth (CCD) (Zachos *et al.* 1996; Coxall *et al.* 2005). Coincident with these changes in the deep-sea, significant glaciomarine sedimentation commences around the margins of both East and West Antarctica indicating the first Cenozoic advance of continental-scale ice-sheets in southern high latitudes (Breza & Wise 1992; Wise *et al.* 1991, 1992; Zachos *et al.* 1992; Ivany *et al.* 2006).

One of the effects of this rapid climate switch is a pronounced positive step-change in global compilations of Cenozoic deep-sea benthic foraminiferal oxygen isotope records at the end of a long-term trend of increasing oxygen isotope values through the Middle to late Eocene (Figure 1.1; Zachos *et al.* 2001a). The existence of such rapid climatic transitions is compelling evidence for the strongly non-linear response of the earth's climate system to external forcing via internal biogeochemical and climate feedback mechanisms (Zachos *et al.* 2001b; De Conto & Pollard 2003a; Zachos & Kump 2005). The suggestion that this rapid climate switch, into a pronounced glacial state, occurred under conditions of steadily declining concentrations of atmospheric carbon dioxide, below a threshold level of between 840 and 560ppmv (De Conto & Pollard 2003a, 2003b), is of profound concern for long-term predictions of future climate where rapidly increasing atmospheric pCO_2 is set to approach, if not exceed this estimated threshold for the Eocene-Oligocene transition (IPCC 2007) with the potential for a

similarly rapid non-linear but reversed (deglacial) response.

Photosynthetic primary producers are a fundamental component of the earth's biogeochemical cycles, using solar energy to drive the conversion of carbon dioxide into organic polysaccharides with an associated release of molecular oxygen. In the Cenozoic oceans, photosynthetic primary production has been and is dominated by three major groups of single celled phytoplankton; the dinoflagellates, diatoms and coccolithophores. The ubiquitous preservation of the calcitic plates, or coccoliths, produced by the coccolithophores provides the most complete Cenozoic fossil record of these phytoplankton groups (Bown *et al.* 2004). The massive scale of coccolith production, across almost all latitudes of the global oceans, makes coccolithophore productivity a major component of oceanic carbonate production and the global carbon cycle (Hay 2004; Rost & Riebesell 2004). During times of rapid climatic and carbon cycle change, such as the Eocene-Oligocene transition, quantifying the responses of the calcareous phytoplankton is crucial for an accurate understanding of temporal changes in global biogeochemical cycles. In addition, the coccolithophore production of

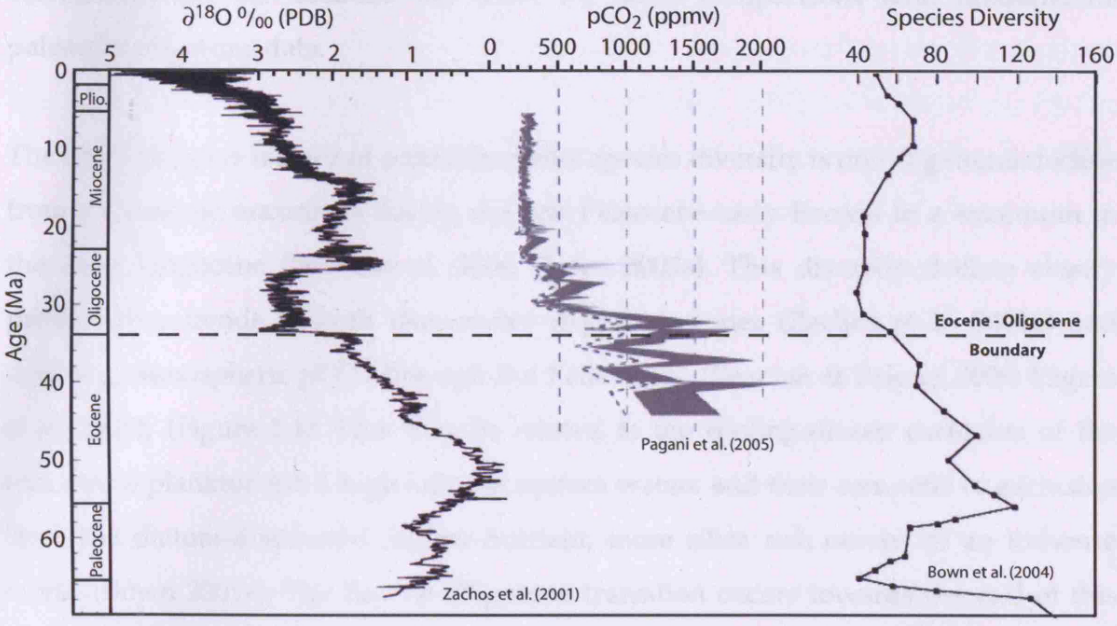

Figure 1.1 Comparison of Cenozoic climate records and calcareous nannofossil species diversity; left - compiled deep-sea benthic foraminiferal oxygen isotope record (Zachos *et al.* 2001a); centre - estimated atmospheric carbon dioxide concentrations based on alkenone proxy data (Pagani *et al.* 2005); right - compilation of global calcareous nannofossil species diversity (Bown *et al.* 2004).

dimethylsulphate (DMS) plays a large role in the global sulphur-cycle (Malin & Steinke 2004) and the production of long-chain alkenone biomarkers by some coccolithophore taxa is now being widely used for paleothermometry and more controversially for the estimation of deep-time atmospheric pCO_2, including across the Eocene-Oligocene transition (Pagani *et al.* 2002, 2005).

The common occurrence and great abundance of coccoliths in most supralysoclinal, Cenozoic marine sediments make the coccolithophores an ideal group for quantitative studies of biotic change at high temporal resolutions. Where the fossil records of larger, less productive organisms inevitably contain significant temporal gaps, often coupled with low preservation potentials within their particular habitats, the temporal resolution of the coccolithophore fossil record is usually constrained only by the accumulation rates of the depositional environment and the costs of labour-intensive data acquisition. In addition, marine sections with high-quality records of coccolithophore assemblages are also likely to yield a range of biostratigraphic, geochemical and paleomagnetic data, which provide accurate age-control, detailed correlations between sections and allow for direct comparisons with fundamental paleoclimatic proxy data.

The late Paleogene history of coccolithophore species diversity is one of general decline from a Cenozoic maximum during the late Paleocene-early Eocene to a minimum in the early Oligocene (Bown *et al.* 2004; Bown 2005a). This diversity decline closely parallels the trends in both deep-water oxygen isotopes (Zachos *et al.* 2001a) and declining atmospheric pCO2 through the Palaeogene (Pearson & Palmer 2000; Pagani *et al.* 2005), (Figure 1.1). This may be related to the cooling-driven exclusion of the calcareous plankton from high-latitude surface waters and their competitive exclusion from the diatom-dominated, higher-nutrient, more silica rich oceans of an icehouse world (Bown 2005a). The Eocene-Oligocene transition occurs towards the end of this general decline in coccolithophore species diversity, and although it is clearly the most concentrated period of very rapid climatic cooling it appears to have had little impact on global coccolithophore diversity (Bown *et al.* 2004; Bown 2005a). If this is true, then a close coupling between climatic change and coccolithophore macroevolution is either

questionable, only operative on longer timescales (1-10 myrs), or mediated by a complex interaction with the fortunes of other phytoplankton groups.

Although the Cenozoic fossil record of the major groups of marine calcareous plankton – the planktonic foraminifera and coccolithophores – are considered to be the most complete of any major fossil group, the small size of their calcite tests/scales make them susceptible to dissolution and recrystallization, both within the water-column and during burial-diagensis. These processes, such as the dissolution of calcareous microfossils below the lysocline, have been known for decades (Honjo 1976), however it is only in recent years that micropalaeontologists have come to recognize the effects of more subtle, often micron or sub-micron scale recrystallization within calcareous microfossils. In the case of the planktonic foraminifera such fine scale recrystallization is now acknowledged to have a potentially significant effect on the stable isotopic composition of foraminiferal tests (Pearson *et al.* 2001; Sexton *et al.* 2006) and in the smaller calcareous nannofossils, recent studies have revealed a strong bias against the preservation of smaller and more fragile taxa (Young *et al.* 2005). It is within this context that recent research efforts have focused on the recovery of "pristine" or "exceptional" calcareous microfossil assemblages, in the first instance for the recovery of accurate geochemical proxy data (Pearson *et al.* 2001, 2007) but increasingly for the associated wealth of high-quality paleobiological and diversity data (Bown 2005b; Bown & Dunkley Jones 2006; Bown *et al.* 2007, in press).

This thesis interweaves the three themes of Eocene-Oligocene climatic change, the coccolithophore response to this change and the role of preservational quality in recording this biotic signal. In the following sections of this chapter each of these three issues will be briefly introduced, including an overview of the relevant literature and the background to this study. The final sections of this chapter present the main objectives for this study, the scheme of work undertaken and the structure of the subsequent chapters.

1.2 The Eocene-Oligocene Transition

The Eocene-Oligocene boundary (EOB) is defined by the Global Stratotype Section and Point (GSSP) at the Massignano Quarry, Ancona, Italy (Premoli Silva & Jenkins, 1993), at a level corresponding to the last occurrence of the Hantkeninidae family of planktonic foraminifera (Coccioni *et al.* 1988; Primoli-Silva & Jenkins 1993; Berggren *et al.* 1995). This level is used as a tie point on the time scale of Cande & Kent (1995) at 33.7Ma, although a more recent astronomically tuned age model from equatorial Pacific ODP Site 1218 proposes a slightly older age for the EOB (Coxall *et al.* 2005). There is however, some uncertainty in the biostratigraphic data from this site and as a result most paleoclimate studies of this interval continue to work with the time-scales of Cande & Kent (1995) and Berggren *et al.* (1995). Around the EOB itself there is a longer period of climatic and biotic change, lasting ~300-400kyr, which is best referred to as the Eocene-Oligocene transition (EOT) (Coxall & Pearson in press)(Figure 1.2). The EOT commences with a brief phase of relatively negative carbon isotope values, observed in a variety of records at several sites (Zachos *et al.* 1996; Coxall *et al.* 2005), followed by positive shifts in global ocean oxygen and carbon isotopic values to a maximum in the earliest Oligocene, which marks the end of the EOT. The EOB event falls within this broader period of climatic and biotic change.

There has been some confusion in the literature concerning the use of the term "Oi-1", which refers to a relatively long "isotope zone" that encompasses much of the lower Oligocene, beginning and ending with two pronounced positive peaks in global oxygen isotope values (Miller *et al.* 1991). Many authors have used this term to denote either the first, relatively short-lived (~400kyr) peak in oxygen isotopes in the earliest Oligocene or the shift in oxygen isotopes into this peak, which occurs through much of the EOT (Zachos *et al.* 2001a; Van Mourik & Brinkhuis 2005; Gale *et al.* 2006). For clarity two new terms, which will be used in this work, have been proposed to identify 1) the ~300-400kyr period of increasing oxygen isotopic values as the "shift" and 2) the ~400kyr period of maximum positive oxygen isotope values in the earliest Oligocene as the early Oligocene Glacial Maximum (EOGM) (Liu *et al.* 2004; Coxall & Pearson in press) (Figure 1.2).

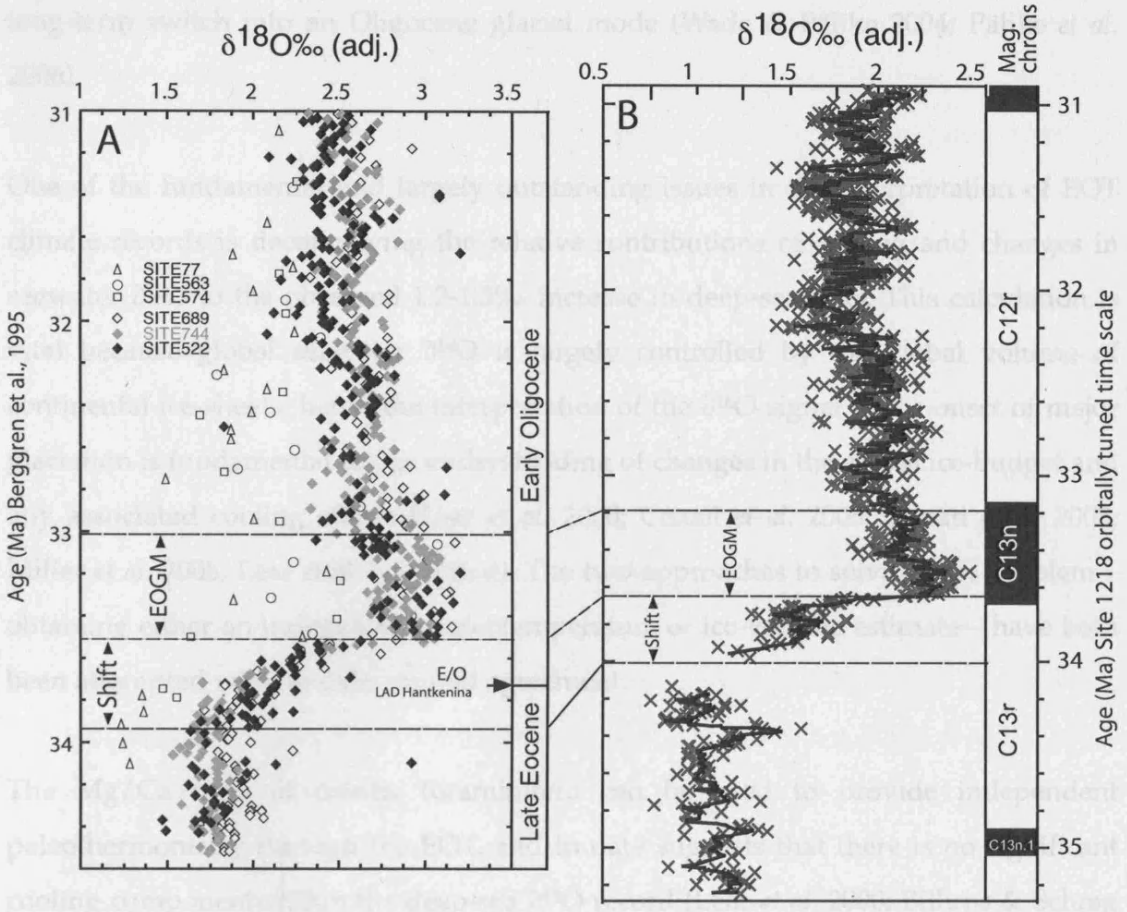

Figure 1.2 High-resolution oxygen isotope records of the EOT; left - compiled benthic foraminifera oxygen isotope data of Zachos *et al.* (2001a), plotted on the common time scale of Berggren *et al.* (1995), showing the commonly recognized ~1.5‰ positive shift into the EOGM and the last occurrence of *Hantkenina* placed at the level determined at DSDP Site 522 (Poore 1984); right - *Cibicidoides* oxygen isotope record from equatorial Pacific ODP Site 1218, plotted on the site-specific orbitally tuned time scale, showing the two step "shift" and EOGM. From Coxall *et al.* (in press).

The positive oxygen isotope values of the EOGM and the ~1.2–1.5‰ shift into this event have now been recorded in many deep-sea sections (Oberhansli *et al.* 1984; Zachos *et al.* 1996; Coxall *et al.* 2005), the most recent of which has identified a structure to the shift of two short steps, of approximately 40kyr each, separated by an ~200kyr plateau (Coxall *et al.* 2005). The first, and smaller, of these steps and the plateau occur in the uppermost part of magnetochron C13r, whilst the second step reaches the maximum positive $\partial^{18}O$ values of the EOGM directly at the base of chron C13n (Coxall *et al.* 2005) (Figure 1.2). After the EOGM deep-sea oxygen isotope values stabilize at slightly less positive values, roughly 1‰ greater than in the late Eocene, suggesting a

long-term switch into an Oligocene glacial mode (Wade & Pälike 2004; Pälike *et al.* 2006).

One of the fundamental and largely outstanding issues in the interpretation of EOT climate records is deconvolving the relative contributions of cooling and changes in seawater $\partial^{18}O$ to the observed 1.2-1.5‰ increase in deep-sea $\partial^{18}O$. This calculation is vital because global seawater $\partial^{18}O$ is largely controlled by the global volume of continental ice-sheets, hence the interpretation of the $\partial^{18}O$ signal at the onset of major glaciation is fundamental to our understanding of changes in the global ice-budget and any associated cooling effects (Lear *et al.* 2000; Coxall *et al.* 2005; Tripati *et al.* 2005; Miller *et al.* 2008; Lear *et al.* submitted). The two approaches to solving this problem – obtaining either an independent paleotemperature or ice-volume estimate – have both been attempted with, to date, limited agreement.

The Mg/Ca ratio of calcitic foraminifera can be used to provide independent paleothermometry through the EOT, and to date suggests that there is no significant cooling component within the deep-sea $\partial^{18}O$ record (Lear *et al.* 2000; Billups & Schrag 2003; Lear *et al.* 2004). This poses a significant problem, implying that all of the change in deep-sea $\partial^{18}O$ is due to changes in seawater $\partial^{18}O$ driven by an ice-volume increase of 1.6 to 2.7 times the present day Antarctic ice-volume, depending on the estimated $\partial^{18}O$ value used for "Oligocene" ice (Coxall *et al.* 2005). Such a volume of ice cannot be realistically accommodated on the Antarctic continent and implies extensive northern hemisphere glaciation (Coxall *et al.* 2005; Tripati *et al.* 2005) and a eustatic sea level fall of ~150m (Miller *et al.* 2008). Although there is compelling evidence for some glacial activity in the northern hemisphere during the EOT, in the form of glaciomarine sediments in the Greenland sea, these were probably sourced from isolated glaciers on the East Greenland margin and are not evidence for extensive northern hemisphere glaciation (Eldrett *et al.* 2007).

The second approach is to estimate the extent of eustatic sea-level fall, and hence ice-volume increase, associated with the EOT. Extensive sequence stratigraphic studies of the New Jersey continental margin estimate a sea level fall of 70m through the EOT

(Pekar *et al.* 2002); these have recently been corroborated by similar studies from the US Gulf Coast, which produced an estimate of 55m of sea level fall through the same interval (Miller *et al.* 2008). These results imply a significantly smaller global ice-budget, which could be largely accommodated on Antarctica and are in good agreement with models of Antarctic ice-sheet development under declining atmospheric pCO_2 (De Conto & Pollard 2003a, 2003b). If correct this interpretation of the deep-sea $\partial^{18}O$ record, which attributes only around half of the $\partial^{18}O$ change to ice-volume, implies a significant cooling of ~2-3°C in the deep-sea that has so far gone undetected by Mg/Ca paleothermometry.

At the opposite extreme of the "ice *versus* cooling" argument are Hay *et al.* (2005) who, largely on the basis of older global sea level studies that found little change around the EOB, suggest that all of the increase in $\partial^{18}O$ can be accommodated by cold water filling the deep ocean, the formation of polar sea ice and changes in seawater alkalinity. This scenario is largely redundant with the growing evidence for sea-level fall directly correlated to the EOT from New Jersey (Pekar *et al.* 2002), the US Gulf Coast (Miller *et al.* 1991; Miller *et al.* 2008), west Africa (Séranne 1999), the North Sea (Vandenberghe *et al.* 2003), South Australia (McGowran *et al.* 1992) and the UK (Gale *et al.* 2006). In addition, there is also direct sedimentary evidence for significant but episodic east Antarctic glaciation in the late Eocene followed by extensive glaciation in the earliest Oligocene (Barrett *et al.* 1989; Wise *et al.* 1991; Breza & Wise 1992; Zachos *et al.* 1992, 1999) and the significant early Oligocene glaciation of west Antarctica (Birkenmajer 1996; Gilbert *et al.* 2003; Birkenmajer *et al.* 2005; Ivany *et al.* 2006).

The major ocean-wide increase in $\partial^{13}C$, which is closely coupled to the shift in $\partial^{18}O$ – at equatorial Pacific ODP Site 1218 it lags $\partial^{18}O$ by ~10kyr (Coxall *et al.* 2005) – is compelling evidence for a significant perturbation in the global carbon cycle through the EOT (Zachos *et al.* 1996, 2001a; Diester-Haass & Zachos 2003). This positive shift in $\partial^{13}C$ would suggest an increase in the removal of light carbon from the ocean-atmosphere system - most likely due to the enhanced burial of organic carbon coupled to a peak in surface water export production. There is evidence for significantly increased primary production through the EOT and EOGM, especially in the Southern

Ocean where marked increases in benthic and planktonic foraminifera, radiolaria, fish, echinoderm and ostracod accumulation rates occur through this interval (Ehrmann & Mackensen 1992; Diester-Haass 1995; Diester-Haass *et al.* 1996; Diester-Haass & Zahn 1996, 2001; Salamy & Zachos 1999). This increase in productivity has been linked to high latitude cooling and an increased latitudinal temperature gradient, which in turn increased ocean-atmosphere circulation and the upwelling of nutrient-rich deep waters (Diester-Haass 1995; Zachos *et al.* 1996), but may also be stimulated by weathering-derived nutrients during a rapid sea-level fall. An increase in surface water productivity and burial of organic carbon, with the associated drawdown of atmospheric carbon dioxide, has been modeled as one of the positive feedback mechanisms that may have driven the climate system into a strongly glaciated state during the EOGM (Zachos & Kump 2005).

The third major change in the chemistry of the global oceans through the EOT, which again is closely coupled to the shift in $\partial^{18}O$, is an increase in deep-ocean carbonate ion concentrations and a dramatic deepening of the calcium carbonate compensation depth (CCD) (Van Andel 1975; Hsü & al. 1984; Moore *et al.* 1984; Peterson & Backman 1990; Coxall *et al.* 2005; Rea & Lyle 2005). Although this increase in the carbonate saturation of the deep ocean is probably the largest single change in the history of Cenozoic oceanic chemistry, the underlying controls on this are still poorly constrained (Rea & Lyle 2005). The most likely causes are one or a combination of: 1) the loss of shelf carbonate production during this major regression (Berger & Winterer 1974; Opdyke & Wilkinson 1989; Coxall *et al.* 2005), with the subsequent rise in oceanic carbonate alkalinity being buffered by a deepening of the CCD and an increase in deep-sea carbonate deposition; 2) a weathering-driven increase in the flux of calcium to the oceans, suggested by Rea & Lyle (2005) who argue that the loss of shelf carbonate production alone is not large enough to account for the observed increase in deep-sea carbonate deposition; or 3) enhanced siliceous export production causing the increased burial of organic carbon and associated removal of CO_2 from the ocean-atmosphere system, which in turn shifts the carbonate dissolution equilibrium towards the precipitation of calcium carbonate (Harrison 2000), however, this requires the extensive deposition of organic carbon in marine sediments, which has not been observed during

this interval (Rea & Lyle 2005).

Although marine records indicate a major shift in ocean chemistry coupled to the development of major ice sheets on Antarctica, and at least some component of northern hemisphere glaciation, there is continuing uncertainty as to the nature and severity of this event in the terrestrial realm. Some of the most recent terrestrial records, with good calibration to the marine isotope record, indicate a drop in mean annual temperatures of ~8°C in continental North America (Zanazzi *et al.* 2007) and the onset of aridification in central Asia (Dupont-Nivet *et al.* 2007) but conflicting terrestrial records have shown no significant fall in temperatures in either the northern (Grimes *et al.* 2005) or southern hemispheres (Kohn *et al.* 2004).

The record of biotic change across the Eocene-Oligocene transition has been hampered by correlation difficulties between marine and terrestrial records (Prothero 1994; Ivany *et al.* 2003) and between low and high-latitude marine records (Van Mourik & Brinkhuis 2005). In the marine realm there is considerable evidence for a significant biotic response to climatic changes in both planktic and benthic ecosystems, but this is a mixture of extinction, radiation and shifting biogeographic provincialism rather than a uniform extinction event. Perhaps the clearest extinctions during this interval are the sequential last occurrences of two widespread and long-lived groups of planktonic foraminifera just prior to and at the EOB, with the extinction of the *Turborotalia cerroazulensis* group ~65kyr before that of the Hantkeninidae at the EOB (Coccioni *et al.* 1988; Berggren & Pearson 2005). The relationship between these events at the EOB *sensu stricto* and the onset of glaciation during the EOT is as yet unresolved, with some suggesting that the EOB is simply an isolated extinction event in the planktonic foraminifera which is uncorrelated to the major biotic changes that take place at the peak of the EOGM (Prothero 1994; Prothero & Heaton 1996; Van Mourik & Brinkhuis 2005).

New records of radiolaria assemblages from the equatorial Pacific also show a significant extinction and turnover event in the siliceous heterotrophic plankton during the isotopic shift into the EOGM (Funakawa *et al.* 2006). The dinoflagellate record also

indicates surface water cooling through the EOT, with the influx of high-latitude species in the Massignano section, (Van Mourik & Brinkhuis 2005) and the onset of upwelling in the Southern Ocean (Sluijs *et al.* 2003). The most fundamental change in the distribution and diversity of marine microplankton between the Eocene and Oligocene is seen in the record of biosiliceous phyto- and microzooplankton from the Southern Ocean. Radiolarian and diatom records, along with the distribution of biosiliceous sediments, all strongly indicate the early Oligocene development of a distinct cold-water Southern Ocean province, bounded to the north by a well-defined Polar Front, which is dominated by upwelling, biosiliceous deposition and a strong Antarctic Circumpolar Current (Lazarus & Caulet 1994; Olney *et al.* 2005; Whithead 2005). Coincident with this is an explosive diversification of diatom species focused on the Southern Ocean (Spencer-Cervato 1999), which transforms the sediments of this region into a major sink for biogenic opal (Cervato & Burckle 2003).

Although there is no major overturn in deep-sea benthic foraminifera assemblages at the EOB (Thomas 1992; Coccioni & Galeotti 2003) there is evidence for an increase in primary production causing a peak in benthic foraminifera accumulation rates (Diester-Haass & Zahn 2001; Diester-Haass & Zachos 2003) and a decline in diversity with a shift towards more opportunistic, phytodetritus-exploiting species (Thomas & Gooday 1996). In contrast, the large shallow-water benthic foraminifera, which are a major component of Eocene shallow-water carbonate production, undergo a significant decline through the EOB (Kiessling *et al.* 2003; Nebelsick *et al.* 2005) with the extinction of the long-ranging genera *Asterocyclina* and *Discocyclina* in the Indo-Pacific (Adams *et al.* 1986). There is a similar marked turnover in the earliest Oligocene molluscan record from the US Gulf Coast and Atlantic margin (Dockery III 1986; Dockery III & Lozouet 2003) and the western USA (Hickman 2003; Nesbitt 2003; Squires 2003).

In summary, although there appears to be both a geographically and taxonomically widespread biotic response to global change through the EOT, there may be a variety of causal mechanisms behind this change including cooling, sea level fall, eutrophication and increased productivity. Most of these records, although constrained to the EOT, lack the temporal resolution to determine the nature and rate of biotic

changes at each stage of the climatic shifts that occur through the EOT.

1.3 The calcareous phytoplankton

The calcareous nannoplankton, predominantly the coccolithophore group of calcareous-scale producing haptophyte algae, are ideal for constructing high-resolution records of biotic and ecological change in the marine realm. Their common occurrence and high-abundances in calcareous marine sediments allows for the production of continuous, high-resolution records of species abundance changes and ecological diversity, both of which are highly sensitive to changes in their surface-ocean habitat. For example, high-resolution nannofossil assemblage data from the Southern Ocean has demonstrated that there was a significant fall in nannofossil diversity and an increase in "cold-water" (*Chiasmolithus* spp. group and *Reticulofenestra daviesii*) and decrease in "temperate-water" taxa (*Coccolithus pelagicus* group, *Reticulofenestra umbilicus* group, *Dictyococites bisectus* group and *Isthmolithus recurvus*) directly coincident with the onset of Antarctic glaciation in the early Oligocene (Persico & Villa 2004) (Figure 1.3).

At present there is no comparable dataset from the low-latitudes that documents the detailed timing and response of the calcareous phytoplankton through the Eocene-Oligocene transition, with previous studies being either at low ~100kyr resolution (Backman 1987; Wei & Wise 1990; Wei *et al.* 1992) or severely compromised by poor-preservation (Monechi 1986; Coccioni *et al.* 1988). Early attempts to define the biogeographic provincialism of Paleogene nannofossil species (Haq & Lohmann 1976) were followed by the association of Eocene and Oligocene latitudinal species distributions with supposed water temperature preferences, to construct groupings of warm- (*Coccolithus formosus*, discoasters, helicosphaerids and sphenoliths), temperate- (*Coccolithus pelagicus, Cyclicargolithus floridanus* group, *Reticulofenestra bisecta, Reticulofenestra samodurovii/umbilica*) and cool-water (chiasmoliths, *Isthmolithus recurvus* and *Reticulofenestra daviesii*) taxa (Wei & Wise 1990). A similar latitudinal distribution of Eocene and Oligocene taxa was found between equatorial and high

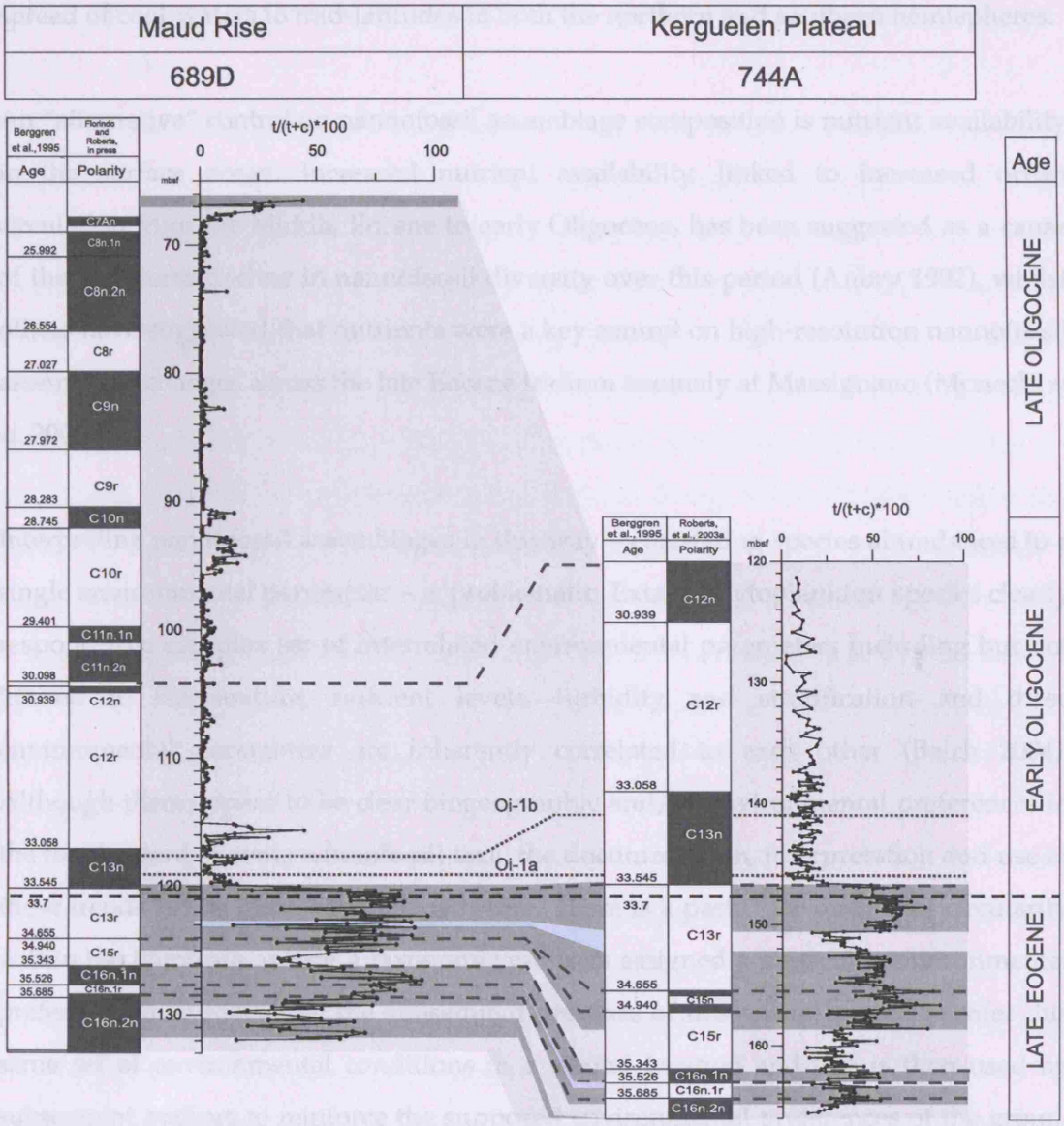

Figure 1.3 The temperate-water taxa index of Persico & Villa (2004) through the late Eocene and early Oligocene of Southern Ocean ODP Sites 689D and 744A. Note the rapid transition at the base of Chron C13n from assemblages dominated by warm-water taxa in the late Eocene (highlighted dark grey) to assemblages dominated by cool-water taxa in the early Oligocene (light grey).

latitude sites in the Indian Ocean (Wei *et al.* 1992). Together these studies laid the basis for the more detailed description of temperature dependent assemblages from Eocene and Oligocene sediments of the Southern Ocean (Persico & Villa 2004; Villa & Persico 2006). A peak in the abundance of *Isthmolithus recurvus*, coincident with the extinction of the planktonic foraminifera genus *Hantkenina* in both the Gubbio section, Italy (Monechi 1986) and the South Atlantic DSDP Site 522 (Backman 1987), may indicate the

spread of cool-waters to mid-latitudes in both the northern and southern hemispheres.

An "alternative" control on nannofossil assemblage composition is nutrient availability in the surface ocean. Increased nutrient availability, linked to increased ocean circulation from the Middle Eocene to early Oligocene, has been suggested as a cause of the long term decline in nannofossil diversity over this period (Aubry 1992), whilst others have suggested that nutrients were a key control on high-resolution nannofossil assemblage changes across the late Eocene iridium anomaly at Massignano (Monechi *et al.* 2000).

Interpreting nannofossil assemblages in this way – correlating species abundances to a single environmental parameter – is problematic. Extant phytoplankton species clearly respond to a complex set of interrelated environmental parameters including but not limited to temperature, nutrient levels, turbidity and stratification and these environmental parameters are inherently correlated to each other (Balch 2004). Although there appear to be clear biogeographic and/or environmental preferences in the fossil record of some nannofossil taxa, the documentation, interpretation and use of these trends needs to be handled with care. There is a particular danger of circularity within the literature, where a taxonomic group is assigned a particular environmental preference in one location; the subsequent presence of this group is used to infer this same set of environmental conditions in a second location and this is then used by subsequent authors to reinforce the supposed environmental preferences of the group. There are also issues of taxonomic consistency between authors, especially were assemblage data is published without figured material or references to clearly illustrated taxonomic descriptions in support of the authors' taxonomic concepts. More fundamentally, a high-resolution study of Milankovitch-scale climate cycles in mid-Pliocene sediments has shown that only a limited number of taxa - discoasters, sphenoliths and the deep-photic zone *Florisphaera profunda* - respond in a coherent way to external, abiotic climate forcing (Gibbs *et al.* 2004). Determining meaningful correlations between environmental conditions and given taxa needs to be undertaken with care - if these do exist then they should be apparent though periods of major climatic change, such as the EOT.

1.4 Preservation

Fossil konservat-lagerstätte - sedimentary units that contain extraordinary well preserved fossil material (Briggs 2001) – are the only source of information for many taxonomic groups that have limited preservation potential in standard sedimentary environments, such as the preservation of soft-bodied organisms in the Middle Cambrian Burgess Shale or Upper Jurassic Solnhofen Limestone. The consistent presence and often great abundance of calcareous microfossils in a variety of sedimentary environments might suggest that these, often robust, skeletal remains are not subject to significant taphonomic losses between living and fossil assemblages and hence do not require exceptional sedimentary conditions for the preservation of a representative flora or fauna. Although this may be true to some extent for the relatively large and robust calcareous foraminifera, it is becoming clear that the minute size, typically <10μm, and fragile nature of many calcareous nannofossil species can introduce a significant preservational bias into their fossil record (Young *et al.* 2005; Bown *et al.* 2008).

The fossil record of coccolithophores, in the form of calcareous nannofossils, extends from the Upper Triassic to the present (Bown *et al.* 2004), with occurrences that often reach rock-forming abundances in deep-sea calcareous oozes and chalks. In spite of this apparently complete, continuous Mesozoic and Cenozoic fossil record, comparisons of living coccolithophore communities in surface waters with sediment trap and core top assemblages have revealed a significant loss of small <3μm and fragile taxa within the water column (Andruleit *et al.* 2004; Young *et al.* 2005). Additional comparisons between global species diversities and coccolith size distributions of extant coccolithophore and Holocene nannofossil taxa show that their preservation potential, even in recent sediments, is highly size dependent – more than 90% of living taxa with coccoliths >3μm have a Holocene fossil record, compared with only 20% of taxa with coccoliths <3μm (Young *et al.* 2005). This loss of the small size fraction species diversity is not insignificant, with only ~30% of living taxa being found as fossils in typical Holocene sedimentary environments (Young *et al.* 2005).

Certain groups of coccolithophore species produce distinct coccolith morphologies in the two phases of their haplo-diplontic life cycle; robust heterococcoliths formed of interlocking calcite crystals in the diploid phase and fragile holococcoliths formed of small equidimensional crystallites in the haploid phase (Young *et al.* 2003). These differences in construction make the more robust heterococcoliths the most common form preserved in the fossil record - of the 90 living holococcolith taxa only one, slightly larger (3-4μm) form, *Syracolithus schilleri*, is commonly preserved in Neogene sediments (Young *et al.* 2003). Although there are a number of well known Cretaceous and Palaeogene holococcolith species, which are generally larger and hence more robust than extant forms, it is almost certain that the fossil record of holococcoliths significantly undersamples the living community, severely limiting our knowledge of fossil holococcolith diversity, taxonomy and paleobiology.

The extensive use of calcareous nannofossils for detailed biostratigraphy (Perch-Nielsen 1985; Bown 1998) and paleoceanographic reconstructions (e.g. Beaufort *et al.* 2001), is generally based upon commonly preserved heterococcoliths and nannoliths. This familiarity with a 'good', reliable and useful fossil record may disguise the inherent incompleteness of this record when viewed from the perspective of paleobiology and paleoecology. In addition, the development of molecular genetic techniques has produced a series of phylogenetic hypotheses for a large proportion of living taxa (Sáez *et al.* 2004), which can only be rigorously tested by comparison with fossil assemblages that preserve a high proportion of the actual coccolithophore diversity at a given time.

1.5 Objectives

This study focuses on the three themes of calcareous nannofossil preservation, climatic change through the EOT and the response of calcareous nannofossil assemblages through this interval. The specific objectives for this project were:

- the identification of suitable Eocene-Oligocene boundary sections for this study, namely those with continuous sedimentation through the EOT, adequate age control, stable isotope stratigraphy and good to excellent preservation of calcareous nannofossils;
- the collection of high resolution nannofossil assemblage data through these sections, with the aim of determining both the response of the calcareous phytoplankton to global climatic change but also using this response to constrain the timing and nature of the physical changes in the low-latitude surface water environment coincident with the onset of high-latitude glaciation;
- to compare the taxonomic composition and preservational states of the calcareous nannofossil assemblages from the selected study sites and use this to assess the effects of preservation on nannofossil assemblage data; and,
- to document the diversity and taxonomic composition of the exceptionally well-preserved late Eocene to early Oligocene calcareous nannofossils recovered from the Tanzanian sections and use this to inform discussions of the Cenozoic history of the coccolithophores.

1.6 Scheme of Work

This project was undertaken as part of the Tanzanian Drilling Project, a multi-disciplinary, international collaboration of micropalaeontologists, geochemists and sedimentologists aimed at the recovery of high-quality paleoclimatic and paleobiological data from the Cretaceous and Paleogene sediments of southern Tanzania. Involvement in this project naturally led to other collaborations and helped identify suitable Eocene-Oligocene comparison sites for this study. There is vital geochemical, biostratigraphic and sedimentological data presented in this thesis that has been sourced from project partners and this is referenced as such to either a published source or with a personal attribution. Conversely there is a significant amount of nannofossil and geological data that has been gathered during the course of this thesis but which falls outside the scope of this written presentation; the main components of this are listed in Table 1.1. Where this work lead to the authorship or co-

authorship of publications these are included on the supplementary data disk and are listed below.

Publications:

Bown, P. R., **Dunkley Jones, T.**, Lees, J. A., Randell, R., Mizzi, J., Pearson, P. N., Coxall, H. K., Young, J.R., Nicholas, C.J., Karega, A., Singano, J and Wade, B. S. 2008. The Paleogene Kilwa Group of coastal Tanzania: a calcareous microfossil Konservat-Lagerstätte. *Geological Society of America Bulletin* **120**: 3-12.

Pearson, P. N. McMillan, I. K., Wade, B. S., **Dunkley Jones, T.**, Coxall, H. K., Bown, P. R. and Lear, C. H. 2008. Extinction and environmental change across the Eocene-Oligocene boundary in Tanzania. *Geology* **36**: 179-182.

Dunkley Jones, T. and Bown, P. R. 2007. Post-sampling dissolution and the consistency of nannofossil diversity measures: A case study from freshly cored sediments of coastal Tanzania. *Marine Micropaleontology*, **62**(4):254-268.

Bown, P. R., **Dunkley Jones, T.** and Young, J. R. 2007. *Umbilicosphaera jordanii* Bown, 2005 from the Palaeogene of Tanzania: confirmation of generic assignment and a Palaeocene origination for the family Calcidiscaceae. *Journal of Nannoplankton Research*, **29**(1):25-30.

Bown, P. R. and **Dunkley Jones, T.** 2006. New Paleogene calcareous nannofossil taxa from coastal Tanzania: Tanzania Drilling Project Sites 11 to 14. *Journal of Nannoplankton Research*, **28**(1):17-34.

Nicholas, C. J., Pearson, P. N., Bown, P. R., **Dunkley Jones, T.**, Huber, B. T., Karega, A., Lees, J. A., McMillan, I. K., O'Halloran, A., Singano, J. M. and Wade, B. S. 2006. Stratigraphy and sedimentology of the Upper Cretaceous to Paleogene Kilwa Group, southern coastal Tanzania. *Journal of African Earth Sciences*, **45**(4-5):431-466.

Date	Activity
August - October 2004	TDP field season - mapping the Upper Cretaceous of Nangurukuru and Paleogene of the Pande Peninsular; drilling TDP Sites 11, 12, 13 and 14 (Pande Peninsular).
November 2004 - June 2005	Preliminary biostratigraphy of TDP Sites 11, 12 and 13. Contributions to the combined stratigraphy paper (Nicholas *et al.* 2006).
	Post-sampling dissolution study on TDP Sites 12 and 13 (Dunkley Jones & Bown 2007).
	Light microscope taxonomy of TDP Sites 11, 12 and 13 contributing to the taxonomy paper (Bown & Dunkley Jones 2006).
July - August 2005	TDP field season - drilling TDP Sites 15 (Nangurukuru) 16a, 16b, 17, 18, 19 (Pande Peninsular) & 20 (Kilwa Masoko).
September - December 2005	Geochemical (organic carbon, carbonate, sulphide and sulphate) analyses on sediments from TDP Sites 12 & 13 for the dissolution study (Dunkley Jones & Bown 2007).
January 2006	Drilling project in western Java, Indonesia targeting a Middle Eocene - early Oligocene sequences with excellent calcareous microfossil preservation.
February - May 2006	Nannofossil biostratigraphy of Java cores.
June 2006	Preliminary field work in Mississippi, USA (assistant on the Cretaceous project of Jackie Lees) - collected late Eocene and early Oligocene material from Mississippi and Alabama.
July - August 2006	Participant at the 3rd Urbino Summer School in Paleoclimatology
April - May 2007	Field work in Mississippi and Alabama to collect samples from key successions and cores through the EOB (Chapter 5).
June - August 2007	Co-supervision of MSc project/pilot study on the Eocene-Oligocene Mossey Grove core, Jackson, Mississippi; including assemblage counts, taxonomy and TEX86 paleothermometry.

Table 1.1 Main periods of field work, additional studies not included in this thesis and collaborations undertaken during this project.

1.7 Structure

This thesis does not explicitly follow the more traditional pattern of Methods/Results/Discussion. Instead I have structured the chapters into semi-contained site-by-site studies for two reasons; first the methodologies employed are relatively straightforward and are better incorporated into the geological setting/materials section for each site; and second, the more site-specific aspects of the results from each site are best discussed alongside the primary data for the site. This format relies upon the general introduction presented in this chapter and the more extensive discussion presented in Chapter 6, which highlights the comparisons between sites and the implications for more general questions of biotic, oceanographic and climatic change through the EOT.

Chapter 2 is a presentation of high-resolution nannofossil assemblage data from two TDP boreholes that recovered sediments through the EOT. The collection of this assemblage data, along with the taxonomic study of the same material presented in Chapter 3, forms the core of this thesis. The detailed documentation of these nannofossil assemblage changes through the EOT was undertaken alongside the collection of high-resolution stable isotope (Pearson *et al.* 2008), trace element (Lear *et al.* submitted), and detailed paleoecological data for both planktonic (Wade & Pearson submitted) and benthic (McMillan *et al.* in prep) foraminifera. The combination of these high resolution biotic records along with detailed geochemical proxy data has produced the most detailed correlation of biotic and climatic change through the EOT to date, as well as the correlation of the EOB to climatic changes within the EOT. The taxonomic data collected from the Eocene-Oligocene calcareous nannofossil assemblages of Tanzania, as presented in Chapter 3, are truly unique, representing the most diverse and well-preserved Eocene-Oligocene nannofossil flora known to date, but also in its preservation of many extant coccolithophore taxa that previously had no or a very limited fossil record. These assemblages, located as they are between the high diversity, coccolithophore dominated oceans of the early Palaeogene and the evolution of a recognizably modern flora in the Neogene, provide a detailed view of the ecology and diversity of the coccolithophores during this transition period. Chapter 3 forms a

largely self-contained taxonomic study, the implications of which are discussed within the Chapter itself.

Chapters 4 and 5 test the ideas established in Chapters 2 and 3 by collecting both nannofossil assemblage and taxonomic data from two additional low-latitude (paleolatitudes <30° N/S) sites - DSDP Site 242 in the Mozambique Channel, western Indian Ocean (Chapter 4) and St Stephens Quarry, Alabama, USA (Chapter 5) (Figure 1.4). DSDP Site 242 is the closest deep-sea Eocene-Oligocene boundary to the TDP sections and, for a deep-sea section, contains relatively well-preserved nannofossil assemblages. Quantifying these assemblages through the EOT provides data from an open-ocean locality relatively near to the TDP sites, allowing for the determination of local versus regional controls on these assemblages. The Eocene-Oligocene section exposed at St Stephens Quarry has been and continues to be extensively studied for geochemical proxy data, sequence stratigraphy and biotic change through the EOT (see Miller *et al.* 1991, in press and references therein). There is surprisingly no high-resolution record of calcareous nannofossil assemblage change though this section, even though calcareous nannofossil preservation is considerably better than the extensively studied nannofossil assemblages of Massignano (Monechi 1986; Monechi *et al.* 2000). The production of nannofossil assemblage data from St Stephens provides a

Figure 1.4 Paleogeographic reconstruction for the late Eocene (34Ma) showing the locations of the three studied sites; TDP - Tanzania Drilling Project sites, 242 - DSDP Site 242, SSQ - St Stephens Quarry, Alabama. Paleogeographic reconstruction from the Ocean Drilling Stratigraphic Network http://www.odsn.de/odsn/index.html.

far-field comparison, from a northern hemisphere site in a different ocean basin, to the data from the TDP sites and DSDP Site 242, allowing for an assessment of the geographical extent and relative timing of the biotic response. The locations of the three study sites are shown in relation to a late Eocene (~34Ma) paleogeographic reconstruction in Figure 1.4.

2. NANNOFOSSIL ASSEMBLAGE CHANGES THROUGH THE EOCENE-OLIGOCENE BOUNDARY OF COASTAL TANZANIA

2.1 Introduction

This study is part of an ongoing paleoclimate research project, the Tanzanian Drilling Project (TDP), which has focused on recovering geochemical and paleobiological data using exceptionally well-preserved calcareous microfossils from the Cretaceous and Paleogene sediments of the Kilwa Group, coastal Tanzania (Pearson *et al.* 2001, 2004, 2006, 2007). In its initial stages, this project concentrated on collecting very well-preserved planktonic foraminifera shells with which to test the fidelity of the oxygen isotope record of planktonic foraminifera recovered from deep-sea sediments and quantify the effects of calcite diagenesis and recrystallization on these geochemical records (Pearson *et al.* 2001). Subsequent collaborations with specialists from a number of other disciplines (sedimentology, organic geochemistry, palynology and calcareous nannofossil micropaleontology) led to a broadening of focus and a number of exciting new research possibilities. Of these, perhaps the most remarkable was the discovery of a hitherto unknown, or undocumented, diversity of Paleogene calcareous nannofossil species, including many new taxa, which are already contributing to significant revisions of the Cenozoic paleobiology and history of the group (Bown 2005b; Bown & Dunkley Jones 2006; Bown *et al.* 2007, in press).

After a number of years of exploratory fieldwork (1998-2001), followed by four consecutive seasons of 4-6 weeks drilling operations (2002-2005), the improved understanding of the local geology and stratigraphy allowed for the targeting of short stratigraphic intervals of rapid global change, such as the Paleocene-Eocene Thermal Maximum (PETM) and the Eocene-Oligocene Boundary (EOB). In the final two years of drilling operations (2004-5) the project recovered three sequences of cores through each of these critical intervals. These successions have the advantage of both yielding exceptionally well-preserved calcareous microfossils - enabling both detailed

paleobiological and geochemical investigations - and having high sedimentation rates and expanded sequences, which are ideal for high temporal resolution investigations.

This chapter presents the results of a detailed, high-resolution investigation of nannofossil assemblage changes through the EOB. It is designed to answer some of the questions discussed in Chapter 1, particularly addressing the nature and timing of the response of low-latitude phytoplankton to high-latitude glaciation during the Eocene-Oligocene transition. The quality of preservation, diversity and, it is hoped, fidelity of these nannofossil assemblages to the living phytoplankton community provides a unique opportunity to investigate climate-biosphere interactions through the EOB. This work was undertaken in parallel with a number of other studies on the same material including planktonic foraminiferal stable isotopes and paleobiology (Paul Pearson, Helen Coxall, Bridget Wade), benthic foraminiferal evolutionary turnover (Ian McMillan), trace element geochemistry (Carrie Lear), sedimentology (Chris Nicholas, Aoife O'Halloran), organic geochemistry (Richard Pancost, Luke Handley), palynology (Henk Brinkhuis, Appy Sluijs) and calcareous nannofossil taxonomy and paleobiology (Tom Dunkley Jones, Paul Bown - see Chapter 3).

2.2 Materials and Methods

Two sets of cores were examined for this study, TDP Site 12 (drilled October 2004; UTM 37L 560222 8981309; total depth 147.44m) and TDP Site 17 (drilled August 2005; UTM 37L 560539 8984483; total depth 125.9m) located on the Pande Peninsular, approximately 3km apart, between the villages of Pande and Mkazambo, Lindi District, Tanzania (Nicholas *et al.* 2006) (Figure 2.1). The cores were recovered using a simple truck mounted water-flush rotary percussion drilling rig, with water sourced from a local river without the addition of bentonite or other additives. The 2 inch (~5 cm) diameter cores were normally recovered in 3m lengths, which were then divided into 1m core sections for lithological description and sampling. Sample identification numbers follow the protocol of the Ocean Drilling Program detailing site, core number, section number and depth interval; for example TDP12/26-2, 62cm indicates a sample from TDP Site 12, core 26, at 62cm into section 2. Both boreholes cored a succession of

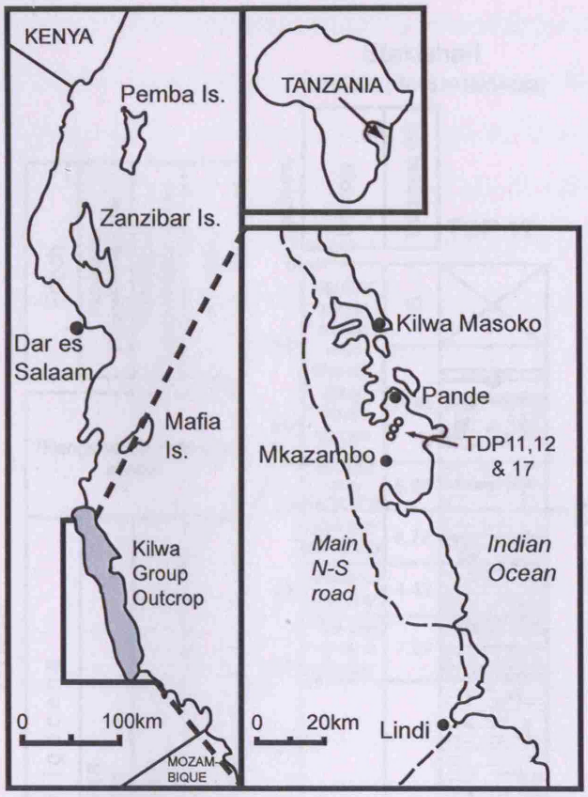

Figure 2.1 Location of the EOB boreholes used in this chapter and Chapter 3 (TDP Sites 11, 12 & 17).

dark greenish-grey marly clays - with carbonate contents of between 5 and 35 wt% (Dunkley Jones & Bown 2007) - with occasional limestone interbeds (Figure 2.2), which are typical of the middle Eocene to lower Oligocene Pande Formation (Nicholas *et al.* 2006). The cores span the EOB, nannofossil zones NP19/20 and 21 (Martini 1971) and planktonic foraminifera zones E16 and O1 (Berggren & Pearson 2005). The notation NP19/20 is used because of ongoing taxonomic uncertainty between *Sphenolithus radians* and *Sphenolithus pseudoradians,* with the first occurrence of the later defining the base of the Martini (1971) zone NP20. Following Martini (1976) and later workers (Aubry 1983; Perch-Nielsen 1985) I use the combined zone NP19/20 with a top defined by the last occurrence of *Discoaster saipanensis*. In high latitudes the base of this zone is defined by the first occurrence of *Isthmolithus recurvus* but this is often absent in low latitudes, and an alternative marker of the last occurrence of *Chiasmolithus grandis* was proposed for sites in the low latitude equatorial Pacific (Martini 1976); both *I. recurvus* and *Ch. grandis* are absent from the TDP Sites and the assignment of the zone NP19/20 to the lower part of the sections is based upon the placement of the the last occurrence of *Discoaster saipanensis*, which marks the base of NP21, within the sections combined with the absence of *Discoaster barbadiensis,* whose last occurrence falls just below that of *D. saipanensis* in NP19/20, at the base of the section (Berggren *et al.* 1995). This implies an age of topmost NP19/20, which is consistent with the planktonic foraminiferal biostratigraphy. The top NP21 is defined by the last occurrence of *Coccolithus formosus*, which is present throughout the sections.

Figure 2.2 Lithologic logs for TDP12 and TDP17, Pande Peninsular, Tanzania (after Nicholas *et al.* 2006)

The *in situ* benthic foraminiferal assemblage of the Pande clays, recovered at TDP Sites 12 and 17, consists of 'flysch'-style agglutinated forms, dominated by *Bathysiphon*, and a deep-water calcareous fauna typical of outer shelf to upper slope environments (300-500m water depth) (Nicholas *et al.* 2006). Abundant allocthonous microscopic shell debris, transported from the innermost shelf, is present throughout the succession and often dominates benthic foraminiferal assemblages. Planktonic foraminiferal and dinoflagellate assemblages may indicate a slightly shallower mid-shelf environment, but the identification of the deep-photic zone calcareous phytoplankton *Gladiolithus* and *Algirosphaera* (see Chapter 3) constrains the setting to a clear-water, open-ocean environment (Jordan & Chamberlain 1997; Takahashi & Okada 2000).

The age model and correlation between the two cores is primarily based on the planktonic foraminifera and calcareous nannofossil bioevents listed in Table 2.1. The two boreholes were then correlated in detail onto a composite depth scale based on these bioevents as well as locally distinct benthic foraminifera acme and extinction horizons and the stable isotope stratigraphy of both successions (Nicholas *et al.* 2006; Pearson *et al.* 2008). The final age model for these sites was then developed by correlating the spliced planktonic foraminiferal (*T. ampliapertura*) oxygen isotope

Datum	Age (Ma)	Composite depth (m)
LAD *Pseudohastigerina micra* (F)	32.0	*P. micra* present throughout
LAD *Coccolithus formosus* (N)	32.7	*C. formosus* present throughout
Base Oi-1 (I)	33.545	89.90
LAD Hantkeninidae (F)	33.7	102.70
LAD *Turborotalia cerroazulensis* (F)	33.765	107.40
LAD *Discoaster saipanensis* (N)	34.2	130.35
LAD *Discoaster barbadiensis* (N)	34.3	*D. barbadiensis* absent at base
LAD *Globigerinatheka index* (F)	34.3	*G. index* absent at base

Table 2.1 Age model data for planktonic foraminifera (F), calcareous nannofossil (N) and stable isotope (I) events in TDP Sites 12 and 17. The base of Oi-1, which is defined as the maximum benthic foraminifera ∂18O value at Site 522 (Miller *et al.* 1991), equates to an age of 33.494 Ma on the geomagnetic polarity time scale of Cande & Kent (1995). The LAD of *T. cerroazulensis* is a revised age from Berggren & Pearson (2005), all other ages are from Berggren *et al.* (1995).

records of TDP Sites 12 and 17 to the benthic foraminiferal (*Cibicidoides*) oxygen isotope records from three deep-sea sections with good or excellent age constraints - ODP Sites 522, 744 (Zachos *et al.* 1996) and 1218 (Coxall *et al.* 2005) - using the time scale of Cande & Kent (1995); this correlation is presented in Pearson *et al.* (in press) and is shown in Figure 2.3. All depths presented in this chapter are meters composite depth (mcd) and ages are based on this time scale of Pearson *et al.* (in press). The detailed stratigraphic correlation between TDP Sites 12 and 17 indicates the presence of a ~12m disconformity at the level of the EOB in TDP17. The location of this missing section is indicated on the axis of all the following data plots for TDP Site 17.

Figure 2.3 Planktonic foraminiferal (*T. ampliapertura*) oxygen isotope stratigraphy of TDP Sites 12 and 17 correlated to the deep-sea benthic foraminiferal (*Cibicidoides*) records of ODP Sites 522, 744 (Zachos *et al.* 1996) and 1218 (Coxall *et al.* 2005). Also shown are the extinction events in the calcareous plankton (far left) and the depth tie points between TDP12 & 17 (right). Time scale of Cande & Kent (1995). After Pearson *et al.* (in press).

The Berggren *et al.* (1995) age assessment of the LAD of *D. saipanensis* in low to mid-latitudes is based on the Italian sections at Massignano and the Contessa Road, where it falls within the lower part of Chron C13r with an estimated age of 34.2Ma. There is some uncertainty in this estimate due to both the latitudinal diachroneity of this event (Berggren *et al.* 1995) and the typically low abundance of *D. saipanensis* immediately prior to its last occurrence (Backman 1987). Records from various other mid and low-latitude sites have recorded a longer range of *D. saipanensis* into the upper part of Chron C13r (Poore *et al.* 1982; Wei & Wise 1989; Marino & Flores 2002). As in many other sections the low abundance of *D. saipanensis* in the Tanzanian cores makes the determination of this bioevent somewhat uncertain, however based on the new age model for these sites the placement of this bioevent in the Tanzanian sections supports a younger age estimates for the LAD of *D. saipanensis* of ~34.0Ma (Figure 2.3).

Sediment samples, approximately $2cm^3$ in volume, were extracted at a frequency of one per 1m-core section in the on-site field laboratory in Tanzania. These were thoroughly scraped clean to remove any possibility of contamination from the drilling mud and shipped back to University College London (UCL). Simple smear-slides were made by mixing a small quantity of sediment and distilled/de-ionised water on a cover slip and smearing evenly across the surface with a tooth-pick. All slides were prepared to a similar thickness by maintaining a constant opacity of the smeared sediment between each preparation. The use of simple smear-slides was judged the most suitable approach for these diverse assemblages, which include a significant number of fragile taxa, as it minimizes the amount of sample processing, with the attendant risks of nannofossil fragmentation and dissolution. This approach also allows for the assessment of sediment mineralogy alongside nannofossil assemblage counts. This smear slide preparation technique is used as standard for Chapters 3, 4 and 5.

The transport and storage of these sediments between coring and smear slide preparation are judged not to have had a significant deleterious effect on nannofossil preservation or the assemblage data collected from this material, as discussed in Dunkley Jones & Bown (2007). This study also validates the consistency and reproducibility of the assemblage data collected using the smear-slide technique

employed in this thesis (Dunkley Jones & Bown 2007). Sediments from both boreholes contain exceptionally well-preserved, diverse and abundant nannofossil assemblages (see Chapter 3 for a full description), with species richness values logged during preliminary light microscope biostratigraphy often exceeding 60, including a significant number of holococcolith taxa.

A total of 111 slides were examined for calcareous nannofossils from TDP12 (range in original depth scale 147.8 to 11.56mbgl), and 86 slides from TDP17 (range in original depth scale 125.24 to 31.15mbgl), using standard light microscope techniques at a magnification of 1250x on an Olympus BX40 microscope. Up to 20 consecutive fields of view (FOV) were initially examined for each slide, with all whole, identifiable nannofossil specimens counted. Specimens were identified to species level wherever possible, following the taxonomy of Bown (2005b) and Bown & Dunkley Jones (2006). During this count, the number of whole, reworked Cretaceous nannofossils and the number of cubic and framboidal pyrite, glauconite and amorphous carbonate grains were counted per FOV. Counts were terminated when at least 400 complete, *in situ*, identifiable nannofossils had been counted; where necessary, counts were extended beyond 20 FOV, along continuous transects, until 400 specimens had been counted. Occasional samples from both boreholes contained very low nannofossil abundances (~4 or less per FOV) and these were examined and counted as normal for 20 FOV to obtain nannofossil abundance, Cretaceous reworking and mineralogical counts but were then abandoned. Samples and slides are curated at the Department of Earth Sciences, University College London; count data is included on the supplementary data disk.

Nannofossil diversity was represented using the "SHE" analysis (Species richness - H Shannon's diversity - Evenness) approach detailed in Hayek & Buzas (1997). Shannon's information parameter H is widely used in the analysis of ecological diversity as it is sensitive to both raw species diversities (the number of taxa) with a measure of the dominance/evenness of assemblages. For example a community of ten taxa with relative abundances of 10% each would be considered more ecologically diverse than one with ten taxa where one has a relative abundance of 91% and the rest of 1% each.

This is strongly reflected in the H diversities of these communities (2.3 and 0.5 respectively) but not in the simple species richness measure, which is 10 in both cases. The SHE analysis is a graphical method of representing simple species richness together with H diversity and a measure of evenness . This is achieved by plotting the natural log of species richness, ln(S) alongside Shannon's diversity (H) with the resulting difference between the two being related to the evenness of a given assemblage. If H plots on top of ln(S), the assemblage has "maximum" evenness with the exactly equal partitioning of species abundances across all taxa; an increasing distance between these two measures indicates the increasing dominance of assemblages by a few taxa and a reduced "evenness".

A Principal Component Analysis (PCA) was performed on a reduced set of relative abundance data, for a total of 29 species, with the exclusion of species whose standard deviation of their relative abundances was less than 0.5%, followed by the re-scaling of the data to sum to 100%. This eliminates rarely occurring species, with relative abundances typically less than 1%, and follows the standard procedure for the multivariate analysis of subcomposition data (Pawlowsky-Glahn & Egozcue 2006). Before analysis, zero data were replaced using the rounded zero replacement routine of the CoDaPack multivariate data analysis software (Thió-Henestrosa & Martín-Fernández 2006) and then additive-log-ratio (ALR) transformed, with the most dominant species, the small form of *Cyclicargolithus floridanus* (sml), used as the denominator. This allows the use of standard multivariate methods on percentage compositional data, although the denominator variable, *Cyclicargolithus floridanus* (sml), is not present in the transformed data set (Pawlowsky-Glahn & Egozcue 2006). The transformed data were standardized before running the PCA.

PCA was carried out on a combined data set from both boreholes. PCA returns component loadings for each species, the scores of each principal component for each sample and the principal component variances (eigenvalues). The "percentage explained" by each of the principal components can be derived by calculating the percentage of the variance of each of the principal components with respect to the sum of the variances of all components (Trauth 2006).

Metric Multi-dimensional Scaling (MMDS) was performed on the same ALR transformed, standardized data set, using the Euclidean distance measure to obtain a dissimilarity matrix between the multi-dimensional data, and squared stress as the goodness-of-fit criterion between the multi-dimensional and two-dimensional distances. This method produces a two-dimensional representation of the samples that seeks to preserve and represent the distances between samples in the multi-dimensional space defined by the variables analyzed – in this case species relative abundances. Both the PCA and MMDS were performed in MATLAB, using the standard statistics toolbox.

2.3 Results

Mixed-layer planktonic foraminiferal (*Turborotalia ampliapertura*) stable isotope data (data from Paul Pearson and Helen Coxall; see Pearson *et al.* 2008), counts of reworked Cretaceous nannofossils and cubic pyrite grains, and nannofossil abundances are shown on Figure 2.4. The stable isotope record is similar in structure to the most complete benthic foraminifera isotope records from the deep-sea (Oberhansli *et al.* 1984; Zachos *et al.* 1996; Coxall *et al.* 2005; and see Figure 2.3), with a ~1 per mil increase in oxygen isotopes occurring over two steps (maxima of each step at ~107 and 97mcd) into the most positive isotope values of the EOGM. Planktonic foraminiferal carbon isotope values from the Tanzanian sections also shift to higher values coincident with the positive shift in oxygen isotopes, which is consistent with the deep-sea benthic foraminiferal records (Zachos *et al.* 1996; Coxall *et al.* 2005).

There is very little to no reworking of Cretaceous nannofossils in the lower half of TDP12 (from 205.8 to 126.53mcd, mean of 3.9 specimens/mm^2), but significant reworking appears at 125.56mcd and continues to be variably but consistently present to the top of the section (125.56 to 69.56mcd, mean 36 specimens/mm^2). A similar pattern is seen in TDP17, where significant reworking appears at 122.2mcd and continues up to the top of the section (mean below this point is 5.7 specimens/mm^2;

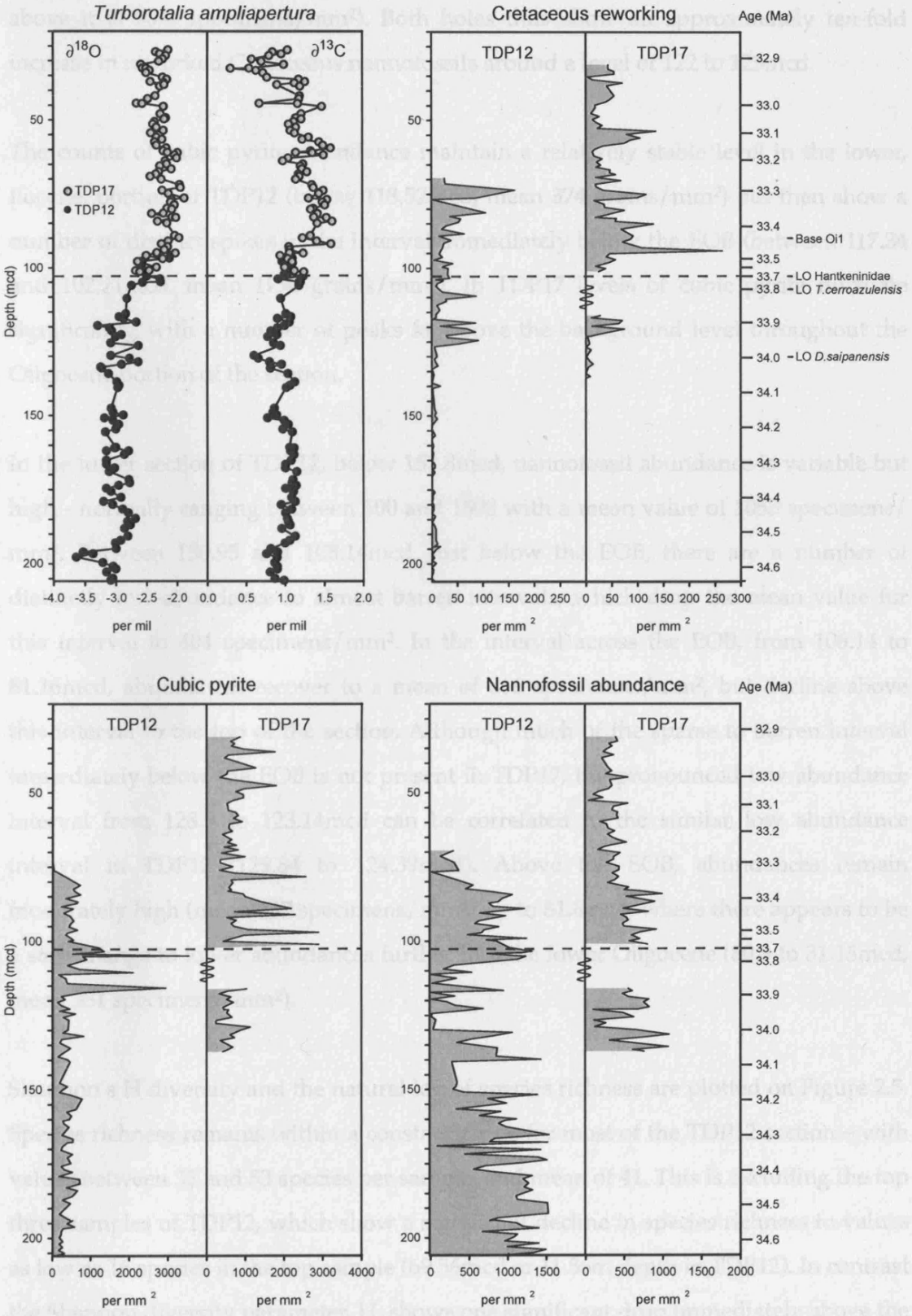

Figure 2.4 Planktonic foraminiferal stable isotopes (*T. ampliapertura*), reworked Cretaceous nannofossil and cubic pyrite abundance against depth (mcd). Ages from Pearson *et al.* (in press) based on the time scale of Cande & Kent (1995).

above it is 50.4 specimens/mm^2). Both holes thus show an approximately ten-fold increase in reworked Cretaceous nannofossils around a level of 122 to 125mcd.

The counts of cubic pyrite abundance maintain a relatively stable level in the lower, Eocene, portion of TDP12 (below 118.52mcd, mean 374 grains/mm^2) but then show a number of distinct spikes in the interval immediately below the EOB (between 117.34 and 102.21mcd, mean 1150 grains/mm^2). In TDP17 levels of cubic pyrite fluctuate significantly, with a number of peaks far above the background level throughout the Oligocene portion of the section.

In the lower section of TDP12, below 151.8mcd, nannofossil abundance is variable but high - normally ranging between 500 and 1500 with a mean value of 1053 specimens/ mm^2. Between 150.95 and 108.14mcd, just below the EOB, there are a number of distinctly low-abundance to almost barren intervals, which drop the mean value for this interval to 404 specimens/mm^2. In the interval across the EOB, from 106.14 to 81.16mcd, abundances recover to a mean of 866 specimens/mm^2, but decline above this interval to the top of the section. Although much of the sparse to barren interval immediately below the EOB is not present in TDP17, the pronounced low abundance interval from 128.9 to 123.14mcd can be correlated to the similar low abundance interval in TDP12 (129.84 to 124.39mcd). Above the EOB, abundances remain moderately high (mean 647 specimens/mm^2) up to 81.8mcd, where there appears to be a step-change to lower abundances further into the lower Oligocene (80.3 to 31.15mcd, mean 331 specimens/mm^2).

Shannon's H diversity and the natural log of species richness are plotted on Figure 2.5. Species richness remains within a constant range for most of the TDP12 section – with values between 32 and 53 species per sample, and mean of 41. This is excluding the top three samples of TDP12, which show a significant decline in species richness to values as low as 16 species in the top sample (69.56mcd or 11.56m depth in TDP12). In contrast the Shannon diversity parameter, H, shows one significant drop immediately above the EOB (102.7mcd), from 2.97 at 102.21mcd to 2.14 at 100.04mcd. This point separates the lower, mostly Eocene, part of the borehole, which has mean H diversity of 2.65 and the

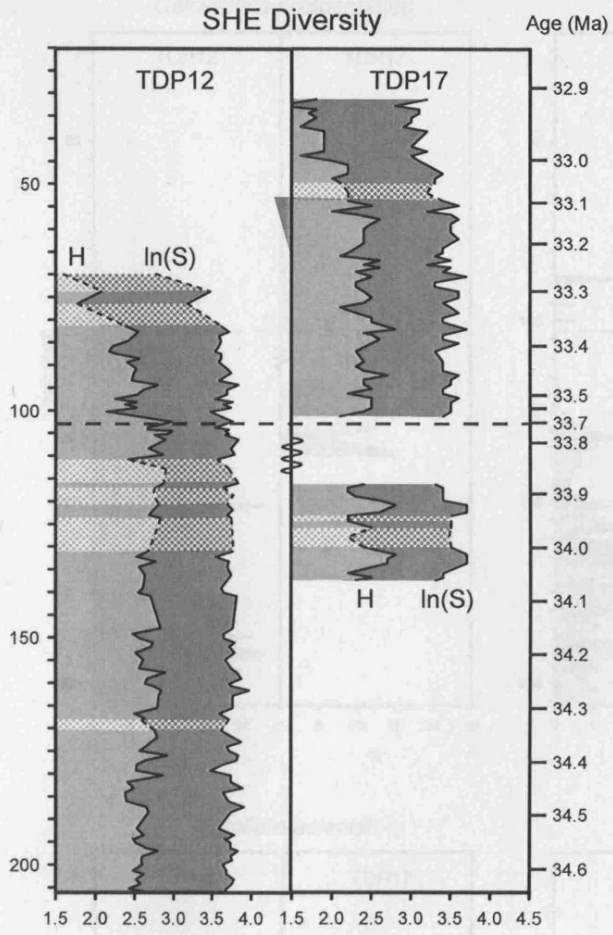

Figure 2.5 Shannon's H diversity and log species richness, ln(S), against depth (mcd). Ages from Pearson *et al.* (in press) based on the time scale of Cande & Kent (1995). Stippled areas indicate low abundance intervals where count data was not obtainable.

upper, mostly Oligocene section, with mean H of 2.43 - this does not include the topmost three data points, which show anomalously low H values, and may have been adversely affected by surface weathering.

As in TDP12, species richness in TDP17 is broadly constant throughout the section (from 137.24 to 53.55mcd, range is 24 to 42 species per sample, mean 32) but begins to decline slightly above 51.55mcd (mean 51.55 to 31.15mcd is 23 species per sample). Shannon's diversity parameter, H, follows a similar trend with mean values below 53.55mcd of 2.40 and above 51.55mcd of 1.86. There is no noticeable change in H across the EOB in TDP17, but the critical interval across the actual boundary is not present in this section. In general, TDP17 has both lower species richness and H values than TDP12.

Plots of the relative abundance of the main species components are shown in Figures 2.6 to 2.12. Species shown on Figures 2.6 and 2.7 all show a clear trend of decreased relative abundance between the latest Eocene and early Oligocene, with many of them not present or rarely occurring above the EOB. *Calcidiscus protoannulus* and *Lanternithus minutus* are the most abundant of this group, with mean abundances, across both boreholes, in the Eocene of 12.3 to 7.3% respectively, but which drop to 0.4 and 0.5% in the Oligocene. The notable difference between the records of these two species is their

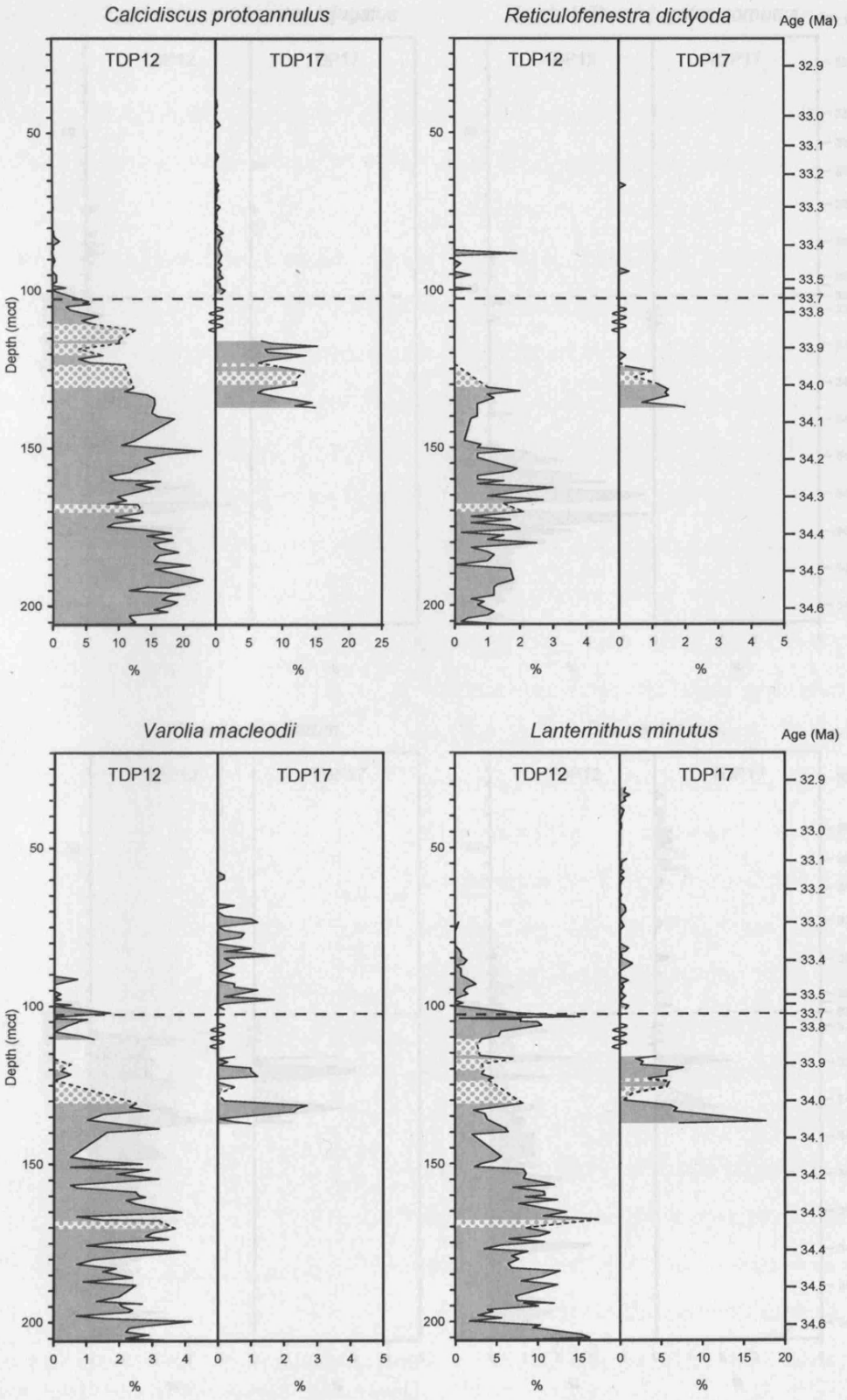

Figure 2.6 Species relative abundances against depth (mcd) - *Calcidiscus protoannulus*, *Reticulofenestra dictyoda*, *Varolia macleodii* and *Lanternithus minutus*. Ages from Pearson *et al.* (in press) based on the time scale of Cande & Kent (1995). Stippled areas indicate low abundance intervals where count data was not obtainable.

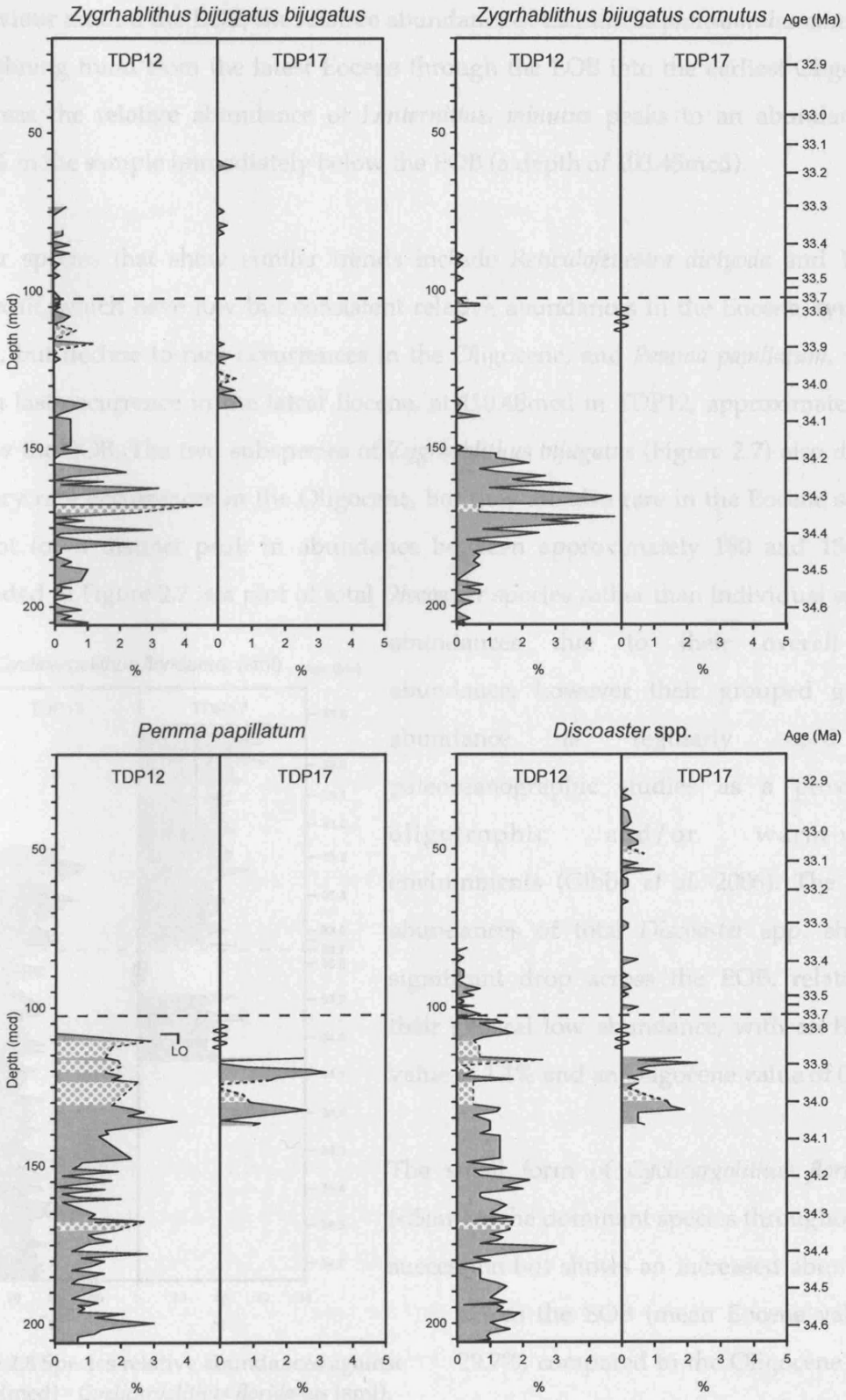

Figure 2.7 Species relative abundances against depth (mcd) - *Zygrhablithus bijugatus bijugatus*, *Zygrhablithus bijugatus cornutus*, *Pemma papillatum* and grouped *Discoaster* species. Ages from Pearson *et al.* (in press) based on the time scale of Cande & Kent (1995). Stippled areas indicate low abundance intervals where count data was not obtainable.

behaviour around the EOB; the relative abundance of *Calcidiscus protoannulus* continues a declining trend from the latest Eocene through the EOB into the earliest Oligocene, whereas the relative abundance of *Lanternithus minutus* peaks to an abundance of 15.1% in the sample immediately below the EOB (a depth of 103.45mcd).

Other species that show similar trends include *Reticulofenestra dictyoda* and *Varolia macleodii*, which have low but consistent relative abundances in the Eocene, typically 2-5%, but decline to rare occurrences in the Oligocene, and *Pemma papillatum*, which has a last occurrence in the latest Eocene, at 110.48mcd in TDP12, approximately 7m below the EOB. The two subspecies of *Zygrhablithus bijugatus* (Figure 2.7) also decline to very rare occurrences in the Oligocene, but they are also rare in the Eocene section except for a distinct peak in abundance between approximately 180 and 150mcd. Included in Figure 2.7 is a plot of total *Discoaster* species rather than individual species abundances due to their overall low abundance, however their grouped generic abundance is regularly used in paleoceanographic studies as a proxy for oligotrophic and/or warm-water environments (Gibbs *et al.* 2006). The mean abundances of total *Discoaster* spp. show a significant drop across the EOB, relative to their general low abundance, with an Eocene value of 1.1% and an Oligocene value of 0.2%.

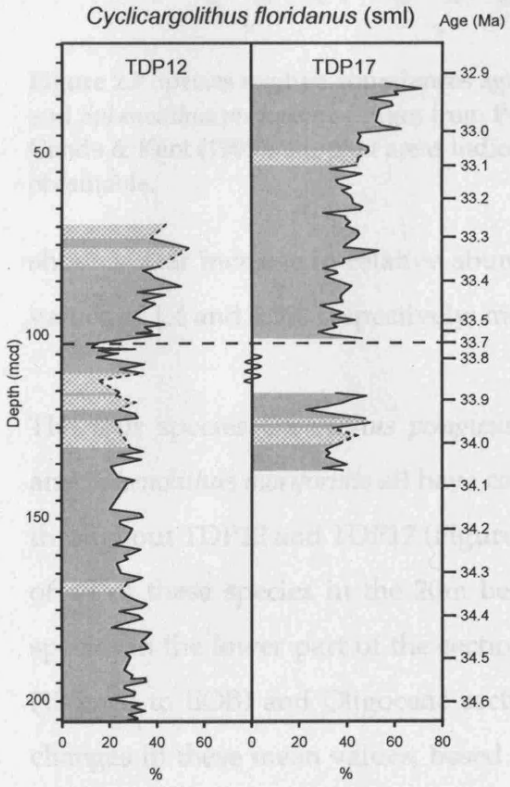

Figure 2.8 Species relative abundances against depth (mcd) - *Cyclicargolithus floridanus* (sml). Ages from Pearson *et al.* (in press) based on the time scale of Cande & Kent (1995). Stippled areas indicate low abundance intervals where count data was not obtainable.

The small form of *Cyclicargolithus floridanus* (<5μm) is the dominant species throughout the succession but shows an increased abundance across the EOB (mean Eocene value of 29.7%, compared to the Oligocene value of 41.4%) (Figure 2.8). Likewise the larger form of *Cyclicargolithus floridanus* (>5μm) and *Sphenolithus predistentus*,

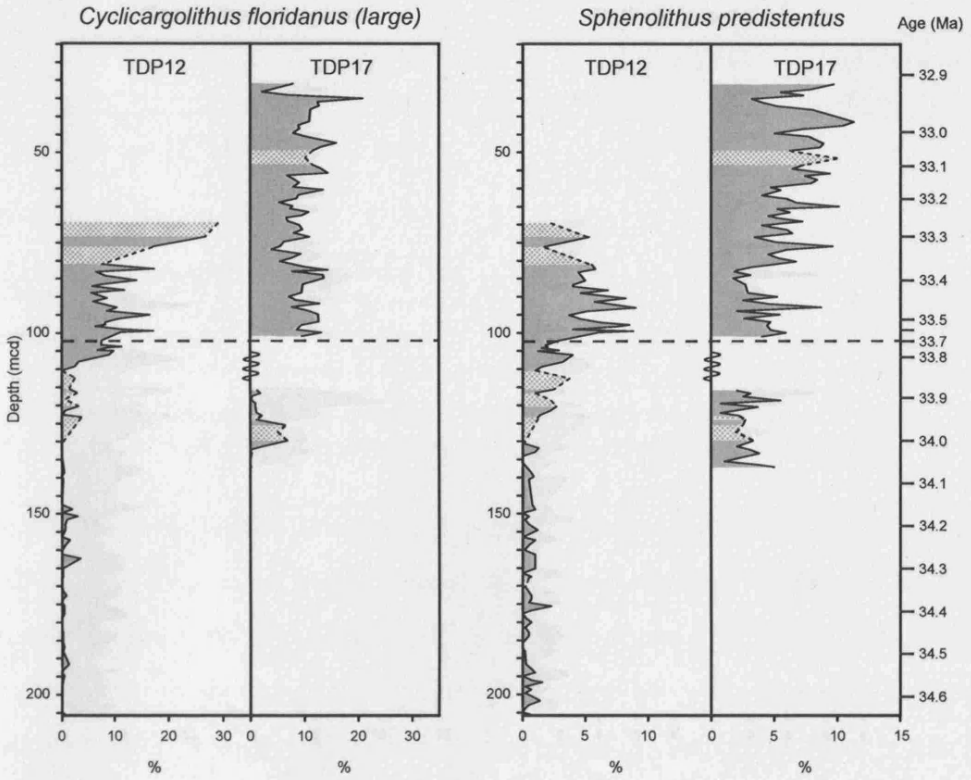

Figure 2.9 Species relative abundances against depth (mcd) - *Cyclicargolithus floridanus* (large) and *Sphenolithus predistentus*. Ages from Pearson *et al.* (in press) based on the time scale of Cande & Kent (1995). Stippled areas indicate low abundance intervals where count data was not obtainable.

show a clear increase in relative abundance across the EOB (Figure 2.9) (mean Eocene values of 1.4 and 1.3% respectively; mean Oligocene values of 10.2 and 5.7%).

The four species *Coccolithus pelagicus*, *Reticulofenestra bisecta*, *Reticulofenestra filewiczii* and *Sphenolithus moriformis* all have consistent moderate to low abundances (~2 to 10%) throughout TDP12 and TDP17 (Figure 2.10). There is a subtle increase in the abundance of all of these species in the 20m below the EOB; mean abundance values for these species in the lower part of the sections (base to 125mcd), the topmost Eocene portion (125mcd to EOB) and Oligocene sections are given in Table 2.2. Although subtle, the changes in these mean values, based on tens of data points, all support an increase in relative abundances of these four species in the interval 125mcd to the EOB.

Other species that are consistently present through TDP12 and TDP17, but do not show clear trends across the EOB, are shown in Figures 2.11 and 2.12. *Reticulofenestra minuta*

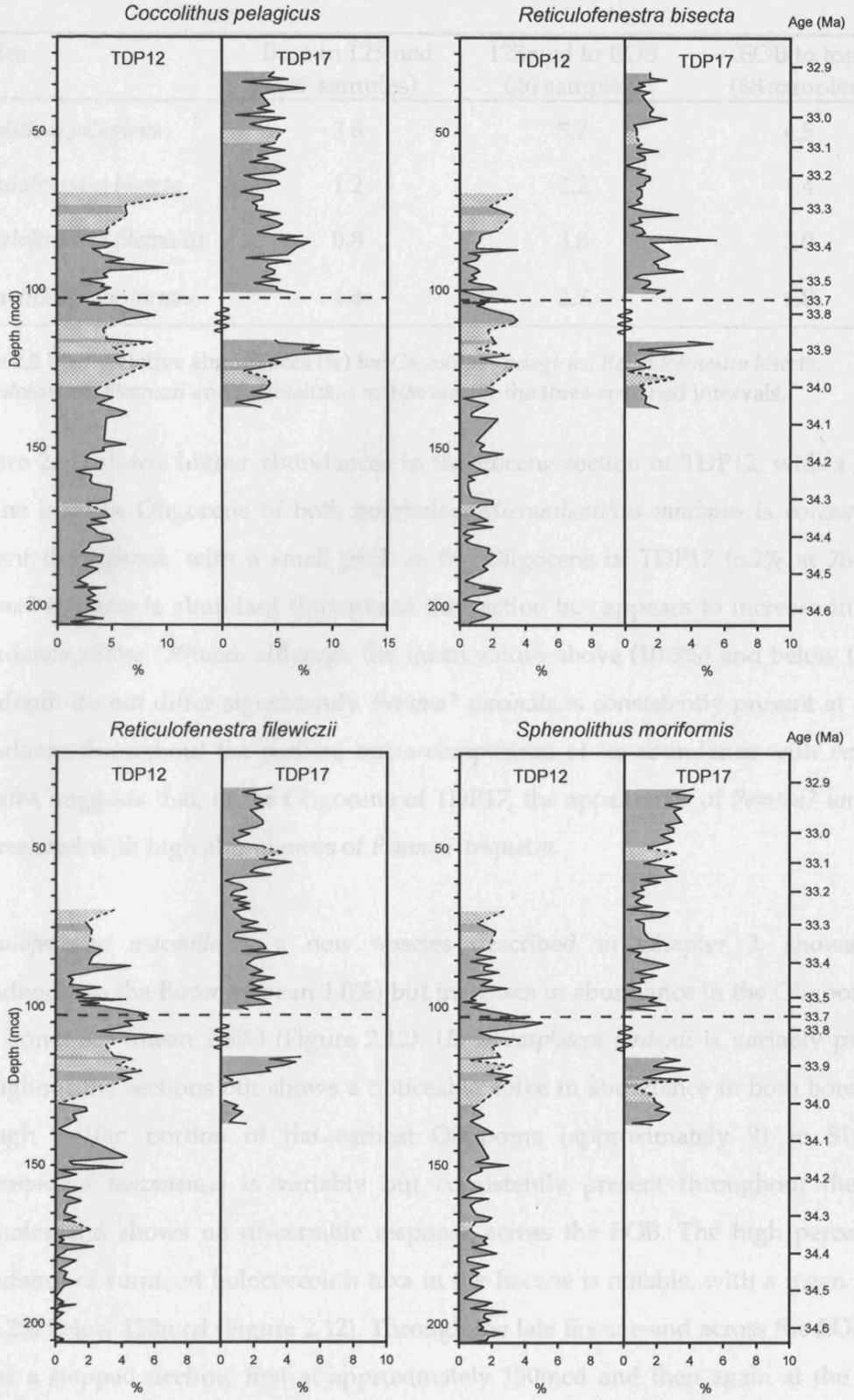

Figure 2.10 Species relative abundances against depth (mcd) - *Coccolithus pelagicus*, *Reticulofenestra bisecta*, *Reticulofenestra filewiczii* and *Sphenolithus moriformis*. Ages from Pearson *et al.* (in press) based on the time scale of Cande & Kent (1995). Stippled areas indicate low abundance intervals where count data was not obtainable.

Species	Base to 125mcd (67 samples)	125mcd to EOB (26 samples)	EOB to top (88 samples)
Coccolithus pelagicus	3.6	5.7	4.5
Reticulofenestra bisecta	1.2	2.2	1.4
Reticulofenestra filewiczii	0.8	3.8	2.0
Sphenolithus moriformis	1.4	2.7	1.8

Table 2.2 Mean relative abundances (%) for *Coccolithus pelagicus, Reticulofenestra bisecta, Reticulofenestra filewiczii* and *Sphenolithus moriformis* for the three specified intervals.

(Figure 2.11) shows higher abundances in the Eocene section of TDP12, with a slight decline into the Oligocene of both boreholes. *Micrantholithus minimus* is consistently present throughout, with a small peak in the Oligocene of TDP17 (6.2% at 76mcd). *Pemma? triquetra* is abundant throughout the section but appears to increase in peak abundance above 139mcd, although the mean values above (10.3%) and below (9.6%) this depth do not differ significantly. *Pemma? uncinata* is consistently present at a low abundance throughout the section, but a comparison of its abundance with *Pemma? triquetra,* suggests that, in the Oligocene of TDP17, the appearance of *Pemma? uncinata* is correlated with high abundances of *Pemma? triquetra.*

Reticulofenestra macmillanii, a new species described in Chapter 3, shows low abundances in the Eocene (mean 1.0%) but increases in abundance in the Oligocene of both boreholes (mean 2.6%) (Figure 2.12). *Umbilicosphaera jordanii* is variably present throughout the sections but shows a noticeable spike in abundance in both boreholes through a 10m portion of the earliest Oligocene (approximately 91 to 81mcd). *Syracosphaera tanzanensis* is variably but consistently present throughout the two boreholes and shows no discernible response across the EOB. The high percentage abundance of summed holococcolith taxa in the Eocene is notable, with a mean value of 15.2% below 150mcd (Figure 2.12). Through the late Eocene and across the EOB this shows a stepped decline, first at approximately 150mcd and then again at the EOB, with mean values of 9.2% between 150mcd and the EOB, and 2.8% above the EOB.

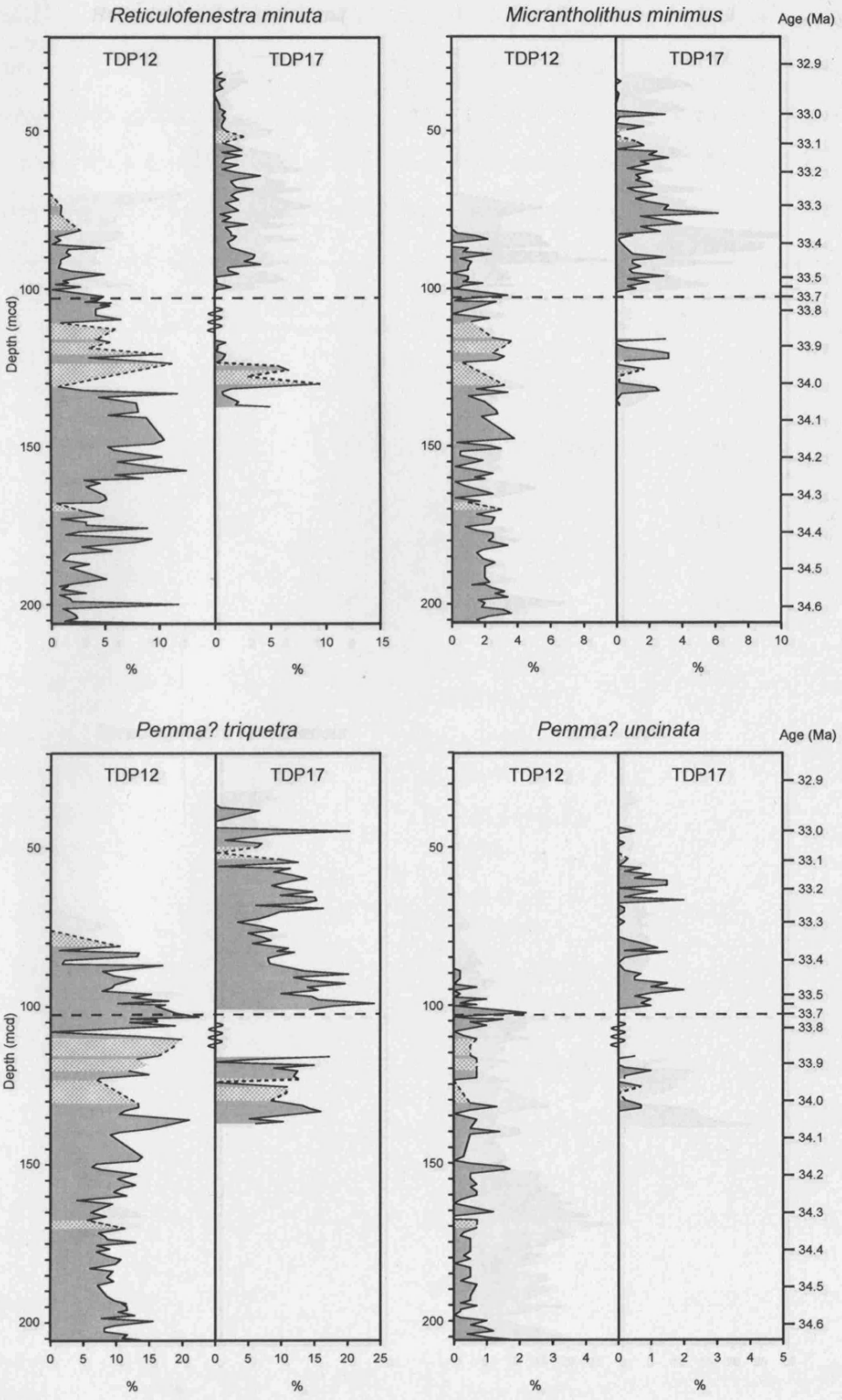

Figure 2.11 Species relative abundances against depth (mcd) - *Reticulofenestra minuta, Micrantholithus minimus, Pemma? triquetra* and *Pemma? uncinata*. Ages from Pearson *et al.* (in press) based on the time scale of Cande & Kent (1995). Stippled areas indicate low abundance intervals where count data was not obtainable.

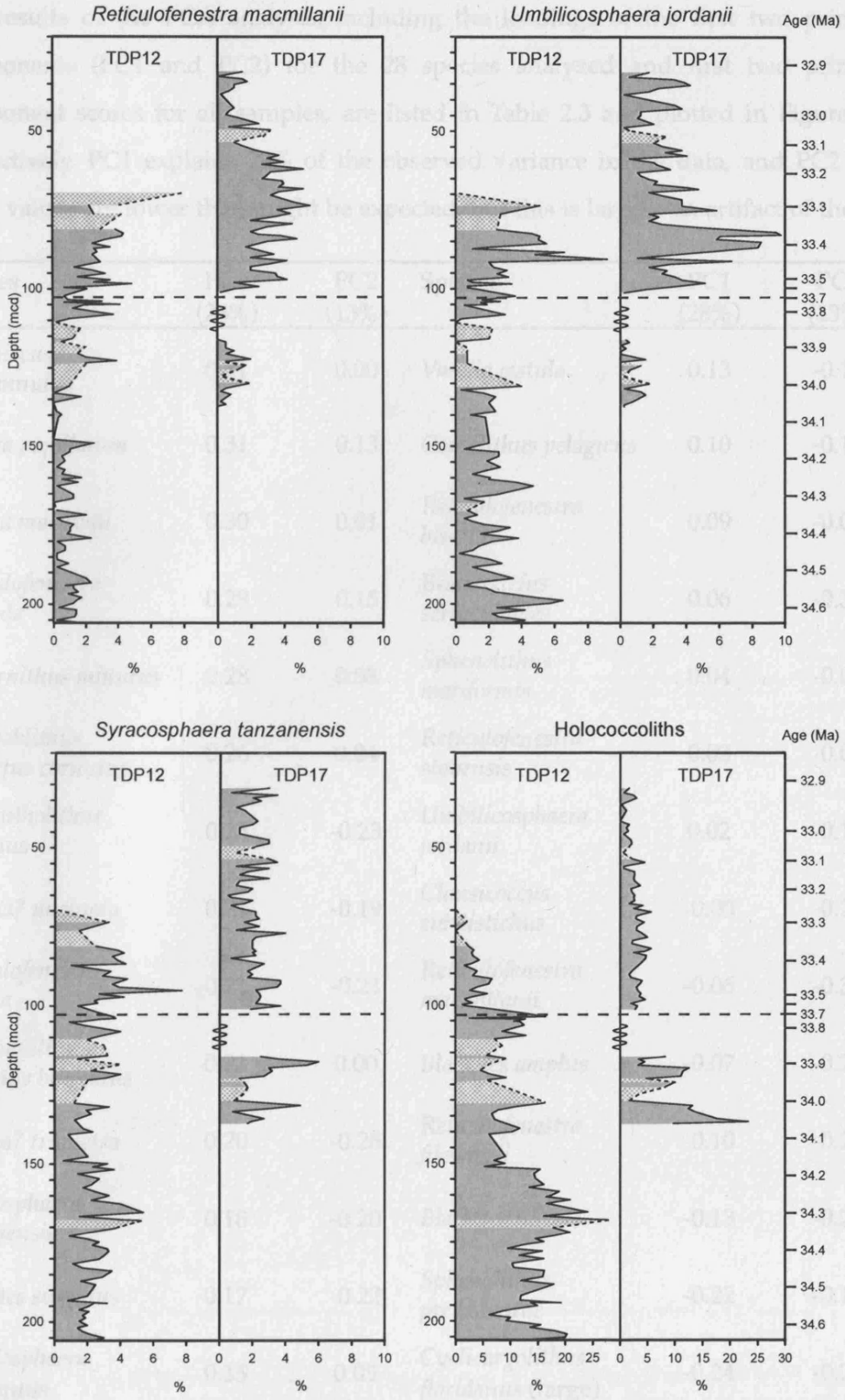

Figure 2.12 Species relative abundances against depth (mcd) - *Reticulofenestra macmillanii, Umbilicosphaera jordanii, Syracosphaera tanzanensis* and grouped holococcoliths. Ages from Pearson *et al.* (in press) based on the time scale of Cande & Kent (1995). Stippled areas indicate low abundance intervals where count data was not obtainable.

The results of the PCA analysis, including the loadings of the first two principal components (PC1 and PC2) for the 28 species analyzed and first two principal component scores for all samples, are listed in Table 2.3 and plotted in Figure 2.13 respectively. PC1 explains 28% of the observed variance in the data, and PC2 13%; these values are lower than might be expected, but this is largely an artifact of the log-

Species	PC1 (28%)	PC2 (13%)	Species	PC1 (28%)	PC2 (13%)
Calcidiscus protoannulus	0.31	0.00	*Varolia cistula*	0.13	-0.19
Pemma papillatum	0.31	0.13	*Coccolithus pelagicus*	0.10	-0.17
Varolia macleodii	0.30	0.01	*Reticulofenestra bisecta*	0.09	-0.04
Reticulofenestra dictyoda	0.29	0.15	*Bramletteius serraculoides*	0.06	-0.32
Lanternithus minutus	0.28	0.08	*Sphenolithus moriformis*	0.04	-0.01
Zygrhablithus bijugatus cornutus	0.26	0.04	*Reticulofenestra stavensis*	0.03	-0.07
Micrantholithus minimus	0.23	-0.23	*Umbilicosphaera jordanii*	0.02	-0.19
Pemma? uncinata	0.21	-0.19	*Clausicoccus subdistichus*	-0.03	-0.23
Reticulofenestra minuta	0.21	-0.21	*Reticulofenestra macmillanii*	-0.06	-0.33
Zygrhablithus bijugatus bijugatus	0.21	0.00	*Blackites amplus*	-0.07	-0.29
Pemma? triquetra	0.20	-0.26	*Reticulofenestra filewiczii*	-0.10	-0.21
Syracosphaera tanzanensis	0.18	-0.20	*Blackites furvus*	-0.13	-0.27
Blackites singulus	0.17	-0.22	*Sphenolithus predistentus*	-0.22	-0.19
Rhabdosphaera gracilentus	0.15	0.05	*Cyclicargolithus floridanus* (large)	-0.24	-0.24

Table 2.3 Principal component loadings for the first two principal components (PC1 & PC2) on the 28 species used as variables in the analysis. The percent of total variance explained by each principal component is shown in the header row. Listed in order of decreasing PC1 values.

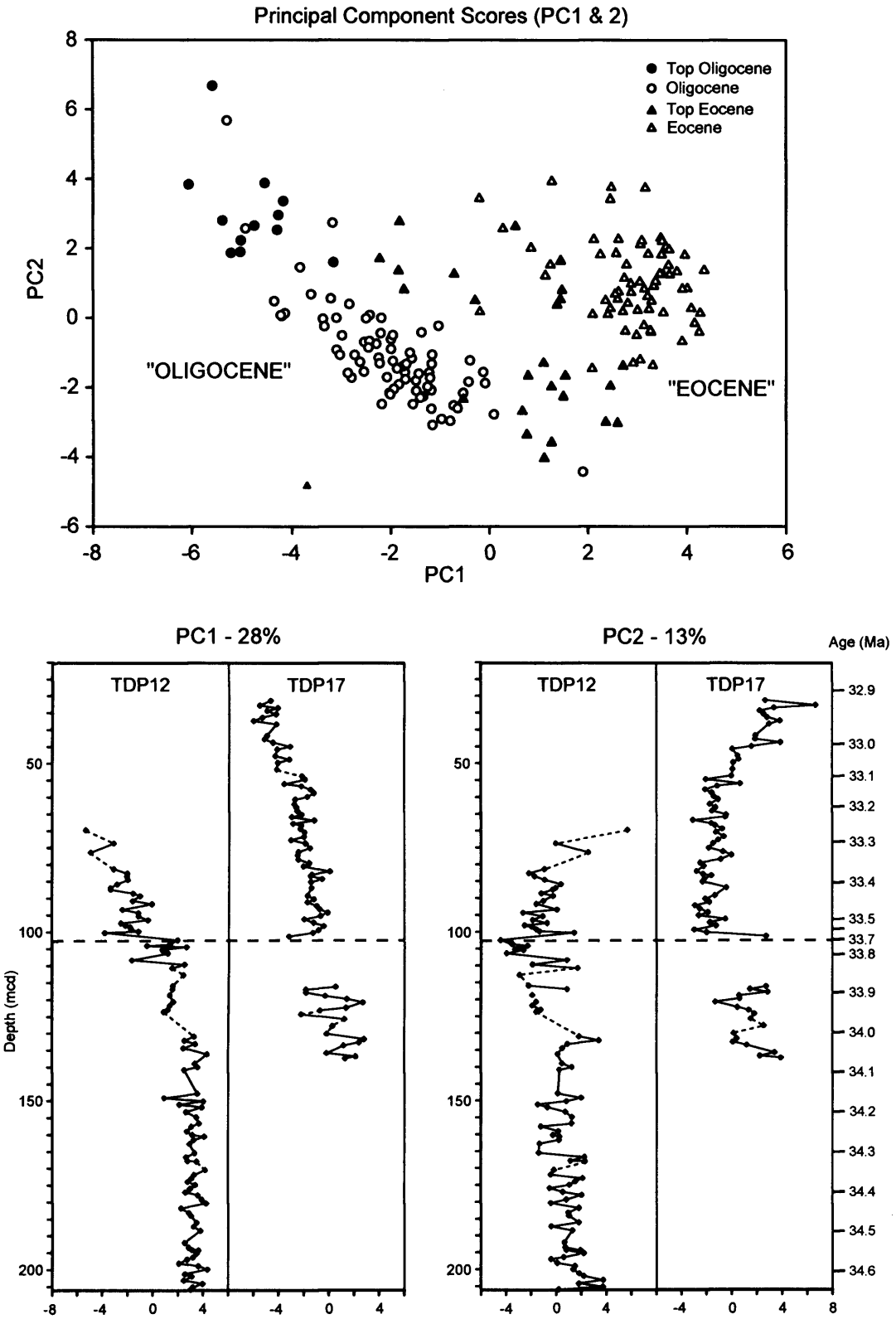

Figure 2.13 Principal component scores for the first two principal components; plotted against each other for all samples (top) and plotted against sample depth in TDP12 and 17 (mcd). In the upper figure, "Eocene" samples are from below 125mcd, "Top Eocene" are between 125mcd and the EOB, "Oligocene" are from the EOB to 44.75mcd and "Top Oligocene" are from above 44.75mcd. Ages from Pearson *et al.* (in press) based on the time scale of Cande & Kent (1995).

based ALR transformation, which increases the weighting of low-abundance taxa when the strongest 'signal' is present in the variations of the dominant taxa. The PCA loadings can be used to discriminate groups of species that have similar loadings in both principal components. For example *Calcidiscus protoannulus, Pemma papillatum, Varolia macleodii, Reticulofenestra dictyoda, Lanternithus minutus, Zygrhablithus bijugatus cornutus* and *Zygrhablithus bijugatus bijugatus* (termed Group 1) have the largest positive loadings on PC1 and non-negative loadings on PC2. The two species with the largest negative loadings on PC1 are *Cyclicargolithus floridanus* (large) and *Sphenolithus predistentus* (termed Group 2), which also have negative loadings on PC2. The remaining species are spread between these two end-members and have been divided into two further groups; Group 3a consists of the taxa, discussed above, that show an increase in abundance between 125mcd and the EOB (*Coccolithus pelagicus, Reticulofenestra bisecta, Reticulofenestra filewiczii, Sphenolithus moriformis*) (Figure 2.10) and the less abundant *Reticulofenestra stavensis*, which all have intermediate loadings on PC1 and low-negative loadings on PC2. Group 3b are a distinct group, including the two uncertain taxa *Pemma? triquetra* and *Pemma? uncinata*, with high positive loadings on PC1 and high negative loadings on PC2.

Plots of the principal component scores for PC1 and PC2 against depth in TDP12 and TDP17 are shown in Figure 2.13. PC1 is stable through the lower, Eocene, section of TDP12 (mean value 3.2), but then shows stepped reduction, first at 125mcd and then at the EOB, with mean values between 125m and the EOB of 1.1 and in the Oligocene of -2.1. TDP17 shows an almost continuous decline in PC1 through the uppermost Eocene and into the Oligocene (mean value Eocene 0.6, Oligocene –2.5). At 125mcd in TDP12, scores of PC2 show a similar step-change to lower values as PC1 (mean below 125mcd is 0.9, above is –1.8), however these shift back to slightly higher values in the Oligocene (mean –0.7). In TDP17, values of PC2 immediately above the EOB are lower than in the Eocene portion of the record (mean for Eocene is 1.4, mean EOB to 54.55mcd is –1.4), however the section immediately preceding the boundary is not present at this location. Values are then roughly stable until 54.55mcd, where they trend towards positive values, similar to those of the late Eocene (mean above 54.55mcd is 1.9).

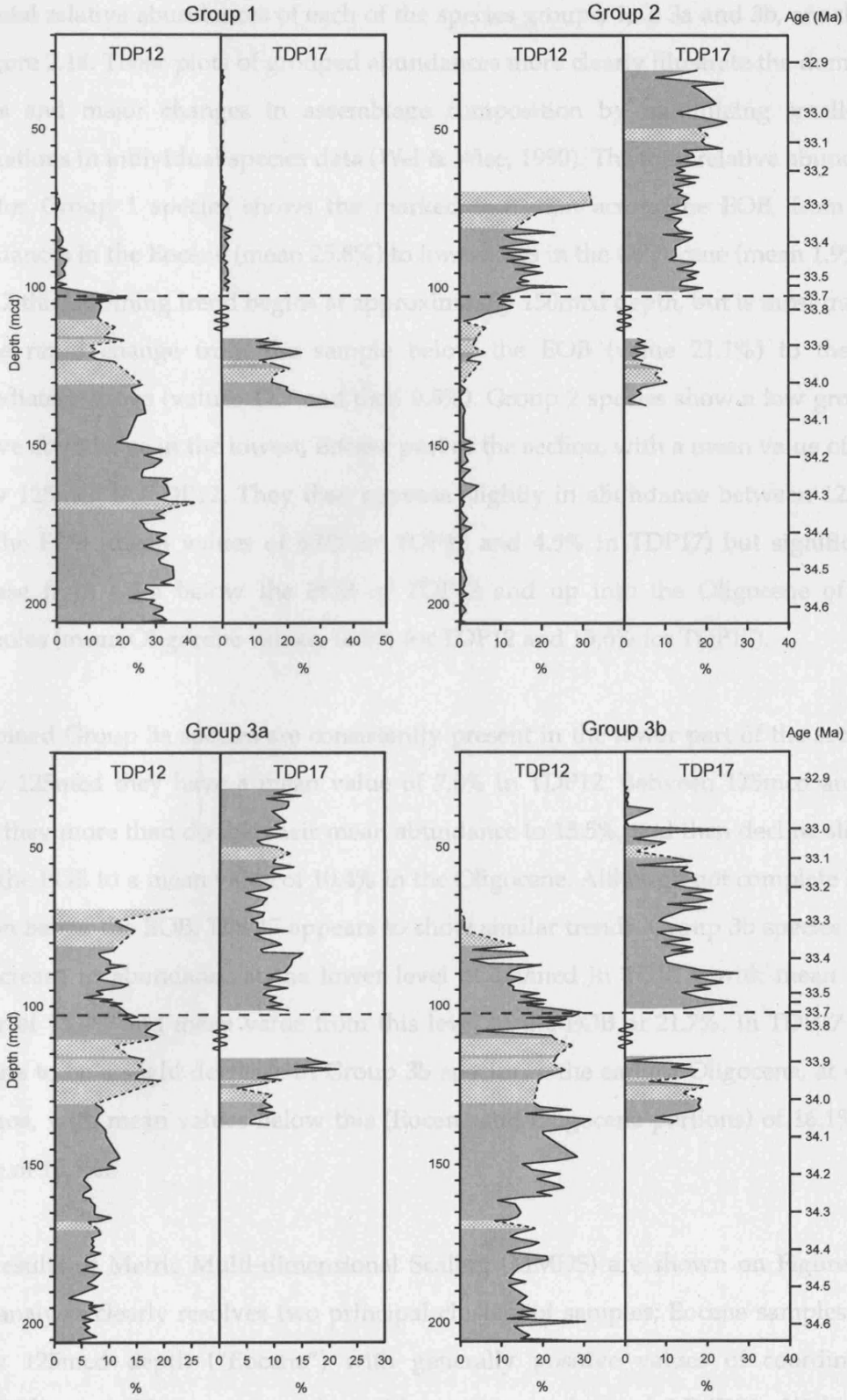

Figure 2.14 Percent relative abundances for Group 1, 2, 3a and 3b species against depth (mcd). Ages from Pearson *et al.* (in press) based on the time scale of Cande & Kent (1995). Stippled areas indicate low abundance intervals where count data was not obtainable.

The total relative abundances of each of the species groups, 1, 2, 3a and 3b, are shown in Figure 2.14. These plots of grouped abundances more clearly illustrate the dominant trends and major changes in assemblage composition by minimizing small-scale fluctuations in individual species data (Wei & Wise, 1990). The total relative abundance plot for Group 1 species shows the marked transition across the EOB, from high abundances in the Eocene (mean 25.8%) to low values in the Oligocene (mean 1.9%). In TDP12 this declining trend begins at approximately 150mcd depth, but is most marked in the rapid change from the sample below the EOB (value 21.1%) to the two immediately above (values 12.7 and then 0.5%). Group 2 species show a low grouped relative abundance in the lowest, Eocene part of the section, with a mean value of 1.0% below 125mcd in TDP12. They then increase slightly in abundance between 125mcd and the EOB (mean values of 6.5% in TDP12 and 4.5% in TDP17) but significantly increase from 4.5m below the EOB of TDP12 and up into the Oligocene of both boreholes (mean Oligocene values, 16.8% for TDP12 and 15.6% for TDP17).

Combined Group 3a species are consistently present in the lower part of the section - below 125mcd they have a mean value of 7.0% in TDP12. Between 125mcd and the EOB, they more than double their mean abundance to 15.5%, and then decline slightly after the EOB to a mean value of 10.4% in the Oligocene. Although not complete in the section below the EOB, TDP17 appears to show similar trends. Group 3b species show an increase in abundance at the lower level of 160mcd in TDP12, with mean value below of 15.3% and mean value from this level to the EOB of 21.7%. In TDP17 there appears to be a slight decrease in Group 3b species in the earliest Oligocene, at depth 86.7mcd, with mean values below this (Eocene and Oligocene portions) of 16.1% and above of 10.5%.

The results of Metric Multi-dimensional Scaling (MMDS) are shown on Figure 2.15. This analysis clearly resolves two principal clusters of samples; Eocene samples from below 125mcd depth ("Eocene") with generally positive values of coordinate 1 (MMDS1), and Oligocene samples with negative values of MMDS1. Within the Oligocene group, a subset of "Top Oligocene" samples can be identified from above 44.75mcd in TDP17, which tend to plot with more positive values of coordinate 2

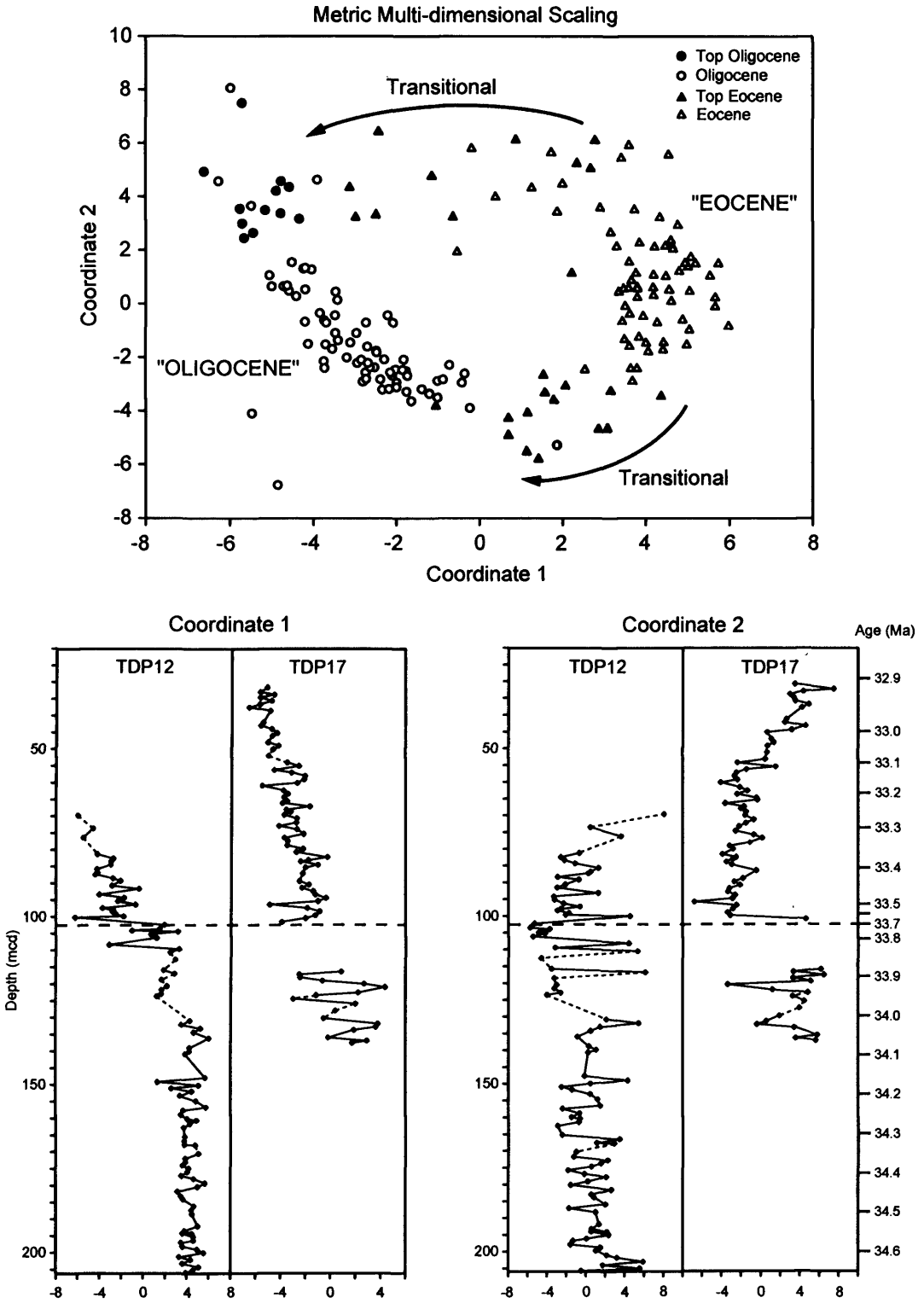

Figure 2.15 Results of the Metric Multi-dimensional Scaling analysis; coordinates 1 and 2 plotted against each other for all samples (top) and plotted against sample depth in TDP12 and 17 (mcd). In the upper figure, "Eocene" samples are from below 125mcd, "Top Eocene" are between 125mcd and the EOB, "Oligocene" are from the EOB to 44.75mcd and "Top Oligocene" are from above 44.75mcd. Ages from Pearson *et al.* (in press) based on the time scale of Cande & Kent (1995).

(MMDS2). Samples from between 125mcd and the EOB, labeled "Top Eocene", plot with MMDS1 values between the Eocene and Oligocene samples but show a broadly positive/negative bimodal pattern of MMDS2 values. This is largely but not entirely, correlated with samples from the different boreholes; 89% of TDP17 samples have positive values of MMDS2 and 82% of TDP12 samples have negative values.

2.4 Discussion

In order to integrate the results presented above, the following discussion consists of a brief summary of three key intervals that have coherent features and illustrate the temporal changes in surface water environment through the Eocene-Oligocene transition at this locality, followed by a discussion of the taxon-specific response to the EOT and finally the implications of these results for paleoceanographic and paleoclimatic changes through this interval. The three intervals discussed are the late Eocene from 205.8 to 125mcd; the topmost late Eocene from 125mcd to the EOB at 102.7mcd; and finally the EOB itself and the early Oligocene above 102.7mcd. Although the results and discussion presented here primarily use core depths, estimated age ranges will be given for each of the intervals discussed, based on the age model of Pearson *et al.* (in press) and discussed in section 2.2 above.

Late Eocene nannofossil assemblages; 205.8 to 125mcd (~34.65 to 33.95Ma)

The late Eocene interval, from the base of TDP Site 12 to 125mcd, is characterized by broad stability in the nannofossil records, with some subtle changes in the uppermost portion. The stability is apparent in the plots of Cretaceous reworking, H diversity (Figures 2.4 & 2.5) and PC1/MMDS1 (Figures 2.13 & 2.15), none of which show significant trends before 125mcd. In general, nannofossil abundance is high but variable, there is little or no reworking of Cretaceous nannofossils, cubic pyrite abundance is low and both H diversity and species richness are stable and relatively high (Figure 2.4 & 2.5). The nannofossil assemblages are dominated by Group 1 species (~30%), *Cyclicargolithus floridanus* (sml) (~25%) and to a lesser degree Group 3b species

(10-20%) (Figures 2.6, 2.7, & 2.12). The similarity of nannofossil assemblages within this interval is illustrated by the close clustering of these "Eocene" samples in the multivariate analyses (Figures 2.13 & 2.15). The only distinct "event" below 150mcd is the broad peak in *Zygrhablithus* abundance, between 180 and 150mcd (Figure 2.7), which may be a species-specific response to some subtle environmental or ecological change. The first perturbation of this stability is at 150mcd, when there is a marked drop in nannofossil abundances (Figure 2.4) and a stepped decline in the relative abundance of Group 1 species and holococcoliths, and an increase in Group 3a species (Figure 2.12 & 2.14). The assemblages stabilize once again, along with a recovery in nannofossil abundances, between ~140 and 125mcd.

Latest Eocene transition interval; 125 to 102.7mcd (~33.95 to EOB at 33.7Ma)

The base of this interval is marked by a distinct series of samples with very low nannofossil abundances (129.84 to 124.39mcd in TDP12; 128.90 to 123.14mcd in TDP17) (Figure 2.4). The first peaks in Cretaceous reworking begin towards the top of these low abundance intervals (Figure 2.4) and they are followed by a marked reduction in Group 1 species and an increase in Group 3a species (Figure 2.14). The last occurrence of *Discoaster saipanensis* occurs just below this low abundance interval at 130.32mcd. A number of thinner low abundance levels, together with continued spikes in Cretaceous reworking and the first significant peaks in cubic pyrite abundance are present above the initial low abundance-barren interval (Figure 2.4).

Between 111.26mcd and the EOB (102.70mcd) there are further pronounced shifts in the nannofossil assemblages coincident with a recovery in nannofossil abundance; these include the first significant occurrences of the large form of *Cyclicargolithus floridanus* and a distinct peak in the abundance of *Lanternithus minutus*. This interval contains the last occurrences of *Pemma papillatum*, at 110.48mcd, and the *Turborotalia cerroazulensis* group of planktonic foraminifera, at 107.40mcd. The changes in nannofossil assemblage are reflected by the start of a negative shift in PC1/MMDS1 and a negative step-change in PC2/MMDS2 at 125mcd followed by a rapid negative shift in PC1/MMDS1 at 108.14mcd (Figures 2.13 & 2.15). The plots of PC1/MMDS1 versus PC2/MMDS2

clearly distinguishes the assemblages between 125mcd and the EOB ("Top Eocene") from the majority of the Eocene samples.

The Eocene-Oligocene Boundary Event (33.7Ma)

The changes in nannofossil assemblages across the EOB itself, as recorded in TDP12, consist of a short interval of transition (106.14 to 102.21mcd; LO of the Hantkeninidae is at 102.7mcd), which is then terminated by a rapid step change (102.21 to 100.04mcd). The short-transition period is immediately above the last occurrence of *Turborotalia cerroazulensis*, at 107.40mcd, which is estimated to be 65kyr before the EOB/LO of the Hantkeninidae (Berggren & Pearson, 2005). Above 106.14mcd there is a recovery of nannofossil abundances, an increase in abundance of *Cyclicargolithus floridanus* (large) (Figure 2.9) and an approximate doubling in the abundance of *Lanternithus minutus* (Figure 2.6). This exact interval (106.14 to 102.21mcd) also has the most negative PC2/MMDS2 scores (Figures 2.13 & 2.15). The step change at the end of this interval (between 102.21 to 100.04mcd in TDP12) is defined by a marked drop in Shannon diversity linked to the increasing dominance of a few species, the largest step change in both PC1/MMDS1 and PC2/MMDS2 (Figures 2.13 & 2.15) and a rapid decline in Group 1 species and increase in Group 2 species (Figure 2.14). This is the most marked shift in nannofossil assemblages throughout the entire section and occurs within the 2.3m (~30kyr) interval above the LO of the Hantkeninidae. The events associated with the EOB appear to occur within a period of relatively stable $\partial^{18}O$ values just prior to the second step in $\partial^{18}O$ into the EOGM (Figure 2.4). The $\partial^{13}C$ isotopes show a slight, negative-tending reversal in their overall positive shift, immediately following the EOB (Figure 2.4), which is similar to the two-step pattern of decreasing $\partial^{13}C$ observed in other locations (Zachos & Kump 2005).

The taxon-specific response to the EOT

From the above summary it is clear that there is a large overturn in the taxonomic composition of nannofossil assemblages though the EOT in the Tanzanian successions, with the almost complete loss of Group 1 species, which form ~30% of the late Eocene

assemblage, and an increase in abundance of Group 2 species from very low levels to form ~20% of the total assemblage in the early Oligocene. This is a very strong biotic response, to what must be a major perturbation to the surface water environment at this location. Whilst trying to avoid circular arguments, a consideration of the both the taxa that respond during this transition and the independent geochemical proxy data through the same interval can increase our confidence in both the nature of the surface water environmental changes occurring at this time and the ecological preferences of the taxa involved.

The Group 1 taxa, which show a strong trend of declining abundance through the EOT, are dominated by the holococcolith species *Varolia macleodii, Lanternithus minutus, Zygrhablithus bijugatus bijugatus* and *Zygrhablithus bijugatus cornutus.* This decline in holococcolith abundance through the EOT is clearly shown in the grouped relative abundance of all holococcolith taxa (Figure 2.12). Holococcolith production during the haploid phase of the coccolithophore life-cycle, and heterococcoliths during the diploid phase, has only recently been established (Billard 1994; Young *et al.* 1999) and understanding the environmental trigger and adaptive function of the holococcolith-heterococcolith (haploid-diploid) transition in the coccolithophores is at an early stage (Cros *et al.* 2000 ; Noël *et al.* 2004). Plankton sampling of the modern oceans has established an association between holococcolith abundance, water-depth - with greater holococcolith abundances in near surface waters - and generally oligotrophic conditions (Kleijne 1991; Cros *et al.* 2000). For example, in the hetero-holococcolith association of *Helicosphaera carteri* (heterococcolith diploid stage) and *Syracolithus cartilliferus* (holococcolith haploid stage) in the Western Mediterranean there is a characteristic pattern of higher abundances of the holococcolith *S. cartilliferus* in the near surface, while the heterococcolith *H. carteri* reaches peak abundances at depths of 40-70m (Cros *et al.* 2000). This depth partitioning may be related to differences in the optical adsorption properties of hetero- and holococcoliths, as suggested by recent modeling which showed that the layered crystallites of many holococcolith taxa efficiently backscatter harmful ultra-violet radiation away from the cell whilst allowing the transmission of wavelengths within the photosynthetically active band of 400 to 700nm (Quintero-Torres *et al.* 2006). Culture studies have managed to induce the

haploid to diploid transition in one coccolithophore species, the holococcolith-bearing *Calyptrosphaera sphaeroidea,* via environmental stress including an increase in nutrient concentrations, although this may be a species specific response in which the heterococcolith-phase is adapted to the temporary colonization of coastal environments (Noël *et al.* 2004).

In spite of the environmental sensitivity of holococcoliths their use in paleoceanographic reconstructions has been minimal due to their generally low preservation potential (Ziveri *et al.* 2000; Young *et al.* 2005). One attempt to do this used well-preserved nannofossil assemblages from Holocene and late Pleistocene sediments of the Mediterranean that have species compositions, and hopefully an ecology, directly comparable to modern assemblages (Crudeli *et al.* 2006). The exceptional preservation of the Tanzanian sections through the EOT provides a unique deep-time record of the response of the holococcolith-bearing phase to a major environmental perturbation. In the light of the above discussion, the strong decline in the relative abundance of holococcoliths through the EOT in the Tanzanian sections appears to indicate a shift away from oligotrophic surface water conditions. This assumes that there is no systematic worsening of the preservational state of this material through the EOT, which would strongly affect the record of holococcoliths, but this is unlikely as very fragile holococcolith taxa, such as *Orthozygus,* are still preserved in the basal Oligocene, whereas the species lost are more robust forms such as *Lanternithus* and *Zygrhablithus.*

The decline in the abundance of discoasters - a taxon associated with warm, oligotrophic waters (Chepstow-Lusty *et al.* 1989, 1992; Chapman & Chepstow-Lusty 1997; Gibbs *et al.* 2004), in parallel with the fall in Group 1 species and holococcolith abundance, is consistent with increasingly eutrophic conditions through the EOT at this site. The other Group 1 species, *Calcidiscus protoannulus* and *Reticulofenestra dictyoda* also show pronounced declines through the EOT. In the case of *Calcidiscus protoannulus* this decline precedes its last occurrence in the earliest Oligocene (Bybell 1982; Bralower & Mutterlose 1995). As noted in the introduction, it is difficult to unravel the often co-varying parameters of temperature and nutrient levels, especially through an interval

with potentially strong cooling and productivity signals, and the declines in all these taxa may be related to cooling and/or increasing nutrient levels. However, most of these taxa tend to show a marked decline before the EOB itself, with a stronger response to the first step in $\partial^{18}O$ from ~125m upwards, which new trace element data from the Tanzanian sites suggests is mostly due to surface water cooling (Lear *et al.* submitted).

The dominance of *C. floridanus* and sphenoliths in the early Oligocene of Tanzania, with combined abundances of ~60% or more, has also been observed in Oligocene assemblages of the equatorial Pacific Ocean, which are dominated by *C. floridanus* and show increased sphenolith abundance during high productivity intervals (Wade & Pälike 2004). The paleoecology of sphenoliths is problematic. They appear to have a clear warm-water affinity, based on, for example, Eocene and Oligocene biogeographic gradients in both the Atlantic and Indian Oceans that record greatest sphenolith abundances in equatorial locations (Wei & Wise 1990; Wei *et al.* 1992). In addition, the cyclic co-variance of sphenoliths with discoaster species and *Florisphaera profunda* in mid-Pliocene sediments strongly indicates that they are part of a warm-water, oligotrophic assemblage (Gibbs *et al.* 2004). In contrast, sphenoliths have been shown to occur as almost monospecific assemblages in diatom-rich, high-productivity sediments of the Messinian (Wade & Bown 2006), more in line with their association with high-productivity intervals during the Oligocene in the equatorial Pacific (Wade & Pälike 2004). This difference may be related to species-specific tolerances and adaptations or may indicate that sphenoliths in general are capable of more opportunistic adaptations, taking advantage of disturbed environmental conditions, as seen through the EOT in Tanzania. This ecological opportunism may partly explain the broad trend in low-latitude assemblages from discoaster-dominated floras of the Eocene to sphenolith-dominated floras of the Oligocene, coupled to the general increase in ocean overturning and productivity (Salamy & Zachos 1999).

As with the sphenoliths, the ecological affinities of *Cyclicargolithus* are uncertain; it was included as a temperate-water taxa in the biogeographic study of Wei & Wise (1990) but was assigned no temperature affinity in the work of Persico & Villa (2004). In terms

of nutrients it has been associated with high-nutrient events in the late Eocene (Monechi *et al.* 2000) and is considered to be a bloom-forming taxon capable of exploiting eutrophic conditions by Aubry (1992). The abundance of *Cyclicargolithus floridanus* in the low-latitude Tanzanian sections and its very low abundances in contemporary high-latitude sections (Persico & Villa 2004), would strongly indicate that this is a tropical, warm-water taxon. The strong trend of increasing *Cyclicargolithus* abundance directly associated with the EOB, however, indicates that it is taking advantage of environmental changes in the surface ocean at this time; most likely an increase in nutrient levels as there is no significant cooling at this level recorded by $\partial^{18}O$ or trace metal data (Lear *et al.* submitted), which supports the inference that this is a bloom-forming taxon that thrives in higher nutrient conditions.

The Tanzanian sections are also notable for the absence or very low abundance of relatively common late Eocene taxa, such as *Chiasmolithus* spp., *Isthmolithus recurvus* and the grill-bearing reticulofenestrids of the *Reticulofenestra daviesii* / *Reticulofenestra lockerii* group. This confirms the findings of previous late Eocene biogeographic studies, that found *Chiasmolithus* spp. abundantly at high-latitudes in the Indian Ocean but rarely in equatorial regions (Wei *et al.* 1992) and that the *Reticulofenestra daviesii* group was generally absent from low-latitude sites in the Atlantic but abundant in the high-latitudes of both the Atlantic and Indian Oceans (Wei & Wise 1990; Wei *et al.* 1992) as well as having a cool-water preference during the late Eocene and early Oligocene in the Southern Ocean (Persico & Villa 2004). *Isthmolithus recurvus* has been shown to commonly occur in deep-sea sites north and south of 30° but then decline in abundance towards equator (Bukry 1978) and be abundant but restricted to high-latitudes of the Indian Ocean (Wei *et al.* 1992). Recent studies of Southern Ocean sites, however, show reduced abundances of *I. recurvus* during the coolest intervals of the late Eocene-early Oligocene, which may suggest a more temperate water association (Persico & Villa 2004). Peak abundances in *Isthmolithus recurvus* in the Gubbio section (Monechi 1986) and South Atlantic Site 522 (Backman 1987) are directly coincident with the EOB and may indicate a significant cooling of mid-latitude surface waters at this time.

The low-latitude surface water environment through the EOT

The general stability that characterizes the lower, late Eocene interval of these successions is first interrupted by a brief negative excursion in $\partial^{13}C$ coincident with an extended interval of samples with very low nannofossil abundances and etched planktonic foraminifera (Paul Pearson, Bridget Wade pers. comm.). This same negative $\partial^{13}C$ excursion together with poor carbonate preservation is also observed in many of the more complete deep-sea records (Zachos *et al.* 1996; Coxall *et al.* 2005), The maximum estimated paleodepths of these Tanzanian sites (300-500m) (Nicholas *et al.* 2006) places them significantly above the CCD, however the preservation state of both nannofossil and planktonic foraminifera indicate a transient period of significant supra-lysoclinal carbonate dissolution (Milliman *et al.* 1999). The meaning of the apparent correlation of this interval to globally negative $\partial^{13}C$ values and horizons of zero carbonate accumulation in the deep-sea (Coxall *et al.* 2005) is intriguing but at present difficult to assess. What is clear is that this interval in the Tanzanian cores is immediately followed by the first positive shift in $\partial^{18}O$, the first significant reworking of Cretaceous nannofossils into these sediments and the first major change in nannofossil assemblages. New trace metal data, which will be illustrated and further discussed in Chapter 6, indicate that this first step in $\partial^{18}O$ is largely related to cooling of ~2-3°C, in this case of tropical surface waters. This is consistent with the almost coincident shifts in nannofossil assemblages, most clearly shown by MMDS1, and $\partial^{18}O$ through the early stages of the EOT, as phytoplankton assemblages should be sensitive to a major fall in surface water temperature. Although this first step in $\partial^{18}O$ may be dominated by cooling, the independent record of reworked Cretaceous nannofossils, interpreted as driven by falls in local base level and enhanced erosion, indicates an ice-volume component to the $\partial^{18}O$ signal from the earliest stages of the EOT.

The environmental perturbations associated with the first step in $\partial^{18}O$ appear to correlate with the series of extinctions observed in the calcareous plankton in the period immediately preceding the EOB, from the LO of the calcareous nannofossils

Discoaster saipanensis and *Pemma papillatum*, to the LO of the *Turborotalia cerroazulensis* group of planktonic foraminifera and finally the extinction of the Hantkeninidae at the EOB. This transition period, from ~125m to the EOB, as identified in the analysis of nannofossil assemblages outlined above, is marked by a distinct assemblage composition that is established early on in the first step in $\partial^{18}O$, which in turn correlates to the main cooling signal in Mg/Ca data from planktonic foraminifera. The distinct nature of the nannofossil assemblages through this interval is shown, for example, by the increase in Group 3a species abundances (Figure 2.14) and the plot of MMDS first and second coordinate values (Figure 2.15). This interval is then terminated by the rapid assemblage changes directly associated with the EOB itself. The drop in nannofossil H diversity across the EOB, the shift to assemblages dominated by *Cyclicargolithus floridanus* and *Sphenolithus predistentus* and major step change in PC1/MMDS1 all indicate a major perturbation in the surface ocean environment well beyond the idea of a limited extinction confined to the planktonic foraminifera (Van Mourik & Brinkhuis 2005). It is perhaps surprising that this major biotic event is not coincident with any significant shift in either stable isotope or trace metal records available to date (Pearson *et al.* 2008; Lear *et al.* submitted). The nannofossil data from the Tanzanian sections, including the reduced diversity of assemblages and the nature of the taxonomic shifts, suggest that this transition is associated with a shift to more eutrophic conditions. The timing and nature of the observed step change in nannofossils assemblages at the EOB is remarkably similar to the rapid decline in H diversity and increase in cosmopolitan species observed in the radiolarian record from the equatorial Pacific Ocean, which also occurs immediately prior to second step in Oi-1 (Funakawa *et al.* 2006). This further illustrates the widespread impact of the EOB both geographically and across the major plankton groups.

After the EOB there is surprisingly little change in the nannofossil assemblages through the second step in $\partial^{18}O$ and the peak glacial conditions of the EOGM. In this case the new trace metal data from the Tanzanian sections indicate that this second step is dominated by an increase in continental ice-volume, with relatively little or no surface water cooling at this location (Lear *et al.* submitted). Again this is supported by

the limited response of the nannofossil assemblages to this shift in $\partial^{18}O$, indicating that there is little further change in the tropical surface water environment at this level. The record of reworked Cretaceous nannofossils, however, clearly peaks in the earliest Oligocene of TDP Site 17, directly coincident with the second step in $\partial^{18}O$ between 100 and 90mbgl (Figure 2.4). This validates both the connection between the reworking signal and sea level fall/ice-volume increases and the results of the trace metal data that indicate the onset of major glaciation at this level.

The apparent slight reduction in nannofossil abundances in the earliest Oligocene, although not corrected for changes in sedimentation rate, suggests that there is no major increase in the productivity of the calcareous phytoplankton in the earliest Oligocene. This is consistent with the hypothesis that increased global productivity in the earliest Oligocene is dominated by biosiliceous production (Nilsen *et al.* 2003), most significantly in the Southern Ocean (Salamy & Zachos 1999). The increase in biosiliceous productivity in the early Oligocene would have had a major impact on the rain ratio of organic carbon:carbonate carbon and if this resulted in increased organic carbon burial in marine sediments, would have been capable of driving a significant drawdown of atmospheric CO_2 and is thought to be the main cause of the positive shift in $\partial^{13}C$ through the EOT (Salamy & Zachos 1999; Zachos & Kump 2005). The records presented here indicate that this switch from calcareous to biosiliceous primary productivity was not due to direct competition between the coccolithophores and the diatoms but is linked to a shift in the general oceanic environment from oligotrophic to more eutrophic conditions, which favoured diatom productivity, especially in the Southern Ocean (Bown 2005a). This fundamental switch in primary productivity, from calcareous to siliceous organisms, which occurred through the EOT and into the earliest Oligocene, may be one of the key feedback mechanisms that maintained atmospheric CO_2 at significantly reduced levels and locked the early Oligocene climate system into its predominantly glacial-mode (Zachos & Kump 2005).

The Tanzanian calcareous nannofossil assemblages, with correlations to the other study sites, will form the basis of further discussion in Chapter 6, including the presentation of the new trace element geochemical data from TDP Sites 12 & 17 (Lear *et al.*

submitted), which combined with the nannofossil and stable isotope data presented here, provides the most detailed record to date of the nature and timing of climatic and biotic events through the EOT.

3. TAXONOMY OF UPPER EOCENE TO LOWER OLIGOCENE CALCAREOUS NANNOFOSSILS, PANDE FORMATION, TANZANIA

3.1. Introduction

The purpose of this chapter is to document the exceptionally diverse and well-preserved calcareous nannofossils from three TDP boreholes - Sites 11, 12 and 17 - which recovered similar successions of upper Eocene to lower Oligocene sediments. The detailed taxonomic data presented here is designed to compliment the set of high-resolution nannofossil assemblage data collected from two of these boreholes (TDP Sites 12 & 17), which is presented in Chapter 2. Together these chapters provide an unprecedented view of both the taxonomic diversity and ecological responses of low latitude calcareous phytoplankton to global climate change through the Eocene-Oligocene boundary. The detailed description of this, the most diverse and well-preserved Paleogene - and possibly Cenozoic - calcareous nannofossil assemblage described to date, provides vital palaeontological data with which to test recent advances in coccolithophore molecular phylogeny and classification (Young & Bown 1997; Edvardsen *et al.* 2000; Young *et al.* 2003; Jordan *et al.* 2004; Sáez *et al.* 2004).

The distinct and truly exceptional nature of the Tanzania calcareous nannofossil assemblages becomes apparent when their species composition and overall diversity is compared to contemporaneous open-ocean sites. Data for three standard "moderately to well-preserved" upper Eocene nannofossil assemblages from recent Ocean Drilling Program sites in the Pacific (Shatsky Rise Site 1209; Bralower 2005), Atlantic (Iberia Abyssal Plain Hole 900A; Liu 1996) and Southern Ocean (Agulhas Ridge Hole 1090B; Marino & Flores 2002) are compared to the Tanzanian assemblage in Table 3.1. The most striking feature is the difference in overall species diversities, with values of 16, 47 and 44 for the open-ocean sites compared to the 117 species-equivalent morphotypes described from Tanzania. The additional diversity in the Tanzanian sections is dominated by holococcoliths (22 species in Tanzania; maximum of 5 species in open-ocean sites) and members of the Rhabdosphaeraceae (20 species in Tanzania; maximum

of 2 species in open-ocean sites); typically members of both these groups are fragile and highly susceptible to fragmentation and dissolution.

Taxonomic Group	Shatsky Rise (Site 1209)	Iberia Abyssal Plain (Hole 900A)	Agulhas Ridge (Hole 1090B)	Tanzania (TDP11, 12, 17)
Total Species	16	47	44	117
Rhabdosphaeraceae	1 (6%)	2 (4%)	1 (2%)	20 (17%)
Zygodiscales	0 (0%)	8 (17%)	3 (7%)	14 (12 %)
Holococcoliths	1 (6%)	5 (11%)	2 (5%)	22 (19%)
Braarudosphaeraceae	0 (0%)	2 (4%)	1 (2%)	8 (7%)

Table 3.1 Comparison of species diversity across taxonomic groups and between the Tanzanian sections and open-ocean sites. Number of species in each group with percentage contribution to total species diversity in brackets. Note that data for open-ocean sections are compiled across the majority of the upper Eocene whereas the Tanzanian sections only span the uppermost upper Eocene and so the observed differential in total species diversity is conservative. See text for references.

This apparent bias against the preservation of fragile taxa in the open-ocean sites may partially explain the "excess" species diversity in the Tanzanian sections, however when compared to similar contemporaneous low-latitude shelf-slope clay facies, with generally excellent preservation, such as the Yazoo Clay of Mississippi, USA (Dockery III *et al.* 1991) and the Tegalsari Marls of Java (Lunt & Sugiatno in press), the Tanzanian material still shows considerable additional species diversity (species diversities of 54 for the Yazoo Clay and 40 for the Tegalsari Marls) (pers. obs.). Again, this differential is largely due to the preservation of a diverse holococcolith and rhabdolith assemblage in Tanzania, as well as the presence of previously unknown Paleogene deep-photic zone coccolithophores.

In addition to the extraordinary diversity of the Tanzanian assemblages, the preservation of the very small (<3 μm) size class of hetero- and holococcoliths - which are almost never observed in the Holocene or Neogene sediment record (Young *et al.* 2005) - and original sub-micron structures in many taxa is further evidence for the exceptional nature of the Tanzanian assemblages.

The causes of exceptional calcareous microfossil preservation in the Tanzanian material remain perplexing; an impermeable clay facies, rapid burial and low organic carbon contents may all be prerequisites for excellent preservation but the quality of holococcolith preservation, which is poor even in modern sediment traps (Andruleit *et al.* 2004), suggests that, in the Tanzanian setting, nannoplankton remains were rapidly transported from the photic zone to the sediment surface, limiting dissolution and fragmentation within the water-column. An alternate or complementary control on the Tanzanian holococcolith record may be genuine enhanced holococcolith production in this particular paleoenvironment. The environmental controls on the diploid-haploid transition and holococcolith production in the modern ocean are still poorly understood (Cros *et al.* 2000) but the Kilwa Group of Tanzania offers a unique opportunity to study holococcolith productivity and diversity through much of the Paleogene.

Another striking feature of the Tanzanian assemblages is the Paleogene occurrence of a number of living taxa that have no or only a highly sporadic and limited fossil record. These include the first report of the living genus *Rhabdosphaera* from Paleogene sediments, the consistent presence of the Neogene to modern genus *Umbilicosphaera* (Bown *et al.* 2007) and, most impressively, the frequent occurrence of the modern deep-photic zone genera *Gladiolithus* and *Algirosphaera*, which both had fossil records limited to very rare occurrences within Quaternary sediments (Lars Legge *et al.* 2006; Okada & Matsuoka 1996). These new Paleogene occurrences of modern genera and species have three main implications: 1) they constrain the origin of these taxa to the Paleogene, providing supporting evidence for molecular phylogenies and their estimated divergence times (Sáez *et al.* 2004); 2) they imply long Neogene ghost ranges for these taxa, and the possibility that Neogene deposits with similar exceptional preservation may preserve some of this "missing" diversity; 3) they document the highly conservative nature of many coccolithophore morphologies over tens of millions of years, such as *Gladiolithus flabellatus*, indicating a strong stabilizing selection on these morphologies and a high degree of coccolith functionality – presumably in the case of *Gladiolithus* this represents a long-term and successful adaptation to the lower photic zone environment.

The detailed systematic descriptions, from order to species level, presented in this chapter are based on, and so test the robustness of, recent advances in coccolithophore systematics and higher taxonomy (Young & Bown 1997; Edvardsen *et al.* 2000; Young *et al.* 2003; Jordan *et al.* 2004; Sáez *et al.* 2004). The taxonomy of the coccolithophores is largely based upon the structure of the calcite scales, or coccoliths, produced by these single celled algae. This contrasts with the taxonomy of other extant unmineralized haptophyte algae, which is based upon cell cytology, biology and, increasingly, molecular genetics, with organic scale morphology never being used in classifications above species level (Sáez *et al.* 2004). However, the specific nature of calcite biomineralization - involving the controlled growth of an anisotropic crystalline medium - requires the operation of complex biochemical processes, which appear to be highly conservative and hence closely correspond with coccolithophore phylogeny (Sáez *et al.* 2004). Indeed the taxonomy of coccolithophores, which has largely been the work of palaeontologists, has generally been proved robust by subsequent cytological and molecular genetic studies on extant taxa (Sáez *et al.* 2004).

The classification of coccolithophores, based upon the complex structure of their coccoliths, depends upon the reliable recognition of homologous structural elements. It is now understood that there is an underlying deep homology in coccolith structure rooted in the fundamental biomineralization mechanism common to all calcifying haptophytes (Young *et al.* 1992, 2004). In all cases of heterococcolith formation observed to date, biomineralization begins with the nucleation of a ring of calcite crystals - the proto-coccolith ring - upon an organic base-plate scale within an intra-cellular vesicle. The proto-coccolith ring is formed of regularly spaced calcite crystals with alternating sub-vertical and sub-radial c-axis orientations (Young *et al.* 1992, 2004). These have been termed V- and R-units respectively, and their subsequent growth into complex coccolith structures forms the basis for coccolithophore taxonomy (Figure 3.1). One of the fundamental advances of this "V/R model" of coccolith formation is the identification of characters useful for higher taxonomy - those stemming from initial growth from the proto-coccolith ring, notably rim/shield structure and crystallography - and those formed late in the process of coccolith biomineralization, which exhibit a high degree of plasticity and are only useful for species level taxonomy, such as central

Figure 3.1 V/R model of coccolith growth (after Young *et al.* 2004). Growth pattern of *Coccolithus pelagicus* from proto-coccolith ring of alternating V- and R-units (left) and final coccolith structure (right).

area structures and process/spine morphologies. The characteristic shield structure and V/R crystallography of five extant (and Paleogene) families are shown in Figure 3.2 (after Young *et al.* 2004).

The V/R model has proved to be a powerful tool for coccolithophore taxonomy and systematics, forming the basis of recent revisions to the classification of Cenozoic nannoplankton (Young & Bown 1997). This, purely coccolith-structure based

Figure 3.2 Coccolith structure of five extant (and Paleogene) coccolithophore families - R-units are white, V-units dark gray, circles indicate the location of the proto-coccolith ring. The Syracosphaeraceae have additional T-units, which form the radial lath cycle, and have a tangential c-axis orientation (after Young *et al.* 2004).

classification, is now being gradually integrated with new phylogenetic data from the molecular genetic analysis of extant haptophyte algae (Edvardsen *et al.* 2000; Sáez *et al.* 2004). Where molecular genetic data is available it has become clear that the clades identified by coccolith-structure analysis are robust - Figure 3.3 presents a summary of extant haptophyte phylogeny based on molecular genetics integrated with coccolith-structure analysis (after Young *et al.* 2005; see also Jordan *et al.* 2004). The main discrepancy between these two approaches is in the assignment of the appropriate levels of higher classification and the relationships between families within the "holococcolithophore producing clade" identified on Figure 3.3. On the basis of molecular genetics, Sáez *et al.* (2004) recognize this entire group as an order level clade, the "Coccolithales", consisting of the well-supported sub-clade of the Coccolithaceae, Calcidiscaceae, Hymenomonadaceae and Pleurochrysidaceae, and a number of other groups with poorly resolved relationships. In this study, following Jordan *et al.* (2004) and Young *et al.* (2005), the order Coccolithales has a more restricted use denoting the sub-clade Coccolithaceae, Calcidiscaceae, Hymenomonadaceae and Pleurochrysidaceae, whilst the orders Zygodiscales and Syracosphaerales are retained based on the homologies of coccolith structure - this is not inconsistent with the available molecular genetic data. Recent analyses of single cell SSU rDNA had confirmed the placement of the enigmatic genus *Braarudosphaera* within the coccolithophore clade but its affinities within this group are still uncertain (Takano *et al.* 2006).

It is hoped that this study is a further step in the integration of paleontological/ coccolith-structure data with the molecular genetic approach to coccolithophore phylogeny and classification. The description of such well-preserved material will both aid, and hopefully encourage, future detailed taxonomic studies of Paleogene coccolithophores - in this thesis it provides the taxonomic framework for the subsequent description of nannofossil assemblages from DSDP Site 242 (Chapter 4) and St Stephens Quarry (Chapter 5).

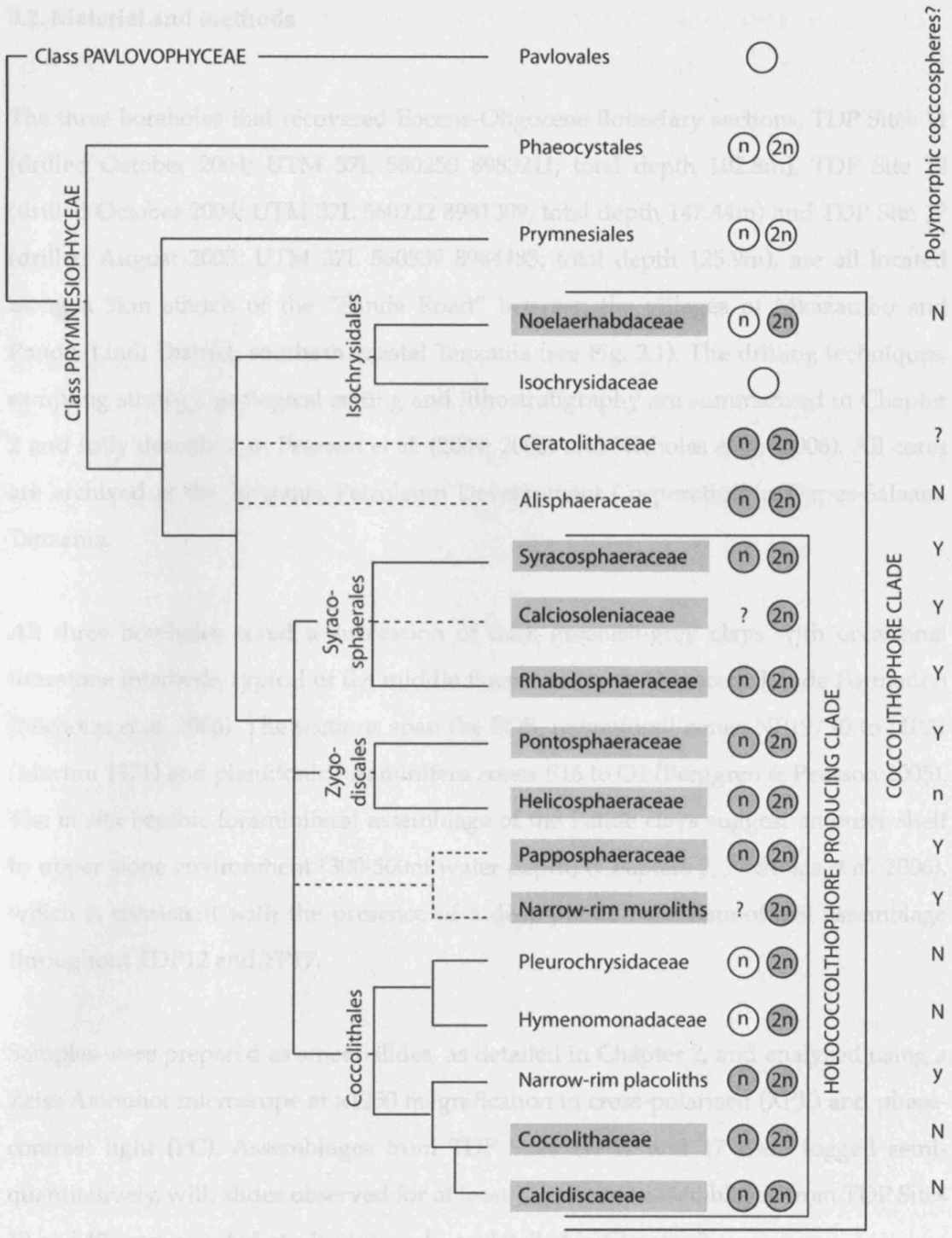

Figure 3.3 Consensus phylogeny of extant Haptophyte families based on molecular genetics - dotted lines indicate inferred relationships where genetic data is not available (after Young *et al.* 2005). Shaded circles indicate life-cycle phases that produce coccoliths (n - haploid phase, 2n - diploid phase; no shading indicates a life-cycle phase that does not produce coccoliths). Right hand column indicates the presence of polymorphic coccospheres (N - no polymorphism, n - variomorphism but no true polymorphism, y/Y - polymorphism rare/common in group). Families highlighted in grey are represented in the Eocene-Oligocene sediments described herein.

3.2. Material and methods

The three boreholes that recovered Eocene-Oligocene Boundary sections, TDP Sites 11 (drilled October 2004; UTM 37L 560250 8983211; total depth 102.8m), TDP Site 12 (drilled October 2004; UTM 37L 560222 8981309; total depth 147.44m) and TDP Site 17 (drilled August 2005; UTM 37L 560539 8984483; total depth 125.9m), are all located along a 3km stretch of the "Pande Road" between the villages of Mkazambo and Pande, Lindi District, southern coastal Tanzania (see Fig. 2.1). The drilling techniques, sampling strategy, geological setting and lithostratigraphy are summarized in Chapter 2 and fully described in Pearson *et al.* (2004; 2006) and Nicholas *et al.* (2006). All cores are archived at the Tanzania Petroleum Development Corporation in Dar-es-Salaam, Tanzania.

All three boreholes cored a succession of dark greenish-grey clays with occasional limestone interbeds, typical of the middle Eocene to lower Oligocene Pande Formation (Nicholas *et al.* 2006). The sections span the EOB, nannofossil zones NP19/20 to NP21 (Martini 1971) and planktonic foraminifera zones E16 to O1 (Berggren & Pearson 2005). The *in situ* benthic foraminiferal assemblage of the Pande clays suggest an outer shelf to upper slope environment (300-500m water depth) (Chapters 2; Nicholas *et al.* 2006), which is consistent with the presence of a deep-photic zone nannofossil assemblage throughout TDP12 and TP17.

Samples were prepared as smear-slides, as detailed in Chapter 2, and analyzed using a Zeiss Axiophot microscope at x1250 magnification in cross-polarised (XPL) and phase-contrast light (PC). Assemblages from TDP Sites 11, 12 and 17 were logged semi-quantitatively, with slides observed for at least 45 minutes; assemblages from TDP Sites 12 and 17 were counted at ~1m intervals, as detailed in Chapter 2.

Light microscope images were captured using Scion Image software and macros written by Dr. Jeremy Young (Bown & Young 1998). Scanning Electron Microscope (SEM) studies were conducted on broken rock-surfaces using a JEOL Digital JSM-6480LV SEM (Lees *et al.* 2004). All light microscope images were captured at the

same magnification with a two-micron scale bars shown on each plate (magnification ~x 2180); a 1μm scale bar is shown on all SEM images unless otherwise indicated. Consecutive light microscope images of the same specimen are only labeled once, beneath the first figure in the series.

3.3 Systematic descriptions

Descriptive terminology follows the guidelines of Young *et al.* (1997). All new taxonomic names are in latin with the meaning given in each case. The layout of the taxonomy and the higher taxonomic rationale follows recent classification schemes for extant coccolithophores (Young *et al.* 2003; Jordan *et al.* 2004) combined with the review of Cenozoic coccolithophore taxonomy by Young & Bown (1997). The term "diagnosis" is used for taxa above the species level to denote a summary diagnosis of current taxonomic understanding. This is based on both the original descriptions and later modifications or clarifications, and is not a verbatim statement of the original diagnosis or description of the taxon concerned. The term "diagnosis" is also used where new species level taxa are being defined.

Abundance and occurrence of species is noted using the terms 'very rare' (sporadic occurrences; ~1-2 per slide), 'rare' (<1 specimen per FOV), 'frequent' (1 per FOV), 'common' (1-10 per FOV) and 'abundant' (>10 per FOV). Size classes, based on long-axis length, are 'very small' (<3 μm), 'small' (3-5 μm), 'medium' (5-8 μm), 'large' (8-12 μm) and 'very large' (>12 μm) (Young *et al.* 1997). Morphometric data are given for all new taxa.

Range information is given for the stratigraphic distribution within the Tanzanian sites studied. All calcareous nannofossil zones refer to the NP biozones of Martini (1971). The abbreviations FO and LO are used to denote first occurrence, i.e., oldest/lowest occurrence in the sections, and last occurrence, i.e., youngest/highest occurrence in the sections, respectively. Additional abbreviations used in the descriptions are: Ds - distal shield, Pr - proximal shield, LM – light microscope, XPL cross-polarised light, PC –

phase-contrast illumination, L – length, H – height, W – width, D – diameter. Type material and images are stored in the Department of Earth Sciences, University College London.

3.3.1 Placolith coccoliths

Order **ISOCHRYSIDALES** Pascher 1910

DIAGNOSIS: Includes the extant placolith-forming Noelaerhabdaceae and the non-calcifying Isochrysidaceae as well as the extinct family Prinsiaceae. The grouping of the extant families Noelaerhabdaceae and Isochrysidaceae is based on flagellar characteristics (haptonema vestigial), the production of alkenones and molecular genetics (Edvardsen *et al.* 2000; Fujiwara *et al.* 2001; Sáez *et al.* 2004; Young *et al.* 2003). The inclusion of the Prinsiaceae is based on a shared coccolith structure with the Noelaerhabdaceae, namely a well developed R-unit that forms the proximal shield-element, two-tube elements with opposite senses of imbrication and usually a central-area element (Young & Bown 1997). Central-area structures are always conjunct and formed from either the central-area element or the inner tube-element of the proximal shield.

Family **NOELAERHABDACEAE** Jerkovic 1970 emend. Young & Bown 1997

DIAGNOSIS: Placolith-bearing forms with *Reticulofenestra*-type placolith structure; i.e. V-unit virtually absent with R-units forming the proximal and distal shields, the inner and outer tube-cycles, grill and any central-area structures (Figure 3.2). Strongly birefringent in XPL.

Genus ***CYCLICARGOLITHUS*** Bukry 1971

DIAGNOSIS: Sub-circular to circular *Reticulofenestra*-type placoliths with a narrow central opening. Often possess a higher tube cycle than typical *Reticulofenestra* coccoliths.

Cyclicargolithus floridanus (Roth & Hay in Hay *et al.* 1967) Bukry 1971 (Pl. 3.1, figs 1-3; Pl. 3.2, figs 1-3, 7)

DESCRIPTION: Small to large subcircular reticulofenestrid coccoliths with a high tube-cycle and in light-microscopy a narrow, apparently vacant, central-area. REMARKS: During SEM analysis a finely perforate net, or remnants of one, was consistently present within the central areas of all observed specimens (Pl. 3.2, figs 1-3, 7). These more distally protruding central area nets appear to be distinct from the nets observed within *Reticulofenestra* species, which appear to lay flat on the distal surface (Pl. 3.2, figs 5 & 9). The presence of central area nets does not conflict with the original description of the genus (Bukry 1971), which makes no specific mention of central area structures. SEM images of the distal shield clearly show a raised tube-cycle surrounding the central area (Pl. 3.2, figs 2-3, 7). Specimens were informally divided into small (<5μm) and large (>5μm) morphotypes. OCCURRENCE: The small morphotype is common throughout the section (NP19/20-21) but the first common occurrence of the large form, in this section, is immediately below the EOB and is then consistently present from this point upwards into the lower Oligocene (NP21). The large morphotype is, however, commonly observed in middle Eocene sediments from Tanzania (Bown 2005b).

Genus ***RETICULOFENESTRA*** Hay, Mohler & Wade 1966

DIAGNOSIS: Circular or elliptical *Reticulofenestra*-type placoliths lacking in distinctive features; central-area can be open, partially closed by extensions of the inner tube-elements or spanned by a net or plug.

Reticulofenestra bisecta (Hay *et al.* 1966) Roth 1970 (Pl. 3.1, fig. 4; Pl. 3.2, fig. 8; Pl. 3.4, fig. 7).

DESCRIPTION: Medium to large reticulofenestrid coccoliths with a central plug that are <10 μm (NB. the holotype is ~8 μm). REMARKS: Most specimens of the *R. bisecta* morphology are within the 8-10μm size range, although occasional specimens within the 10-11μm range were observed and classified as *R. stavensis* (below) following Bown (2005b). These larger forms, however, do not appear to represent a distinct taxonomic entity in these sections. OCCURRENCE: Frequent to common throughout the section.

Reticulofenestra stavensis (Levin & Joerger 1967) Varol 1989 (not figured)

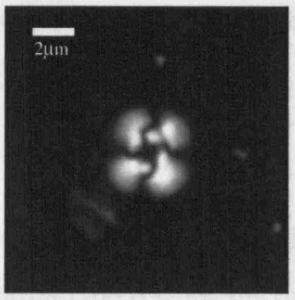

1. *Cy. floridanus* (<5 µm) TDP17/5-1

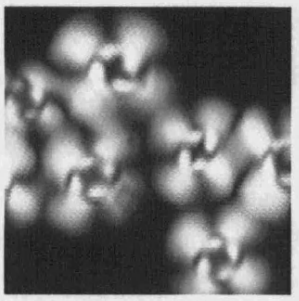

2. *Cyclcarg. floridanus* TDP17/15-1

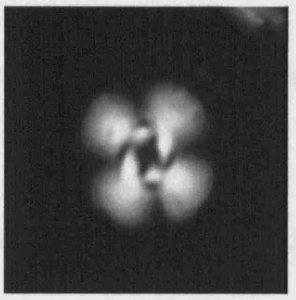

3. *Cyclicarg. floridanus* TDP17/5-1

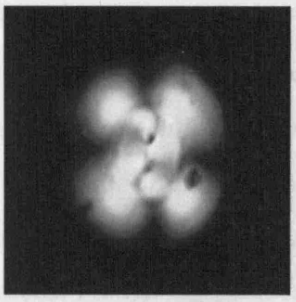

4. *Reticulofen. bisecta* TDP12/10-1

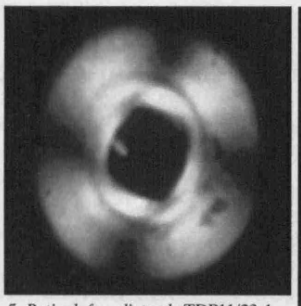

5. *Reticulofen. dictyoda* TDP11/23-1

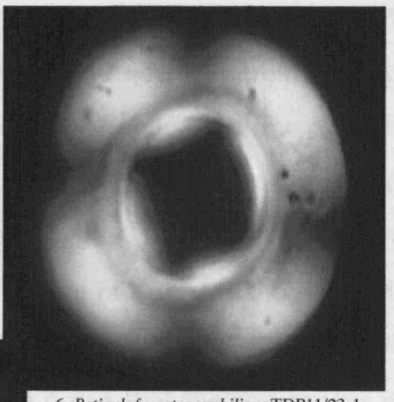

6. *Reticulofenestra umbilicus* TDP11/23-1

7. *Reticulofen. macmillanii* TDP11/23-1

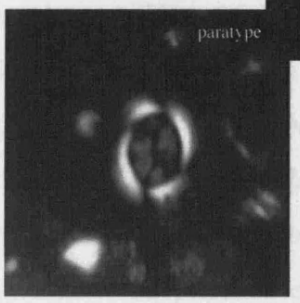

8. *Reticulofen. macmillanii* TDP12/10-1

9. *Reticulofenestra minuta* TDP12/47-1

10. *Reticulofen. filewiczii* TDP11/23-1

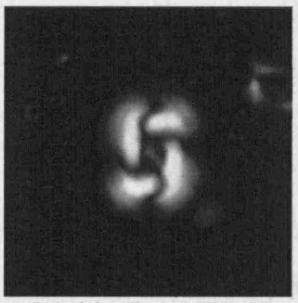

11. *Reticulofen. filewiczii* TDP11/23-1

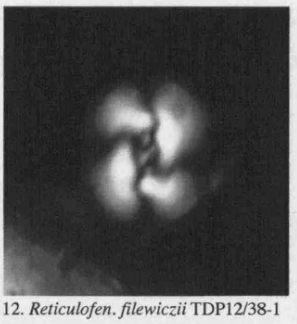

12. *Reticulofen. filewiczii* TDP12/38-1

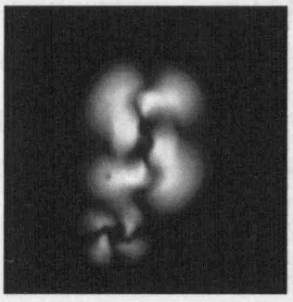

13. *Reticulofen. filewiczii* TDP11/15-1

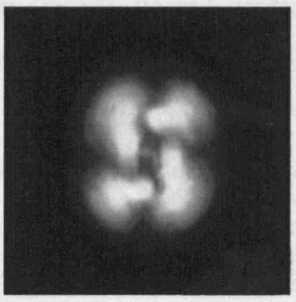

14. *Reticulofen. filewiczii* TDP12/10-1

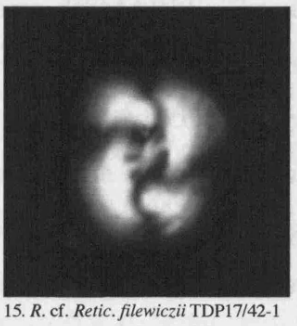

15. *R.* cf. *Retic. filewiczii* TDP17/42-1

Plate 3.1 LM images of *Cyclicargolithus* and *Reticulofenestra* placoliths.

DESCRIPTION: Large to very large (>10μm) reticulofenestrid coccoliths with a central plug (NB. the holotype is ~14 μm). OCCURRENCE: Occurs rarely throughout the section.

Reticulofenestra dictyoda (Deflandre *in* Deflandre & Fert 1954) Stradner *in* Stradner & Edwards 1968 (Pl. 3.1, fig. 5; Pl. 3.2, figs 4-6)

DESCRIPTION: Used here for all elliptical reticulofenestrid coccoliths between 3 and 14 μm with a relatively wide and, in LM, apparently vacant central area. REMARKS: As with *C. floridanus*, SEM imaging reveals the consistent presence of a fine central-area net in all specimens observed (Pl. 3.2, figs 4-6). Specimens smaller than 3μm are included in *Reticulofenestra minuta* and those larger than 14μm in *Reticulofenestra umbilicus*. Following Bralower & Mutterlose (1995) I have not used the "intermediate" reticulofenestrid taxon, *R. samodurovii* (Hay, Mohler & Wade 1966) Roth 1970, to separate specimens in the 3-14μm range. It should be noted that the size ranges of the original descriptions of both species overlap – *R. samodurovii* holotype length is 5.9 μm; the size range of the original description of *R. dictyoda* is 5.6-6.6μm. The majority of *R. dictyoda* specimens in these sections are large (~10-14 μm) and probably intergrade with *R. umbilicus*, however without detailed morphometric study, ideally from a number of locations, it is difficult to reliably separate these late Eocene forms into meaningful size classes. OCCURRENCE: Common in the upper Eocene (NP19/20 and lower NP21) but becomes very rare in the lower Oligocene (upper NP21).

Reticulofenestra umbilicus (Levin 1965) Martini & Ritzkowski 1968 (Pl. 3.1, fig. 6)

DESCRIPTION: Very large (>14 μm) elliptical reticulofenestrid coccoliths with a relatively wide and, in LM, apparently vacant central area. REMARKS: The use of a placolith length of 14 μm as the lower boundary for *R. umbilicus* follows the morphometric work of Backman & Hermelin (1986), which concluded that this condition was the most precise for the biostratigraphic use of the FO of *R. umbilicus* in the middle Eocene. The size distribution of large reticulofenestrids varies through time in the late Eocene and early Oligocene (Backman & Hermelin 1986) and probably varies biogeographically as well, making species concepts somewhat arbitrary without detailed, site-specific morphometric data. *R. hillae* Bukry & Percival 1971 has been used

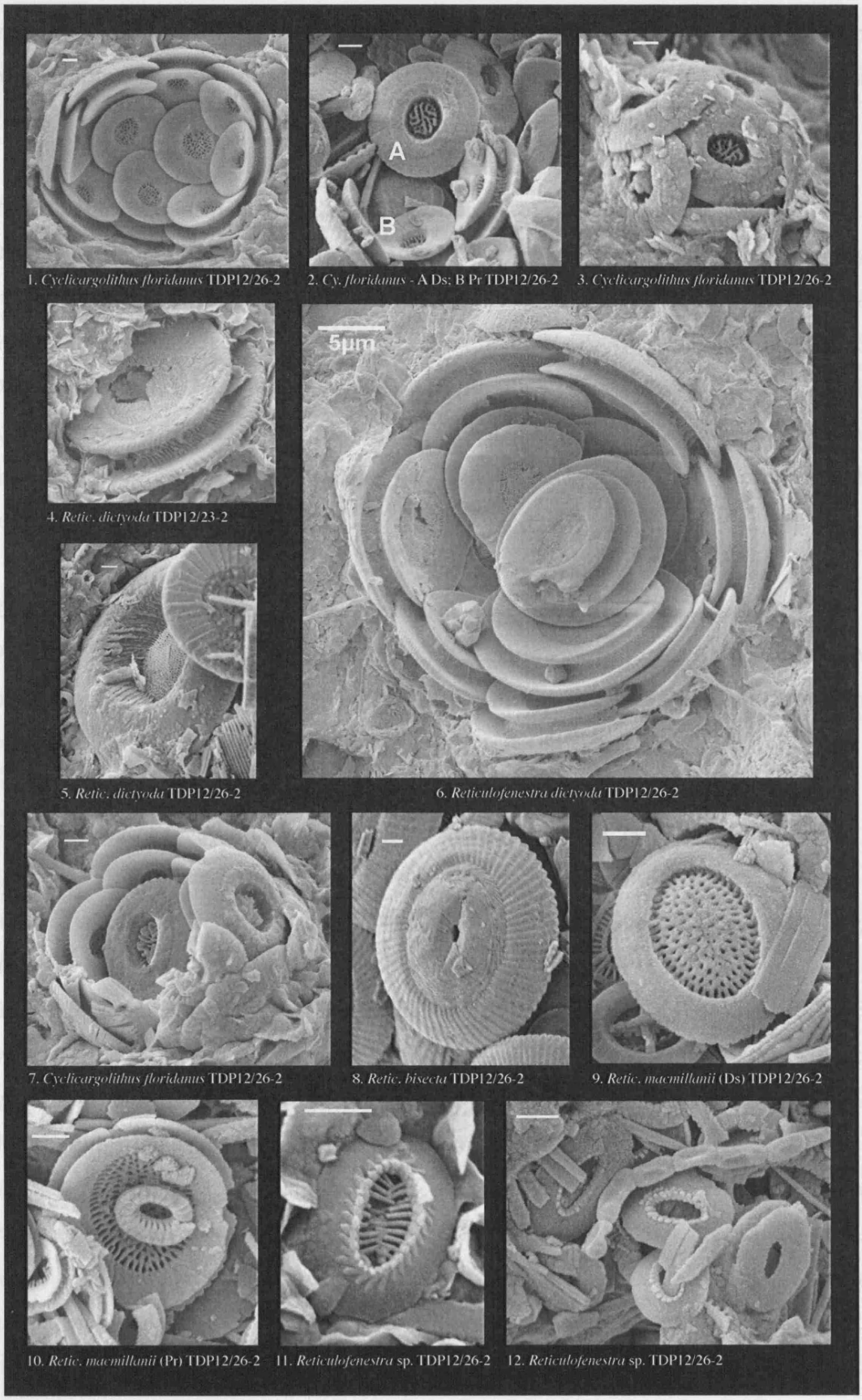

Plate 3.2 SEM images of *Cyclicargolithus* and *Reticulofenestra* placoliths.

for large late Eocene and early Oligocene reticulofenestrids with a more narrow central area opening of less than a third of the placolith width. OCCURRENCE: Rare throughout the section.

Reticulofenestra macmillanii sp. nov. (Pl. 3.1, figs 7-8; Pl. 3.2, figs 9-10)
DERIVATION OF NAME: Named after Dr. Ian McMillan (Cardiff University), micropalaeontologist. DIAGNOSIS: Small elliptical reticulofenestrids with a narrow rim and very wide central area spanned by a uniform, weakly birefringent grill. DIMENSIONS: L 4.7 μm, W 4.3 μm. HOLOTYPE: Pl. 3.1, fig. 7. PARATYPE: Pl. 3.1, fig. 8. TYPE LOCALITY: TDP Site 11, Pande, Tanzania. TYPE LEVEL: Lower Oligocene, Sample TDP11/23-1, 23cm (Subzone NP21). OCCURRENCE: Rare throughout the section; NP19/20-21; TDP Site 11, 12, 17.

Reticulofenestra minuta Roth 1970 (Pl. 3.1, fig. 9)
DESCRIPTION: Very small (<3 μm) elliptical reticulofenestrid coccoliths with, in LM, an apparently vacant central area. OCCURRENCE: Common to abundant throughout the section.

Reticulofenestra filewiczii Wise & Wiegand *in* Wise 1983 stat. nov. (Pl. 3.1, figs 10-14)
BASIONYM: *Reticulofenestra bisecta filewiczii* Wise & Wiegand *in* Wise 1983, pl. 6, fig. 2; *Initial Reports of the Deep Sea Drilling Project*, **71**: 481-550. DIAGNOSIS: Medium to large, elliptical reticulofenestrids with a narrow, elongated central area spanned by a weakly birefringent central area net. REMARKS: This upper Eocene subspecies of *R. bisecta* was described by Wise & Wiegand, on the basis of SEM images only, as an *R. bisecta* type morphology with a central area that is only partially closed, unlike the fully closed central area in *R. bisecta bisecta.* LM images of a form described as *R. bisecta filewiczii,* and similar to those figured here, are shown in de Kaenel & Villa (1996). This morphology, which is clearly distinct from specimens of *R. bisecta* with its closed central area, and is common in upper Eocene and lower Oligocene sediments, warrants species status. A number of LM images are presented here (Pl. 3.1) as the distinction between elliptical reticulofenestrids with central area grills of varying widths - *R. filewiczii, R. lockeri* and *R. daviesii* - is difficult but vital when members of this group are

used as paleoceanographic proxies, e.g. the use of *R. daviesii* as a "cold-water" species (Persico & Villa 2004). DIMENSIONS: L 5.7-8.3 μm, W 4.7-7.3 μm OCCURRENCE: Frequent throughout the section.

Reticulofenestra* cf. *R. filewiczii Wise & Wiegand *in* Wise 1983 stat. nov. (Pl. 3.1, fig. 15)
DIAGNOSIS: Medium to large, elliptical reticulofenestrids with a *R. filewiczii* form but with slightly wider central areas that are spanned by a faint grill that has a ring of pores near its outer margin. REMARKS: The presence of a faint central area grill perforated by a ring of pores at its margin is similar to descriptions of both *R. lockeri* Müller, 1970 and *R. daviesii* (Haq, 1968) Haq, 1971, however both these species appear to have a significantly wider central area and, in these sections, this form appears to intergrade with *R. filewiczii*. OCCURRENCE: Rare throughout the section.

***Reticulofenestra* sp.** (Pl. 3.2, fig. 11-12)
DESCRIPTION: Small (~3μm), elliptical reticulofenestrids observed in SEM with a distinctly raised but narrow tube cycle, giving the appearance of a beaded rim around the central area, which in turn is spanned by a coarse grill. OCCURRENCE: Rare in SEM.

Order **COCCOLITHALES** Schwarz 1932 emend. Edvardsen & Eikrem in Edvardsen *et al.* 2000

DIAGNOSIS: Includes the placolith-forming families Coccolithaceae, Calcidiscaceae and Pleurochrysidaceae and the murolith-forming Hymenomonadaceae (Young *et al.* 2003; Jordan *et al.* 2004). The placolith-forming families share two common structural features; first, growth occurs downward as well as upwards from the proto-coccolith ring, which becomes embedded within the rim (Figure 3.2) and second, the distal shield and most of the tube is formed of V-units, whereas the proximal shield and sometimes part of the tube is formed of R-units, making the distal shield dark and the proximal shield bright in XPL (Young *et al.* 2004).

Family **COCCOLITHACEAE** Poche 1913 emend. Young & Bown 1997

DIAGNOSIS: Produce placoliths with V-unit forming both the distal shield and the proximal layer of the inner tube, while the R-unit forms a bicyclic proximal shield and the distal layer of the inner tube (Figure 3.1) (Young *et al.* 1992).

Genus ***COCCOLITHUS*** Schwarz 1894

DIAGNOSIS: Placoliths with a Coccolithaceae-type structure and an open or closed central area, sometimes spanned by a disjunt bar or diminutive cross. REMARKS: Although *Cruciplacolithus* and *Chiasmolithus* are the two accepted Coccolithaceae genera with axial/non-axial central area crosses, the genus *Coccolithus* does include a number of Eocene species with reasonably well-developed central area crosses (*C. mutatus, C. staurion, C. crucis;* see Bown 2005b).

Coccolithus pelagicus (Wallich 1877) Schiller 1930 (Pl. 3.3, fig. 1; Pl 3.4, figs. 1-2 & 7)

DESCRIPTION: Small and medium sized elliptical placoliths with *Coccolithus*-type structure and an apparently open central area in LM. REMARKS: There are two accepted extant sub-species of *C. pelagicus;* a subarctic form, *C. pelagicus pelagicus,* and a temperate form, *C. pelagicus braarudii,* which have been consistently distinguished on the basis of heterococcolith size, the production of distinct holococcolith morphologies in the haploid phase and molecular genetics (Geisen *et al.* 2002; Sáez *et al.* 2003). The estimated divergence time for these two subspecies is between 1.6 and 2.7 Ma (Sáez *et al.* 2003). SEM imaging of *C. pelagicus* in this study confirms the presence of a morphotype with a gracile central-area cross (Pl. 3.4, fig. 2), similar to those observed in upper Paleocene/lower Eocene sediments of Tanzania (Bown *et al.* 2008). The subtle morphological variations observed within the Paleogene *C. pelagicus,* combined with our knowledge of the genetic and morphological variation within the modern species, suggests the presence of multiple sub- or pseudo-cryptic species within the Paleogene *C. pelagicus* species-concept. The presence of considerable genetic variability within the modern *C. pelagicus,* combined with the observed persistence of a relatively conservative morphotype from the earliest Paleogene to the recent, indicates the action of a strong stabilizing selection on this coccolith morphology (Sáez *et al.* 2003). OCCURRENCE: Common throughout the section.

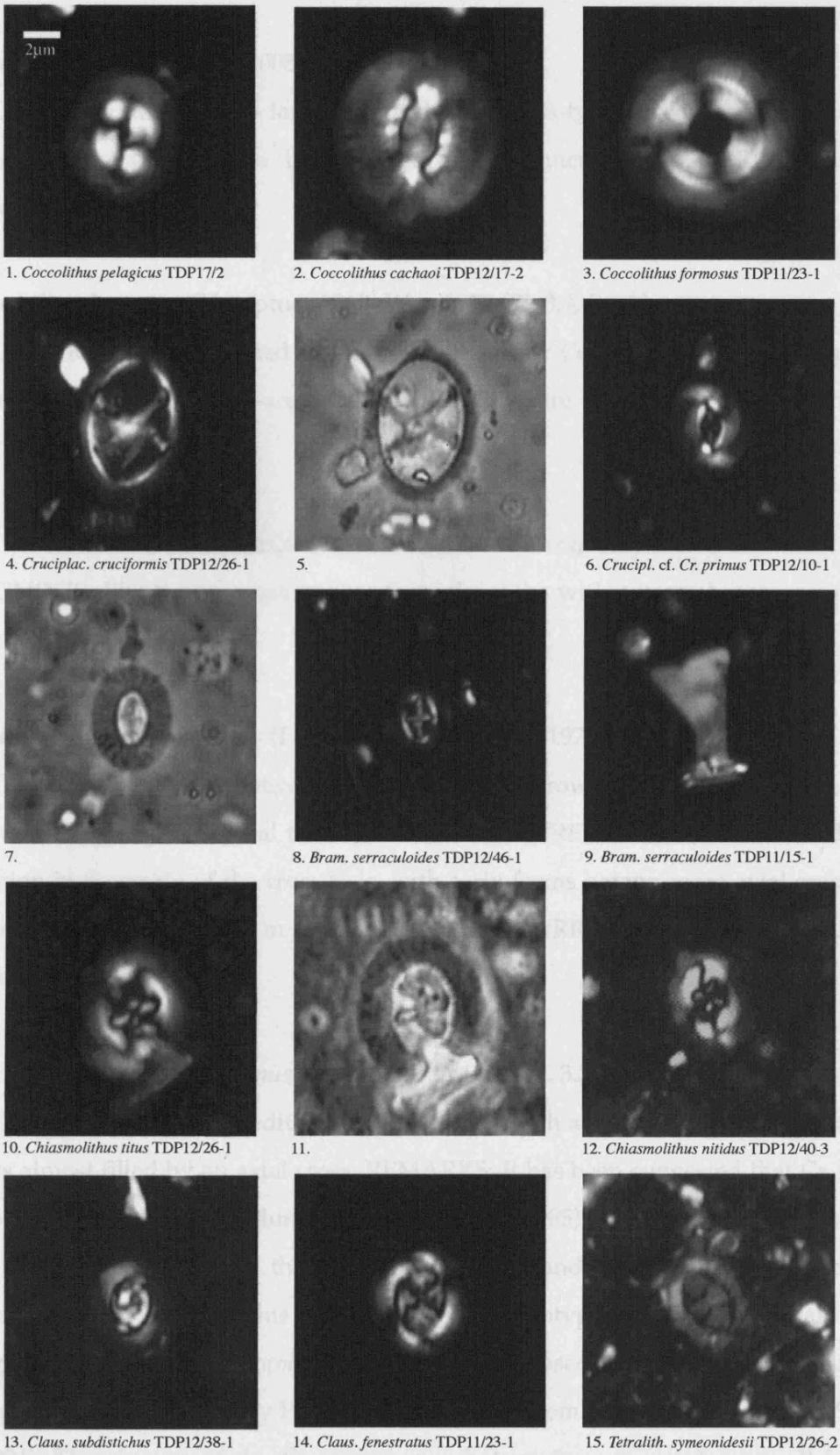

1. *Coccolithus pelagicus* TDP17/2
2. *Coccolithus cachaoi* TDP12/17-2
3. *Coccolithus formosus* TDP11/23-1
4. *Cruciplac. cruciformis* TDP12/26-1
5.
6. *Crucipl.* cf. *Cr. primus* TDP12/10-1
7.
8. *Bram. serraculoides* TDP12/46-1
9. *Bram. serraculoides* TDP11/15-1
10. *Chiasmolithus titus* TDP12/26-1
11.
12. *Chiasmolithus nitidus* TDP12/40-3
13. *Claus. subdistichus* TDP12/38-1
14. *Claus. fenestratus* TDP11/23-1
15. *Tetralith. symeonidesii* TDP12/26-2

Plate 3.3 LM images of *Coccolithus*, *Cruciplacolithus*, *Bramletteius*, *Chiasmolithus*, *Clausicoccus* and *Tetralithoides* placoliths.

Coccolithus cachaoi Bown 2005 (Pl. 3.3, fig. 2)

DESCRIPTION: Medium to large elliptical *Coccolithus*-type coccoliths with a narrow central area spanned by a broad transverse disjunct bar. OCCURRENCE: Rare throughout the section.

Coccolithus formosus (Kamptner 1963) Wise 1973 (Pl. 3.4, fig. 3)

DESCRIPTION: Medium sized circular to sub-circular *Coccolithus*-type coccoliths with a circular and open central-area. OCCURRENCE: Rare to frequently throughout the section.

Genus ***CRUCIPLACOLITHUS*** Hay & Mohler *in* Hay *et al.* 1967

DIAGNOSIS: Elliptical Coccolithaceae-type placoliths with a central-area spanned by an axial or near-axial cross.

Cruciplacolithus cruciformis (Hay & Towe 1962) Roth 1970 (Pl. 3.3, figs 4-5)

DESCRIPTION: Large elliptical placoliths with narrow shields and a wide, open central area spanned by axial to diagonal cross bars. REMARKS: Shows considerable variation in the angle of the cross bars, with early forms having more axial cross bars, which justifies its inclusion in *Cruciplacolithus*. OCCURRENCE: Very rare throughout the section.

Cruciplacolithus* cf. *Cr. primus Perch-Nielsen 1977 (Pl. 3.3, figs 6-7)

DESCRIPTION: Small to medium sized placoliths with a narrow elliptical central-area that is almost filled by an axial cross. REMARKS: It has been suggested that *Cr. primus* is restricted to Paleocene sediments (Perch-Nielsen 1985), however this closely related form is consistently present throughout the Eocene and into the lower Oligocene of Tanzania (Bown 2005b). This long-ranging morphotype may be ancestral to the Neogene and extant *Cruciplacolithus neohelis*, which based on recent molecular genetic data appears to have an early Paleocene divergence from the genus *Coccolithus* (Sáez *et al.* 2004). The absence of the *Cr. primus* morphotype from many deep-sea Paleogene sequences may be due to either a low preservation potential or a long history of

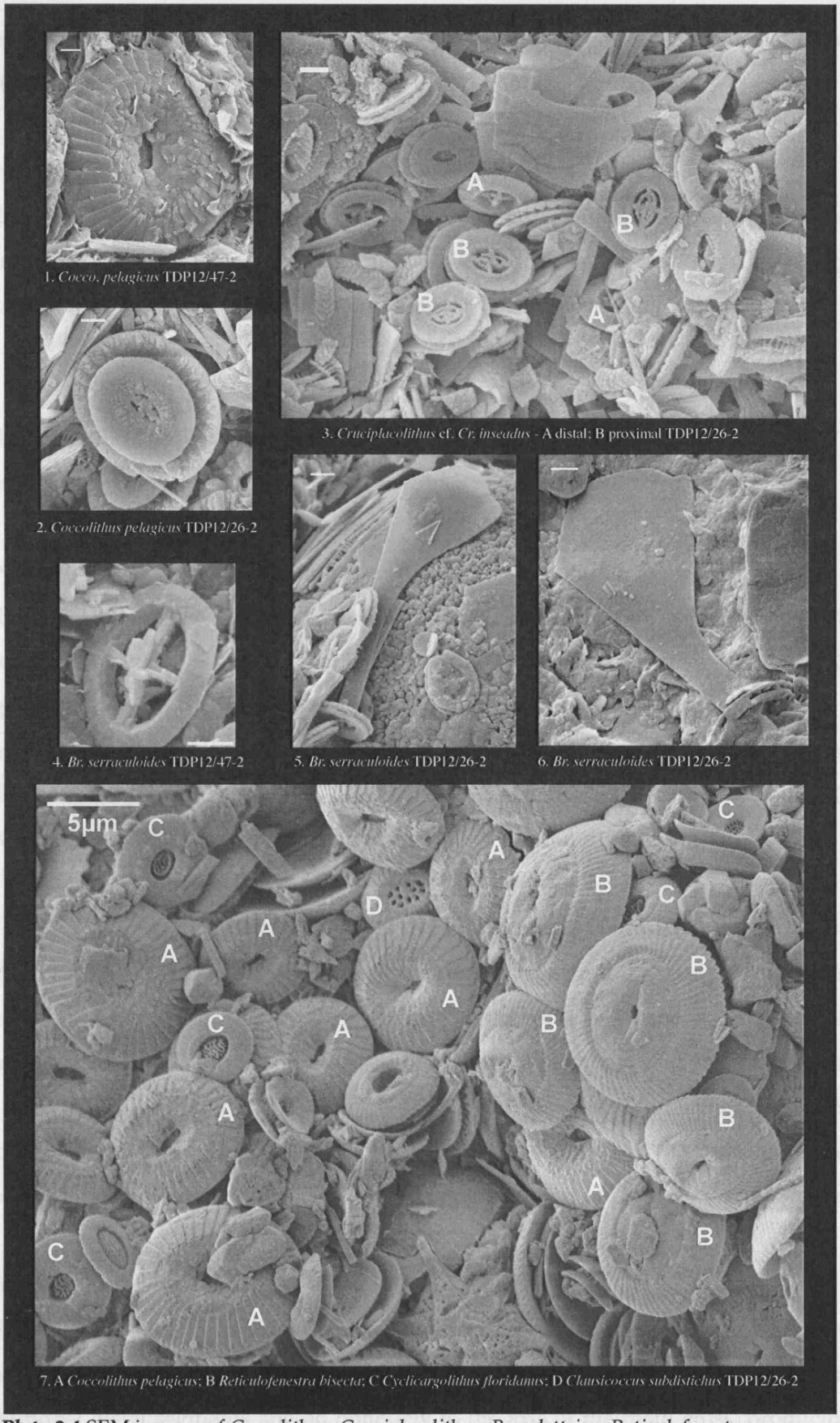

Plate 3.4 SEM images of *Coccolithus*, *Cruciplacolithus*, *Bramletteius*, *Reticulofenestra*, *Cyclicargolithus* and *Clausicoccus* placoliths.

restriction to neritic/coastal environments, as observed for the extant *Cr. neohelis* (Young *et al.* 2003). OCCURRENCE: Rare throughout the section.

Cruciplacolithus* cf. *Cr. inseadus Perch-Nielsen 1969 (Pl. 3.4, fig. 3)

DESCRIPTION: Occasional proximal views of *Cruciplacolithus*-like placoliths show a central area cross surrounded by an additional elliptical ring of elements (Pl. 3.4, fig. 3) similar to the Paleocene *Cruciplacolithus inseadus*. OCCURRENCE: Rare in SEM.

Genus ***BRAMLETTEIUS*** Gartner 1969

DIAGNOSIS: *Cruciplacolithus*-like base with a very large monocrystalline "paddle" or spine.

Bramletteius serraculoides Gartner 1969 (Pl. 3.3, figs 8-9; Pl. 3.4, figs 4-6)

DESCRIPTION: Small placoliths with a *Cruciplacolithus*-like rim and an open central area spanned by an axial cross that bears a monocrystaline paddle-like process (Pl. 3.3, fig. 9; Pl. 3.4, figs 5-6) along its long-axis. There is a considerable variation in the birefringence of the inner cycle. REMARKS: The axial cross consists of multiple, lath-like elements (Pl. 3.4, fig. 4), one of which becomes extended to form the paddle-like process. OCCURRENCE: Frequent to common throughout the section.

Genus ***CHIASMOLITHUS*** Hay, Mohler & Wade 1966

DIAGNOSIS: Elliptical Coccolithaceae-type placoliths with a diagonal, usually offset, central-area cross. REMARKS: The genus *Chiasmolithus* has been subdivided, into *Chiasmolithus* and *Sullivania*, on the basis of bar morphology and the presence/absence of a distinct collar formed by the centro-distal cycle (Bown & Young 1997; Varol 1992). Here we retain the genus *Chiasmolithus* for all these forms as the most practicable taxonomic grouping, pending an improved understanding of *Chiasmolithus* phylogeny.

Chiasmolithus titus Gartner 1970 (Pl. 3.3, figs 10-11)

DESCRIPTION: Medium sized *Chiasmolithus* species with an oblique central area cross with one-axis composed of simple arms and the other composed of kinked arms due to additional distal segments angled obliquely to the axis of the main cross, producing a

swastika-like appearance. OCCURRENCE: Rare in the upper Eocene becoming very rare in the lower Oligocene.

Chiasmolithus nitidus Perch-Nielsen 1971 (Pl. 3.3, fig. 12)
DESCRIPTION: Medium to small *Chiasmolithus* species with a simple oblique central area cross. OCCURRENCE: Rare in the upper Eocene becoming very rare in the lower Oligocene.

Genus ***CLAUSICOCCUS*** Prins 1979

DIAGNOSIS: Placoliths with typical Coccolithaceae-type rim and a wide central area spanned by a disjunct perforate plate.

Clausicoccus subdistichus (Roth & Hay *in* Hay *et al.* 1967) Prins 1979 (Pl. 3.3, fig. 13; Pl. 3.4, fig. 7)
DESCRIPTION: Small elliptical *Clausicoccus* species with a narrow central area spanned by a disjunt plate with perforations that are only clearly visible in SEM (Pl. 3.4, fig. 7). OCCURRENCE: Rare to frequent throughout the section.

Clausicoccus fenestratus (Deflandre & Fert 1954) Prins 1979 (Pl. 3.3, fig. 14)
DESCRIPTION: Medium sized elliptical *Clausicoccus* species with a wide central area spanned by a disjunct plate with perforations visible in LM. OCCURRENCE: Rare throughout the section.

Family **CALCIDISCACEAE** Young & Bown 1997

DIAGNOSIS: Form elliptical, subcircular and circular placoliths where V-unit forms the (non-birefringent) distal shield and tube, extending to the proximal surface, and R-unit forms the proximal shield (*Calcidiscus*-type rim) (Figure 3.2).

Genus ***CORONOCYCLUS*** Hay, Mohler & Wade 1966

DIAGNOSIS: Open ring-like coccolith without distinct shields, elements of rim complexly intergrown, apparently with outer V-unit and inner R-unit.

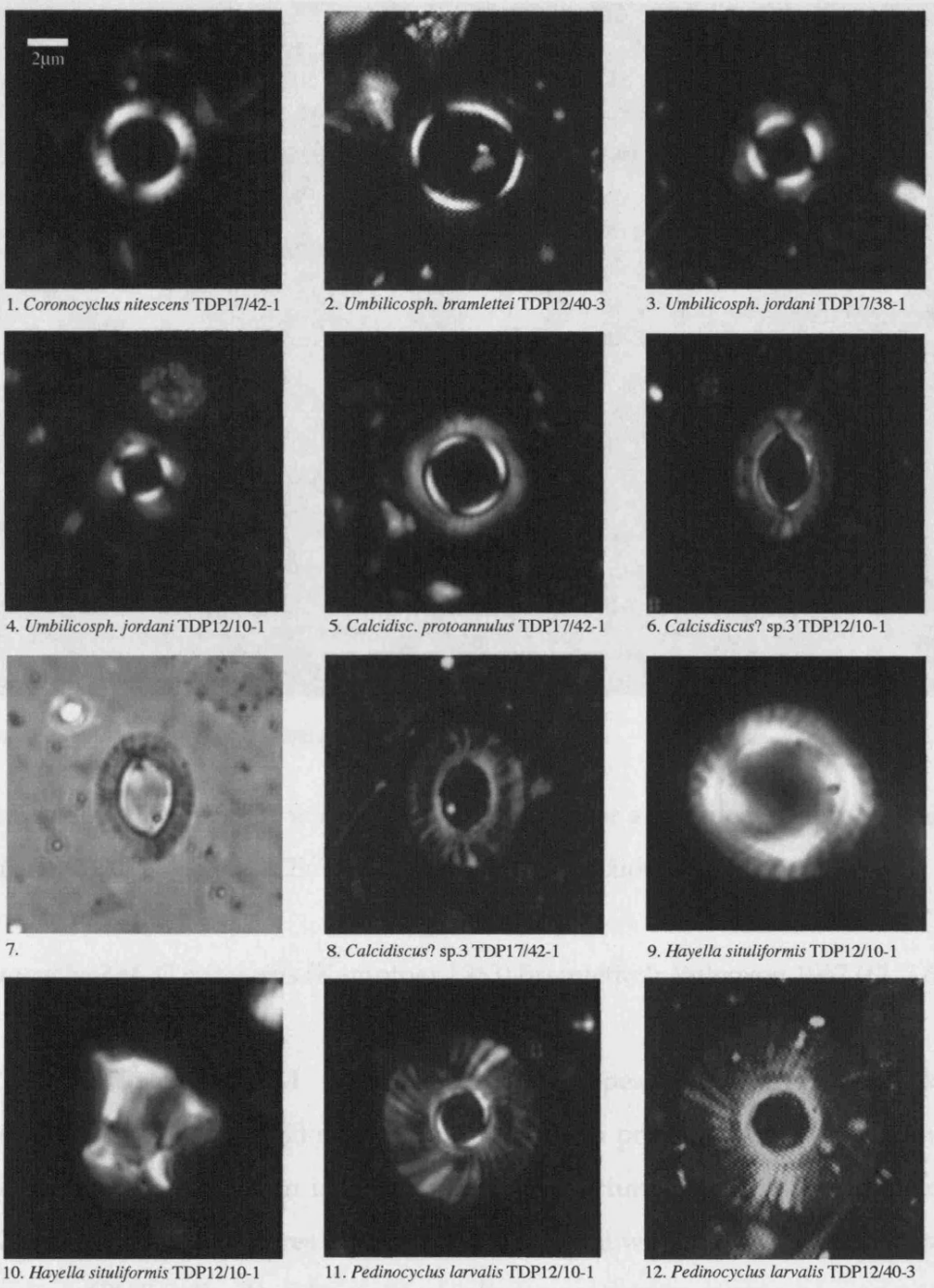

Plate 3.5 LM images of *Coronocyclus*, *Umbilicosphaera*, *Calcidiscus*, *Hayella* and *Pedinocyclus* placoliths.

Coronocyclus nitescens (Kamptner 1963) Bramlette & Wilcoxon 1967 (Pl. 3.5, fig. 1; Pl. 3.6, fig. 3)

DESCRIPTION: Medium to large ring-shaped coccoliths, bicyclic in XPL. The birefringent cycle dominates the XPL image and is crossed by extinction lines that are non-axial. Outer edge appears serrated in LM due to a large number of small radiating

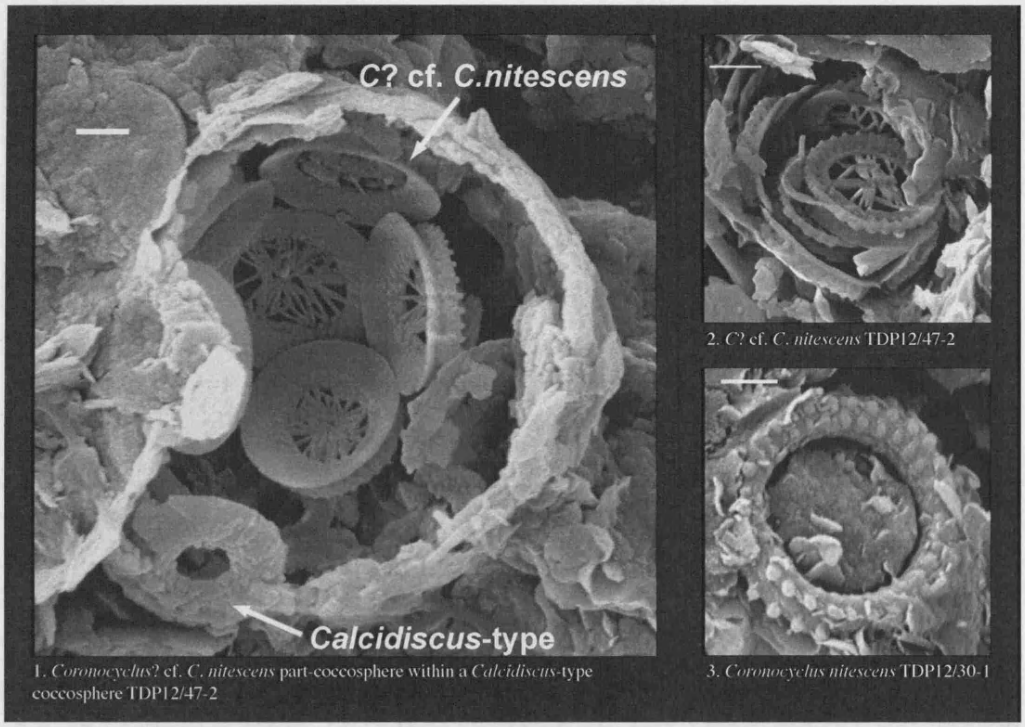

Plate 3.6 SEM images of *Coronocyclus* placoliths.

nodes developed in concentric circles around the lower and outer surfaces of the ring (Pl. 3.6, fig. 3). OCCURRENCE: Rare throughout the section.

Coronocyclus?* cf. *C. nitescens (Kamptner 1963) Bramlette & Wilcoxon 1967 (Pl. 3.6, figs 1-2)

DESCRIPTIONS: Two SEM images of what appear to be *Coronocyclus*-type coccospheres (Pl. 3.6, figs 1-2) show placoliths with a proximal shield slightly wider than the distal shield and an irregular grill-like structure spanning the wide central area. One of these coccospheres is completely contained within a larger *Calcidiscus*-type coccosphere (Pl. 3.6, fig. 1), this may be a chance occurrence, represent a transitional life-cycle stage or be a combination of endo- and exothecal coccoliths on the same coccosphere. OCCURRENCE: Rare in SEM.

Genus ***UMBILICOSPHAERA*** Lohmann 1902

DIAGNOSIS: Circular or elliptical placoliths with wide, open central-area, birefringent tube cycle and complex kinked sutures between distal shield elements. Proximal shield mono- or bi-cyclic.

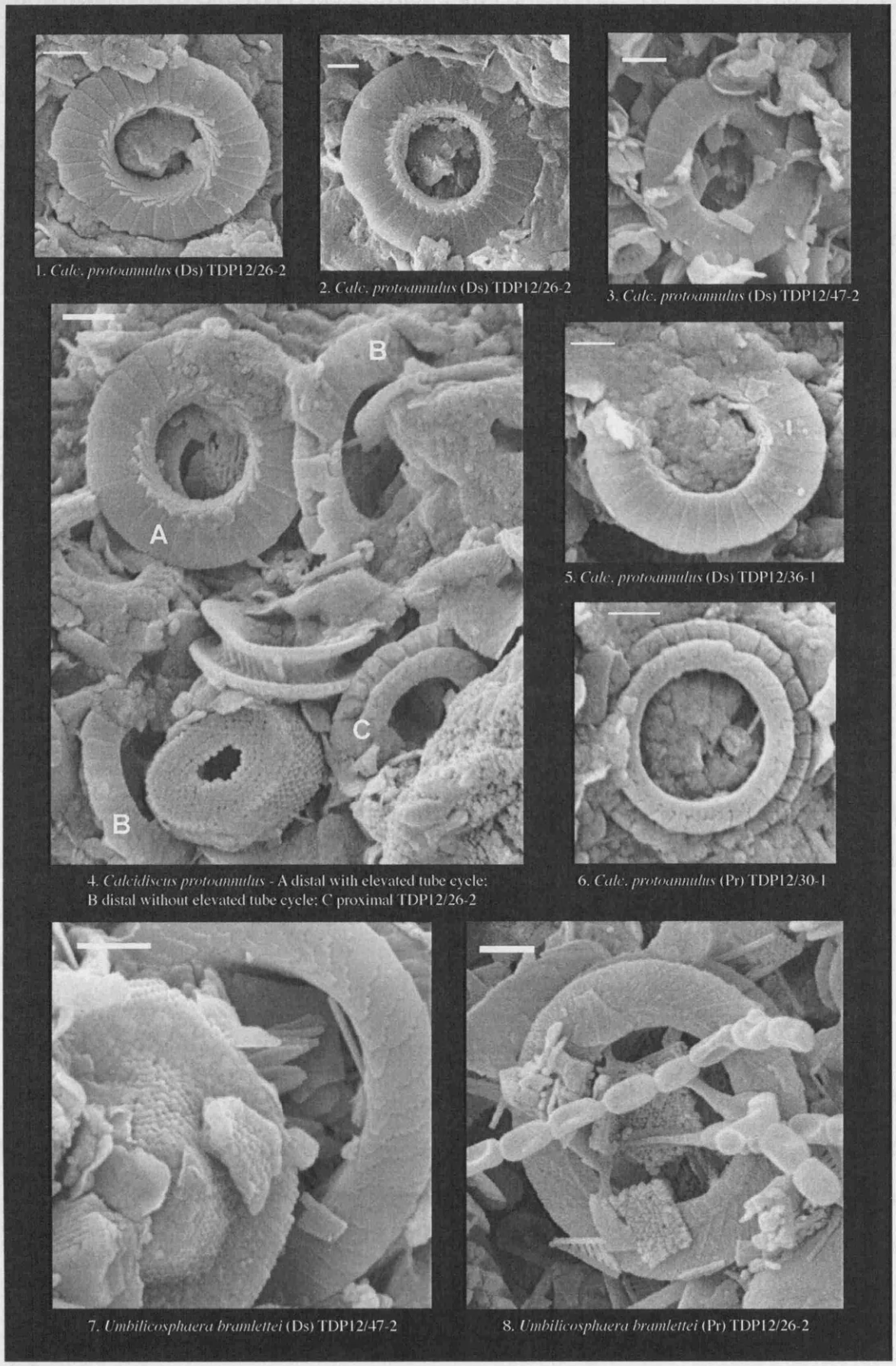

Plate 3.7 SEM images of *Calcidiscus* and *Umbilicosphaera* placoliths.

Umbilicosphaera bramlettei (Hay & Towe 1962) Bown *et al.* 2007 (Pl. 3.5, fig. 2; Pl. 3.7, figs 7-8)

DESCRIPTION: Small to medium sized (3.5-7.5 μm), narrow, ring-shaped coccoliths, distinctly bicyclic in XPL. The two cycles are similar in width; the bright inner cycle is crossed by non-axial extinction lines. REMARKS: SEM images of *U. bramlettei* clearly show its morphological similarities to modern *Umbilicosphaera,* namely the presence of kinked sutures with anticlockwise obliquity on the distal shield (Pl. 3.7, fig. 7) and a proximal shield with a strong clockwise obliquity and a narrow, slightly raised collar at its inner edge (Pl. 3.7, fig. 8). This distal shield element morphology is very similar to the extant *U. sibogae* (Bown *et al.* 2007), supporting its reassignment to the genus *Umbilicosphaera.* OCCURRENCE: Rare throughout the sections.

Umbilicosphaera jordanii Bown 2005 (Pl. 3.5, figs 3-4)

DIAGNOSIS: Medium sized (3.5-6.0 μm) circular ring-shaped placoliths with a non-birefringent distal shield, a narrow bright tube cycle crossed by non-axial extinction lines, and vacant central area that is slightly wider than the shields. REMARKS: As with *U. bramlettei,* recent SEM studies of Paleogene *U. jordanii* from Tanzania have shown that this species has a distal shield element morphology similar to the extant *U. sibogae* (Bown *et al.* 2007) confirming its assignment to the genus *Umbilicosphaera.* OCCURRENCE: Frequent in the upper Eocene becoming common in the lower Oligocene.

Genus ***CALCIDISCUS*** Kamptner 1950

DIAGNOSIS: Sub-circular to circular placoliths with typically monocyclic distal shields with straight sutures between elements; proximal shield either mono- or bicyclic. REMARKS: The placolith morphologies of the genera *Calcidiscus* and *Umbilicosphaera* are similar, with *Umbilicosphaera* being distinguished by its kinked distal-shield sutures and wide, open central-area. This generic distinction is, however, supported by molecular genetic analysis of extant taxa (Sáez *et al.* 2003).

Calcidiscus protoannulus (Gartner 1971) Loeblich & Tappan 1978 (Pl. 3.5, fig. 5; Pl. 3.7, figs 1-6)

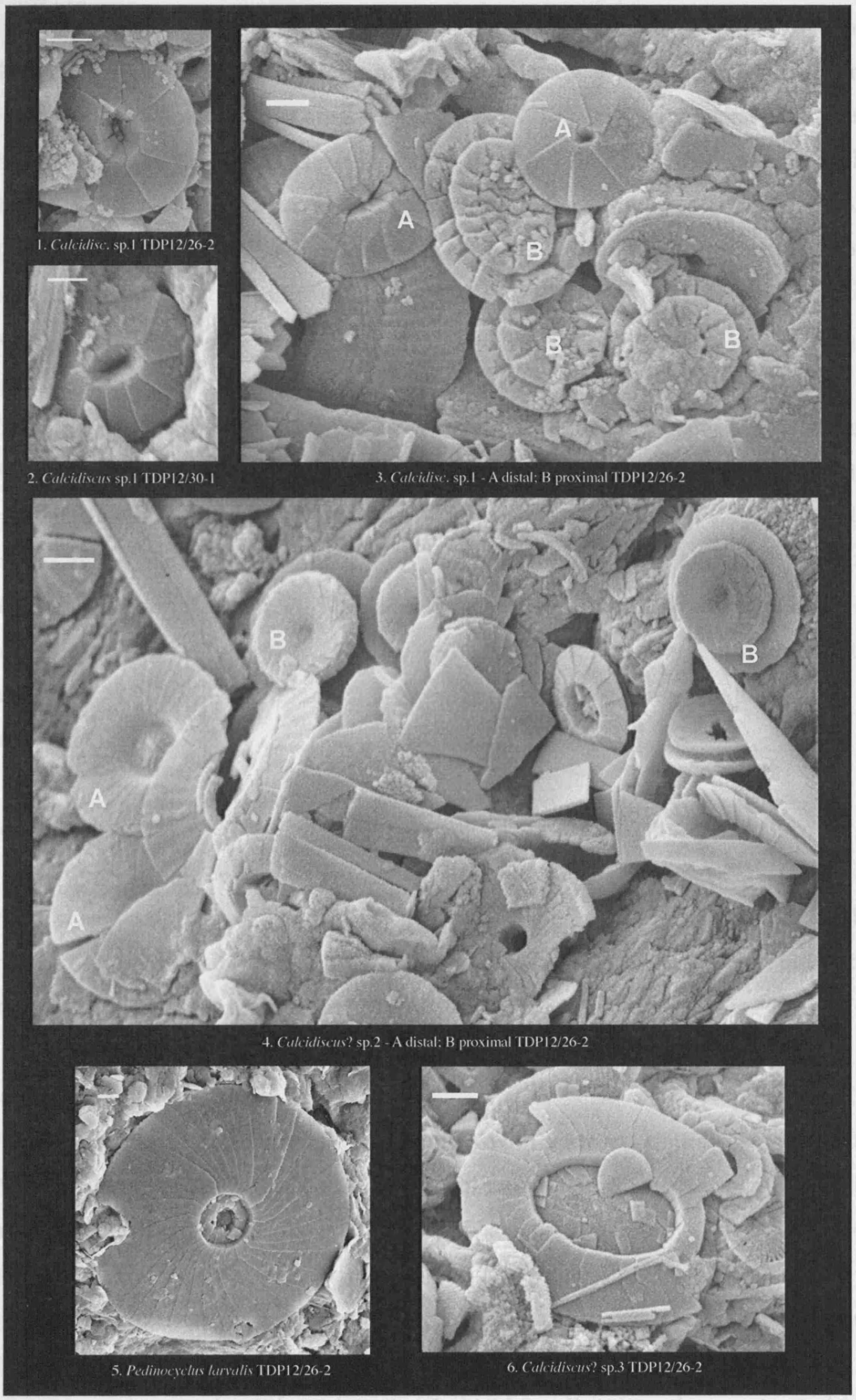

1. *Calcidisc.* sp.1 TDP12/26-2

2. *Calcidiscus* sp.1 TDP12/30-1

3. *Calcidisc.* sp.1 - A distal; B proximal TDP12/26-2

4. *Calcidiscus*? sp.2 - A distal; B proximal TDP12/26-2

5. *Pedinocyclus larvalis* TDP12/26-2

6. *Calcidiscus*? sp.3 TDP12/26-2

Plate 3.8 SEM images of *Calcidiscus*-type and *Pedinocyclus* placoliths.

DIAGNOSIS: Small to medium sized (3.5-8.0 μm) ring-shaped coccoliths that are distinctly bicyclic in XPL; the bright inner cycle is narrower than the outer cycle, and crossed by extinction lines that are near axial. REMARKS: SEM images show that distal shield sutures are straight and near-radial (Pl. 3.7, figs 1-5). At the inner margin of the distal shield there may be a raised tube cycle with strong clockwise imbrication (Pl. 3.7, figs 1-2); this is variably developed between specimens, with some possessing smooth inner margins to the distal shield (Pl. 3.7, figs 3 & 5) and may vary between placoliths from a single coccosphere (Pl. 3.7, fig. 4). This form is similar to the extant *Umbilicosphaera anulus*, which also has a wide central area (characteristic of *Umbilicosphaera*) and straight sutures between elements (characteristic of *Calcidiscus*). Molecular genetic analysis supports the division between *Caclcidiscus*-type species with straight sutures and closed central areas (*C. leptoporus, C. quadriperforatus, Oolithotus fragilis*) and *Umbilicosphaera* species with open central areas and kinked sutures (*U. sibogae, U. foliosa*) (Sáez *et al.* 2003), however data is not yet available for *U. anulus*, so the generic placement of forms with with open central areas and straight sutures is still uncertain. OCCURRENCE: Common in the upper Eocene becoming rare to very rare in the lower Oligocene.

***Calcidiscus* sp. 1** (Pl. 3.8, figs 1-3)

DIAGNOSIS: Small (3-4μm) broadly elliptical to circular *Calcidiscus*-type placoliths with a closed central area; proximal shield smaller than the distal shield and closed by an inner set of irregular elements (Pl. 3.8, fig. 3). REMARKS: These small placoliths have not been reliably identified in LM. OCCURRENCE: Rare in SEM.

***Calcidiscus*? sp. 2** (Pl. 3.8, fig. 4)

DIAGNOSIS: Small (4-5μm) circular placoliths with a closed central area. Proximal shield smaller than distal; distal shield elements show slight clockwise obliquity, whilst proximal shield elements show strong anti-clockwise obliquity (Pl. 3.8, fig. 4). REMARKS: This is a very unusual form, with the strong anti-clockwise obliquity of proximal shield elements being atypical for the Calcidiscaceae, making the generic assignment very uncertain; an alternative interpretation would be that this is a Coccolithaceae-type placolith with a distal shield smaller than the proximal shield

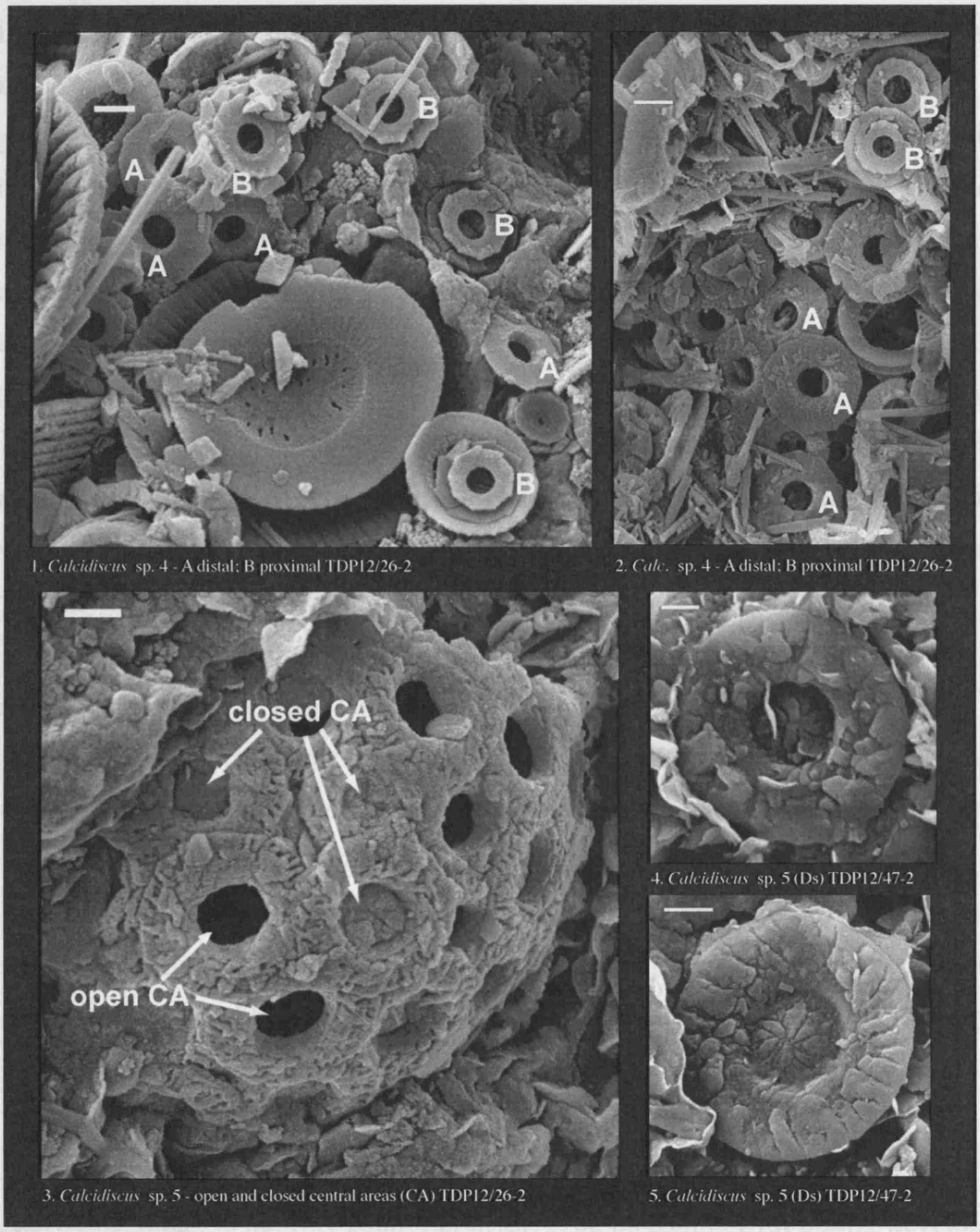

Plate 3.9 SEM images of *Calcidiscus*-type placoliths.

(reverses the identification of distal/proximal shields). The general appearance of the distal (larger) shield is similar to the extant *Oolithotus fragilis*, but the coccoliths of this modern genus have a characteristic asymmetry (Young *et al.* 2003). These small placoliths have not been reliably identified in LM. OCCURRENCE: Rare in SEM.

***Calcidiscus*? sp. 3** (Pl. 3.5, figs 6-8; Pl. 3.8, fig. 6)

DIAGNOSIS: Small to medium sized elliptical placolith observed in SEM with a *Calcidiscus*-type distal shield and a moderately wide central area completely closed by a plate formed of multiple elements (Pl. 3.8, fig. 6). Similar sized elliptical placoliths with a moderately wide, dark outer cycle, very narrow bright inner-cycle and a wide, apparently vacant, central area are frequently observed in LM (Pl. 3.5, figs 6-8) and may correspond to the placoliths observed in SEM. REMARKS: Specimens tentatively assigned to the genus *Calcidiscus* and paired with placoliths observed in LM. Similar forms have been observed in SEM studies of late Paleocene-early Eocene sediments of Tanzania (Paul Bown pers. comm.) and further SEM/LM observations of these forms may justify the creation of a new genus within the Calcidiscaceae. Central-area structure is similar to the extant narrow-rimmed placolith *Tetralithoides quadrilaminata.* OCCURRENCE: Rare to frequent throughout the section.

***Calcidiscus* sp. 4** (Pl. 3.9, figs 1-2)

DIAGNOSIS: Small (3-5μm) circular-polygonal *Calcidiscus*-type placoliths with a narrow, open central area; proximal shield smaller than distal and with clockwise imbrication of elements. REMARKS: The polygonal outline and small number of elements in the distal shield are similar to the modern *Hayaster,* but this form does not have the distinctive diminutive proximal shield of *Hayaster*. These small placoliths have not been reliably identified in LM and generic assignment is tentative. OCCURRENCE: Rare in SEM.

***Calcidiscus* sp. 5** (Pl. 3.9, figs 3-5)

DIAGNOSIS: Small (3-5μm) circular *Calcidiscus*-type placoliths with poorly developed crystal faces on distal shield elements. Central area open or closed by a set of irregular petaloid elements (Pl. 3.9, fig. 4-5). REMARKS: Only seen in distal view and may be related to the similar *Calcidiscus* sp.4. Variation in the presence/absence of the central area structure (Pl. 3.9, fig. 3) may be preservational. These small placoliths have not been reliably identified in LM and generic assignment is tentative. OCCURRENCE: Rare in SEM.

PLACOLITH COCCOLITHS *Incertae Sedis*

Genus ***TETRALITHOIDES*** Theodoridis 1984

DIAGNOSIS: Elliptical narrow-rimmed placoliths with wide central areas filled by four plates.

Tetralithoides symeonidesii Theodoridis 1984 (Pl. 3.3, fig. 15)

DIAGNOSIS: Small, dark, low-birefringence placoliths with wide central area spanned by four distinct plates. OCCURRENCE: Very rare in LM.

Genus ***HAYELLA*** Gartner 1969

DIAGNOSIS: Modified placolith coccoliths (?) formed of a single cycle of subvertical crystal units and a tube cycle with two flanges (Young & Bown 1997).

Hayella situliformis Gartner 1969 (Pl. 3.5, figs 9-10)

DESCRIPTION: Medium-sized circular placolith coccoliths with a wide, open central area and highly birefringent tube cycle. Shield elements are distinct and show obliquity. OCCURRENCE: Rare throughout the section.

Genus ***PEDINOCYCLUS*** Bukry & Bramlette 1971

DIAGNOSIS: Low birefringence circular placoliths.

Pedinocyclus larvalis Bukry & Bramlette 1971 (Pl. 3.5, figs 11-12; Pl. 3.8, fig. 5)

DESCRIPTION: Medium to large circular placoliths with a single thin flat shield of distinct, slightly inclined elements and relatively small open central area. OCCURRENCE: Rare throughout the section.

3.3.2 Murolith Coccoliths

Order **ZYGODISCALES** Young & Bown 1997

DIAGNOSIS: Muroliths and modified descendants with an outer rim-cycle of V-units

showing anti-clockwise imbrication and an inner rim-cycle showing clockwise imbrication.

Family **HELICOSPHAERACEAE** Black 1971

DIAGNOSIS: V-units of outer rim modified to form a helical flange ending in a wing or spike. R-units form the baseplate and extend to form a blanket of small elements.

Genus ***HELICOSPHAERA*** Kamptner 1954

DIAGNOSIS: Coccoliths with a helical flange.

Helicosphaera compacta Bramlette & Wilcoxon 1967 (Pl. 3.10, figs 1-2)

DESCRIPTION: Elliptical coccolith with a well-defined birefringent blanket in XPL and narrow central-area spanned by a conjunct bar. OCCURRENCE: Frequent throughout the section.

Helicosphaera reticulata Bramlette & Wilcoxon 1967 (Pl. 3.10, figs 3-6)

DESCRIPTION: Broadly rhombohedral in outline with a moderately well developed spur in some specimens (Pl. 3.10, figs 4-5), and a broad oblique disjunct bar. Entire distal surface appears to be covered by a blanket with multiple perforations. OCCURRENCE: Rare to frequent in the upper Eocene becoming frequent to common in the lower Oligocene.

Helicosphaera seminulum Bramlette & Sullivan 1961 (Pl. 3.10, figs 7-9)

DESCRIPTION: Elliptical with relatively wide central area spanned by a broad transverse to slightly oblique disjunct bar. REMARKS: Distinguished from *H. bramlettei* by the development of a wider birefringent blanket on one side, producing a distinct asymmetry and the presence of a transverse rather than oblique bar. OCCURRENCE: Rare to frequent throughout the section.

Helicosphaera bramlettei (Müller 1970) Jafar & Martini 1975 (Pl. 3.10, figs 10-12)

DESCRIPTION: Elliptical with relatively wide central area spanned by a broad, oblique disjunct bar. REMARKS: More symmetrical birefringent blanket on each side of the

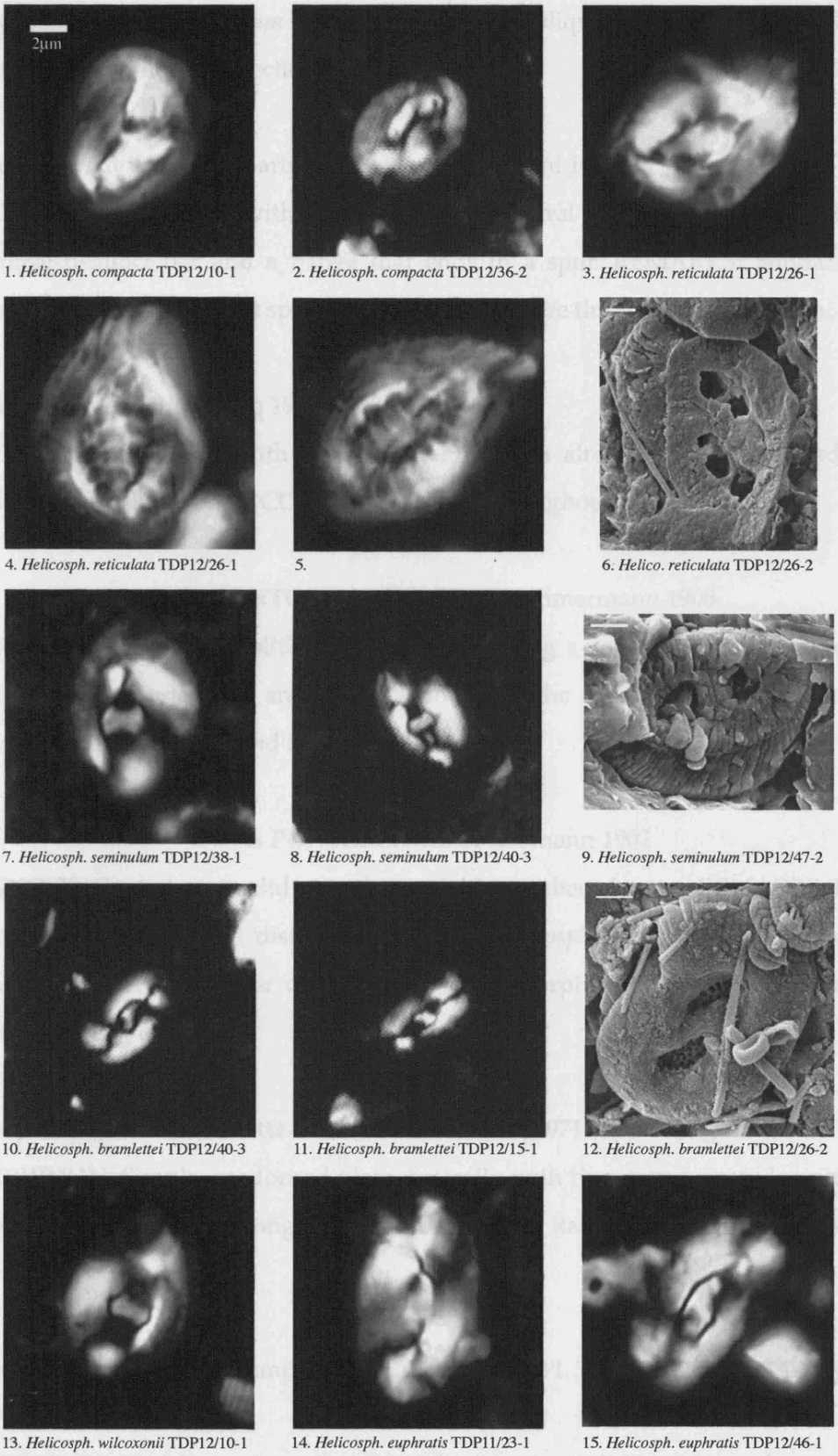

1. *Helicosph. compacta* TDP12/10-1
2. *Helicosph. compacta* TDP12/36-2
3. *Helicosph. reticulata* TDP12/26-1
4. *Helicosph. reticulata* TDP12/26-1
5.
6. *Helico. reticulata* TDP12/26-2
7. *Helicosph. seminulum* TDP12/38-1
8. *Helicosph. seminulum* TDP12/40-3
9. *Helicosph. seminulum* TDP12/47-2
10. *Helicosph. bramlettei* TDP12/40-3
11. *Helicosph. bramlettei* TDP12/15-1
12. *Helicosph. bramlettei* TDP12/26-2
13. *Helicosph. wilcoxonii* TDP12/10-1
14. *Helicosph. euphratis* TDP11/23-1
15. *Helicosph. euphratis* TDP12/46-1

Plate 3.10 LM and SEM images of *Helicosphaera* muroliths.

central-area than *H. seminulum* and more distinctly oblique bar. OCCURRENCE: Rare to frequent throughout the section.

Helicosphaera wilcoxonii (Gartner 1971) Jafar & Martini 1975 (Pl. 3.10, figs 13)
DESCRIPTION: Elliptical with relatively wide central area spanned by a broad, transverse disjunct bar and a flange that ends in a spur. REMARKS: Similar to *H. seminulum* but with a distinct spur. OCCURRENCE: Rare throughout the section.

Helicosphaera euphratis Haq 1966 (Pl. 3.10, figs 14-15)
DESCRIPTION: Elliptical with a narrow central area almost completely filled by a broad oblique disjunct bar. OCCURRENCE: Rare throughout the section.

Family **PONTOSPHAERACEAE** Lemmermann 1908

DIAGNOSIS: Murolith coccoliths with V-units forming a narrow outer rim-cycle with anti-clockwise imbrication and R-units forming the inner rim with clockwise imbrication, the base-plate and blanket.

Genus ***PONTOSPHAERA*** Lohmann 1902

DIAGNOSIS: Central-area solid or with a variable number of pores. REMARKS: Extant members of the genus are distinguished from *Scyphosphaera* by their monomorphic coccospheres – *Scyphosphaera* coccospheres are dimorphic with elevated equatorial coccoliths (Young *et al.* 2003).

Pontosphaera plana (Bramlette & Sullivan 1961) Haq 1971 (Pl. 3.11, fig. 1)
DESCRIPTION: Simple unadorned plate, typically with two very narrow longitudinal slits running parallel to the long-axis. OCCURRENCE: Rare to frequent throughout the section.

Pontosphaera multipora (Kamptner 1948) Roth 1970 (Pl. 3.11, figs 2-3; Pl. 3.12, figs 1 & 3)
DESCRIPTION: Simple unadorned plate with a narrow indistinct rim and up to three concentric cycles of small perforations. REMARKS: As with modern forms (Young *et al.*

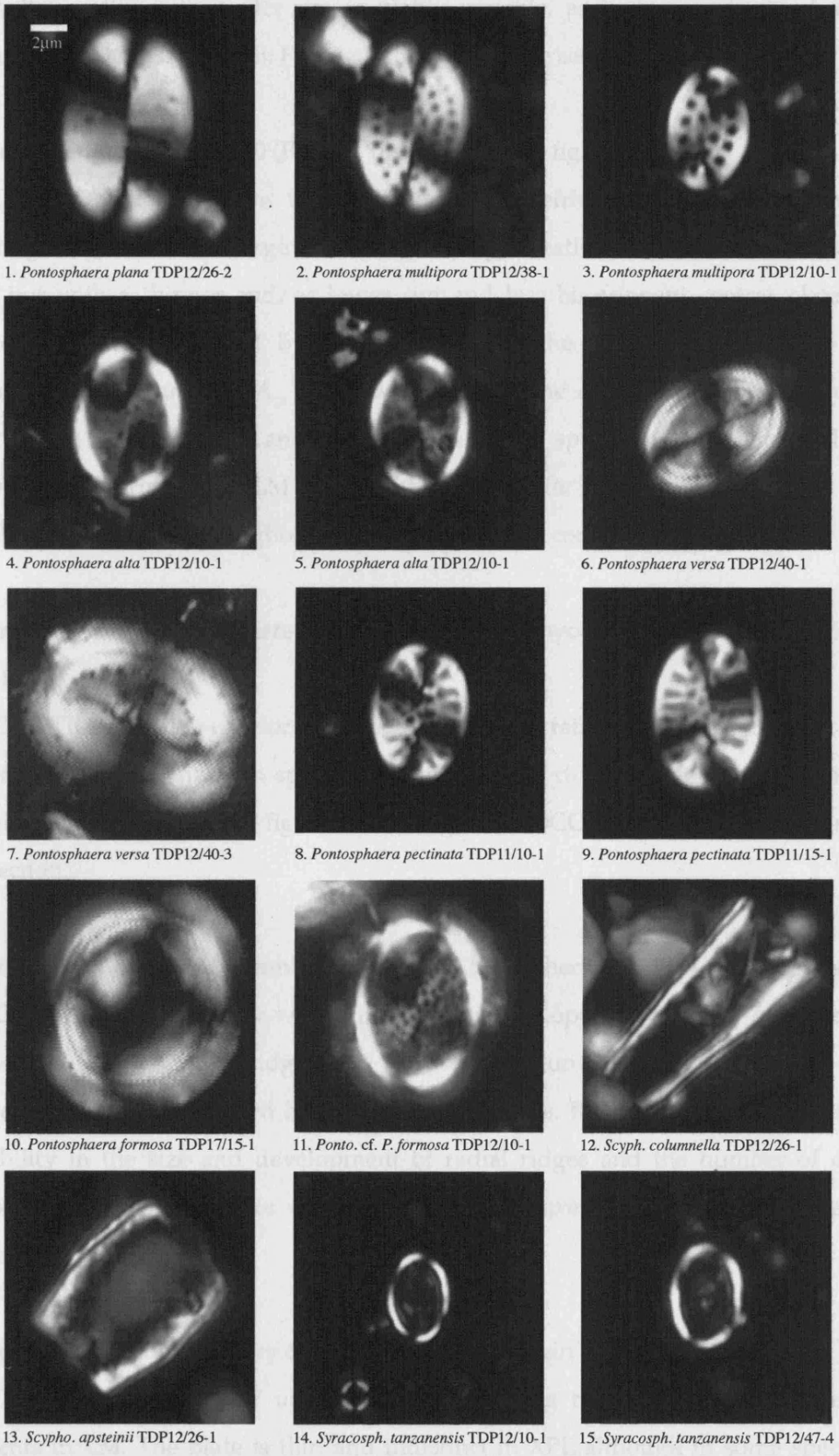

1. *Pontosphaera plana* TDP12/26-2
2. *Pontosphaera multipora* TDP12/38-1
3. *Pontosphaera multipora* TDP12/10-1
4. *Pontosphaera alta* TDP12/10-1
5. *Pontosphaera alta* TDP12/10-1
6. *Pontosphaera versa* TDP12/40-1
7. *Pontosphaera versa* TDP12/40-3
8. *Pontosphaera pectinata* TDP11/10-1
9. *Pontosphaera pectinata* TDP11/15-1
10. *Pontosphaera formosa* TDP17/15-1
11. *Ponto.* cf. *P. formosa* TDP12/10-1
12. *Scyph. columnella* TDP12/26-1
13. *Scypho. apsteinii* TDP12/26-1
14. *Syracosph. tanzanensis* TDP12/10-1
15. *Syracosph. tanzanensis* TDP12/47-4

Plate 3.11 LM images of *Pontosphaera, Scyphosphaera* and *Syracosphaera* muroliths.

2003), the width of the outer rim is highly variable, as is the number and size of perforations. OCCURRENCE: Frequent throughout the section.

Pontosphaera alta Roth 1970 (Pl. 3.11, figs 4-5; Pl. 3.12, fig. 2)
DESCRIPTION: *Pontosphaera* with an elevated, birefringent rim and a thin, low birefringence plate with a large number of small perforations. REMARKS: Similar to *P. versa* but with a thinner and/or lower rim and less birefringent central plate. This species was first described by Roth (1970) from the lower Oligocene Red Bluff Formation of Alabama, USA. The SEM images of the original description are near identical to Pl. 3.12, fig. 2 and LM examination of specimens from the Red Bluff Formation confirmed the LM identification of *P. alta* presented here (pers. obs.). OCCURRENCE: Rare throughout the section but more common than *P. versa.*

Pontosphaera versa (Bramlette & Sullivan 1961) Sherwood 1974 (Pl. 3.11, figs 6-7; Pl. 3.12, fig. 6)
DESCRIPTION: Simple unadorned plate with a broad raised margin/rim. Many of the larger late Eocene Tanzanian specimens have a single ring of perforations around the margin of the plate (Pl 3.11, fig. 7; Pl 3.12, figs 4-5). OCCURRENCE: Rare throughout the section.

Pontosphaera pectinata (Bramlette & Sullivan 1961) Sherwood 1974 (Pl. 3.11, figs 8-9)
DESCRIPTION: *Pontosphaera* with a plate that is scalloped towards its outer edge as defined by narrow radial ridges and furrows that run inwards towards the centre where the plate is perforated by multiple small holes. REMARKS: Shows significant variability in the size and development of radial ridges and the number of central perforations. May intergrade with forms of *P. multipora.* OCCURRENCE: Frequent throughout the section.

Pontosphaera formosa (Bukry & Bramlette 1968) Romein 1979 (Pl. 3.11, figs 10-11)
DESCRIPTION: Large (9-17 μm) with a high flaring rim that displays discernible elements in LM. The plate is thin and indistinct in XPL although in some specimens multiple perforations are clearly visible (Pl. 3.11, fig 11). OCCURRENCE: Rare

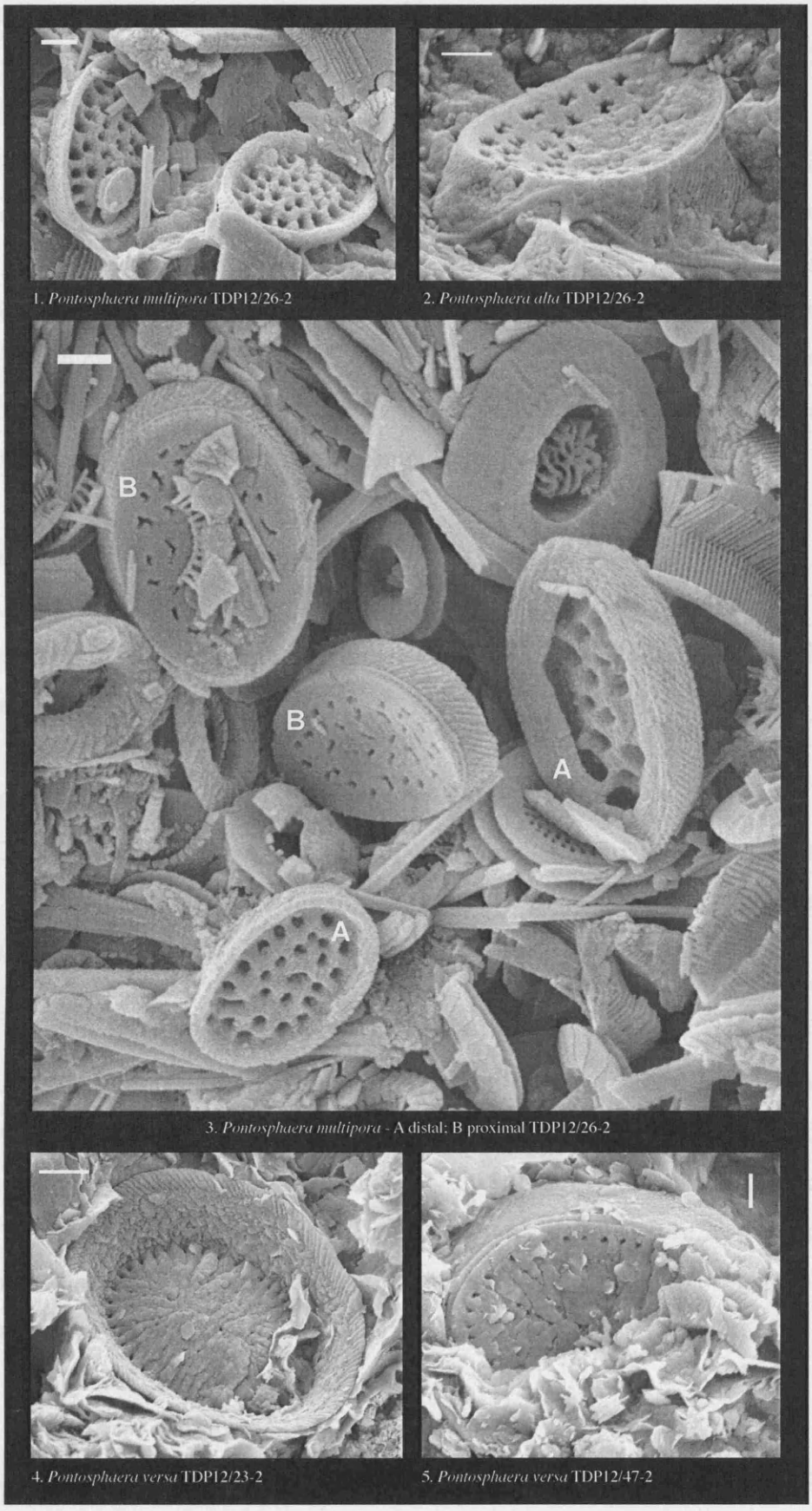

Plate 3.12 SEM images of *Pontosphaera* muroliths.

throughout the section.

Genus ***SCYPHOSPHAERA*** Lohmann 1902

DIAGNOSIS: Extant forms are similar to *Pontosphaera* but with dimorphic coccospheres consisting of elevated equatorial coccoliths, known as lopadoliths, and *Pontosphaera*-type muroliths. REMARKS: Fossil coccoliths with a lopadolith morphology are included within this genus. The, presumably, *Pontosphaera*-like coccoliths that would be expected to occur on 'fossil' *Scyphosphaera* coccospheres would not be distinguishable from true *Pontosphaera* coccoliths (unless preserved on a fossil coccosphere), and so are almost certainly included within the genus *Pontosphaera*.

Scyphosphaera columella Stradner 1969 (Pl. 3.11, fig. 12)

DESCRIPTION: Tall narrow murolith with near-straight walls that run parallel or flare slightly to a maximum width at the distal end. OCCURRENCE: Very rare throughout the section.

Scyphosphaera apsteinii Lohmann 1902 (Pl. 3.11, fig. 13)

DESCRIPTION: Large elevated murolith with variable morphology but typically broad with curved, gently flaring walls that may narrow distally. OCCURRENCE: Very rare throughout the section.

Order **SYRACOSPHAERALES** Hay 1977 emend. Young *et al.* 2003

DIAGNOSIS: Produce complex coccoliths typically consisting of three components: 1) a rim with normal V/R structure but with proto-coccolith ring embedded within it; 2) a radial lath cycle, formed of crystallites with sub-tangential c-axis orientation ("T-units") that interdigitate with rim elements; 3) an axial structure in the centre of the coccolith that may be formed from radial lath elements and/or from additional, disjunct elements (Figure 3.2) (Young *et al.* 2003).

Family **CALCIOSOLENIACEAE** Kamptner 1927

DIAGNOSIS: Produce murolith coccoliths without flanges, usually termed scapholiths. Rim predominantly formed of V-units with small R-units at the base/inner margin

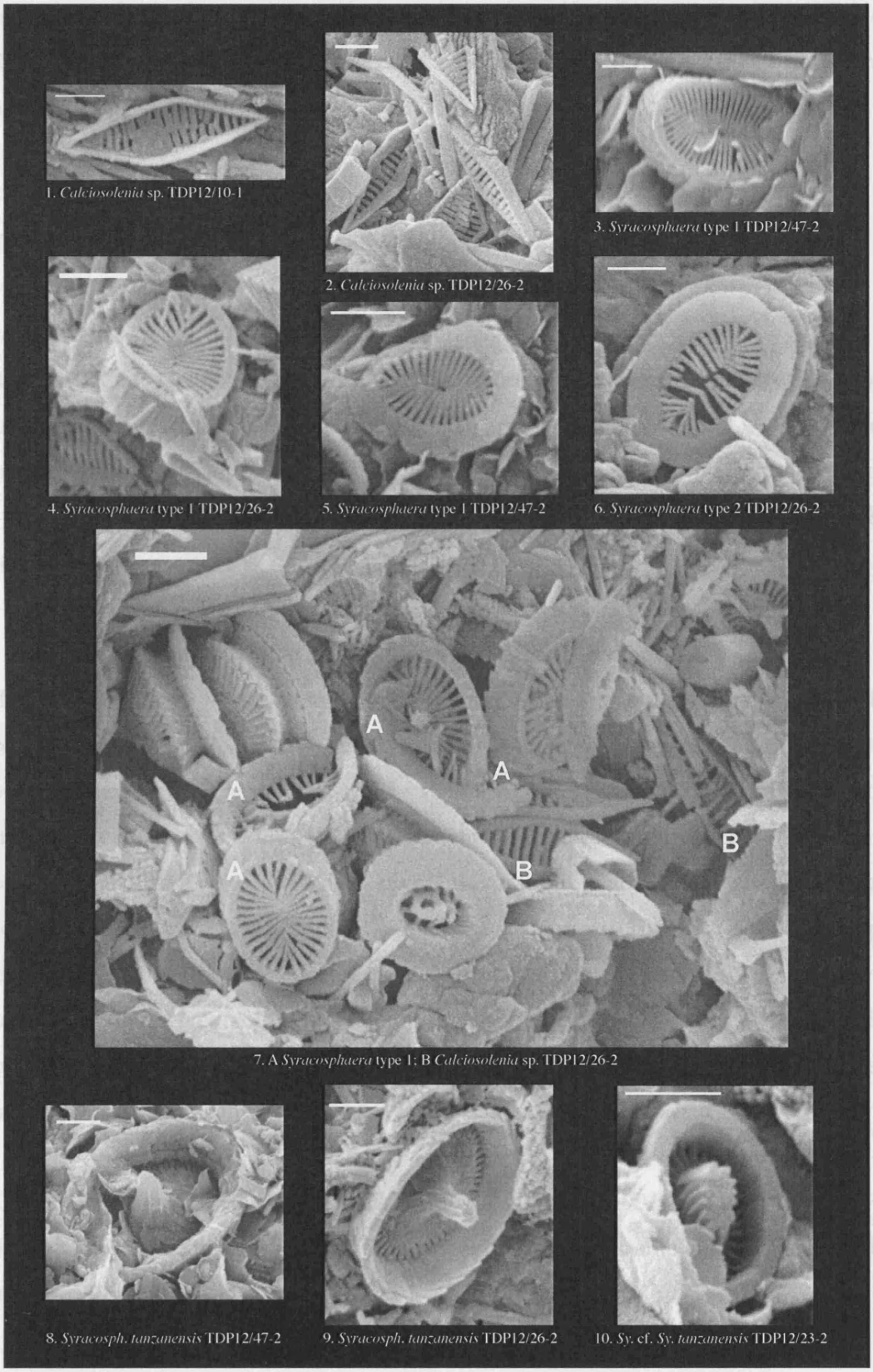

Plate 3.13 SEM images of *Calciosolenia* and *Syracosphaera* muroliths.

(Young *et al.* 2003). Central-area structure formed of a single lath-cycle with pairs of laths from opposite sides of the coccolith rim meeting to form a series of transverse bars.

Genus ***CALCIOSOLENIA*** (Gran 1912) Young *et al.* 2003

DIAGNOSIS: Forms rhombic muroliths (scapholiths).

***Calciosolenia* sp.** (Pl. 3.13, figs 1-2 & 7)

DESCRIPTION: Isolated rhombic muroliths (scapholiths) were frequently observed during SEM investigations of rock chip surfaces and rarely observed in LM. These have not been given a species assignment but in SEM are remarkably similar in morphology to the living *C. brasiliensis* (Young *et al.* 2003). OCCURRENCE: Rare throughout the section.

Family **SYRACOSPHAERACEAE** Lemmermann 1908

DIAGNOSIS: Extant forms often develop distinct inner and outer layers of coccoliths around the cell (dithecatism). Endothecal (inner layer) coccoliths are relatively conservative in form, normally muroliths with a well-developed central-area lath-cycle and variable inner central-area (Figure 3.2), whilst exothecal (outer layer) coccoliths are more variable in form including planolith, murolith and dome-shaped forms. Individual coccospheres can show a significant variation in coccolith size and shape dependent on their position on the coccosphere (varimorphism) and may include a number of distinct coccolith morphologies (polymorphism). These traits make the taxonomy of fossil species problematic as a number of distinct coccolith morphologies, and hence fossil taxa, may be produced by the same biological species.

Genus ***SYRACOSPHAERA*** Lohmann 1902

DIAGNOSIS: Coccospheres usually dithecate with highly variable exothecal coccoliths and murolith endothecal coccoliths with 1, 2 or 3 flanges.

Syracosphaera tanzanensis Bown 2005 (Pl. 3.11, figs 14-15; Pl. 3.13, figs 8-9)

DESCRIPTION: Medium sized muroliths with narrow bicyclic rim (bright inner cycle, dark outer cycle) and wide central area. REMARKS: This species was tentatively assigned to the genus *Syracosphaera* on the basis of its appearance in LM (Bown 2005b). This is confirmed by SEM images presented here (Pl. 3.13, figs 8-9), which show muroliths with a typical *Syracosphaera* structure, with a high rim, radial lath cycle and a central boss. The relatively thick and high rim produces the distinct bright cycle in XPL. OCCURRENCE: Frequent to common throughout the section.

Syracosphaera type 1 (Pl. 3.13, figs 3-5 & 7)

DIAGNOSIS: Small (3-4μm) simple elliptical murolith coccolith with a narrow rim and a wide central-area spanned by a well-developed, fragile lath cycle. REMARKS: Rarely observed in SEM but not observed or not differentiated from *S. tanzanensis* in LM. These, and the following two *Syracosphaera* morphotypes, have not been assigned species names until their relationships to each other can be better established. OCCURRENCE: Rare in SEM.

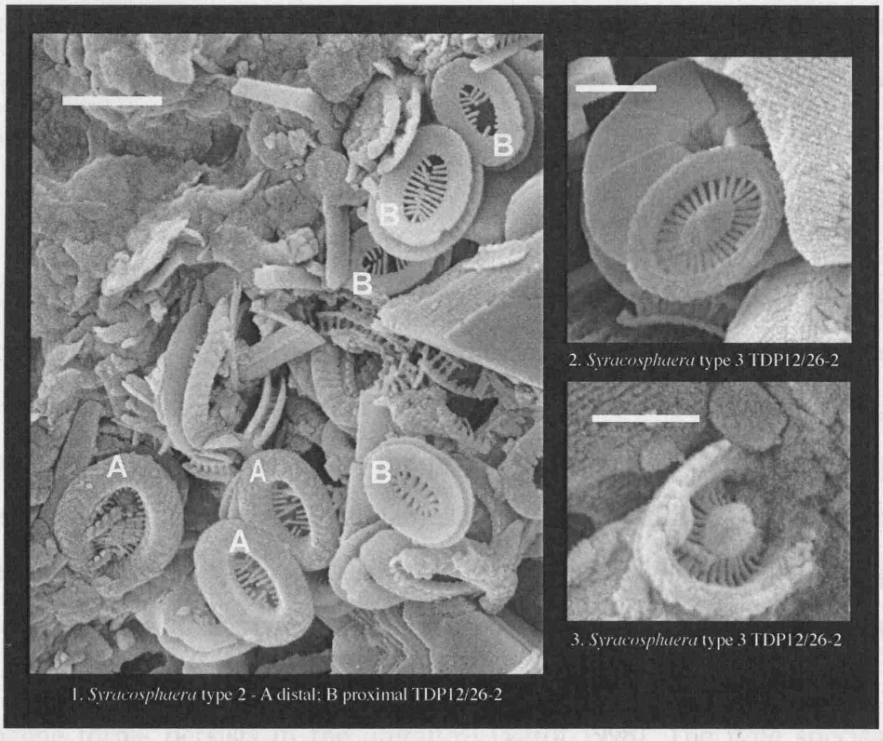

Plate 3.14 SEM images of *Syracosphaera* coccoliths.

Syracosphaera type 2 (Pl. 3.13, figs 6; Pl. 3.14, fig. 1)

DIAGNOSIS: Small (2-4μm) elliptical coccoliths with a relatively narrow rim with two flanges, producing a placolith-like appearance (Young *et al.* 2003), and a wide central-area spanned by a well-developed, fragile lath cycle. REMARKS: Similar to *Syracosphaera* type 1 but with a wider rim with two flanges. OCCURRENCE: Rare throughout the section.

Syracosphaera type 3 (Pl. 3.14, figs 2-3)

DIAGNOSIS: Very small (~2μm) elliptical murolith coccolith with a distinct radial lath cycle and central boss. OCCURRENCE: Very rare in SEM.

Family **RHABDOSPHAERACEAE** Haeckel 1894

DIAGNOSIS: Form typically disc-shaped coccoliths (planoliths) formed of three components: 1) a narrow, slightly elevated rim formed of two cycles of elements, an upper/outer rim cycle of simple non-imbricate V-unit elements and a lower/inner rim cycle with strong obliquity, crystallography uncertain; 2) a radial cycle of radial laths joining rim to lamellar cycle; 3) lamellar cycle(s) formed of lamellar elements showing clockwise imbrication, often multiple cycles with inner cycles more elongate, inclined and in helical arrangement forming spine or protrusion. Coccoliths of the rhabdosphaeraceae are often termed 'rhabdoliths' (Young *et al.* 1997).

Genus ***BLACKITES*** Hay & Towe 1962

DIAGNOSIS: Spine or process bearing coccoliths with a base formed of three components: 1) an outer rim cycle of simple non-imbricate V-unit elements; 2) a radial cycle of radial laths; 3) a lamellar cycle with clockwise imbrication. Simple to highly complex, typically hollow, spines or processes can be formed by multiple lamellar cycles extending up from the basal lamellar cycle. REMARKS: The differentiation of the extant genus *Rhabdosphaera* and extinct Paleogene genus *Blackites* has been problematic. The older genus *Rhabdosphaera* been used by some authors to include Paleogene rhabdoliths with unknown basal structure (Perch-Nielsen 1985) and its use for Paleogene forms persists in the literature (Varol 1998). The type species of the two genera are the extant *Rhabdosphaera clavigera* (Haeckel 1894) and the Eocene/Oligocene

Blackites spinosus (Hay & Towe 1962). The original description of the genus *Blackites* noted the characteristic radial cycle in these coccoliths, which are "characterized by a single circular shield with a perforate ring spanned by interlocking ribs near the periphery" (Hay & Towe 1962). This characteristic was later used as the distinguishing feature between *Blackites* and *Rhabdosphaera*, with the later "compressed elliptically and is lacking the cycle of interlocking ribs characteristic of *Blackites*" (Stradner in Stradner & Edwards 1968). As with other coccolith groups (Young *et al.* 1992), rim structure is the most robust basis for generic taxonomy in the Rhabdosphaeraceae and can be used to distinguish between *Blackites*, which has a radial lath cycle, and *Rhabdosphaera* which lacks this radial cycle. The radial cycle in some *Blackites* species may be greatly reduced but is still present as a series of residual radial elements between the outer cycle and the lamellar cycle.

Detailed morphological analyses of spines and processes have been used to define a number of additional Paleogene rhabdolith genera (Aubry 1999; Shafik 1989). At present we have not attempted to subdivide the genus *Blackites*, which, based on the definition above and the available SEM images appears to include the majority of Paleogene rhabdoliths. Following Bown (2005b) we do use two informal groupings, based on the LM appearance of the coccolith base, which with further SEM analysis may prove taxonomically useful.

Blackites? furvus Bown & Dunkley Jones 2006 (Pl. 3.15, figs 1-2)

DESCRIPTION: Medium-sized, subcircular-circular coccoliths with broad, low-birefringence shields crossed by strongly curving extinction lines. The central area is narrow or closed. REMARKS: Subcircular, spineless *Rhabdosphaera*-type planoliths have been observed in SEM (Pl. 3.17, fig. 5), which may correspond to *Bl. furvus* identified in LM. At present there is not sufficient data to confidently correlate LM and SEM images, hence the retention of the original tentative generic assignment. OCCURRENCE: Frequent throughout the section.

Blackites amplus Roth & Hay 1967 *in* Hay *et al.* 1967 (Pl. 3.15, fig. 3)

DESCRIPTION: A spineless circular rhabdolith with an outer dark cycle and inner bright central cycle in XPL, crossed by curving but roughly north-south trending extinction lines. REMARKS: *Bl. amplus* may be the isolated basal coccolith of a spinose rhabdolith such as *Bl. tenuis* (Aubry, 1999), however the circular, spineless rhabdolith, with a rim and radial lath cycle similar to *Bl. tenuis*, observed in SEM (Pl. 3.16, figs 5-6) may also have a *Bl. amplus* appearance in LM. It is possible that both *Bl. tenuis* bases and this new form appear similar in LM and are both included in LM identifications of *"Bl. amplus"*. Further SEM examination of material containing *Bl. amplus* is required to determine the nature and validity of this taxa. OCCURRENCE: Rare throughout the section.

Blackites morionum Group

Short to moderately tall and wide spines; typical *Blackites* rim structure in which the outer cycle and inner lamellar cycle of the base appear to lie side by side in LM, the outer cycle being smaller.

Blackites deflandrei (Perch-Nielsen 1968) Bown 2005 (Pl. 3.15, fig. 4)

DESCRIPTION: Rhabdolith with a relatively low, wide, hollow sacculiform spine constructed from at least two distinct structural units when viewed in XPL; there may be a small, terminal papilla. The spine broadens slightly to a maximum in the lower cycle, before tapering to a point; the spine is always slightly narrower than the coccolith with a height similar to or slightly greater than the coccolith width. OCCURRENCE: Previously reported from the middle Eocene sub-zones NP14b/15a-c of Tanzania (Bown, 2005b). Occurs very rarely throughout the sections and may be reworked from middle Eocene sediments, although most of the observed specimens show excellent preservation, which is not consistent with reworking.

Blackites clavus Bown 2005 (Pl. 3.15, fig. 5)

DESCRIPTION: Rhabdolith coccoliths with a short spine that tapers rapidly to a point, giving the overall appearance of a nail or pin. Typically the height of the spine is similar to the width of the coccolith. The rim is relatively broad with a small outer cycle that does not lie distally over the inner cycle. OCCURRENCE: Previously reported

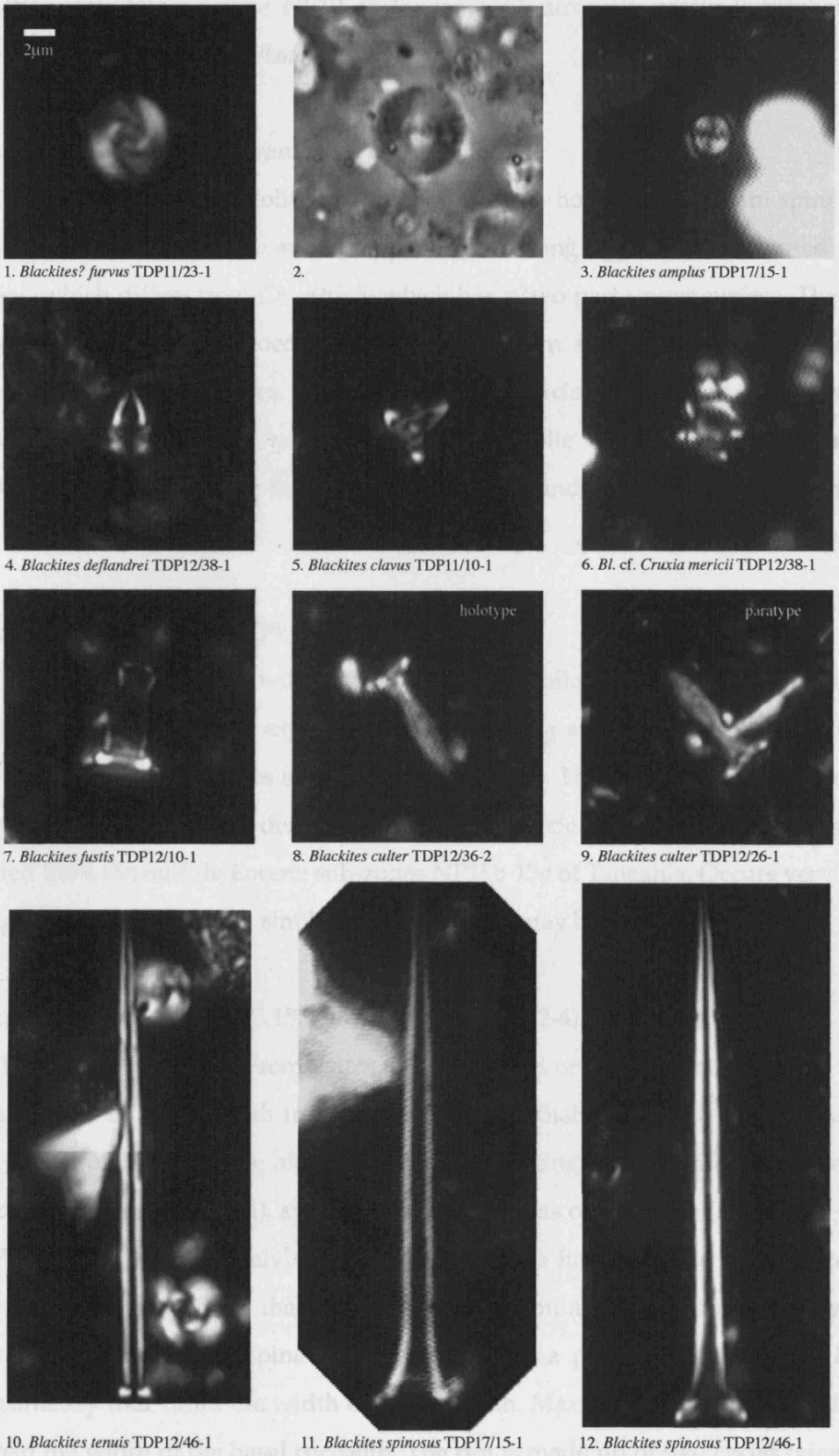

1. *Blackites? furvus* TDP11/23-1
2.
3. *Blackites amplus* TDP17/15-1
4. *Blackites deflandrei* TDP12/38-1
5. *Blackites clavus* TDP11/10-1
6. *Bl.* cf. *Cruxia mericii* TDP12/38-1
7. *Blackites fustis* TDP12/10-1
8. *Blackites culter* TDP12/36-2
9. *Blackites culter* TDP12/26-1
10. *Blackites tenuis* TDP12/46-1
11. *Blackites spinosus* TDP17/15-1
12. *Blackites spinosus* TDP12/46-1

Plate 3.15 LM images of *Blackites* coccoliths.

from the lower Eocene zone NP10 of Tanzania. Occurs very rarely throughout the sections and, similar to *Bl. deflandrei*, may be reworked.

Blackites* cf. *Cruxia mericii Varol 1989 (Pl. 3.15, fig. 6).

DESCRIPTION: Small rhabdoliths with relatively low, hollow sacculiform spines. The spine broadens from the base and is capped by a curving upper surface formed of one element, which differs from *Cr. mericii*, which has a two-part upper surface. The spine is slightly wider than the coccolith. The coccolith rim appears to be narrow and is formed of two bright cycles, whereas only one cycle is observed in *Cr. mericii*. OCCURRENCE: Previously reported from the middle Eocene sub-zone NP15b of Tanzania. Occurs very rarely throughout the sections and, similar to *Bl. deflandrei*, may be reworked.

Blackites fustis Bown 2005 (Pl. 3.15, fig. 7)

DESCRIPTION: Rhabdolith with a relatively wide, hollow ampulliform spine that is initially near parallel-sided, expands distally, reaching a width similar to that of the coccolith, and then terminates sharply in a domed top. The rim is relatively broad and the outer cycle does not lie distally over the inner cycle. OCCURRENCE: Previously reported from the middle Eocene sub-zones NP15b-15c of Tanzania. Occurs very rarely throughout the sections and, similar to *Bl. deflandrei*, may be reworked.

Blackites culter sp. nov. (Pl. 3.15, figs 8-9; Pl. 3.16, figs 2-4)

DERIVATION OF NAME: From *culter* meaning knife or spear-point, referring to the appearance of this rhabdolith in LM. DIAGNOSIS: Rhabdolith with a spine that has concave depressions running along its length, producing either a three (Y-shaped), or possibly four-fold (X-shaped), symmetry across the axis of the spine (Pl. 3.16, figs 2-4). In LM the spine is moderately dark in XPL and has a flat blade-like appearance. The spine broadens away from the coccolith to a maximum width approximately two-thirds of the way up the spine and then tapers to a point with an overall height approximately four times the width of the coccolith. Maximum spine-width is slightly less than the width of the basal coccolith. The rim is made up of two cycles lying side-by-side typical of the *Bl. morionum* group. DIFFERENTIATION: Gross morphology

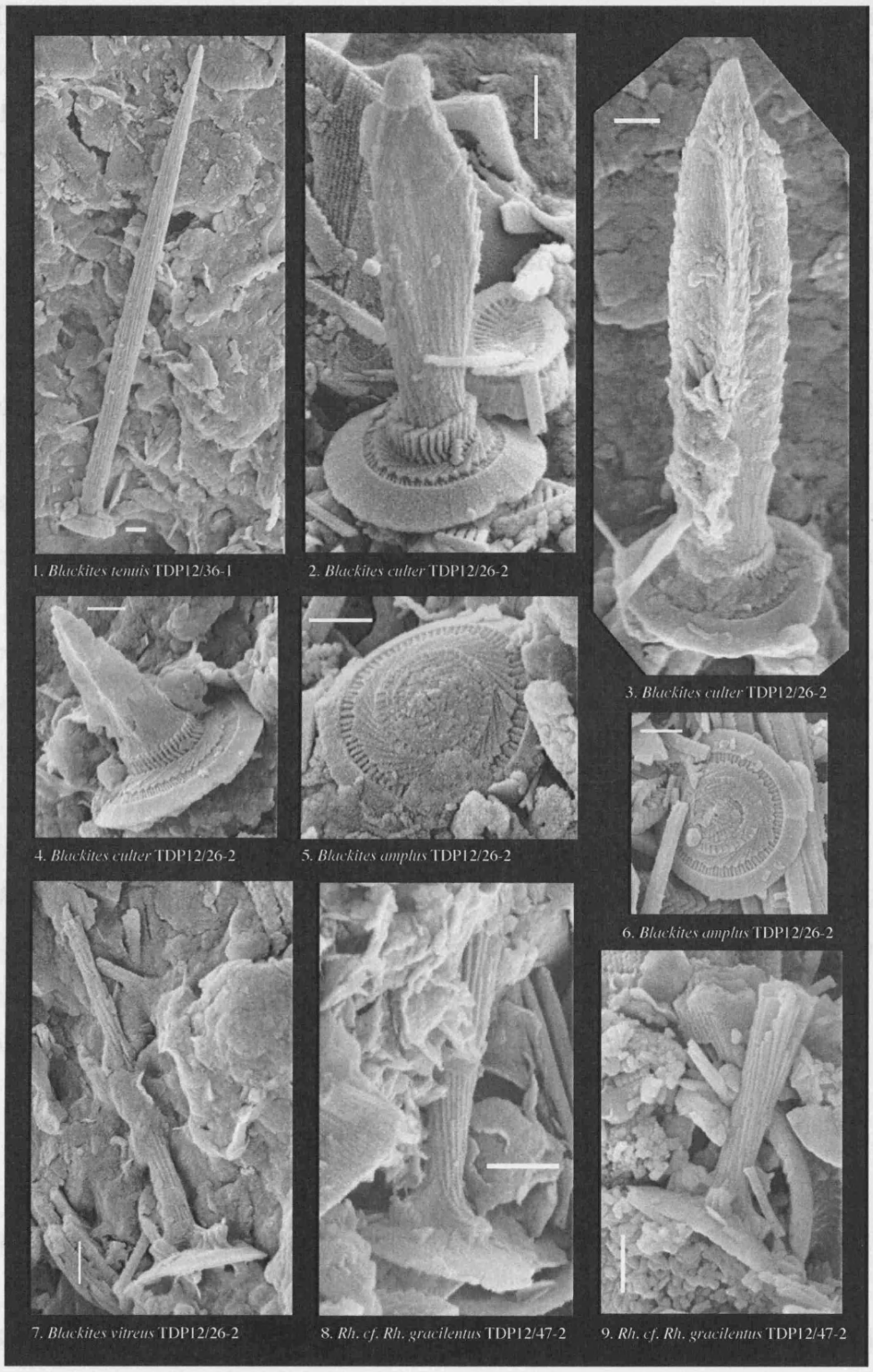

Plate 3.16 SEM images of *Blackites* and *Rhabdosphaera* coccoliths.

similar to *Bl. flammeus* Bown & Dunkley Jones 2006 in LM but *Bl. flammeus* possesses a hollow, slightly asymmetric spine whereas *Bl. culter* has a flat, blade-like spine.

DIMENSIONS: H 6.7 μm; CW 3.3 μm; SW 1.7 μm. HOLOTYPE: Pl. 3.15, fig. 8. PARATYPE: Pl. 3.15, fig. 9. TYPE LOCALITY: TDP Site 12, Pande, Tanzania. TYPE LEVEL: Upper Eocene, Sample TDP12/36-2, 70 cm (Subzone NP19/20). OCCURRENCE: Rare throughout the section; NP19/20-21; TDP Sites 11, 12, 17.

Blackites perlongus Group

Tall, narrow spines and typical *Blackites* rim.

Blackites tenuis (Bramlette & Sullivan 1961) Sherwood 1974 (Pl. 3.15, fig. 10; Pl. 3.16, fig. 1)

DESCRIPTION: Rhabdolith with a tall, narrow styliform spine that is narrow at its base, broadens slightly and then tapers to a point but is never as broad as the coccolith rim. The rim is relatively narrow with a bright inner cycle. REMARKS: Differs from *Bl. spinosus* in having a narrow base to the spine whereas *Bl. spinosus* has a wide base to the spine, from which the spine tapers continuously to a point. OCCURRENCE: Rare throughout the section.

Blackites spinosus (Deflandre & Fert 1954) Hay & Towe 1962 (Pl. 3.15, figs 11-12)

DESCRIPTION: Rhabdolith with a tall, narrow styliform spine that tapers gradually to a point. The width of the spine is around half that of the coccolith but considerable taller (x 4-6). The rim is relatively broad and distinctly convex. OCCURRENCE: Rare throughout the section.

Other *Blackites* coccoliths

Blackites vitreus (Deflandre *in* Deflandre & Fert 1954) Shafik 1981 (Pl. 3.16, fig. 7; Pl. 3.19, fig. 1)

DESCRIPTION: *Bl. vitreus* rhabdoliths are described as having a very narrow styliform spine that typically has a prominent basal collar. The coccolith is broad and thin, and dominated by the inner cycle, with the outer cycle forming only the outermost edge. REMARKS: SEM image (Pl. 3.16, fig. 7) shows the buttress-like structures at the base of the spine that appear as a "collar" in LM. It is also unclear if *Bl. vitreus* has a radial lath

cycle, if this is shown to be missing then this species should be reassigned to the genus *Rhabdosphaera*. OCCURRENCE: Rare throughout the section.

Blackites singulus Bown & Dunkley Jones 2006 (Pl. 3.19, fig. 6)

DESCRIPTION: Long, slender spine that tapers gradually from a slightly thickened broader end. The spine is birefringent when parallel with the polarizing directions and has a narrow, axial canal. REMARKS: The spine has never been observed associated with a basal coccolith. OCCURRENCE: Frequent throughout the sections becoming common in some intervals of the upper Eocene (NP19/20-21).

***Blackites* sp. 1** (Pl. 3.17, figs 6 & 8; Pl. 3.18, fig. 4)

DESCRIPTION: Small, sub-circular to elliptical rhabdoliths with a low domed process and distinct collar formed from an outwardly directed lath cycle. REMARKS: Clusters of associated rhabdoliths, presumably from the same coccosphere, show distinct variomorphism in the degree of process development from domal to distinctly conical (Pl. 3.17, fig. 8). This is similar to many extant members of the rhabdosphaeraceae, which have more pronounced processes in apical or antapical regions (cf. *Acanthoica, Cyrtosphaera, Algirosphaera,* see Young *et al.* 2003). *Blackites* sp. 1 rhabdoliths are similar to those described within the novel genera *Amitha* and *Notiocyrtolithus* from the upper Eocene-lower Oligocene of the Otway Basin, SE Australia (Shafik 1989), which all possess a distinct collar and low domed process. The principal difference observed in the Australian forms is the presence of a broadly spaced - often leaving slits between laths - more radially orientated lath cycle immediately inside of the collar. A similar, but less well developed, more radially orientated lath cycle is visible in some of the Tanzanian specimens (such as lath cycle LC^3 in Pl. 3.18, fig. 3). These forms are retained within the genus *Blackites* on the basis of their structural similarities with other members of the genus (Pl. 3.18). All *Blackites* rhabdoliths have the characteristic rim cycle and radial lath cycle, and then a variable number of lath cycles forming a spine or process. In Pl. 3.18 the lath cycles at the base of the process are labeled as LC^1, LC^2 etc and the whorls of laths that form the bulk of the process as process laths (PL). Using this scheme it becomes clear that the distinct collar observed in *Blackites* sp. 1 - formed of an outward directed, radially oriented lath cycle (LC^2) - is analogous to the vertically

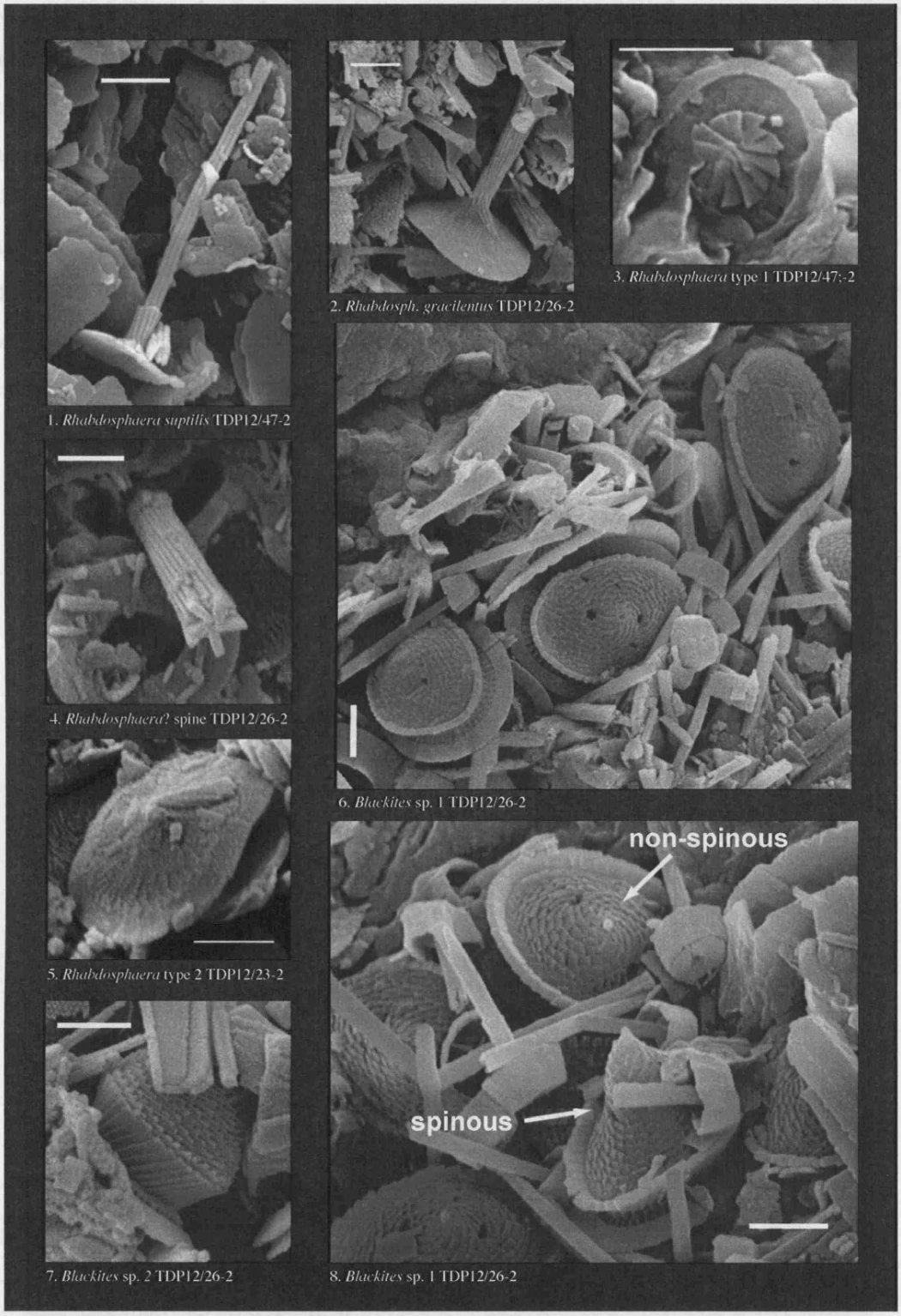

Plate 3.17 SEM images of *Blackites* and *Rhabdosphaera* coccoliths.

directed lath cycle that forms the collar in *Blackites culter* (LC3) and the horizontal, radially orientated lath cycle in *Blackites amplus* (LC2). This demonstrates both the

plasticity of the lath cycle orientation in *Blackites* but also the common structural elements between these species. Retaining all of these, and related species, within the genus *Blackites* prioritizes the similarities of rim and lath cycle construction over more subtle distinctions of lath cycle orientation and process morphology.

***Blackites* sp. 2** (Pl. 3.17, fig. 7)

DESCRIPTIONS: Small domed-shape rhabdolith seen in side view, similar to *Blackites* sp. 1 but with first lamellar cycle forming the lower part of the process rather than a distinct collar. OCCURRENCE: One observation in SEM.

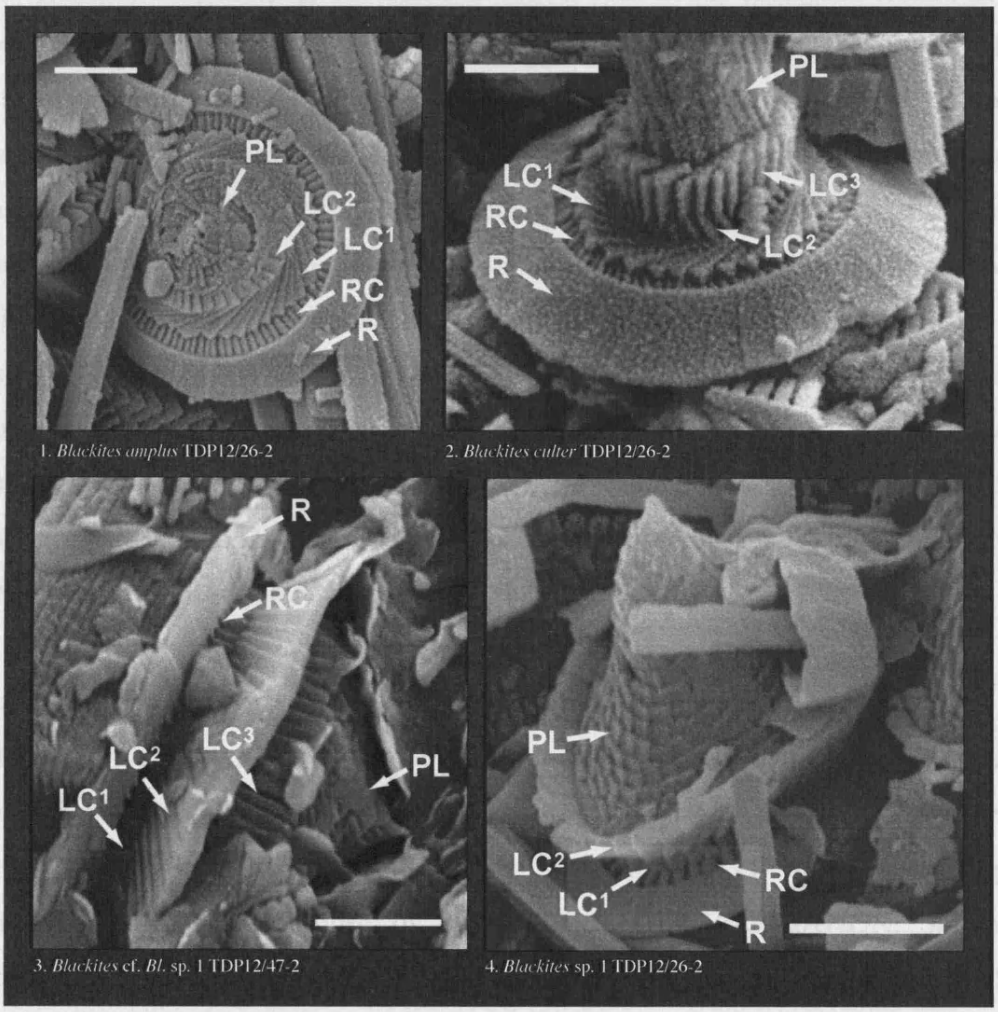

Plate 3.18 SEM images showing structural elements of *Blackites* coccoliths: R - rim cycle; RC - radial cycle; LC - lath cycles (numbered sequentially); PL - process laths.

Genus ***RHABDOSPHAERA*** Haeckel 1894

DIAGNOSIS: Form both spine and non-spine bearing rhabdoliths with no radial cycle. Lamellar cycle fills central-area and forms spine where present. REMARKS: Based on the above discussion of the genera *Blackites*, we restrict the use of the genera *Rhabdosphaera* in fossil material to spine and non-spine bearing rhabdoliths that lack a radial cycle.

Rhabdosphaera gracilentus (Bown & Dunkley Jones 2006) comb. nov. (Pl. 3.16, figs 8-9; Pl. 3.17, fig. 2; Pl. 3.19, figs 2-3)

BASIONYM: *Blackites gracilentus* Bown & Dunkley Jones 2006, p.28, pl.3, fig.21. *J. Nannoplankton Res.*, **28**(1): 17-34. DESCRIPTION: Rhabdolith coccoliths which, in LM, have a thin, narrow coccolith base and a narrow spine with an axial canal. REMARKS: In SEM the spines of *Rh. gracilentus* appear similar in morphology to the extant *Rhabdosphaera clavigera* Murray & Blackman, 1898 but with a wider, more robust spine construction and less rapidly spiraling elements (Pl. 3.17, fig. 2), whilst the rhabdolith base lacks a radial lath-cycle, hence its reassignment to *Rhabdosphaera*. Some, possible variomorphic, forms possess buttress-like structures at the base of the spine (Pl. 3.16, figs 8-9). The original description of *Bl. gracilentus* (Bown & Dunkley Jones 2006) figured a specimen from the lower Oligocene of TDP12 (pl. 3, fig. 20 in Bown & Dunkley Jones; reproduced here as Pl. 3.16, fig. 4), which is now, on the basis of SEM studies, reassigned to *Rhabdosphaera suptilis* sp. nov. described below. OCCURRENCE: Rare to frequent throughout the section.

Rhabdosphaera suptilis sp. nov. (Pl. 3.17, fig. 1; Pl. 3.19, figs 4-5)

DERIVATION OF NAME: From *suptilis* meaning fine, slender, delicate, referring to the spine of this rhabdolith. DIAGNOSIS: Small rhabdolith with a very narrow, gracile spine. A narrow collar is present at the base of the spine (Pl. 3.17 fig. 1); spine height is two to three times the width of the coccolith. DIFFERENTIATION: Similar to *Rhabdosphaera gracilentus* in LM but with a much finer, needle-like spine. In SEM differentiated from *Rh. gracilentus* by the presence of a narrow collar at the base of the spine, which is needle-like (Pl. 3.17, fig. 1), whereas the spine of *Rh. gracilentus* expands distally producing a club-shaped appearance (Pl. 3.17, fig. 2). Appears similar to spine-

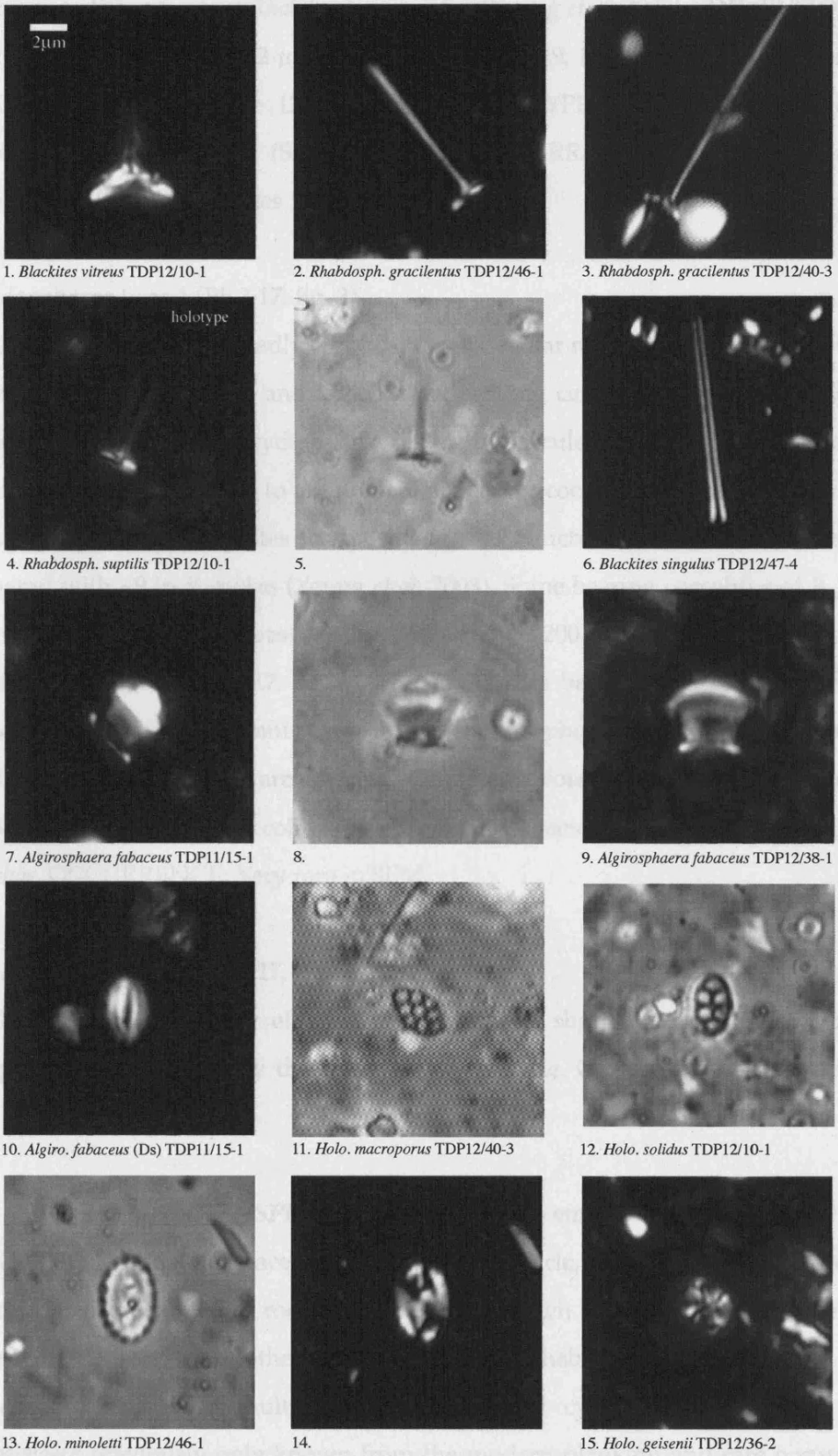

1. *Blackites vitreus* TDP12/10-1
2. *Rhabdosph. gracilentus* TDP12/46-1
3. *Rhabdosph. gracilentus* TDP12/40-3
4. *Rhabdosph. suptilis* TDP12/10-1
5.
6. *Blackites singulus* TDP12/47-4
7. *Algirosphaera fabaceus* TDP11/15-1
8.
9. *Algirosphaera fabaceus* TDP12/38-1
10. *Algiro. fabaceus* (Ds) TDP11/15-1
11. *Holo. macroporus* TDP12/40-3
12. *Holo. solidus* TDP12/10-1
13. *Holo. minoletti* TDP12/46-1
14.
15. *Holo. geisenii* TDP12/36-2

Plate 3.19 LM images of *Blackites, Rhabdosphaera, Algirosphaera* coccoliths and *Holodiscolithus* holococcoliths.

bearing coccoliths of extant *Rhabdosphaera xiphos* (Young *et al.* 2003). DIMENSIONS: H 3.3 μm; CW 2.3 μm; SW ~0.2 μm. HOLOTYPE: Pl. 3.19, fig. 4 (fig. 5 same specimen). TYPE LOCALITY: TDP Site 12, Pande, Tanzania. TYPE LEVEL: Lower Oligocene, Sample TDP12/10-1, 55 cm (Subzone NP21). OCCURRENCE: Rare throughout the section; NP19/20-21; TDP Sites 11, 12, 17.

***Rhabdosphaera* type 1** (Pl. 3.17, fig. 3)

DIAGNOSIS: Very small broadly elliptical to subcircular non-spinose rhabdolith with a narrow rim, no radial cycle and lamellar cycle filling central-area. Approximately 13 imbricate plates of lamellar cycle form a distinctive circular whorl on the distal surface. REMARKS: Appears similar to the non-spine bearing coccoliths of the extant *R. xiphos* but with more imbricate plates within the circular structure on the distal surface; ~13 compared with ~9 in *R. xiphos* (Young *et al.* 2003). Spine bearing coccoliths of *R. xiphos* have gracile spines with a basal collar (Young *et al.* 2003), similar in morphology to *Rhabdosphaera suptilis* (Pl. 3.17, fig. 1). The similarities between the spinose and non-spinose coccoliths of the extant *R. xiphos* and the morphologies of the fossil *R. suptilis* and this *Rhabdosphaera* sp. are striking. These two fossil forms may represent the spinose and non-spinose coccoliths of a dimorphic species of *Rhabdosphaera* similar to *R. xiphos*. OCCURRENCE: Very rare in SEM.

***Rhabdosphaera* type 2** (Pl. 3.17, fig. 5)

DIAGNOSIS: Small broadly elliptical to subcircular, slightly domed, *Rhabdosphaera*-type planolith dominated by the central lamellar cycle. OCCURRENCE: Very rare in SEM.

Genus ***ALGIROSPHAERA*** Schlauder 1945 emend. Norris 1984

DIAGNOSIS: Rhabdosphaeraceae rim with a radial cycle, but with a domal or double-lipped protrusion formed of rod-like elements and often covered with plate-like laths. REMARKS: Differs from other members of the Rhabdosphaeraceae, which have processes formed from multiple sets of lamellar cycles (Probert *et al.* 2007). *Algirosphaera* previously only known from the modern plankton and rare occurrences in Pleistocene sediments (Aubry, 1999; Okada & Matsuoka 1996).

Algirosphaera fabaceus (Bown & Dunkley Jones 2006) comb. nov. (Pl. 3.19, figs, 7-10; Pl. 3.20, figs 1-3; Pl. 3.21, fig. 1)

BASIONYM: *Holodiscolithus fabaceus* Bown & Dunkley Jones 2006, pl. 3, fig. 31; *Journal of Nannoplankton Research,* **28(1)**: 17-34. DIAGNOSIS: Coccolith with typical Rhabdosphaeraceae rim structure but with a low two-part sacculiform spine (a wide dome with narrower base) constructed from a series of vertical and oblique lath-like elements and with distal portion covered with multiple plate-like laths. REMARKS: First described from LM observations of the distal view of the coccolith (holotype figure is reproduced here as Pl. 3.19, fig. 10), which have now been recognized as strikingly similar to LM distal views of extant *Algirosphaera* (J. Young pers. comm.) and linked to side views in LM (Pl. 3.19, figs. 7-9) and a number of SEM images (Pl. 3.20, figs 1-3; Pl. 3.21, fig. 1). Construction of the domal protrusion is similar to the extant *Algirosphaera robusta* (Probert *et al.* 2007), however there are notable differences in both rim and process structure. The basal coccolith structure of *A. fabaceus* consists of an outer rim cycle with radial sutures (R), a radial lath cycle (RC) and a vertically-directed lamellar cycle which has anti-clockwise obliquity (LC) (Pl. 3.20, figs. 1-2). This differs from *A. robusta,* which has an additional lower outer-rim cycle as well as a set of irregular laths that cover the proximal side of the base (Probert *et al.* 2007). The two-part process of *A. fabaceus* appears to be made of up of three structural elements directly comparable to those in *A. robusta,* namely: 1) a thin outer layer of cover laths (CL), which cover the distal, domal portion of the process (Pl. 3.20, fig. 1) ; 2) multiple sets of slightly oblique laths (OL), which appear to form the bulk of the distal, domal part of the process and are organized into two discrete sets, along each side of the hood, with a central cavity running between them (Pl. 3.20, fig. 3) ; 3) a set of vertical laths (VL) that extend vertically from the lamellar cycle within the coccolith base, up to around a third of the total process-height and form the exterior of the lower, narrower part of the process (Pl. 3.20, fig. 1). There appear to be 4 or 5 regular cycles of shorter oblique laths inter-digitated with the vertical laths within the basal section of the process, which potentially extend inwards to form the internal structure of the process (Pl. 3.20, fig. 1). The structure of the process in *A. fabaceus* differs from *A. robusta* in three key ways: 1) the vertical and oblique rods of *A. robusta* are broader in *A. fabaceus*

Plate 3.20 SEM images of *Algirosphaera fabaceus* coccoliths.

(hence termed laths rather than rods) and are organized into distinct cycles, whereas in *A. robusta* they are less regularly distributed in a roughly helical arrangement; 2) *A.*

fabaceus only has cover laths over the more distal, wider, part of the spine, whereas the whole process is covered in *A. robusta;* and 3) the oblique laths in *A. fabaceus* are at a much higher angle, near the vertical, whereas they are ~45° in *A. robusta.* In LM *A. fabaceus* has a distinctly bipartite low sacculiform spine in XPL, with the lower-spine unit broadening away from the coccolith-base to a maximum width approximately equal to the basal coccolith, and an upper-spine of a two part flattened dome, which is bright in XPL (Pl. 3.19, figs 7-9). This is consistent with LM observations of *A. robusta,* where the hood is prominent and formed of crystals with vertically oriented *c*-axes - probably the oblique rods of the process. This correlates with *A. fabaceus,* where the bright (in XPL) distal dome is dominated by oblique laths and the lower, dark, section of the process is dominated by vertical laths and suggests that the vertical and oblique laths have distinct *c*-axis orientations. The rim is indistinct in XPL but appears to show a brighter inner cycle (radial cycle?) and a faint, dark outer cycle (rim?). Typically the spine height is slightly greater than the width of the coccolith. DIFFERENTIATION: In LM gross morphology is similar to *Cruxia mericii* Varol, 1989 but with less distinct elements making up the basal coccolith and lower-process, and bright distinct domal upper-process. OCCURRENCE: Rare throughout the section.

***Algirosphaera* sp. 2** (Pl. 3.21, fig. 2-3)

DIAGNOSIS: Small broadly elliptical coccolith with typical Rhabdosphaeraceae base (rim/radial cycle/lamellar cycle) and a wide open central area. Long lath-like elements protrude vertically upwards from the lamellar cycle, similar to the vertical rods in *A. fabaceus.* REMARKS: Presence of vertical rods suggest placement within *Algirosphaera* as this is the only genus within the Rhabdosphaeraceae which has vertical rods, rather than multiple helical lamellar cycles, forming part of the process (Probert *et al.* 2007). OCCURRENCE: Very rare in SEM.

***Algirosphaera*? sp.** (Pl. 3.21, figs 4)

DIAGNOSIS: Medium sized elliptical coccolith, seen in proximal view, with a narrow rim and distinct radial cycle. Central area of the proximal side of coccolith covered with multiple lath-like elements. REMARKS: Only seen in proximal view but the

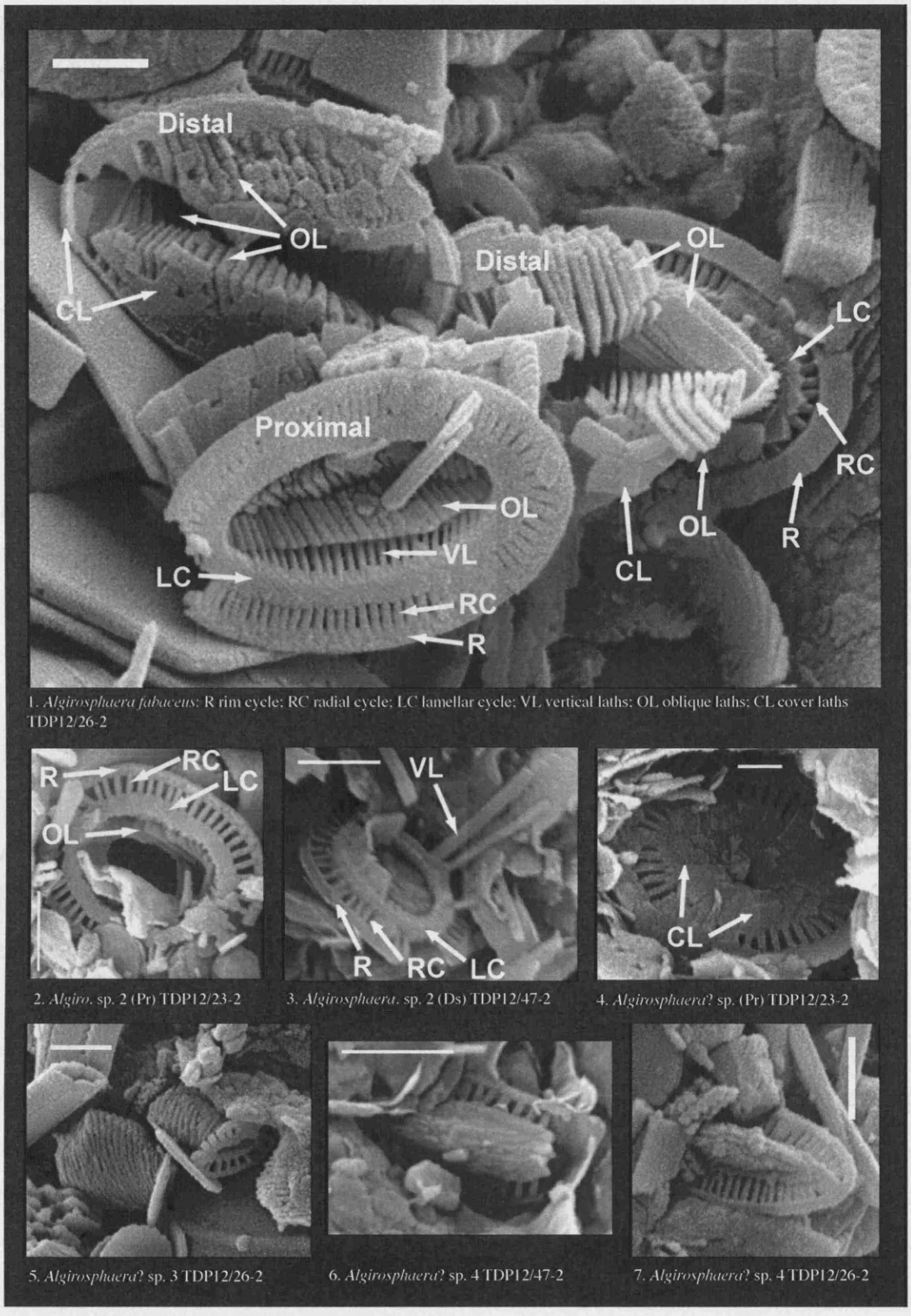

Plate 3.21 SEM images of *Algirosphaera* coccoliths.

covering of lath-like elements on the proximal side of basal coccolith similar to *A. robusta*. OCCURRENCE: One occurrence in upper Eocene zone NP19/20.

***Algirosphaera*? sp. 3** (Pl. 3.21, fig. 5)

DIAGNOSIS: Very small (~2μm) elliptical coccolith with apparently Rhabdosphaeraceae-type rim - only rim and radial cycle clearly visible - and a sacculiform process formed of multiple, helically arranged elements. REMARKS: Tentatively placed in genus *Algirosphaera* on the basis of the multiple elements forming the outer covering(?) of the process. OCCURRENCE: One occurrence in upper Eocene zone NP19/20.

***Algirosphaera*? sp. 4** (Pl. 3.21, figs 6-7)

DIAGNOSIS: Very small (~2μm) long-elliptical coccolith with apparently Rhabdosphaeraceae-type rim - only rim and radial cycle clearly visible - and low, elongate process formed of multiple elements. REMARKS: Very tentatively placed in genus *Algirosphaera* on the basis of the multiple elements forming the process, but may be correctly placed elsewhere in Rhabdosphaeraceae or Syracosphaeraceae. OCCURRENCE: Very rare in SEM.

Genus ***ACANTHOICA*** Lohmann 1903 emend. Schiller 1913 and Kleijne 1992

DIAGNOSIS: Extant forms have polymorphic coccospheres, with well-developed spines on apical and antapical coccoliths; body coccoliths have a well-developed radial cycle and a lamellar cycle that forms a variably developed protrusion.

***Acanthoica* sp.** (Pl. 3.22, figs 1-2)

DIAGNOSIS: Small (2-3μm), broadly elliptical body coccoliths with well-developed rim, radial lath and lamellar cycles. Outer rim cycle appears to be mono-cyclic with sutures oriented radially; radial cycle formed of closely spaced radial laths and lamellar cycle forms very low domed protrusion. One spine-bearing coccolith observed on collapsed coccosphere (Pl. 3.22, fig. 1). REMARKS: Body-coccolith morphology is very similar to extant *Acanthoica* species (cf. *A. quattrospina* - *A. acanthifera*) (Young *et al.* 2003) and the observation of a collapsed coccosphere with only one spine bearing coccolith is consistent with the restriction of spine-bearing coccoliths to the apical-antapical regions of modern *Acanthoica*. OCCURRENCE: Very rare in SEM.

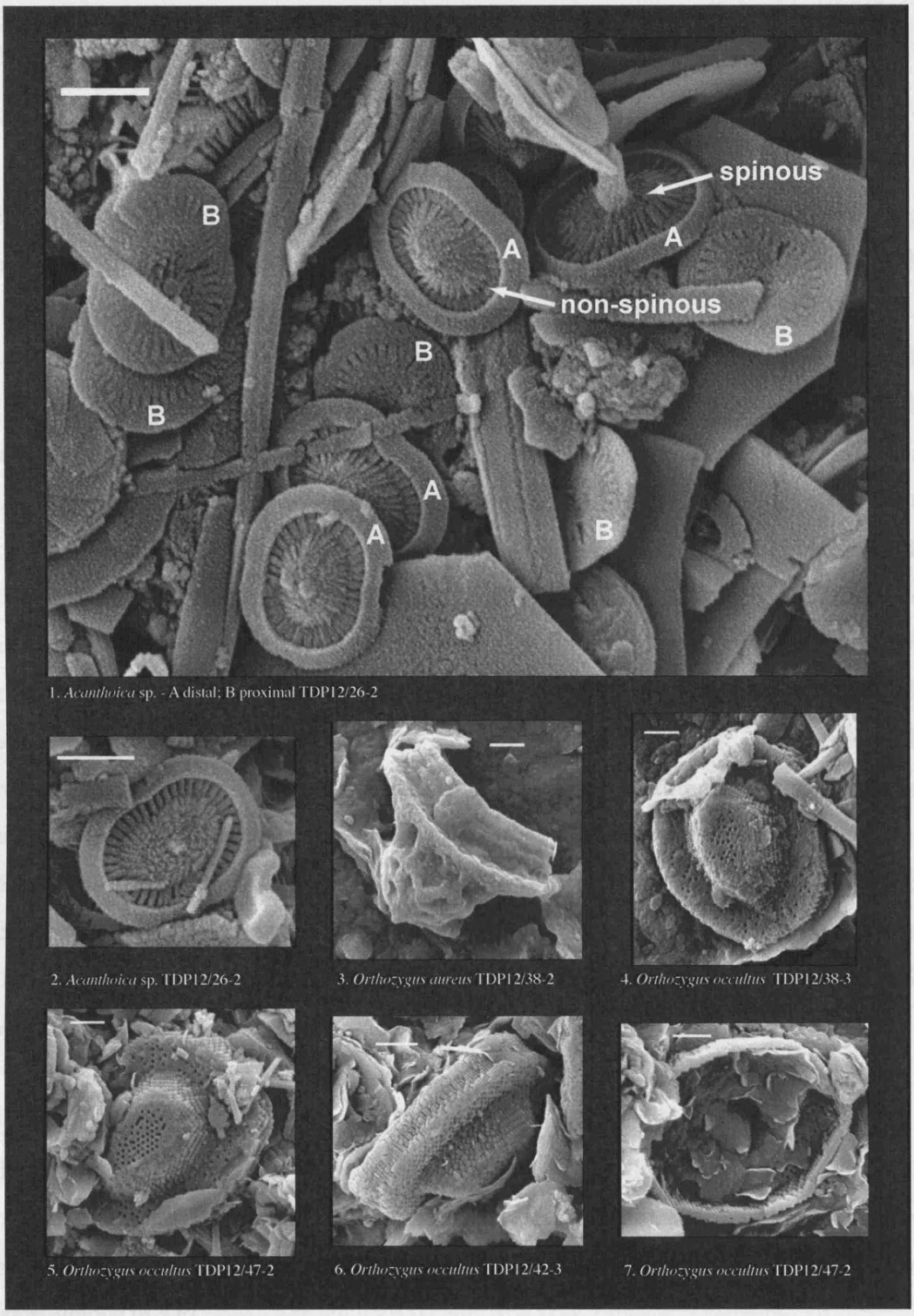

Plate 3.22 SEM images of *Acanthoica* coccoliths and *Orthozygus* holococcoliths.

3.3.3 Holococcoliths

(Formerly of the family Calyptrosphaeraceae Boudreaux & Hay 1969)

All living coccolithophores that are only known from a holococcolith-bearing stage have been traditionally included within the single family Calyptrosphaeraceae. The higher taxonomy of holococcoliths is problematical because: 1) it appears likely that most, if not all, extant holococcolith taxa will prove to have hetercoccolith equivalents; 2) the type species of this family, *Calyptrosphaera oblonga*, has now been shown to be part of the life-cycle, and junior synonym, of *Syracosphaera pulchra*, which in theory makes the Calyptrosphaeraceae a junior synonym of the family Syracosphaeraceae Lohmann, 1902; 3) the rather generalized holococcolith morphologies make taxonomically meaningful homologies difficult to identify (see Young *et al.* 2003 for further discussion). More fundamentally, the family Calyptrosphaeraceae is clearly polyphyletic making its formal use impossible (Jordan *et al.* 2004), however, the consideration of fossil holococcoliths as a single informal grouping is, at present, the only feasible approach to their taxonomy. The identification of associated fossil hetero-/holococcolith life-cycle phases by, for example, observing fossil holo-heterococcolith combination coccospheres is unlikely in the extreme. The following taxonomy is largely consistent with previous taxonomic monographs (e.g. Perch-Nielsen, 1985; Aubry, 1988), applying established generic names where possible but, for the most part, inferring limited phylogenetic information.

Genus ***HOLODISCOLITHUS*** Roth 1970

DIAGNOSIS: Elliptical non-birefringent holococcoliths with perforations. REMARKS: Following Bown (2005b) and Bown & Dunkley Jones (2006), we have employed this genus more widely to include small elliptical holococcoliths with low or no birefringence in XPL.

Holodiscolithus macroporus (Deflandre *in* Deflandre & Fert 1954) Roth 1970 (Pl. 3.19, fig. 11)

DESCRIPTION: Elliptical non-birefringent holococcoliths that appears as a dark plate pierced by a variable number of pores. OCCURRENCE: Rare throughout the section.

Holodiscolithus solidus (Deflandre *in* Deflandre & Fert 1954) Roth 1970 (Pl. 3.19, fig. 12; Pl. 3.24, fig. 4)

DESCRIPTION: Elliptical holococcoliths comprising a rim and six central area bars, which are typically weakly- or non-birefringent. The bars merge centrally to form a central ridge that bifurcates at either end. REMARKS: The specimens observed in this section resemble *H. macroporus* in LM appearing to have six circular perforations rather than holes delineated by distinct bars as seen in early Eocene forms from Tanzania (Bown 2005b). OCCURRENCE: Rare throughout the section.

Holodiscolithus minolettii Bown 2005 (Pl. 3.19, figs 13-14)

DESCRIPTION: A small, elliptical coccolith with a narrow dark rim (visible in PC) and a complexly-constructed, birefringent central-area plate with bright blocks towards each end. OCCURRENCE: Rare throughout the section.

Holodiscolithus geisenii Bown 2005 (Pl. 3.19, fig. 15)

DESCRIPTION: A small, broadly elliptical coccolith with a narrow dark rim and a weakly birefringent central-area plate, which is crossed by gently curving axial sutures. Shows low relief in PC. OCCURRENCE: Rare in the upper Eocene.

Genus ***ORTHOZYGUS*** Bramlette & Wilcoxon 1967

DIAGNOSIS: Basin-shaped holococcoliths with a central bridge. Formed of crystallites with c-axes vertical, hence appears non-birefringent in plan view.

Orthozygus occultus sp. nov. (Pl. 3.22, figs 4-7; Pl. 3.23, figs 1-3)

DERIVATION OF NAME: From *occultus*, meaning hidden, referring to the dark appearance of this holococcolith in XPL. DIAGNOSIS: Small irregularly elliptical to polygonal holococcoliths, which are dark in XPL but have distinctly high relief in PC. Appear to have a central hole in LM, which sometimes contains a poorly developed but bright (in XPL) inner cycle. SEM images show that they are constructed of multiple,

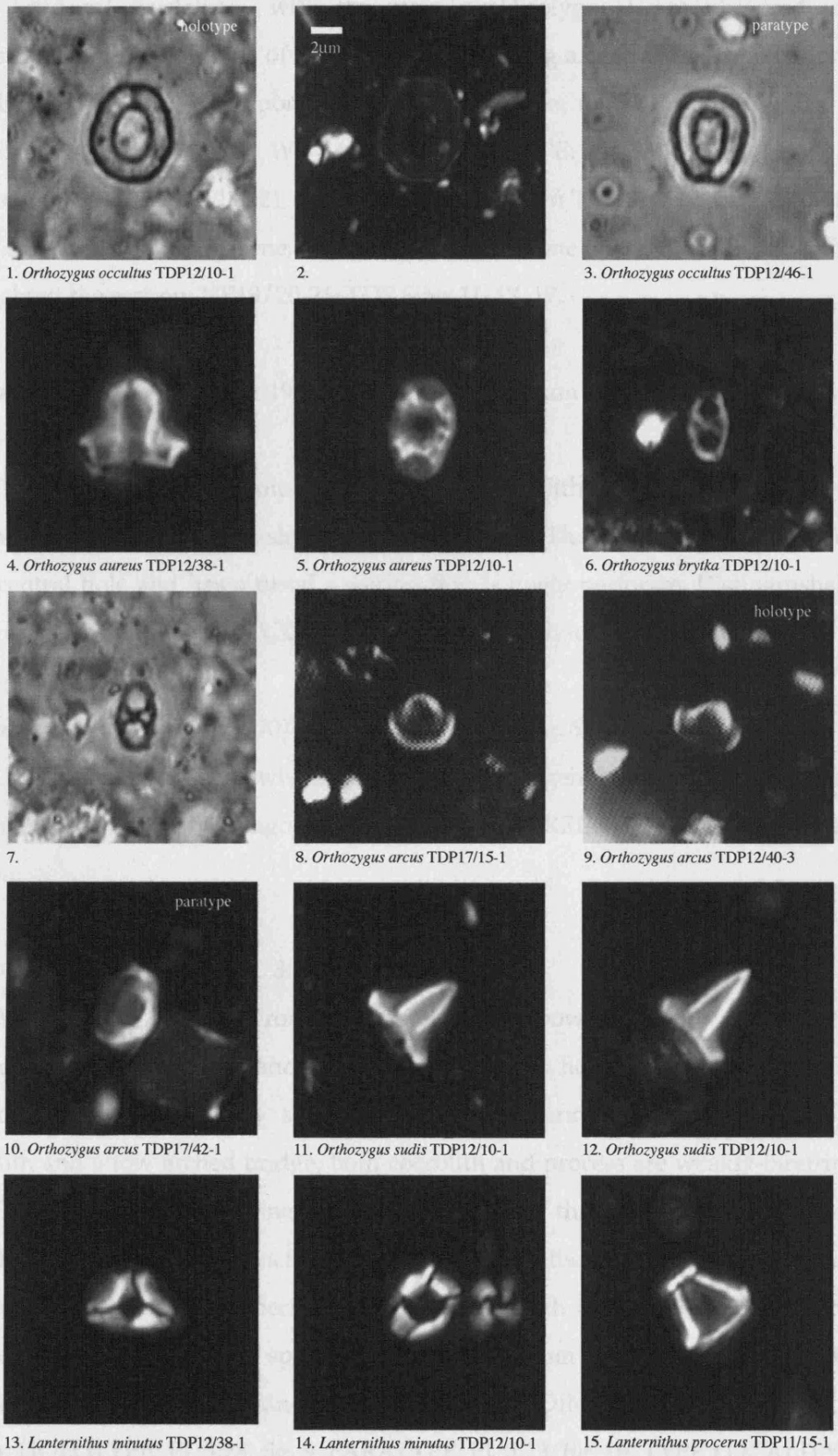

1. *Orthozygus occultus* TDP12/10-1
2.
3. *Orthozygus occultus* TDP12/46-1
4. *Orthozygus aureus* TDP12/38-1
5. *Orthozygus aureus* TDP12/10-1
6. *Orthozygus brytka* TDP12/10-1
7.
8. *Orthozygus arcus* TDP17/15-1
9. *Orthozygus arcus* TDP12/40-3
10. *Orthozygus arcus* TDP17/42-1
11. *Orthozygus sudis* TDP12/10-1
12. *Orthozygus sudis* TDP12/10-1
13. *Lanternithus minutus* TDP12/38-1
14. *Lanternithus minutus* TDP12/10-1
15. *Lanternithus procerus* TDP11/15-1

Plate 3.23 LM images of *Orthozygus* and *Lanternithus* holococcoliths.

small (<0.1μm) crystallites, with the main oval/polygonal rim observed in LM consisting of a thin, flat layer of crystallites surrounding a central, flat-topped dome on the distal side that corresponds to the 'hole' seen in LM (Pl. 3.20, figs 4-6). DIMENSIONS: L = 5.0 μm. W = 4.7 μm. HOLOTYPE: Pl. 3.21, fig. 1 (fig. 2 same specimen). PARATYPE: Pl. 3.21, fig. 3. TYPE LOCALITY: TDP Site 12, Pande, Tanzania. TYPE LEVEL: Lower Oligocene, TDP12/10-1, 55cm (Zone NP21) OCCURRENCE: Rare throughout the section; NP19/20-21; TDP Sites 11, 12, 17.

Orthozygus aureus (Stradner 1962) Bramlette & Wilcoxon 1967 (Pl. 3.22, fig. 3; Pl. 3.23, figs 4-5)

DESCRIPTION: Elliptical non-birefringent holococcolith comprising a narrow rim spanned by an arched, dome-shaped perforate bridge. The bridge is broad and pierced by a central hole and has a distal covering that is finely perforate. Distinguishable in both plan and side views. OCCURRENCE: Rare throughout the section.

Orthozygus brytika (Roth 1970) Aubry 1988 (Pl. 3.23, fig. 6)

DESCRIPTION: Small, narrowly-elliptical non-birefringent holococcolith comprising a narrow rim spanned by diagonal cross-bars. OCCURRENCE: Rare throughout the section.

Orthozygus arcus sp. nov. (Pl. 3.23, figs 8-10)

DERIVATION OF NAME: From *arcus*, meaning a 'bow' or 'arch', referring to the characteristic arched appearance of the bridge of this holococcolith. DIAGNOSIS: A holococcolith that is usually seen in oblique view and comprises of a low basal coccolith and a low arched bridge; both coccolith and process are weakly-birefringent. DIFFERENTIATION: The spine is broader and lower than that of *Orthozygus aureus* and does not have the distinct perforations seen on the distal surface of *O. aureus*. Similar crystallographic properties as *O. sudis* but with a low and smoothly arching bridge instead of pointed spine. Differentiated from *O. occultus* by its visible birefringence in XPL and distinct low arched bridge. DIMENSIONS: H = 3.2μm; W = 4.6μm. HOLOTYPE: Pl. 3.23, fig. 9. PARATYPE: Pl. 3.23, fig. 10. TYPE LOCALITY: TDP Site 12, Pande, Tanzania. TYPE LEVEL: Upper Eocene, Sample TDP12/40-3, 97cm

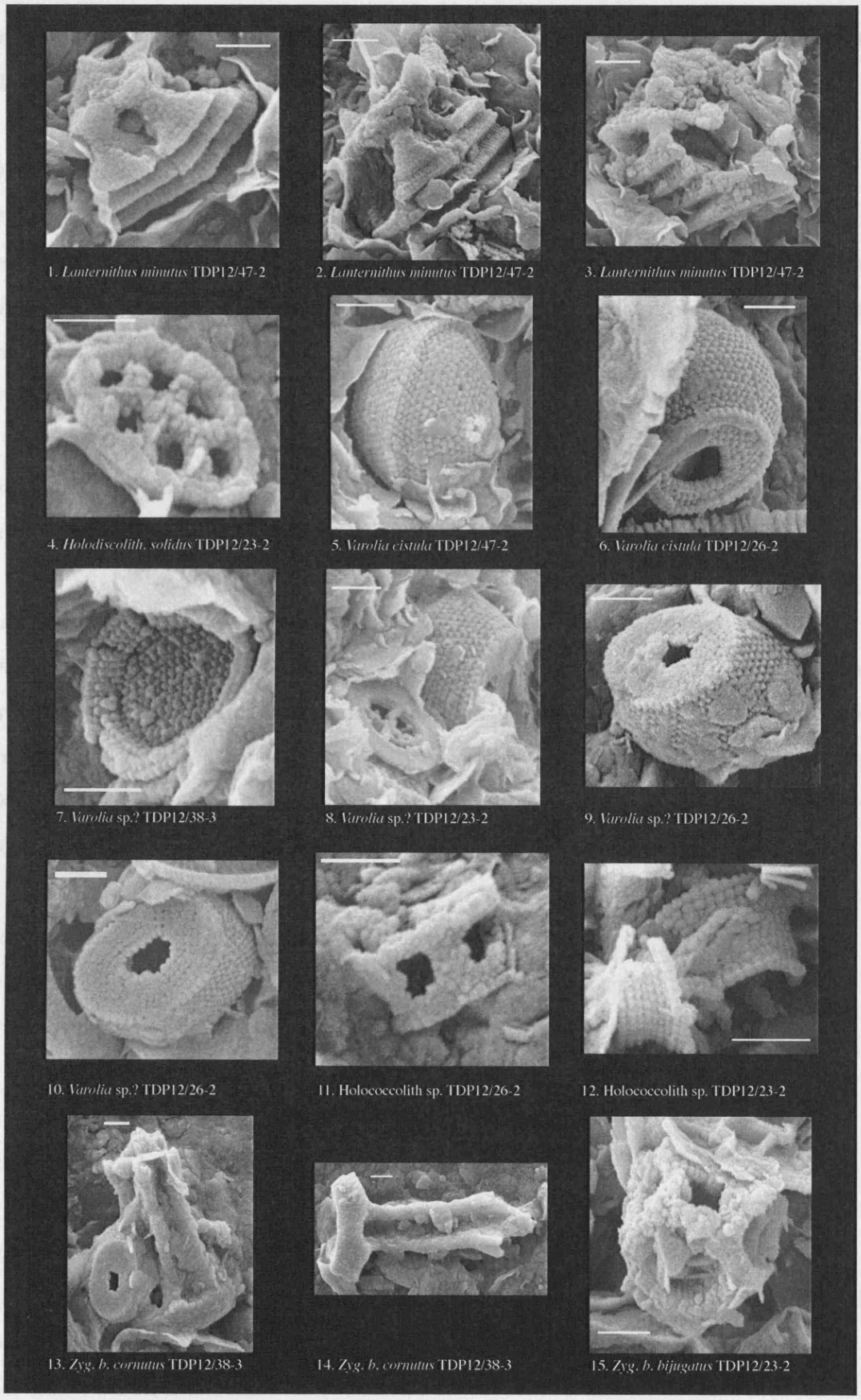

Plate 3.24 SEM images of *Lanternithus*, *Holodiscolithus*, *Varolia*, *Zygrhablithus* and unidentified holococcoliths.

(Zone NP19-20). OCCURRENCE: Rare throughout the section; NP19/20-21; TDP Sites 11, 12, 17.

Orthozygus sudis Bown & Dunkley Jones 2006 (Pl. 3.23, figs 11-12)

DESCRIPTION: A holococcolith that in side-view comprises a low basal coccolith and a relatively tall, hollow spine that tapers to a point; both coccolith and spine are birefringent and crystallographically continuous in XPL. OCCURRENCE: Rare throughout the section.

Genus ***LANTERNITHUS*** Stradner 1962

DIAGNOSIS: Cavate subhexagonal holococcoliths with a series of protruding flanges - birefringent in plan view.

Lanternithus minutus Stradner 1962 (Pl. 3.23, figs 13-14; Pl. 3.24, figs 1-3)

DESCRIPTION: Slightly rectangular holococcolith in plan view, with distinct lateral and end rim blocks and a large central pore. In side view it has a box-like appearance that tapers slightly to one (?the distal) end where it is capped by a distal cover. OCCURRENCE: Frequent to common in the upper Eocene becoming rare in the lower Oligocene.

Lanternithus procerus Bown 2005 (Pl. 3.23, fig. 15)

DESCRIPTION: Similar to *L. minutus* but elongated sides, forming a taller "process" when observed in side view. OCCURRENCE: Rare throughout the section.

Genus ***QUADRILATERIS*** Varol 1991

DIAGNOSIS: Quadrilateral birefringent holococcolith formed of four blocks.

Quadrilateris imparidividuus Varol 1991 (Pl. 3.25, fig. 1)

DESCRIPTION: A small, narrowly rectangular coccolith formed from four thin blocks that are birefringent in XPL. OCCURRENCE: Rare throughout the section.

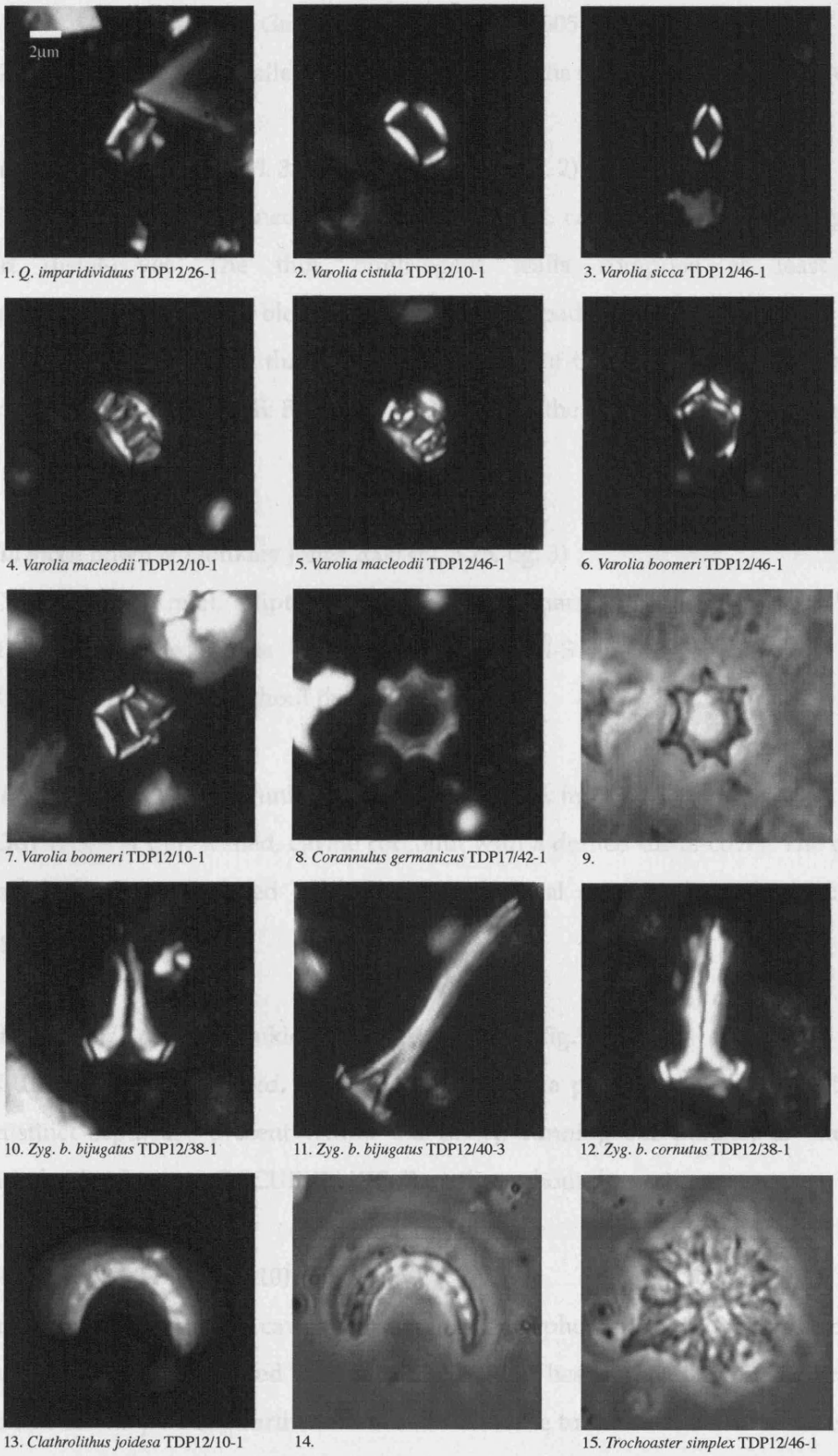

1. *Q. imparidividuus* TDP12/26-1
2. *Varolia cistula* TDP12/10-1
3. *Varolia sicca* TDP12/46-1
4. *Varolia macleodii* TDP12/10-1
5. *Varolia macleodii* TDP12/46-1
6. *Varolia boomeri* TDP12/46-1
7. *Varolia boomeri* TDP12/10-1
8. *Corannulus germanicus* TDP17/42-1
9.
10. *Zyg. b. bijugatus* TDP12/38-1
11. *Zyg. b. bijugatus* TDP12/40-3
12. *Zyg. b. cornutus* TDP12/38-1
13. *Clathrolithus joidesa* TDP12/10-1
14.
15. *Trochoaster simplex* TDP12/46-1

Plate 3.25 LM images of *Quadrilateris*, *Varolia*, *Corannulus*, *Zygrhablithus*, *Clathrolithus* and *Trochoaster* holococcoliths.

Genus *VAROLIA* Bown 2005

DIAGNOSIS: Cavate, thin walled, box-like holococcoliths usually seen in side view.

Varolia cistula Bown 2005 (Pl. 3.24, figs 5-6; Pl. 3.25, fig. 2)

DESCRIPTION: A small to medium-sized, thin-walled, cavate structure with a gently curved distal-cover. The thin, birefringent walls comprise at least four crystallographically-distinct blocks. The structure broadens distally from the basal plate and is typically wider than it is high. Formed of tiny (~0.1μm) crystallites (Pl. 3.24, fig. 5-6). OCCURRENCE: Frequent to common in the upper Eocene becoming rare in the lower Oligocene.

Varolia sicca Bown & Dunkley Jones 2006 (Pl. 3.25, fig. 3)

DESCRIPTION: A small, elliptical coccolith with a narrow, birefringent rim. When orientated at 0° the rim is crossed by narrow N-S and E-W extinction lines. OCCURRENCE: Rare throughout the section.

Varolia macleodii Bown & Dunkley Jones 2006 (Pl. 3.25, fig. 4-5)

DESCRIPTION: A thin-walled, cavate coccolith with a domed distal-cover. The cavate central-area space is spanned by at least two vertical septa. OCCURRENCE: Rare throughout the section.

Varolia boomeri Bown & Dunkley Jones 2006 (Pl. 3.25, fig. 6-7)

DESCRIPTION: A thin-walled, cavate coccolith with a pointed distal-cover. At least two distinct septa are present within the cavity, running sub-parallel to and just beneath the distal-cover. OCCURRENCE: Rare throughout the section.

Varolia? **spp.** (Pl. 3.24, figs 7-10)

A number of <3μm, simple cavate holococcolith morphologies without distal covers (calicalith-type) were observed during SEM studies. These are tentatively assigned to the genera *Varolia* pending further studies of Paleocene to middle Eocene sediments of Tanzania, which contain similar holococcolith morphologies.

Genus ***CORANNULUS*** Stradner 1962

DIAGNOSIS: Non-birefringent, discoidal holococcolith with large central opening and marginal perforations or indentations.

Corannulus germanicus Stradner 1962 (Pl. 3.25, figs 8-9)

DESCRIPTION: Ring-shaped, broadly elliptical, non-birefringent holococcolith with multiple (~7-11) thorn-like projections around the outer edge. Morphology of holococcolith clearest in PC where outer rim shows high relief. OCCURRENCE: Very rare in the upper Eocene of the section (NP19-20)

Genus ***ZYGRHABLITHUS*** Deflandre 1959

DIAGNOSIS: Spinose holococcoliths that are birefringent in side view. In plan view the coccoliths are non-birefringent with a distinct figure-of-eight shaped central structure.

Zygrhablithus bijugatus bijugatus (Deflandre *in* Deflandre & Fert 1954) Deflandre 1959 (Pl. 3.24, fig. 15; Pl. 3.25, fig. 10-11)

DESCRIPTION: Medium to large spinose holococcolith comprising a rim and central process; the spine has a narrow axial canal and tapers uniformly to a distal point or blunt termination. OCCURRENCE: Rare to frequent in the upper Eocene becoming rare to very rare in the lower Oligocene.

Zygrhablithus bijugatus (Deflandre *in* Deflandre & Fert 1954) Deflandre 1959 ***cornutus*** Bown 2005 (Pl. 3.24, figs 13-14; Pl. 3.25, fig. 12)

DESCRIPTION: Medium-sized spinose holococcolith comprising a rim and central process; the spine is relatively long, has a narrow axial canal and short lateral protrusions or horns at its distal end (two in side view). OCCURRENCE: Rare to frequent in the upper Eocene becoming rare to very rare in the lower Oligocene.

Genus ***CLATHROLITHUS*** Deflandre *in* Deflandre & Fert 1954

DIAGNOSIS: Applied here to unusual holococcoliths comprised of a domed, perforate framework.

Clathrolithus joidesa (Bukry & Bramlette 1968) Bown 2005 (Pl. 3.25, figs 13-14)

DESCRIPTION: Large, non-birefringent, c-shaped holococcolith only observed in side view. Inner margin of coccolith usually shows higher birefringence in XPL. No visible pores. OCCURRENCE: Rare throughout the section.

Genus ***TROCHOASTER*** Klumpp 1953

DIAGNOSIS: Non-birefringent, hexaradiate holococcoliths with thin radiating rays and multiple pores.

Trochoaster simplex Klumpp 1953 (Pl. 3.25, fig. 15)

DESCRIPTION: Hexagonal non-birefringent holococcolith. Six thin rays extend a short distance beyond the margin of hexagonal disc with numerous pores. Secondary shorter rays are present between each of the longer rays, which terminate at the disc edge. OCCURRENCE: Very rare in the upper Eocene.

3.3.4 Nannoliths

Family **BRAARUDOSPHAERACEAE** Deflandre 1947

DIAGNOSIS: The extant species *Braarudosphaera bigelowii* has a cell-wall covering of twelve pentaliths forming an imperforate dodecahedron. Recent molecular genetic analysis has confirmed the placement of *B. bigelowii* within the Haptophyta (Takano 2006). Extinct members of the family Braarudosphaeraceae include all pentalith nannoliths. Pentaliths have a laminar ultrastructure with c-axes tangential to pentalith outline.

Genus ***BRAARUDOSPHAERA*** Deflandre 1947

DIAGNOSIS: Pentagonal nannoliths formed of five, non-perforated trapezoidal segments; sutures between segments go to the edges of the pentagon.

Braarudosphaera bigelowii (Gran & Braarud 1935) Deflandre 1947 (Pl. 3.26, figs 1-3; Pl. 3.27, figs 1-2)

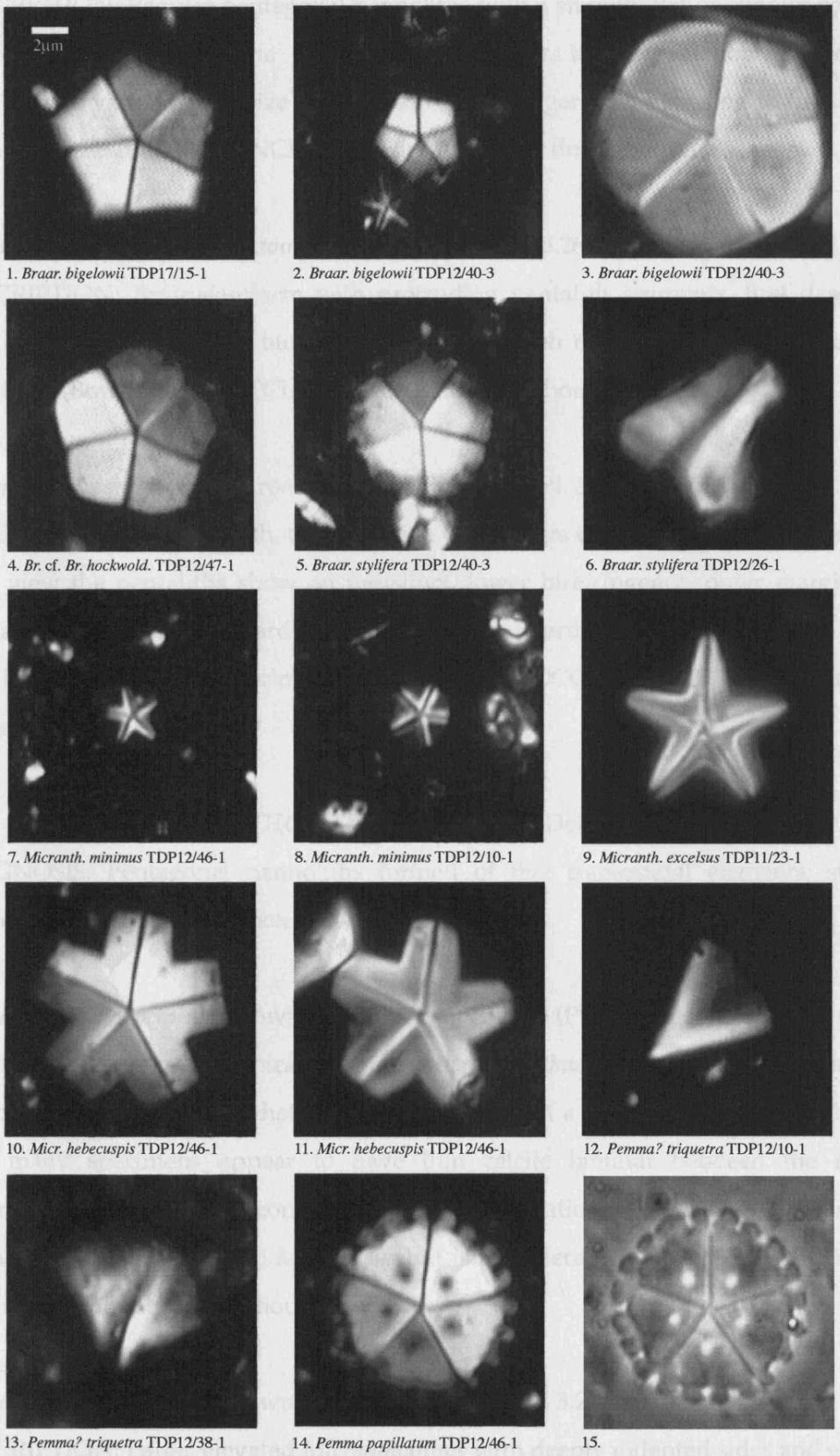

1. *Braar. bigelowii* TDP17/15-1
2. *Braar. bigelowii* TDP12/40-3
3. *Braar. bigelowii* TDP12/40-3
4. *Br.* cf. *Br. hockwold.* TDP12/47-1
5. *Braar. stylifera* TDP12/40-3
6. *Braar. stylifera* TDP12/26-1
7. *Micranth. minimus* TDP12/46-1
8. *Micranth. minimus* TDP12/10-1
9. *Micranth. excelsus* TDP11/23-1
10. *Micr. hebecuspis* TDP12/46-1
11. *Micr. hebecuspis* TDP12/46-1
12. *Pemma? triquetra* TDP12/10-1
13. *Pemma? triquetra* TDP12/38-1
14. *Pemma papillatum* TDP12/46-1
15.

Plate 3.26 LM images of *Braarudosphaera*, *Micrantholithus* and *Pemma* nannoliths.

DESCRIPTION: Regular pentagonal nannoliths with a smooth, flat or slightly concave surface. Type species of the genera *Braarudosphaera*. In these sections it shows a considerable variability in size (3.3-11.6 μm), with larger forms tending to have more rounded apices. OCCURRENCE: Frequent to common throughout the section.

Braarudosphaera* cf. *B. hockwoldensis Black 1973 (Pl. 3.26, fig. 4)
DESCRIPTION: *Braarudosphaera* with protruding pentalith segments, first described from the lower Cretaceous but present through much of the Paleogene of Tanzania (NP10-23) (Bown 2005b). OCCURRENCE: Rare throughout the section.

Braarudosphaera stylifera Troelsen & Quadros 1971 (Pl. 3.26, figs 5-6)
DESCRIPTION: Tall pentalith, which in side view tapers upwards from a wide base. In plan view the pentaliths show an indistinct, lower birefringence, outer margin and increased birefringence towards the centre. The standard pentalith morphology of the base becomes visible by altering the depth of focus. OCCURRENCE: Rare throughout the section.

Genus ***MICRANTHOLITHUS*** Deflandre *in* Deflandre & Fert 1954
DIAGNOSIS: Pentagonal nannoliths formed of five trapezoidal elements; sutures between segments go to the vertices of the pentagon.

Micrantholithus minimus Bown & Dunkley Jones 2006 (Pl. 3.26, figs 7-8; Pl. 3.27, fig. 3)
DESCRIPTION: A small (typically <4 μm) *Micrantholithus* with raised ridges along the line of the segment sutures that give the appearance of a deeply indented pentalith. In LM, many specimens appear to have thin calcite laminar between the raised, birefringent areas, which is confirmed by SEM observations (Pl. 3.27, fig. 3). This form has a similar morphology to *M. excelsus* but is considerably smaller. OCCURRENCE: Frequent to common throughout the section.

Micrantholithus excelsus Bown 2005 (Pl. 3.26, fig. 9; Pl. 3.27, fig. 5)
DESCRIPTION: Large, elevated *Micrantholithus* with deeply indented sides and gracile, long rays. SEM observations show a thin calcite laminar is present between rays at the

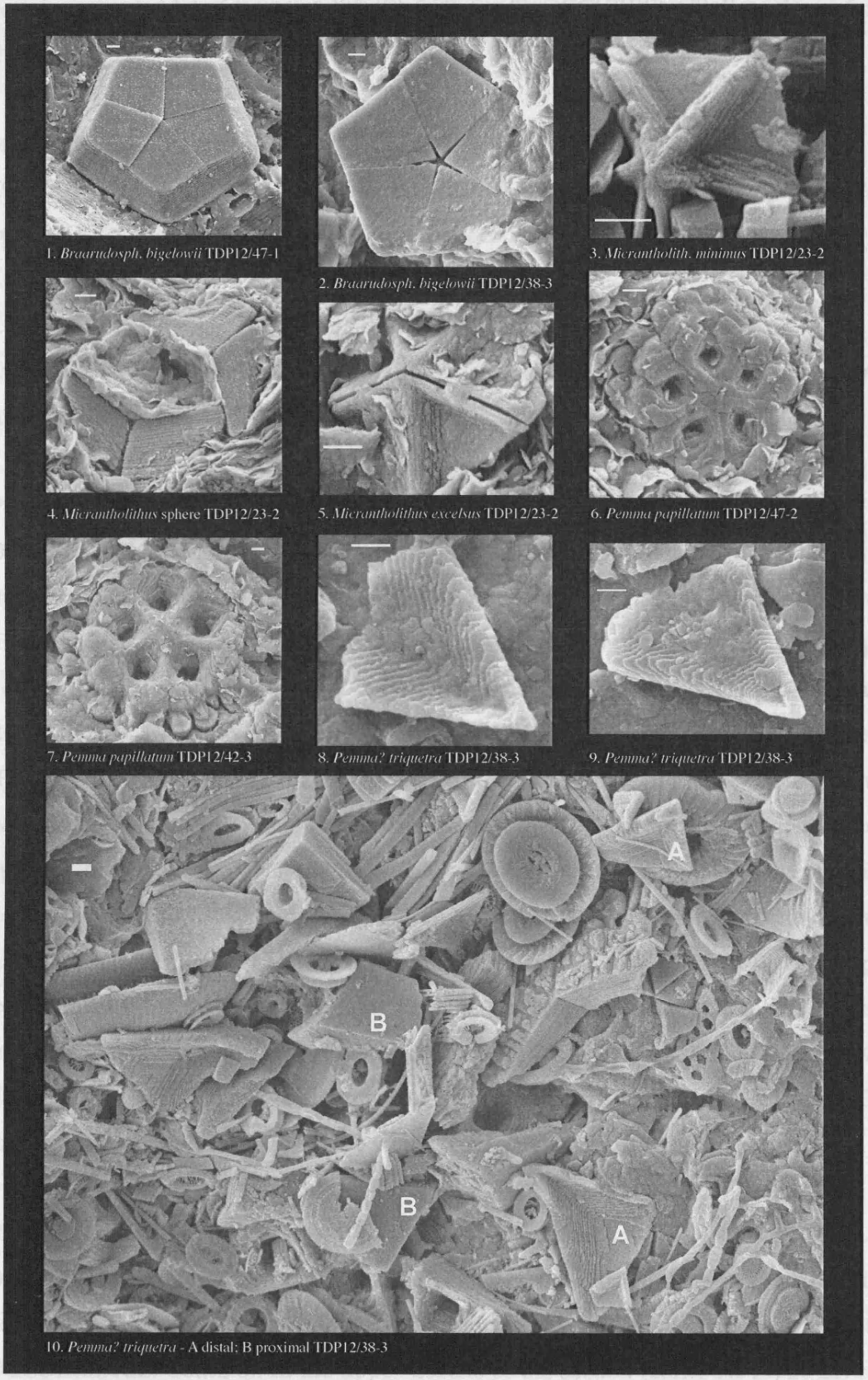

Plate 3.27 SEM images of *Braarudosphaera, Micrantholithus* and *Pemma* nannoliths.

base (proximal side) of the pentalith (Pl. 3.27, fig. 5). OCCURRENCE: Rare throughout the section.

Micrantholithus hebecuspis Bown 2005 (Pl. 3.26, figs 10-11)
DESCRIPTION: Large *Micrantholithus* with deeply indented sides and blunt, flat-ended apices. OCCURRENCE: Rare throughout the section.

Genus ***PEMMA*** Klumpp 1953

DIAGNOSIS: Pentaliths with a perforation in each segment; often producing elevated, robust structures that are commonly observed in side view.

Pemma? triquetra Bown & Dunkley Jones 2006 (Pl. 3.26, figs 12-13; Pl. 3.27, figs 8-10)
DESCRIPTION: Relatively large (typically >5 μm), triangular-shaped nannoliths that thicken along the longer sides, and exhibit low birefringence in XPL. Appear similar to disaggregated *Pemma* or *Micrantholithus* segments in LM but with a more acute angle between the longer edges (~50°-60°, compared to 72° for typical pentaliths). REMARKS: Segments have been very rarely observed lying with long-edges adjacent (Pl. 3.26, fig. 13) similar to disaggregated pentaliths but this may be a chance occurrence. The *c*-axis orientation is similar to other pentaliths, i.e., tangential, but appears to be at a higher-angle, which was the basis for the tentative generic designation. In SEM, segments are observed to consist of a series of fine calcite laminae similar to other members of the Braarudosphaeraceae (Pl. 3.27, figs 8-10). A simple explanation of the more acute opening angle and higher c-axis orientation is that these are segments of *Micrantholithus*-type pentalith with a concave base (cf. Pl. 3.27, fig. 4.). This may warrant future reassignment to the genus *Micrantholithus*. OCCURRENCE: Frequent to common throughout the section.

Pemma papillatum Martini 1959 (Pl. 3.26, figs 14-15; Pl. 3.27, figs 6-7)
DESCRIPTION: Large pentaliths with distinct perforation near the apex of each pentalith and characteristic multiple nodes along the outer margin of each pentalith. OCCURRENCE: Common in the upper Eocene of the section (zones NP19/20-21) but

with a distinct last occurrence in TDP12 ~7m below the LO Hantkeninidae, which characterizes the Eocene-Oligocene boundary.

Family **DISCOASTERACEAE** Tan 1927

DIAGNOSIS: Discoidal nannoliths with 3 to 40 elements radiating from a common centre or axis. c-axes are vertical hence nannoliths, in plan view, are non-birefringent in XPL.

Genus ***DISCOASTER*** Tan 1927

DIAGNOSIS: Star or rosette shaped nannofossils with low birefringence in XPL.

Discoaster saipanensis Bramlette & Riedel 1954 (Pl. 3.28, figs 1-2)

DESCRIPTION: Discoaster with normally six or seven straight or curved rays joined through half their length and which then taper to a point. A central boss and distinct radial sutural ridges and depressions are visible in some specimens (Pl. 3.28, fig. 1). OCCURRENCE: Rare through upper Eocene zone NP19/20; LO defines the top of NP19/20.

Discoaster tanii Bramlette & Riedel 1954 (Pl. 3.28, fig. 3)

DESCRIPTION: Typically five-rayed discoaster with rays of uniform width terminating in a flat or slightly notched ray-end. May show poorly developed unpaired lateral nodes on some rays but does not have the regular paired ray-nodes of *D. nodifer*. This form has close morphological affinities to and may intergrade with *Discoaster nodifer* and *D. ornatus*, which are frequently classified as subspecies or closely related species of *Discoaster tanii*. OCCURRENCE: Rare throughout the section.

Discoaster nodifer Bramlette & Riedel 1954 (Pl. 3.28, figs 4-5)

DESCRIPTION: Potentially 6-9 but typically six-rayed discoaster with rays of uniform width and blunt or notched ray-ends. Differentiated from *D. tanii* by the consistent presence of well-developed paired ray-nodes on all rays. OCCURRENCE: Rare throughout the section.

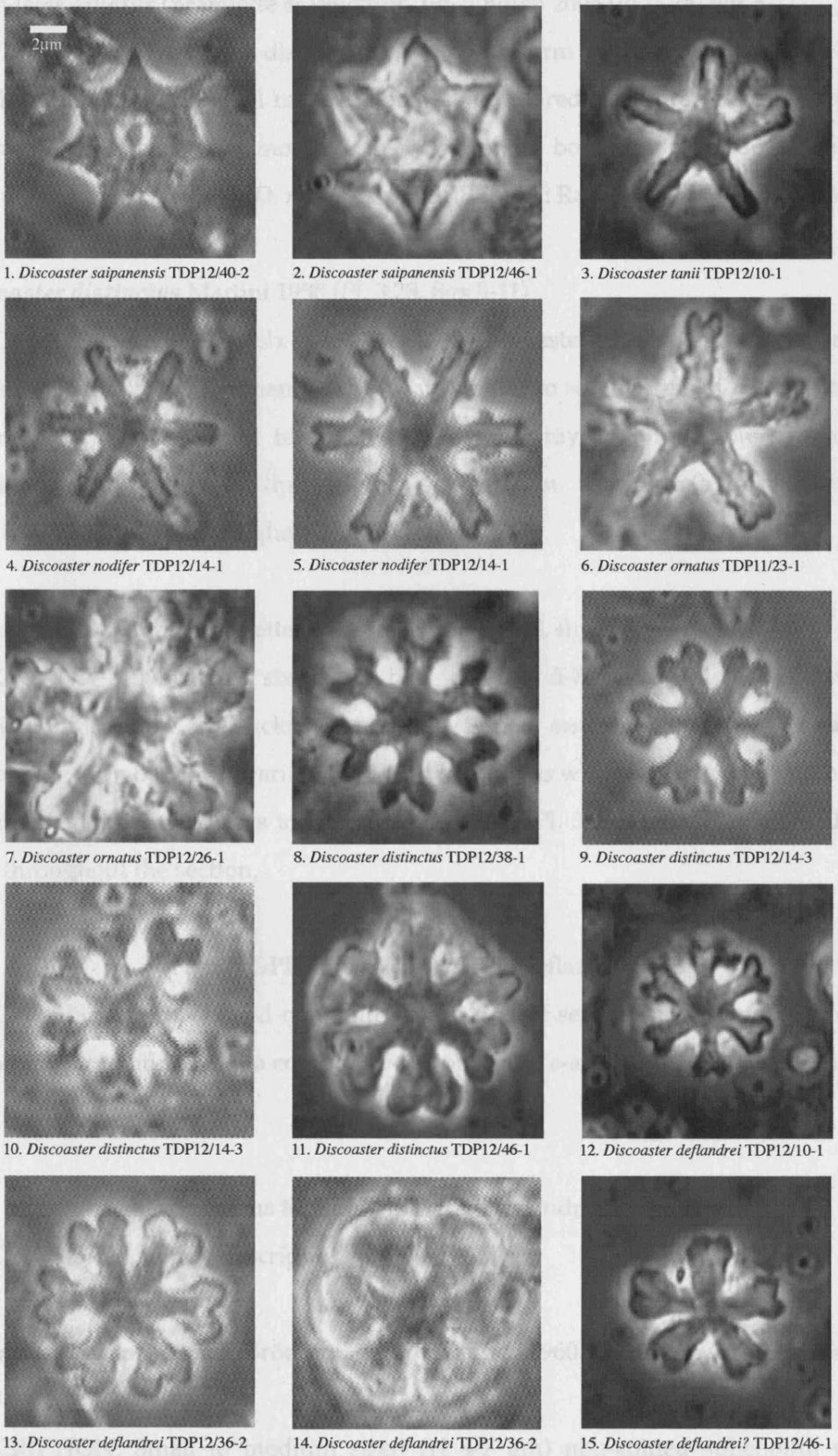

1. *Discoaster saipanensis* TDP12/40-2
2. *Discoaster saipanensis* TDP12/46-1
3. *Discoaster tanii* TDP12/10-1
4. *Discoaster nodifer* TDP12/14-1
5. *Discoaster nodifer* TDP12/14-1
6. *Discoaster ornatus* TDP11/23-1
7. *Discoaster ornatus* TDP12/26-1
8. *Discoaster distinctus* TDP12/38-1
9. *Discoaster distinctus* TDP12/14-3
10. *Discoaster distinctus* TDP12/14-3
11. *Discoaster distinctus* TDP12/46-1
12. *Discoaster deflandrei* TDP12/10-1
13. *Discoaster deflandrei* TDP12/36-2
14. *Discoaster deflandrei* TDP12/36-2
15. *Discoaster deflandrei?* TDP12/46-1

Plate 3.28 LM images of *Discoaster* nannoliths.

Discoaster ornatus (Bramlette & Wilcoxon 1967) Bown 2005 (Pl. 3.28, figs 6-7)

DESCRIPTION: Five-rayed discoaster, rays of uniform width with well-developed, slightly bifurcating, terminal ray-end notches and paired lateral ray-nodes. *D. ornatus* tends to have thicker rays, more conspicuous central boss and better developed ray-end notches than *D. tanii* or *D. nodifer*. OCCURRENCE: Rare throughout the section.

Discoaster distinctus Martini 1958 (Pl. 3.28, figs 8-11)

DESCRIPTION: Five or six-rayed stellate discoasters with prominent ray-tip bifurcations that resemble spanners. Appears similar to some forms of *D. deflandrei* but has rays of uniform width terminated by distinct ray-tip bifurcations whereas *D. deflandrei* often has rays that slightly increase in width towards the ray-tip. OCCURRENCE: Rare throughout the section.

Discoaster deflandrei Bramlette & Riedel 1954 (Pl. 3.28, fig. 12-15)

DESCRIPTION: Normally six-rayed, but includes 5-7 rayed, discoasters with a terminal bifurcation but lacking a well-developed central boss. The general ray-morphology can be highly variable between specimens with some showing a moderate to extreme widening of rays towards the ray-ends (Pl. 3.28, fig. 14). OCCURRENCE: Rare throughout the section.

Family **SPHENOLITHACEAE** Deflandre 1952

DIAGNOSIS: Conical-shaped nannoliths consisting of several superimposed cycles of elements all radiating from a common point of origin. *c*-axes of the elements run along their length.

Genus ***SPHENOLITHUS*** Deflandre 1952

DIAGNOSIS: See family description.

Sphenolithus moriformis (Brönnimann & Stradner 1960) Bramlette & Wilcoxon 1967 (Pl. 3.29, figs 1-2)

DESCRIPTION: Small to medium sized (H 4-7 μm) non-spined sphenolith with a domed upper surface. OCCURRENCE: Frequent to common throughout the section;

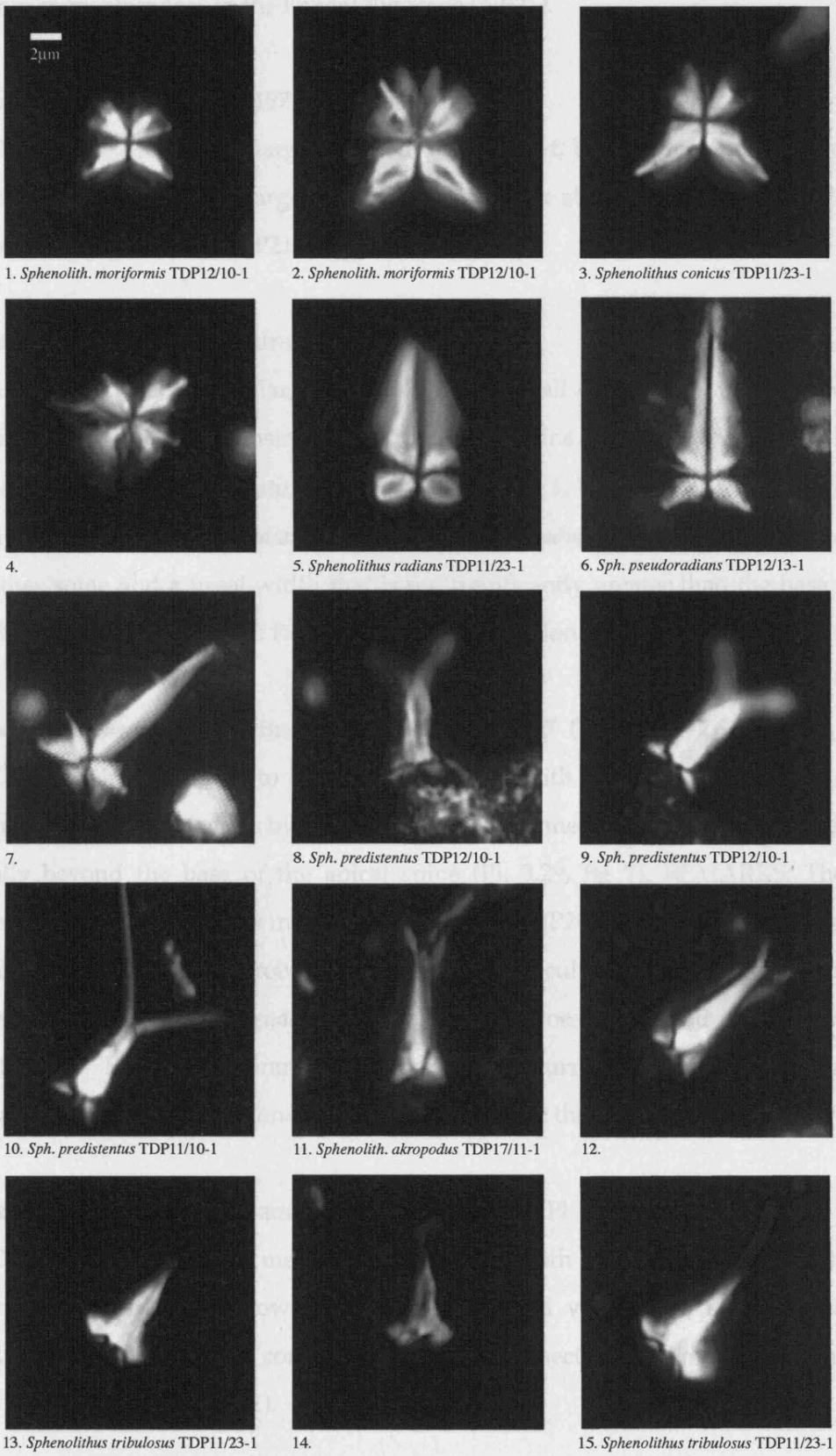

1. *Sphenolith. moriformis* TDP12/10-1
2. *Sphenolith. moriformis* TDP12/10-1
3. *Sphenolithus conicus* TDP11/23-1
4.
5. *Sphenolithus radians* TDP11/23-1
6. *Sph. pseudoradians* TDP12/13-1
7.
8. *Sph. predistentus* TDP12/10-1
9. *Sph. predistentus* TDP12/10-1
10. *Sph. predistentus* TDP11/10-1
11. *Sphenolith. akropodus* TDP17/11-1
12.
13. *Sphenolithus tribulosus* TDP11/23-1
14.
15. *Sphenolithus tribulosus* TDP11/23-1

Plate 3.29 LM images of *Sphenolithus* nannoliths.

becomes more abundant in the lower Oligocene (NP21).

Sphenolithus conicus Bukry 1971 (Pl. 3.29, figs 3-4)

DESCRIPTION: Medium to large sphenolith with short, blunt spine and broad robust base. Lower quadrants are large and the spine is dark at 0°. OCCURRENCE: Rare in the lower Oligocene (zone NP21) of the section.

Sphenolithus radians Deflandre 1952 (Pl. 3.29, fig. 5)

DESCRIPTION: Medium to large sphenolith with a tall compound spine and square shaped base with equidimensional quadrants. The spine is dark but visible at 0° and characterized by a median suture line; at 45° the spine is brightest. Difficult to reliably distinguish from *S. pseudoradians*; in this section *S. radians* is used for forms with a smoother spine and a basal-width that is not significantly greater than the base of the apical spine. OCCURRENCE: Rare throughout the section.

Sphenolithus pseudoradians Bramlette & Wilcoxon 1967 (Pl. 3.29, figs 6-7)

DESCRIPTION: Medium to large sphenolith with a tall compound spine. Distinguished from *S. radians* by its more irregular outline and apical cycles that extend laterally beyond the base of the apical spine (Pl. 3.29, fig 7). REMARKS: The first occurrence of *S. pseudoradians* marks the base of zone NP20 (Martini 1971), however the application of this event is problematic due to the difficulties in reliably distinguishing between *S. radians* and *S. pseudoradians*. This section does not extend far enough back into the late Eocene to comment on the first occurrence of *S. pseudoradians* as recognized within these sections. OCCURRENCE: Rare throughout the section.

Sphenolithus predistentus Bramlette & Wilcoxon 1967 (Pl. 3.29, figs 8-10)

DESCRIPTION: Small to medium sized sphenolith (H 3.4-7.5 μm excluding bifurcations) with tall, narrow bifurcating spine and very short, lower quadrants. OCCURRENCE: Frequent to common throughout the section; becomes more abundant in the lower Oligocene (NP21).

Sphenolithus akropodus de Kaenel & Villa 1996 (Pl. 3.29, figs 11-12)

DESCRIPTION: Medium to large sphenolith with a long tapering apical spine, sometimes bifurcated, and short laterally extending proximal elements forming two pointed feet. In XPL the spine is bright at 45° and weakly birefringent at 0°. Differentiated from *S. predistentus* by the appearance of the basal elements in XPL; at 45° to crossed nicols the basal elements of *S. akropodus* form two bright pointed feet that appear imbedded into the spine (Pl. 3.29, fig. 12), in *S. predistentus* the basal elements form two smaller feet that appear distinct from the main spine of the sphenolith (Pl. 3.29, figs 9-10). OCCURRENCE: Previously reported from lower Oligocene zones NP22 and NP23 of ODP Site 900, Iberia Abyssal Plain; rare in the lower Oligocene zone NP21 of TDP Site 17.

Sphenolithus tribulosus Roth 1970 (Pl. 3.29, figs 13-15)

DESCRIPTION: Like *Sphenolithus predistentus* but the basal part of the sphenolith is considerably broader than the spine, giving an inverted T-shaped outline. OCCURRENCE: Rare throughout the section.

3.3.5 Incertae sedis nannoliths

Pemma? uncinatus Bown & Dunkley Jones 2006 (Pl. 3.30, figs 1-8)

DESCRIPTION: Large (typically >7 μm), triangular-, rectangular- or rhomb-shaped nannoliths, which are thickened along two sides ('base' and 'side') to give a hook-shaped appearance, with a faintly birefringent 'back'. *c*-axis orientation is radial, i.e., parallel with the long axis. SEM imaging shows they are formed of layered rods/ lamellae, which thicken to produce the higher birefringence 'base' and 'side'. Generic designation is almost certainly incorrect, however it is premature to propose a new generic name for this form until its nature is better understood. OCCURRENCE: Rare to frequent throughout the section.

Genus ***POCILLITHUS*** gen. nov.

TYPE SPECIES: *Pocillithus spinulifer* sp. nov. DERIVATION OF NAME: From *pocillum*, meaning 'little cup', referring to murolith structure of these coccoliths. DIAGNOSIS:

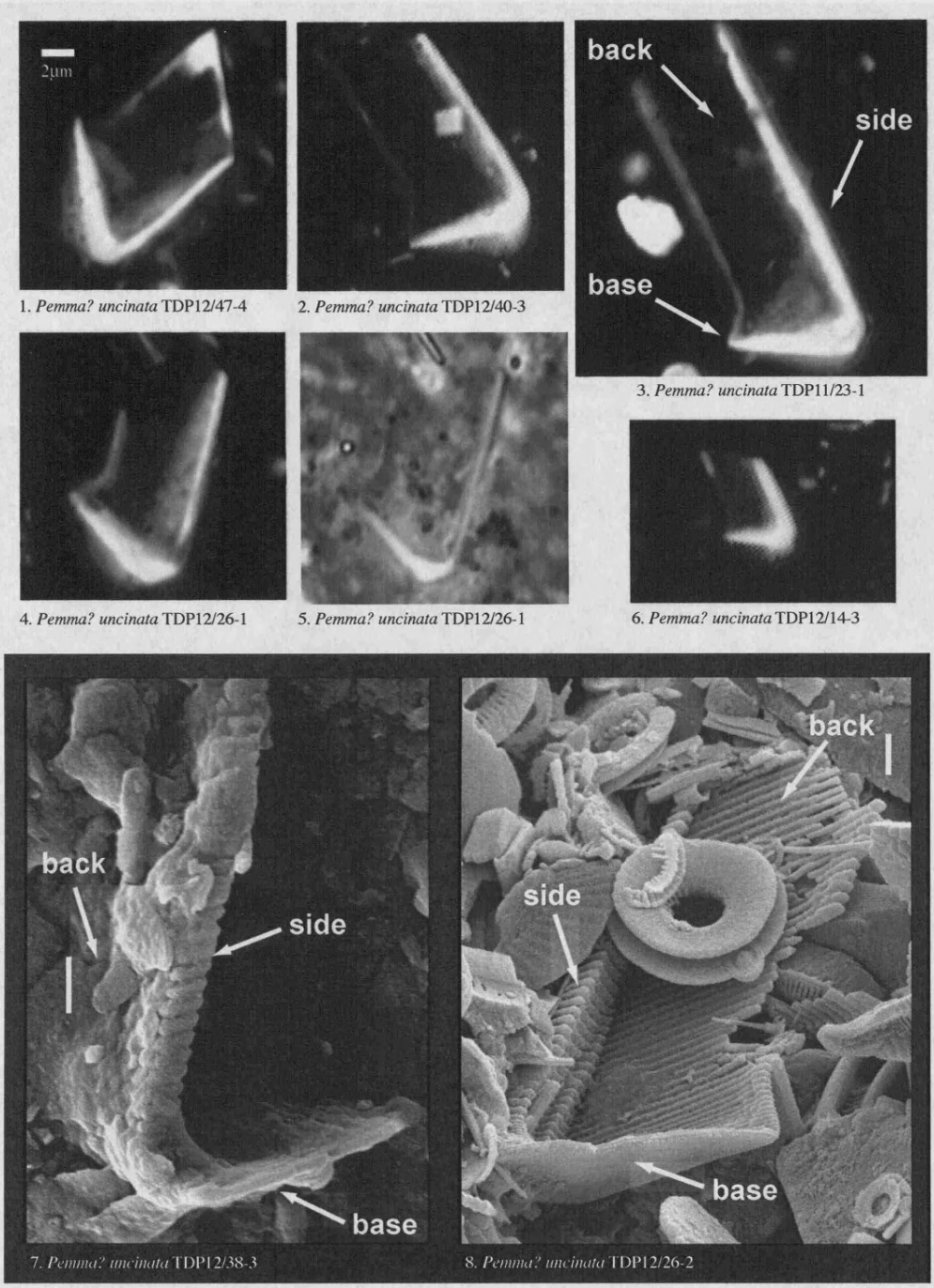

1. *Pemma? uncinata* TDP12/47-4
2. *Pemma? uncinata* TDP12/40-3
3. *Pemma? uncinata* TDP11/23-1
4. *Pemma? uncinata* TDP12/26-1
5. *Pemma? uncinata* TDP12/26-1
6. *Pemma? uncinata* TDP12/14-3
7. *Pemma? uncinata* TDP12/38-3
8. *Pemma? uncinata* TDP12/26-2

Plate 3.30 LM and SEM images of incertae sedis nannolith *Pemma? uncinata*.

Miniscule to small murolith coccoliths which have tall narrow spines in the type species *Poncillithus spinulifer* that extend from a small basal disc. They have a narrow, axial canal and are usually seen in side view.

Pocillithus spinulifer sp. nov. (Pl. 3.31, figs 1-5)

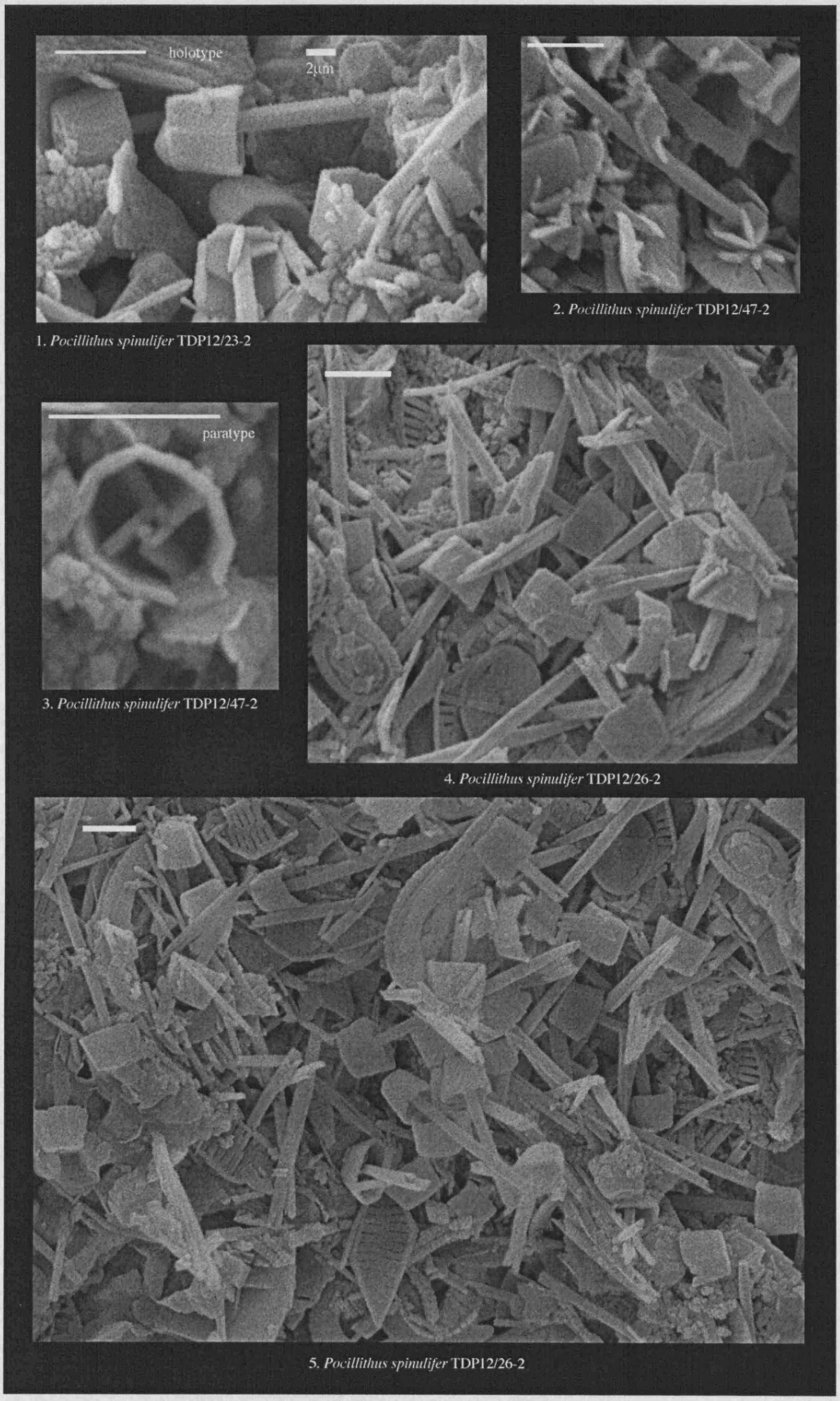

Plate 3.31 SEM images of incertae sedis nannolith *Pocillithus spinulifer*.

DERIVATION OF NAME: From *spinula,* meaning 'small spine' and referring to the tall spines of these coccoliths. DIAGNOSIS: Miniscule to very small murolith (protolith) coccoliths with high, narrow walls and a central areas spanned by an axial cross bearing tall, hollow, near-parallel-sided spines. The coccoliths have not been unequivocally observed in the light microscope. DIFFERENTIATION: Rather similar to the simple murolith coccolith of the early Mesozoic but also shares some characters with extant narrow-rimmed muroliths with affinities to the Pappospheraceae (Young *et al.* 2003), i.e. a small, murolith coccolith with a hollow, square spine, protruding from a central-area cross formed of four simple crystal units. DIMENSIONS: L = 6.0-7.0μm. HOLOTYPE: Pl. 3.31, fig. 1. PARATYPE: Pl. 3.31, fig. 3. TYPE LOCALITY: TDP Site 12, Pande, Tanzania. TYPE LEVEL: Upper Eocene, Sample TDP12/23-2, 79 cm (Zone NP21). OCCURRENCE: Commonly observed in SEM; has also been observed in sediments from TDP Sites 14, 16b, 13, 2, 12 (NP9-21).

Genus ***GLADIOLITHUS*** Jordan & Chamberlain 1993

DIAGNOSIS: Dimorphic deep photic zone extant coccolithophore with basal elliptical plates formed of two elements (lepidoliths) and long hexagonal-section spine.

Gladiolithus flabellatus (Halldal & Markali 1955) Jordan & Chamberlain 1993 (Pl. 3.32, figs 1-3; Pl. 3.33, figs 1-3)

DESCRIPTION: *Gladiolithus* with oval lepidoliths formed from two equidimensional elements joined along a transverse suture. The tube processes are narrow, elongate and free of external ornament. The lepidoliths are very small (<2 μm), smooth on both sides, often observed separating into their constituent elements, and are indistinguishable from those of the living species, *G. flabellatus* (see Pl. 3.32, fig. 1, collected from the Hawaii Ocean Time Series station at 180m, May 2005, courtesy of Jeremy Young). The tube processes are long, narrow and gently tapering, and formed from five to six elongate elements. The elongate elements gently taper, and are narrowest at the proximal end where they terminate bluntly, and widest at the distal end where they have triangular terminations. They are smooth on the inner and outer surfaces but typically have fine serrations along one of the long edges. The lith morphologies, dimensions and coccosphere shape do not differ significantly from

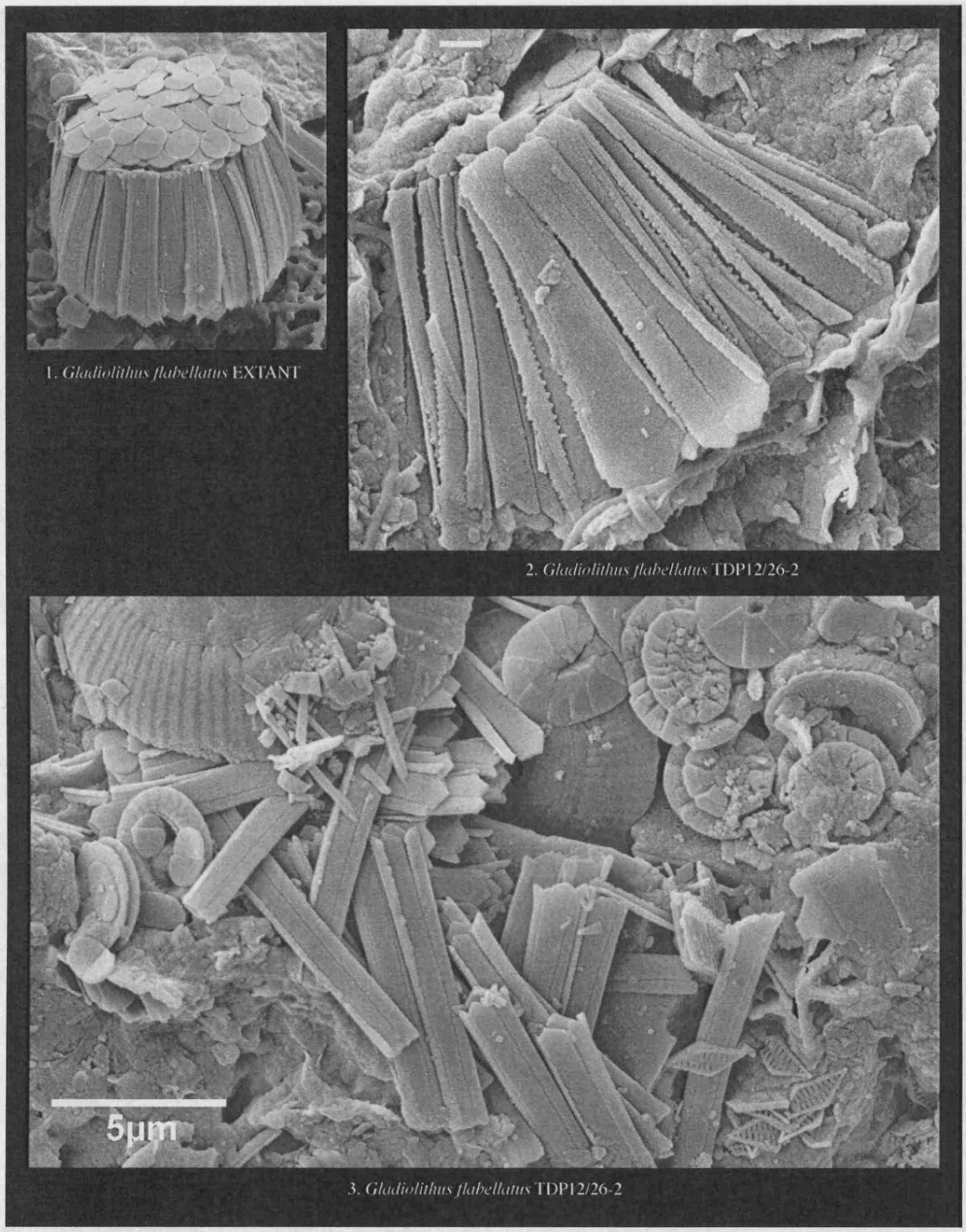

Plate 3.32 SEM images of incertae sedis nannolith *Gladiolithus*.

modern specimens of *G. flabellatus*. Two additional morphotypes, with "short" and "long" tube processes, were consistently observed in SEM (Pl. 3.33, figs 1-3) - these may be additional species as the extant *G. flabellatus* does not show significant variation in process length either within or between coccospheres. OCCURRENCE: Rare to frequent, in SEM studies of rock chip surfaces from the late Eocene of TDP12 (NP19/20-21).

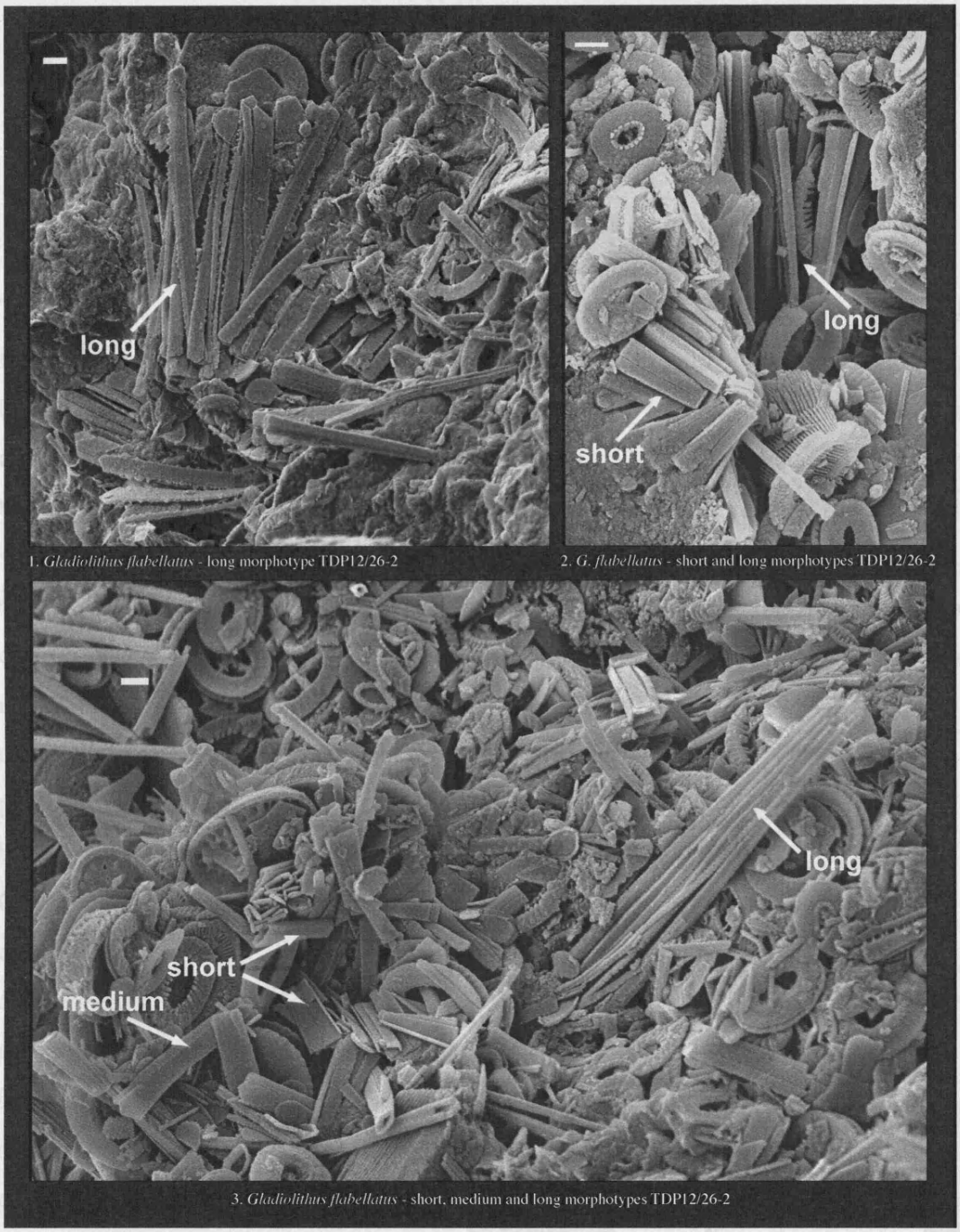

1. *Gladiolithus flabellatus* - long morphotype TDP12/26-2

2. *G. flabellatus* - short and long morphotypes TDP12/26-2

3. *Gladiolithus flabellatus* - short, medium and long morphotypes TDP12/26-2

Plate 3.33 SEM images of incertae sedis nannolith *Gladiolithus* (long and short morphotypes).

4. NANNOFOSSIL ASSEMBLAGE CHANGES THROUGH THE EOCENE-OLIGOCENE BOUNDARY OF DSDP SITE 242

4.1 Introduction

The initial objective of Deep Sea Drilling Project Site 242 (Leg 25), situated within the Mozambique Channel on the eastern flank of the north-south trending Davie Ridge (Figure 4.1), was to constrain the pre-drift position of Madagascar and the tectonic evolution of the Mozambique Channel (Simpson *et al.* 1974). To this end, drilling was targeted at sampling the ridge basement at an estimated depth of 600 to 700m, with spot coring every 50m down to 600m and continuous coring below 600m. A total of 676m of pelagic sediments where encountered at the site, with the near-continuous coring below 600m recovering a succession of late Eocene to early Oligocene nannofossil chalks. Little micropaleontological or paleoceanographical analysis has been undertaken on these Eocene-Oligocene cores in the 30 years since recovery, however, the recent rediscovery of exceptionally preserved calcareous microfossils from sediments of the east African margin (Bown *et al.* 2008) and their paleoceanographic application (Pearson *et al.* 2001, 2007) has encouraged a re-examination of these relatively close deep-sea Paleogene cores.

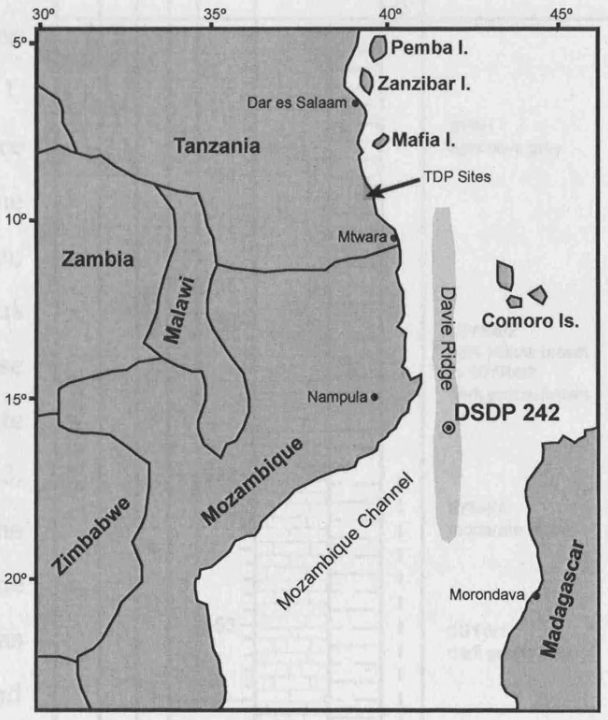

Figure 4.1 Location map of DSDP Site 242.

This study aims to produce high-resolution nannofossil assemblage data through the Eocene-Oligocene boundary in an open-ocean environment relatively near to the

Tanzanian records presented in Chapter 2. This will then be combined with high resolution stable isotope and planktonic foraminifera assemblage data being gathered by Bridget Wade (Texas A&M University).

4.2 Materials and Methods

The Eocene-Oligocene boundary recovered at DSDP Site 242 (15° 50.65'S, 41° 49.23'E) is located within core 15 (649 to 653.5 meters below sea floor (mbsf)), which consists of a "brown clayey nannofossil chalk" (Figures 4.2 & 4.3) (Simpson *et al.* 1974). The initial biostratigraphy of the EOB at the site was somewhat uncertain, with a disagreement between planktonic foraminiferal and calcareous nannofossil age data across the EOB (Simpson *et al.* 1974). Planktonic foraminiferal biostratigraphy placed the EOB in core 15 between samples 15-1, 30-32cm and 15-1, 100-102cm, based on the disappearance of the genus *Hantkenina* and the *Globorotalia cocoaensis* group. However, the presence of the calcareous nannofossil *Discoaster saipanensis*, whose last occurrence marks the top of the late Eocene zone NP19/20, up to core 14-3, 100cm suggests the placement of the EOB within core 14 or higher. One explanation for this discrepancy, as suggested by the generally rare and sporadic occurrences of *D. saipanensis*, is that these are Eocene specimens that have been reworked into early Oligocene sediments (Müller 1974).

Figure 4.2 Summary stratigraphic log for core 15, DSDP Site 242; after Simpson *et al.* (1974).

In this study, revised planktonic foraminiferal and calcareous nannofossil biostratigraphic datums are used based on higher resolution re-sampling of the original cores (Bridget Wade, pers. comm.), with the last occurrence of *Turborotalia cerroazulensis* placed at 15-2, 128cm (651.78m) and the last occurrence of the Hantkeninidae placed at 15-1, 37cm (649.37 mbsf). The last occurrence of *D. saipanensis* recorded within this study was in sample 15-1, 80cm (649.80mbsf), but as with the original report this placement is highly uncertain, as is evidenced by the presence of rare specimens of *D. barbadiensis*, whose last occurrence is generally placed before that of *D. saipanensis* (Berggren *et al.* 1995), throughout core 15. It is likely that some, if not all occurrences of both these forms are due to reworking from older Eocene sediments. The available stable isotope data for the site, undertaken on bulk carbonate as a pilot study prior to future foraminiferal species specific analysis (Figure 4.4; provided by Bridge Wade) shows a clear, marked and coincident positive shift of >1 per mil in both $\delta^{18}O$ and $\delta^{13}C$ at ~651.7mbsf. This is both characteristic of the EOT isotope shifts and, as with the first shift in $\delta^{18}O$ in the Tanzanian record, occurs in close proximity to the last occurrence of *T. cerroazulensis*. This shift can either be interpreted as representing the entire $\delta^{18}O$ shift of the EOT, or as the first step in $\delta^{18}O$ with the slightly more positive peak in $\delta^{18}O$ at ~651.1mbsf as the second step in $\delta^{18}O$. For the purposes of this study, I will assume the later scenario - what is key is that this accurately positions the onset of the EOT. In either case this strongly suggests that the placement of the the LO of the Hantkeninidae is also significantly higher than expected, probably due to reworking and difficulty of picking this event using the generally poorly preserved *Hantkenina* specimens in this section.

Figure 4.3 Core 15, DSDP Site 242 (after Simpson *et al.* 1974).

Sediment samples, approximately $2cm^3$ in volume, were provided by Bridget Wade, at an average sampling frequency of one per 0.10m for the whole of core 15. This study was limited to core 15 because of a 3m coring gap between the base of core 14 and top of core 15, which is too large to provide a meaningful continuation of the high-resolution data collected from core 15. Simple smear-slides were made in the laboratory at UCL following the method described in Chapter 2. All of the samples appeared homogeneous on the millimeter scale with no sign of laminations.

A total of 44 slides were examined for calcareous nannofossils, from 649.08 to 653.48mbsf, using standard light microscope techniques at a magnification of 1250x on an Olympus BX40 microscope. All samples from the studied section contain abundant and diverse moderately to well-preserved nannofossil assemblages. All whole, identifiable nannofossil specimens were counted within each field of view (FOV), and consecutive FOVs where examined until at least 400 complete, *in situ*, identifiable nannofossils had been counted. Specimens were identified to species level wherever possible, following the taxonomy of Bown (2005b) and Bown & Dunkley Jones (2006). During this count the number of cubic and framboidal pyrite, glauconite and amorphous carbonate grains were also counted per FOV. Samples and slides are curated at the Department of Earth Sciences, University College London.

A Principal Component Analysis (PCA) was performed, following the same methodology as in Chapter 2, on a reduced set of relative abundance data of 24 species, with the exclusion of species whose standard deviation of their relative abundances was less than 0.25%. Data was additive-log-ratio (ALR) transformed using the small form of *Cyclicargolithus floridanus* (<5μm) as the denominator. Metric Multi-dimensional Scaling (MMDS) was performed on the same ALR transformed, standardized data set following the methodology of Chapter 2.

4.3 Results

Nannofossil abundance, Shannon diversity (H) and log species richness (S) are shown in Figure 4.4. Nannofossil abundance is variable but high throughout the studied section - ranging from 1763 to 4998 specimens/mm^2 with a mean value of 3037 specimens/mm^2. There is no significant shift in Shannon diversity through the succession, which has a mean value of 2.02, however there is a systematic increase in species richness between 651.28mbsf and 650.67mbsf, with a mean value of 27 below 651.28mbsf and 36 above 650.67mbsf.

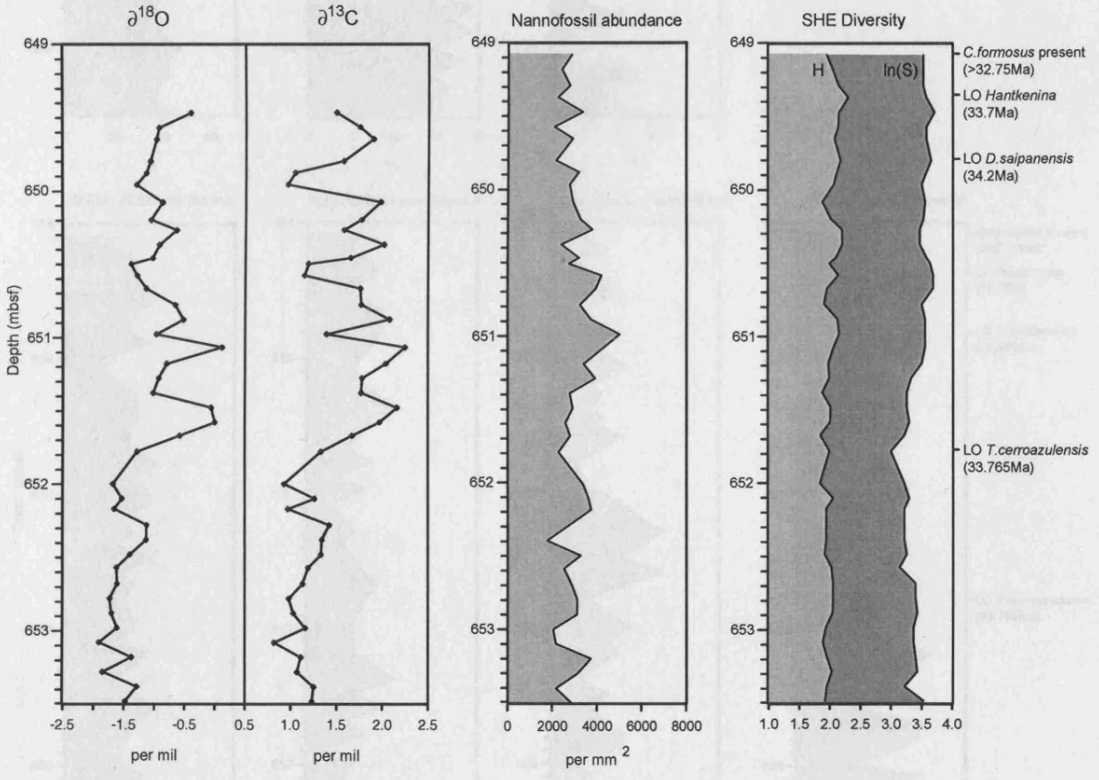

Figure 4.4 Nannofossil abundance, Shannon diversity (H) and log species richness (ln(S)) against depth (mbsf).

Plots of the relative abundance of the main species components are shown in Figures 4.5 and 4.6. Figure 4.5 shows the relative abundances of the dominant and sub-dominant species. The small form of *Cyclicargolithus floridanus* (<5μm) is the dominant species and shows no significant change in abundance through the section, with a mean abundance of 41%. Similarly the relative abundances of the sub-dominant taxa

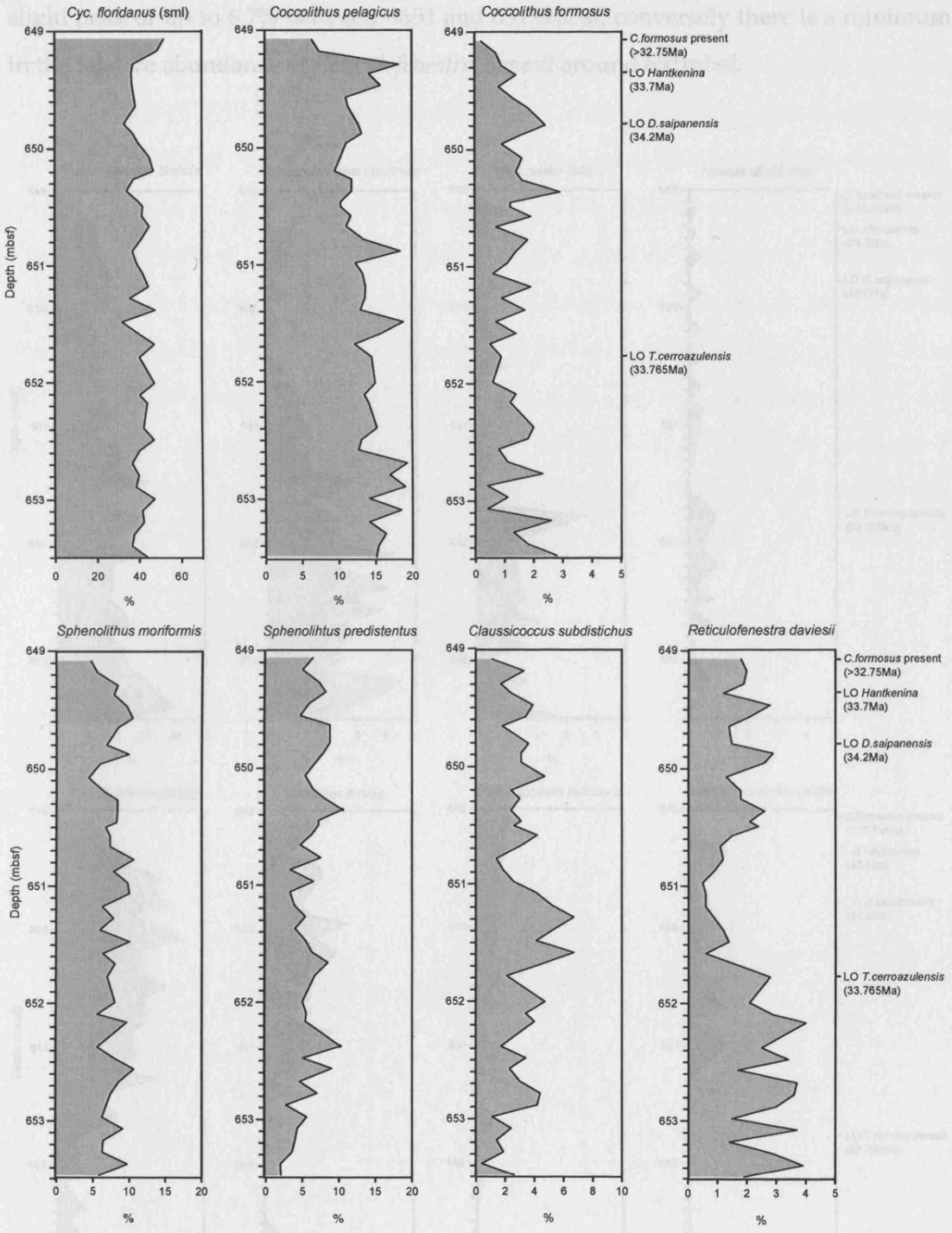

Figure 4.5 Nannofossil species relative abundance data against depth (mbsf) - dominant and sub-dominant taxa.

Coccolithus pelagicus (mean 14%), *Coccolithus formosus* (mean 1.3%), *Sphenolithus moriformis* (mean 7.7%) and *Sphenolithus predistentus* (mean 6.0%) are fairly constant throughout the section. The relative abundance of *Clausicoccus subdistichus* shows a

slight peak of up to 6.7% between ~651 and 651.6mbsf; conversely there is a minimum in the relative abundance of *Reticulofenestra daviesii* around 651mbsf.

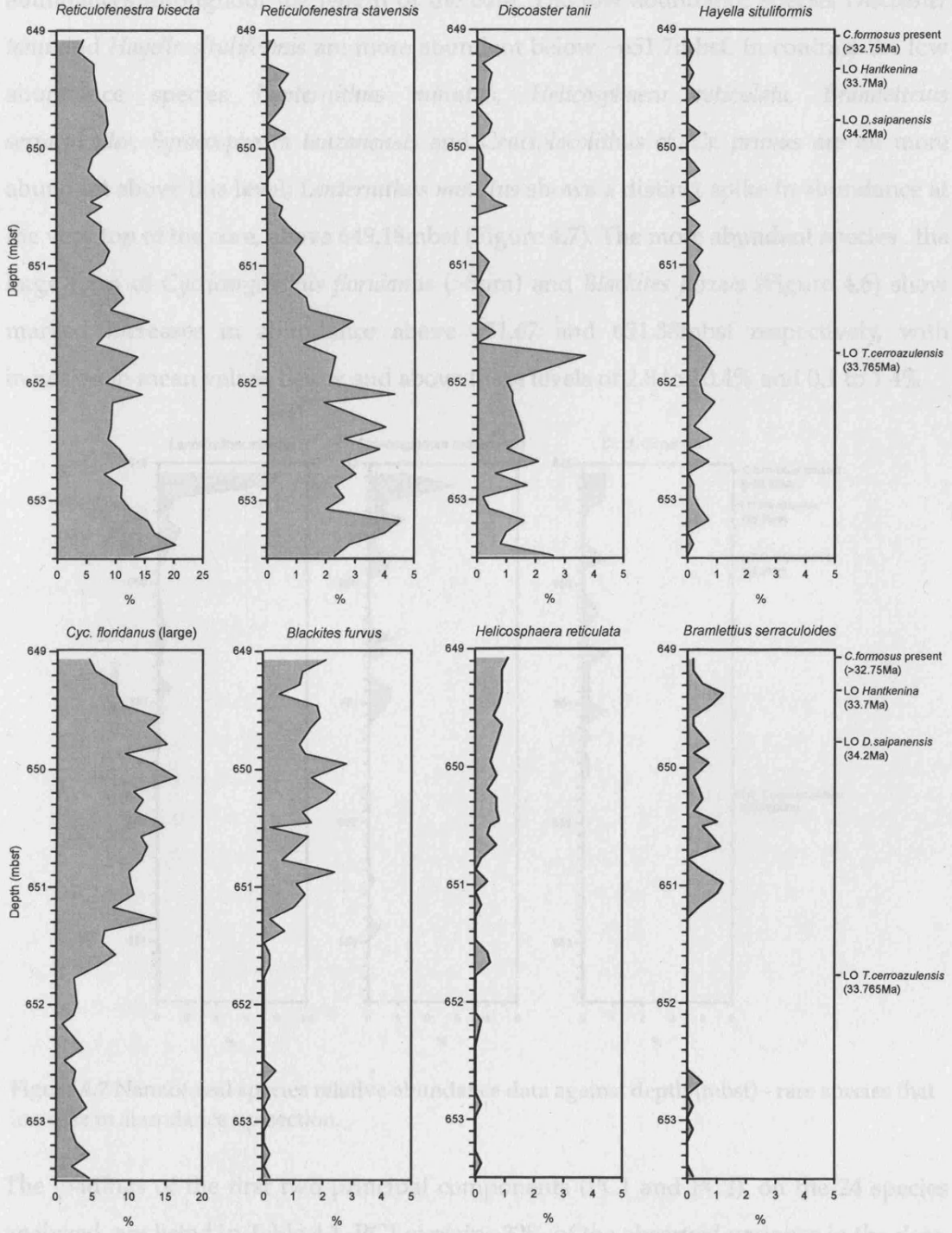

Figure 4.6 Nannofossil species relative abundance data against depth (mbsf) - species with declining (top row) and increasing (bottom row) abundance up-section.

Figures 4.6 & 4.7 show species which have a general trend of either decreasing or increasing relative abundances up-section. The closely related species *Reticulofenestra bisecta* and *Reticulofenestra stavensis* show a similar pattern of steadily declining relative abundances throughout the length of the core. The low abundance species *Discoaster tanii* and *Hayella situliformis* are more abundant below ~651.7mbsf. In contrast the low abundance species *Lanternithus minutus, Helicosphaera reticulata, Bramletteius serraculoides, Syracosphaera tanzanensis* and *Cruciplacolithus* cf. *Cr. primus* are all more abundant above this level; *Lanternithus minutus* shows a distinct spike in abundance at the very top of the core, above 649.18mbsf (Figure 4.7). The more abundant species , the large form of *Cyclicargolithus floridanus* (>5μm) and *Blackites furvus* (Figure 4.6) show marked increases in abundance above 651.67 and 651.38mbsf respectively, with increases in mean values below and above these levels of 2.8 to 10.4% and 0.1 to 1.4%.

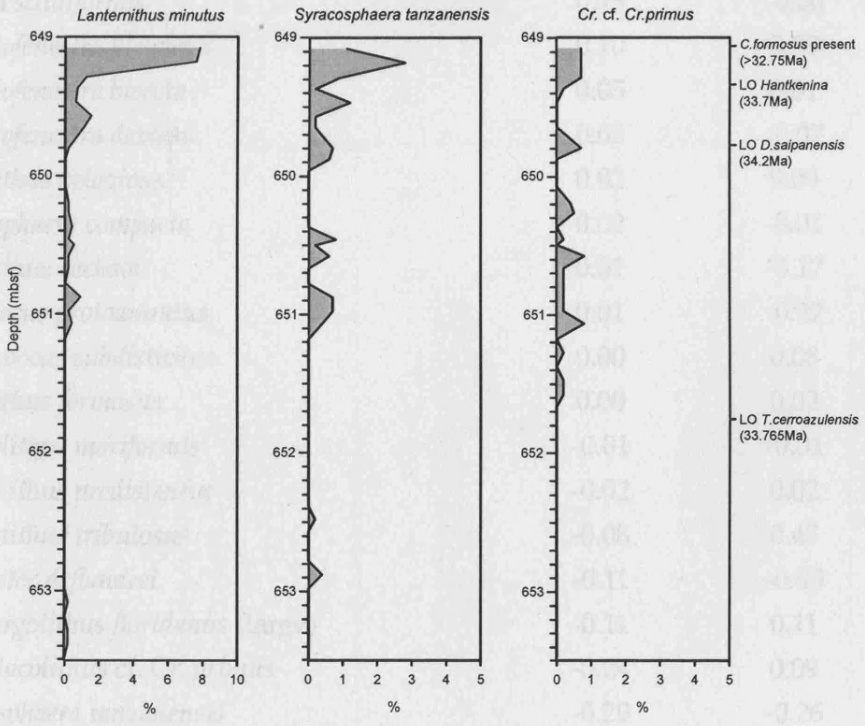

Figure 4.7 Nannofossil species relative abundance data against depth (mbsf) - rare species that increase in abundance up-section.

The loadings of the first two principal components (PC1 and PC2), on the 24 species analyzed, are listed in Table 4.1. PC1 explains 32% of the observed variance in the data, and PC2 11%; these values are lower than might be expected, but this is largely an artifact of the log-based ALR transformation, which increases the weighting of low-

abundance taxa. The PCA loadings can be used to discriminate groups of species that have similar loadings in one or both principal components. *Reticulofenestra stavensis, Discoaster tanii, Hayella situliformis, Reticulofenestra filewiczii* and *Reticulofenestra bisecta* (Group 1) have the largest positive loadings on PC1 (0.29 to 0.05) whereas *Lanternithus minutus, Blackites furvus, Helicosphaera reticulata, Bramletteius serraculoides, Zygrhablithus bijugatus bijugatus, Syracosphaera tanzanensis, Cruciplacolithus* cf. *Cr. primus, Cyclicargolithus floridanus* (large) and *Discoaster deflandrei* (Group 2) have the largest negative loadings on PC1 (-0.40 to –0.11).

	PC1 (32%)	PC2 (11%)
Reticulofenestra stavensis	0.29	-0.11
Discoaster tanii	0.16	-0.26
Hayella situliformis	0.15	-0.20
Reticulofenestra filewiczii	0.10	0.53
Reticulofenestra bisecta	0.05	0.01
Reticulofenestra daviesii	0.03	-0.07
Coccolithus pelagicus	0.02	0.00
Helicosphaera compacta	0.02	-0.01
Coccolithus cachaoi	0.01	-0.17
Calcidiscus protoannulus	0.01	-0.27
Clausicoccus subdistichus	0.00	0.08
Coccolithus formosus	0.00	0.02
Sphenolithus moriformis	-0.01	-0.01
Sphenolithus predistentus	-0.02	0.02
Sphenolithus tribulosus	-0.08	0.45
Discoaster deflandrei	-0.11	-0.05
Cyclicargolithus floridanus (large)	-0.11	0.11
Cruciplacolithus cf. *Cr. primus*	-0.24	0.09
Syracosphaera tanzanensis	-0.29	-0.26
Zygrhablithus bijugatus bijugatus	-0.32	-0.01
Bramletteius serraculoides	-0.36	-0.01
Helicosphaera reticulata	-0.36	0.01
Blackites furvus	-0.39	0.25
Lanternithus minutus	-0.40	-0.35

Table 4.1 Species principal component loadings for PC1 and PC2. Percentage of the total variance explained by each component in brackets.

The plot of the first two principal component scores (PC1 against PC2) for all the samples analyzed and the plots of these scores with depth (Figure 4.8) reveal a systematic change in assemblages through the section. The first principal component scores are relatively stable and positive (mean 5.48) at the base of the section, between 653.48 and 651.78mbsf, but then shift strongly towards negative values up to

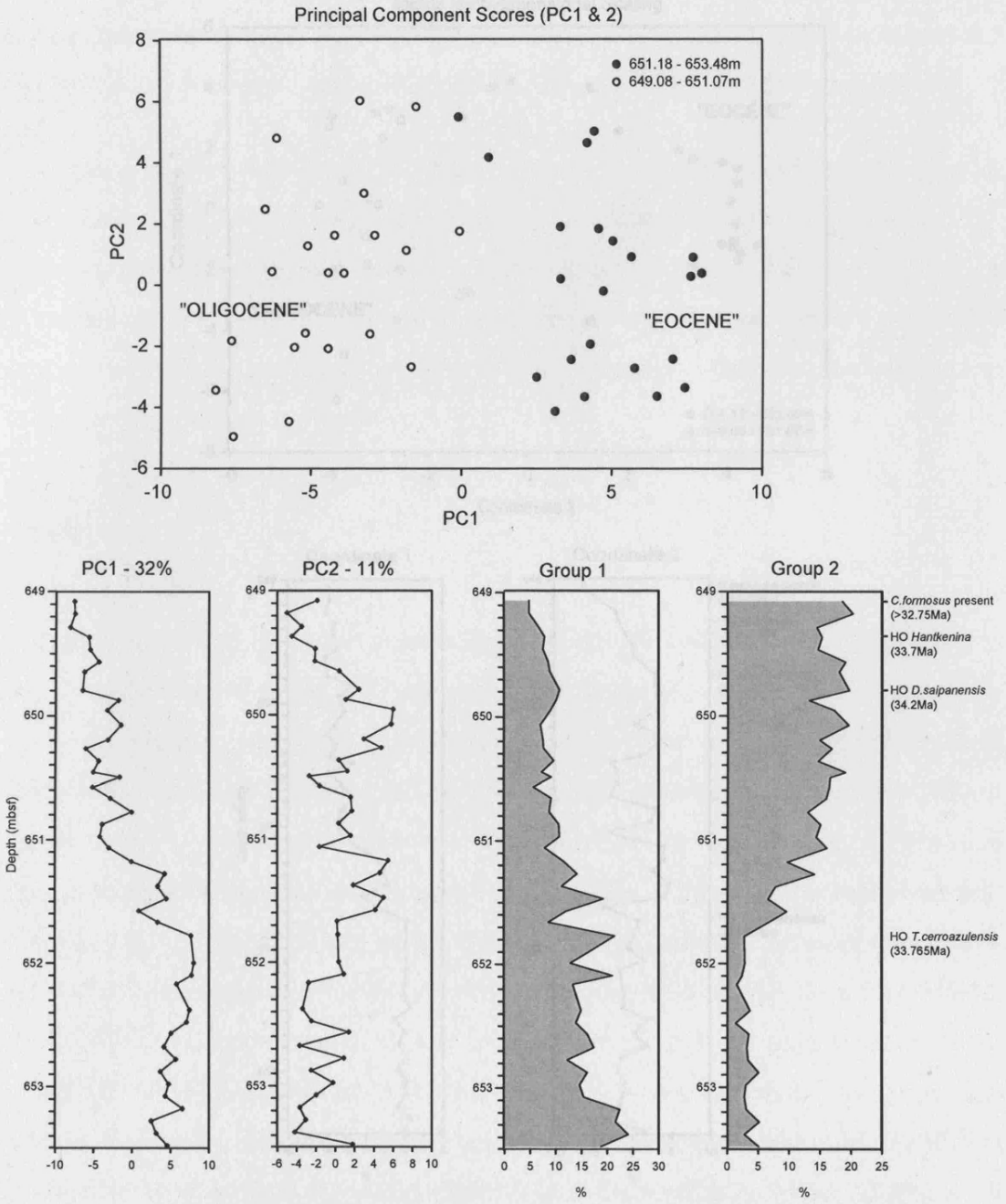

Figure 4.8 Principal Component Analysis; sample principal component scores (PC1 v. PC2) (top), PC1 and PC2 sample scores against depth (bottom left), Group 1 and 2 relative abundance data against depth (bottom right).

651.07mbsf; above this level they continue to move slowly to more negative values with a mean of –4.50. This pattern is visible in the plot of PC1 against PC2 scores (Figure 4.8) where samples below 651.18mbsf in the core plot with positive PC1 scores and those above this level have negative PC1 scores.

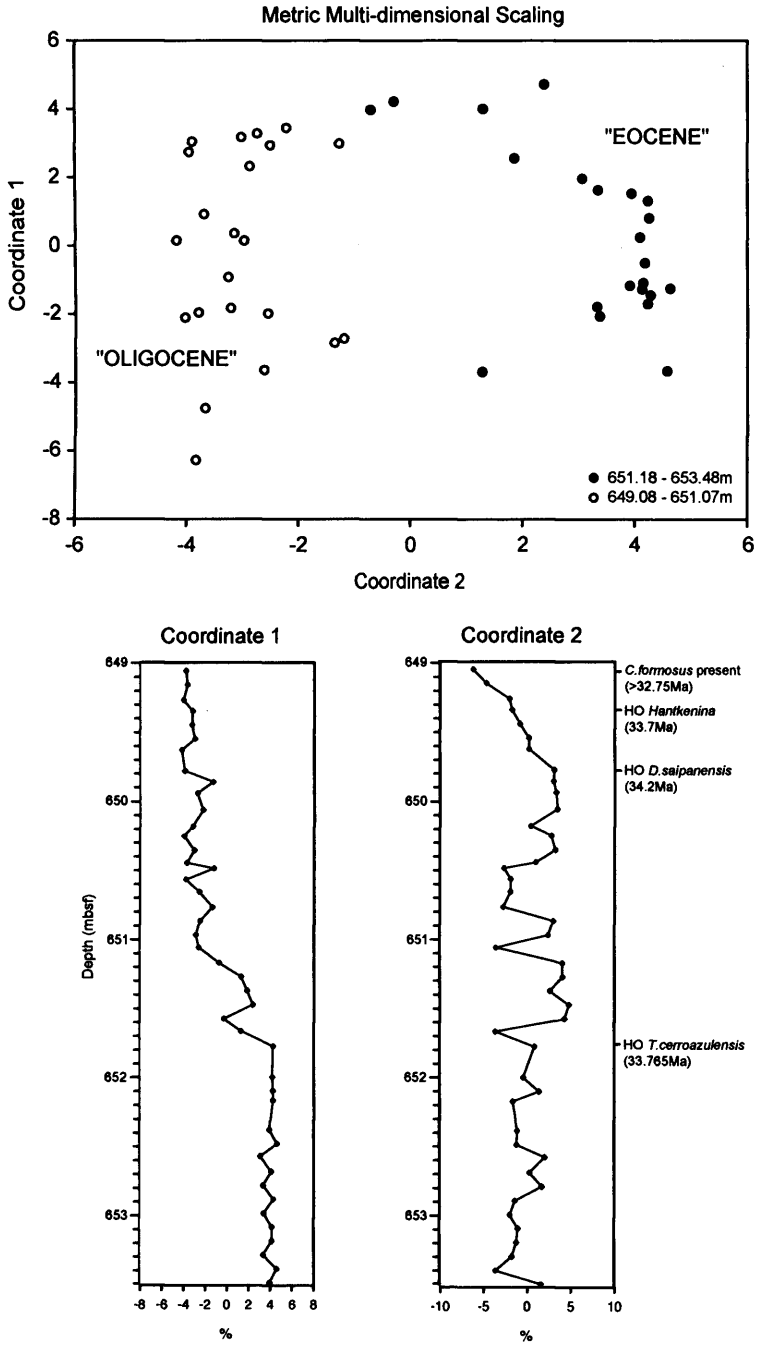

Figure 4.9 Metric Multi-dimensional Scaling; plot of coordinate 1 versus 2 values for all samples (top); coordinate 1 and 2 values plotted against depth (bottom).

Plots of the combined relative abundances for Group 1 and 2 species with depth (Figure 4.8), clearly show a pattern that reflects the changes in PC1 scores with depth. As in Chapter 2, these grouped abundance plots clearly illustrate the dominant trends in assemblage composition by minimizing small-scale fluctuations in individual species data (Wei & Wise 1990). Group 1 abundances appear to steadily decline throughout the section from a high of 24.1% at 653.38m to 4.8% at the top of the core. Group 2 abundance show a more marked increase in abundance between 651.67 and 651.28mbsf, with means below and above this interval of 16% and 3.3% respectively.

The results of the MMDS analysis (Figure 4.9) are similar to the PCA, with samples from below 651.78mbsf plotting with stable positive first coordinate values (mean 3.97), a period of transition to more negative values up to 651.18mbdf, followed by a period of stable negative value to the top of the core (mean –3.01). As in Chapter 2 the MMDS analysis produces a greater differentiation between samples from the top and bottom of the section compared to the PCA.

4.4 Discussion

The general increase in species richness between 651.28 and 650.67mbsf (Figure 4.4) is largely correlated with the first common occurrences of a number of *Pontosphaera* species (*P. formosa, P. multipora, P. pectinata, P. plana, P. versa*) and holococcoliths such as *Lanternithus minutus*. This interval coincides with a general lightening in sediment colour from the green grey to yellow browns of core sections 2 and 3 to a light olive grey in section 1 (Figure 4.2 & 4.3), which is suggestive of increased carbonate content. A marked drop in the CCD and an associated increased carbonate accumulation rate in pelagic sediments through the Eocene-Oligocene transition is well documented (Van Andel 1975), and appears to be closely correlated to the positive oxygen isotope shift into the EOGM (Coxall *et al.* 2005). It is likely that the increase in calcareous nannofossil species richness through this interval is due to the increased preservation of dissolution susceptible taxa, such as the pontosphaerids and holococcoliths (Bown 2005b), with increased deep-water carbonate ion concentrations.

The multivariate analyses of calcareous nannofossil assemblages through this interval reveal a distinct up-section transition, beginning at 651.67mbsf, from relatively stable assemblages at the base of the core (PC1 and MMDS coordinate 1; Figures 4.8 & 4.9), characterized by a marked increase in Group 2 nannofossil species, most notably the large form of *Cyclicargolithus floridanus* and *Blackites furvus*. This transition is immediately above the LO of *T. cerroazulensis* at 651.78mbsf, and closely corresponds to the major positive shift in $\delta^{18}O$ at ~651.7mbsf (Figure 4.4). This transition interval, between ~651.7 and 651.0mbsf, encompasses a number of last common occurrences (*Discoaster tanii, Hayella situliformis*) and first common occurrences (*Helicosphaera reticulata, Bramletteius serraculoides, Syracosphaera tanzanensis, Cruciplacolithus* cf. *Cr. primus*) of low abundance species. Throughout the core there is a longer period decrease in the abundance of the related species *Reticulofenestra bisecta* and *Reticulofenestra stavensis*, which is reflected in the slow decline in Group 1 abundances through the succession.

Although the record of nannofossil assemblages through the EOT of this site may be significantly, if not predominantly, influenced by an increase in the preservation potential of dissolution susceptible taxa with increased deep-sea carbonate saturation, there are some useful comparisons to be made between the assemblages at this, slightly higher latitude Indian Ocean site in comparison to the Tanzanian record. First is the common observation of significantly increased abundances of the large form of *Cyclicargolithus floridanus* through the EOT of both sections. This is difficult to attribute to changes in nannofossil preservation as this placolith is one of the most robust taxa observed at either location, and indicates that this is a more general trend, at least in the western Indian Ocean. The second noticeable difference is the taxonomic composition of the grill-bearing reticulofenestrid assemblages at the two sites, which in the Tanzanian sections is dominated by the larger placoliths with narrower grills of the *Reticulofenestra filewiczii* type, whereas DSPD Site 242 is dominated by smaller placoliths with wider grills of the *Reticulofenestra daviesii* type. In addition, *Isthmolithus recurvus* is rarely but consistently observed throughout the succession in DSPD Site 242, a species which was never observed in the Tanzanian sections. These results are consistent with previous studies that suggest both *R. daviesii* and *I. recurvus* are more

high latitude, cooler water species (Bukry 1978; Wei & Wise 1990; Wei *et al.* 1992; Persico & Villa 2004), what is surprising is the strength of the biogeographic gradient between two sites that differ by only ~5-10° latitude.

The major transition in nannofossil assemblages, beginning close to the LO of *T. cerroazulensis*, is similar to the changes observed in the TDP boreholes, where nannofossil assemblages begin to change coincident with the LO of *T. cerroazulensis* and the first positive oxygen isotope shift into the EOGM. If this correlation holds for DSDP Site 242, then both the LO of *Hantkenina* and *D. saipanensis* are significantly higher than would be expected, as indicated by the preliminary stable isotope record, most likely due to the reworking of older Eocene sediments. If the nannofossil assemblage change is tightly coupled to the first isotope shift in DSDP Site 242, as for the Tanzanian sites, the LO *Hantkenina* and hence the EOB should be between ~651 to 651.5mbsf. A closer correlation between the sites will only be possible with the production of a detailed stable isotope stratigraphy of this succession, which is currently in progress. The correlation of this record to the changes observed at the other study sites and further discussion of environmental changes through the EOT will be presented in Chapter 6.

4.5 Systematic palaeontology

The taxonomy presented here follows the higher taxonomic rationale and species concepts outlined in Chapter 3. Light microscope images were captured using Scion Image software and macros written by Dr. Jeremy Young (Bown & Young 1998). All light microscope images were captured at the same magnification with a two-micron scale bars shown on each plate (magnification ~x 2180). All sample material and images are stored in the Department of Earth Sciences, University College London.

4.5.1 Placolith coccoliths

Order **ISOCHRYSIDALES** Pascher 1910

Family **NOELAERHABDACEAE** Jerkovic 1970 emend. Young & Bown 1997

Genus ***CYCLICARGOLITHUS*** Bukry 1971

Cyclicargolithus floridanus (Roth & Hay in Hay *et al.* 1967) Bukry 1971 (Pl. 4.1, fig. 1-2)
REMARKS: Specimens were informally divided into small (<5μm) and large (>5μm) morphotypes.

Genus ***RETICULOFENESTRA*** Hay, Mohler & Wade 1966

Reticulofenestra dictyoda (Deflandre *in* Deflandre & Fert 1954) Stradner *in* Stradner & Edwards 1968 (Pl. 4.1, fig. 3)

Reticulofenestra umbilicus (Levin 1965) Martini & Ritzkowski 1968 (Pl. 4.1, fig. 4)

Reticulofenestra bisecta (Hay *et al.* 1966) Roth 1970 (Pl. 4.1, fig. 5).

Reticulofenestra stavensis (Levin & Joerger 1967) Varol 1989 (Pl. 4.1, fig. 6)

Reticulofenestra filewiczii Wise & Wiegand *in* Wise 1983 stat. nov. (Pl. 4.1, figs 7-8)

Reticulofenestra daviesii (Haq, 1968) Haq, 1971 (Pl. 4.1, fig. 9-11)
REMARKS: The distinctions between small to medium sized reticulofenestrid species with open central areas spanned by a grill or net is not straightforward. In this classification *R. daviesii* is used for forms that have a moderately wide central area (~half the placolith width), which often show a ring of pores around the outer margin. This is distinguished from *R. lockeri* (below) which has a slightly wider central area and faint perforations often visible across the whole of the central area net.

Reticulofenestra lockeri Müller, 1970 (Pl. 4.1, fig. 12)

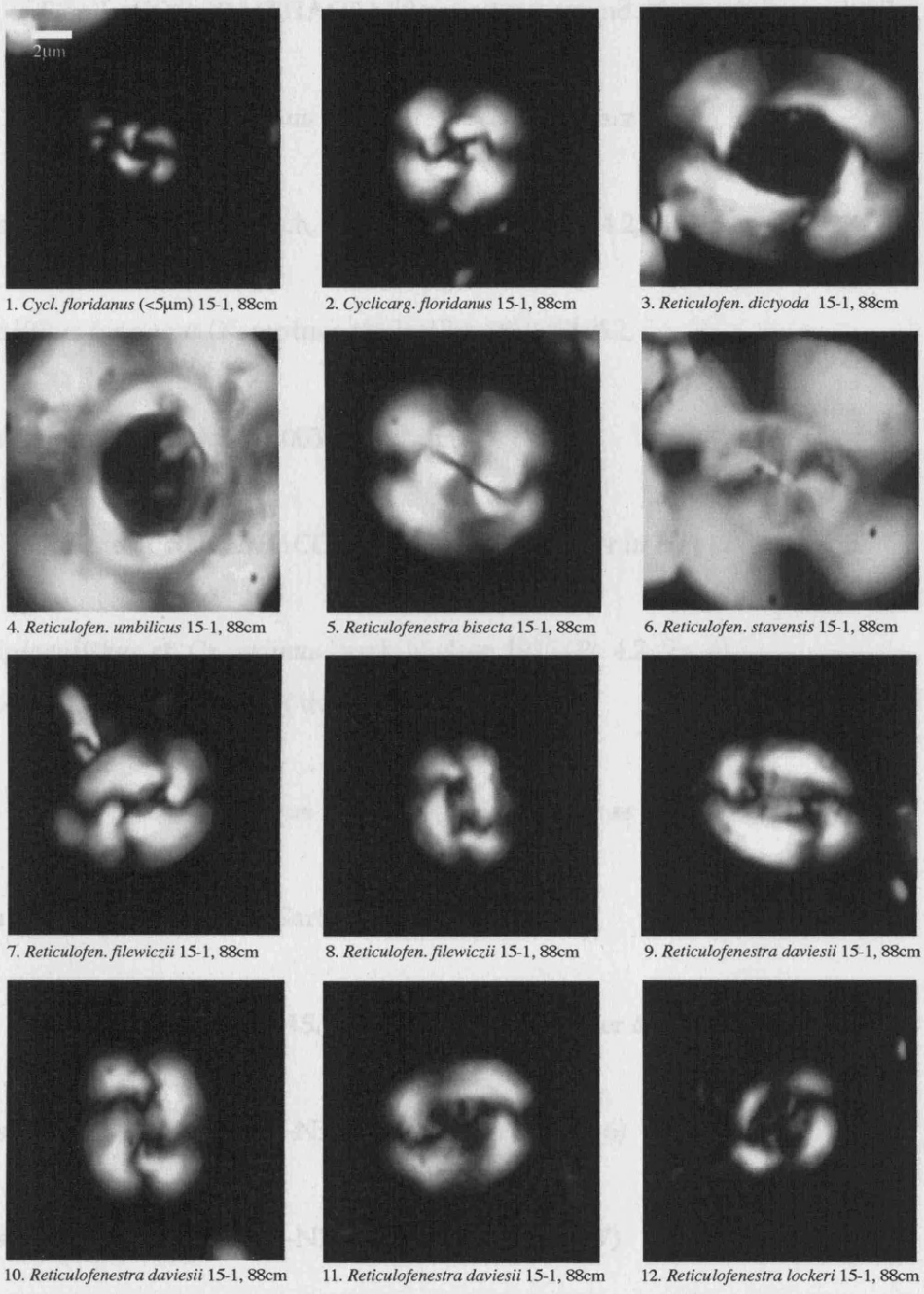

Plate 4.1 LM images of *Cyclicargolithus* and *Reticulofenestra* placoliths.

REMARKS: See remarks for *R. daviesii* above.

Order **COCCOLITHALES** Schwarz 1932 emend. Edvardsen & Eikrem in Edvardsen *et al.* 2000

Family **COCCOLITHACEAE** Poche 1913 emend. Young & Bown 1997

Genus ***COCCOLITHUS*** Schwarz 1894

Coccolithus pelagicus (Wallich, 1877) Schiller 1930 (Pl. 4.2, fig. 1)

Coccolithus formosus (Kamptner 1963) Wise 1973 (Pl. 4.2, fig. 2)

Coccolithus cachaoi Bown 2005 (Pl. 4.2, fig. 3)

Genus ***CRUCIPLACOLITHUS*** Hay & Mohler *in* Hay *et al.* 1967

Cruciplacolithus* cf. *Cr. primus Perch-Nielsen 1977 (Pl. 4.2, fig. 4)
REMARKS: See discussion of this form in Chapter 3.

Genus ***BRAMLETTEIUS*** Gartner 1969

Bramletteius serraculoides Gartner 1969 (Pl. 4.2, fig. 5)

Genus ***CHIASMOLITHUS*** Hay, Mohler & Wade 1966

Chiasmolithus nitidus Perch-Nielsen 1971 (Pl. 4.2, fig. 6)

Chiasmolithus medius Perch-Nielsen 1971 (Pl. 4.2, fig. 7)

Genus ***CLAUSICOCCUS*** Prins 1979

Clausicoccus subdistichus (Roth & Hay *in* Hay *et al.* 1967) Prins 1979 (Pl. 4.2, fig. 8)

Genus ***CAMPYLOSPHAERA***

***Campylosphaera?* sp.** (Pl. 4.2, fig. 9)

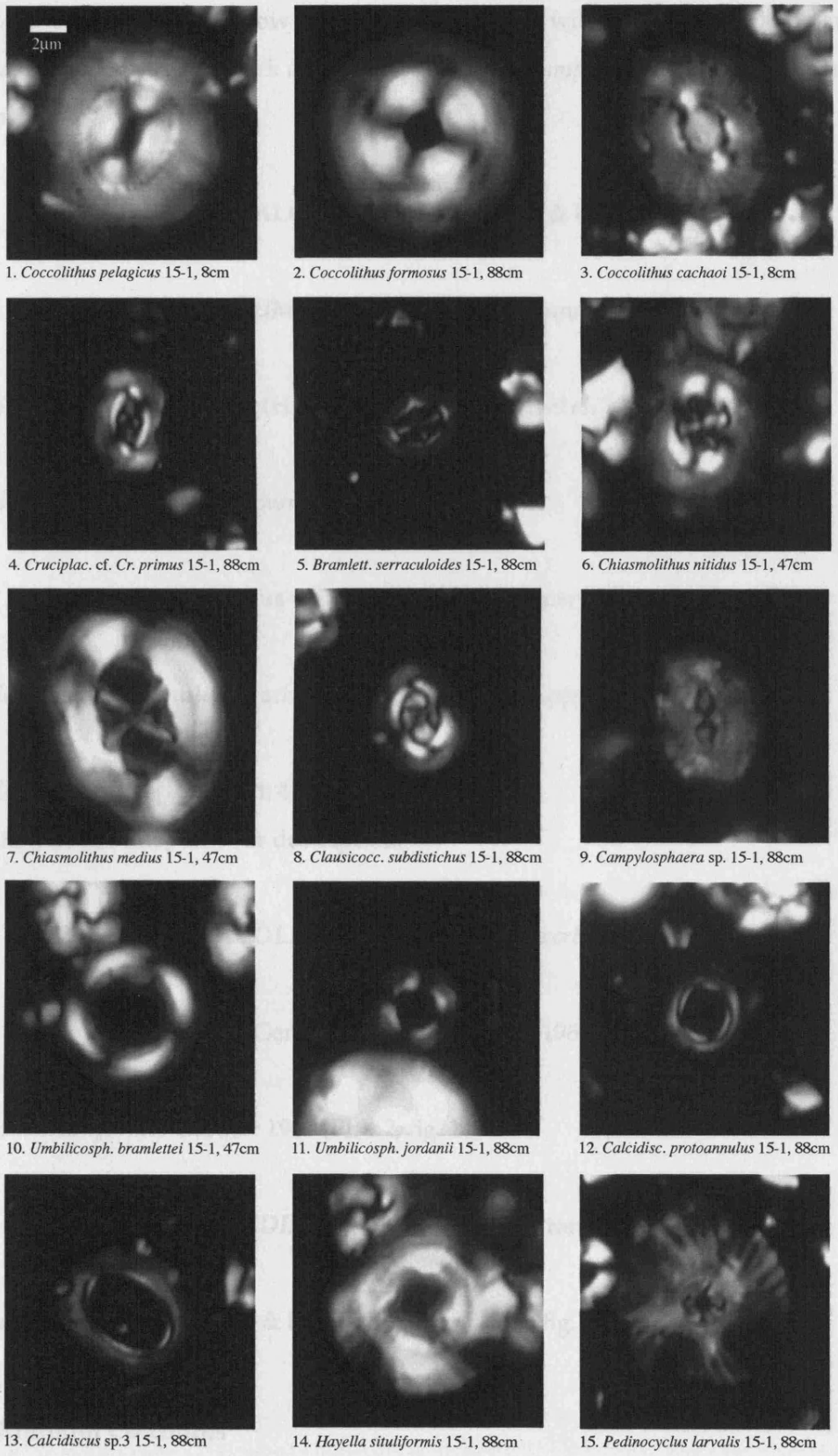

Plate 4.2 LM images of *Coccolithus, Cruciplacolithus, Bramletteius, Chiasmolithus, Clausicoccus, Umbilicosphaera, Calcidiscus, Hayella, Pedinocyclus* and *Campylosphaera* placoliths.

REMARKS: Medium sized, low birefringence placolith with a wide shield and narrow central area spanned by a dark axial cross. Similar to *Campylosphaera* sp. 2 of Bown 2005b.

Family **CALCIDISCACEAE** Young & Bown 1997

Genus ***UMBILICOSPHAERA*** Lohmann 1902

Umbilicosphaera bramlettei (Hay & Towe 1962) Bown *et al.* 2007 (Pl. 4.2, fig. 10)

Umbilicosphaera jordanii Bown 2005 (Pl. 4.2, fig. 11)

Genus ***CALCIDISCUS*** Kamptner 1950

Calcidiscus protoannulus (Gartner 1971) Loeblich & Tappan 1978 (Pl. 4.2, fig. 12)

***Calcidiscus?* sp. 3** sp. nov. (Pl. 4.2, fig. 13)
REMARKS: See Chapter 3 for description.

PLACOLITH COCCOLITHS *Incertae Sedis*

Genus ***HAYELLA*** Gartner 1969

Hayella situliformis Gartner 1969 (Pl. 4.2, fig. 14)

Genus ***PEDINOCYCLUS*** Bukry & Bramlette 1971

Pedinocyclus larvalis Bukry & Bramlette 1971 (Pl. 4.2, fig. 15)

4.5.2 Murolith Coccoliths

Order **ZYGODISCALES** Young & Bown 1997

Family **HELICOSPHAERACEAE** Black 1971

Genus *HELICOSPHAERA* Kamptner 1954

Helicosphaera compacta Bramlette & Wilcoxon 1967 (Pl. 4.3, figs 1-2)

Helicosphaera reticulata Bramlette & Wilcoxon 1967 (Pl. 4.3, figs 3-4)

Helicosphaera seminulum Bramlette & Sullivan 1961 (Pl. 4.3, figs 5-6)

Helicosphaera bramlettei (Müller 1970) Jafar & Martini 1975 (Pl. 4.3, fig. 7)

Helicosphaera euphratis Haq 1966 (Pl. 4.3, fig. 8-9)

Family **PONTOSPHAERACEAE** Lemmermann 1908

Genus *PONTOSPHAERA* Lohmann 1902

Pontosphaera multipora (Kamptner 1948 *ex* Deflandre 1954) Roth 1970 (Pl. 4.3, fig. 10)

Pontosphaera* cf. *P. versa (Bramlette & Sullivan 1961) Sherwood 1974 (Pl. 4.3, figs 11-12)

Pontosphaera pulcheroides (Sullivan 1964) Romein 1979 (Pl. 4.3, fig. 13)

Pontosphaera formosa (Bukry & Bramlette 1968) Romein 1979 (Pl. 4.3, fig. 14)

Genus *SCYPHOSPHAERA* Lohmann 1902

Scyphosphaera apsteinii Lohmann 1902 (Pl. 4.4, fig. 1)

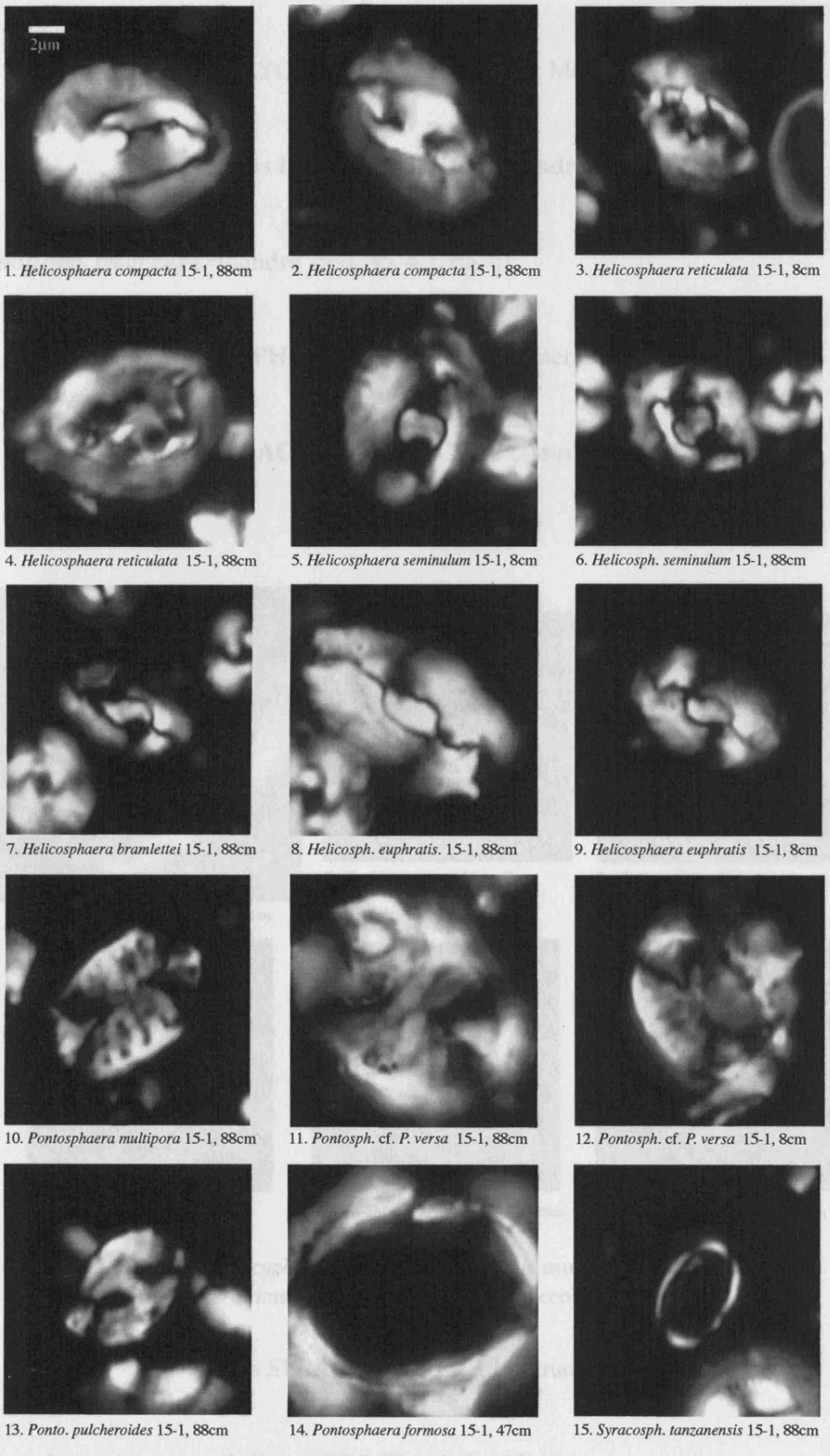

1. *Helicosphaera compacta* 15-1, 88cm
2. *Helicosphaera compacta* 15-1, 88cm
3. *Helicosphaera reticulata* 15-1, 8cm
4. *Helicosphaera reticulata* 15-1, 88cm
5. *Helicosphaera seminulum* 15-1, 8cm
6. *Helicosph. seminulum* 15-1, 88cm
7. *Helicosphaera bramlettei* 15-1, 88cm
8. *Helicosph. euphratis.* 15-1, 88cm
9. *Helicosphaera euphratis* 15-1, 8cm
10. *Pontosphaera multipora* 15-1, 88cm
11. *Pontosph.* cf. *P. versa* 15-1, 88cm
12. *Pontosph.* cf. *P. versa* 15-1, 8cm
13. *Ponto. pulcheroides* 15-1, 88cm
14. *Pontosphaera formosa* 15-1, 47cm
15. *Syracosph. tanzanensis* 15-1, 88cm

Plate 4.3 LM images of *Helicosphaera, Pontosphaera* and *Syracosphaera* muroliths.

Family **ZYGODISCACEAE** Hay & Mohler 1967

Genus ***ISTHMOLITHUS*** Deflandre 1954

Isthmolithus recurvus Deflandre 1954 (Pl. 4.4, fig. 6)

Order **SYRACOSPHAERALES** Hay 1977 emend. Young *et al.* 2003

Family **SYRACOSPHAERACEAE** Lemmermann 1908

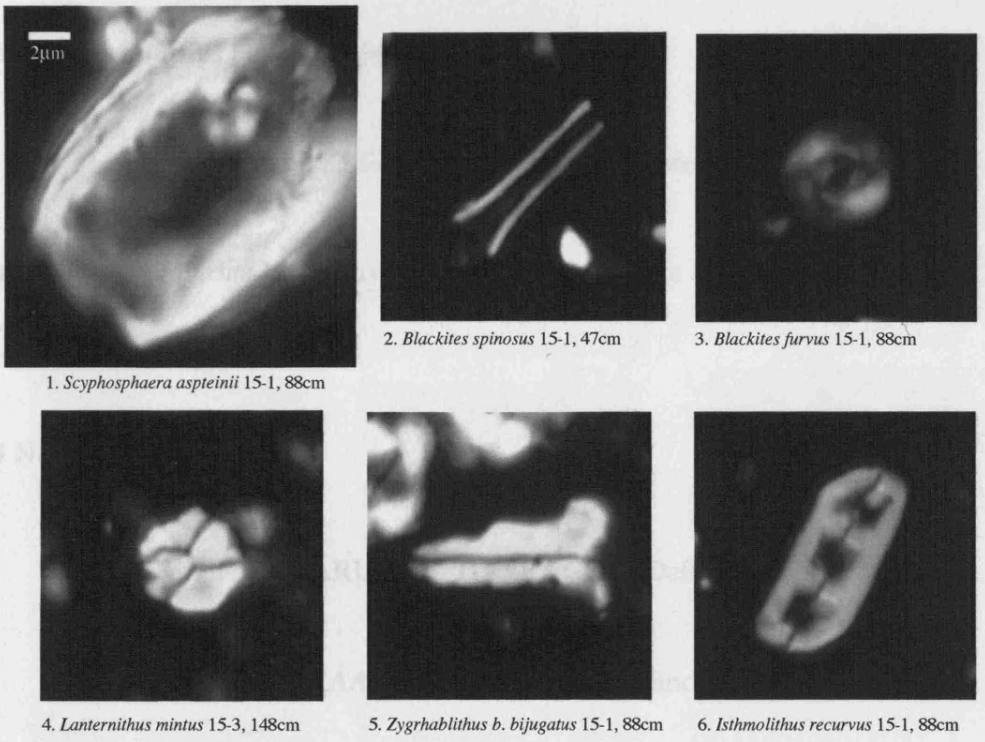

1. *Scyphosphaera aspteinii* 15-1, 88cm
2. *Blackites spinosus* 15-1, 47cm
3. *Blackites furvus* 15-1, 88cm
4. *Lanternithus mintus* 15-3, 148cm
5. *Zygrhablithus b. bijugatus* 15-1, 88cm
6. *Isthmolithus recurvus* 15-1, 88cm

Plate 4.4 LM images of *Scyphosphaera* and *Isthmolithus* muroliths, *Blackites* rhabdoliths and *Lanternithus* and *Zygrhablithus* holococcoliths.

Genus ***SYRACOSPHAERA*** Lohmann 1902

Syracosphaera tanzanensis Bown 2005 (Pl. 4.3, fig. 15)

Family **RHABDOSPHAERACEAE** Haeckel 1894

Genus ***BLACKITES*** Hay & Towe 1962

Blackites spinosus (Deflandre & Fert 1954) Hay & Towe 1962 (Pl. 4.4, fig. 2)

Blackites furvus Bown & Dunkley Jones 2006 (Pl. 4.4, fig. 3)

4.5.3 Holococcoliths

Genus ***LANTERNITHUS*** Stradner 1962

Lanternithus minutus Stradner 1962 (Pl. 4.4, fig. 4)

Genus ***ZYGRHABLITHUS*** Deflandre 1959

Zygrhablithus bijugatus bijugatus (Deflandre *in* Deflandre & Fert 1954) Deflandre 1959 (Pl. 4.4, fig. 5)

4.5.4 Nannoliths

Family **BRAARUDOSPHAERACEAE** Deflandre 1947

Genus ***BRAARUDOSPHAERA*** Deflandre 1947

Braarudosphaera bigelowii (Gran & Braarud 1935) Deflandre 1947 (Pl. 4.5, fig. 1)

Family **DISCOASTERACEAE** Tan 1927

Genus ***DISCOASTER*** Tan 1927

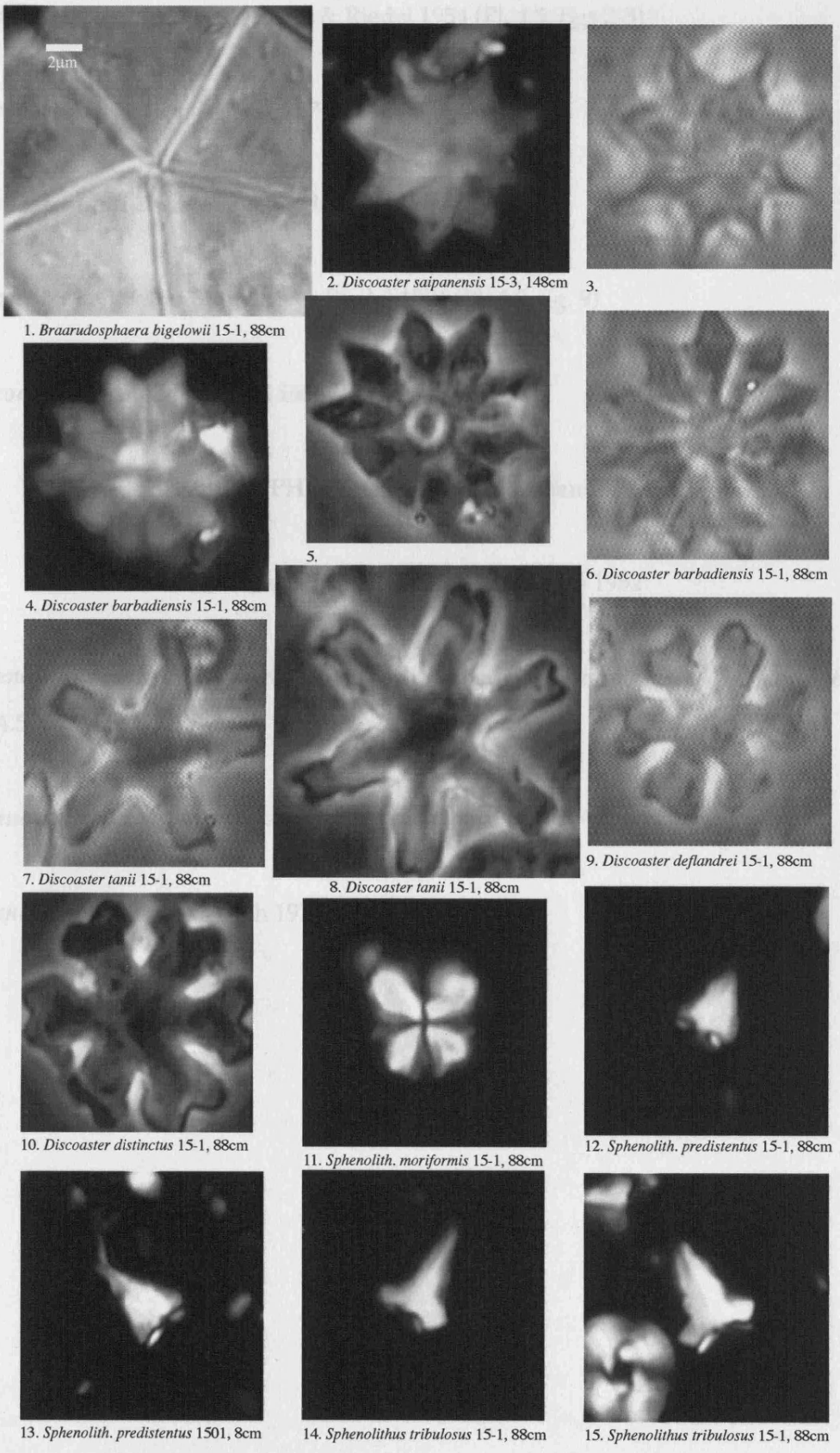

Plate 4.5 LM images of *Braarudosphaera, Discoaster* and *Sphenolithus* nannoliths.

Discoaster saipanensis Bramlette & Riedel 1954 (Pl. 4.5, figs 2-3)

Discoaster barbadiensis Tan, 1927 (Pl. 4.5, figs 4-6)

Discoaster tanii Bramlette & Riedel 1954 (Pl. 4.5, figs 7-8)

Discoaster deflandrei Bramlette & Riedel 1954 (Pl. 4.5, fig. 9)

Discoaster distinctus Martini 1958 (Pl. 4.5, fig. 10)

Family **SPHENOLITHACEAE** Deflandre 1952

Genus ***SPHENOLITHUS*** Deflandre 1952

Sphenolithus moriformis (Brönnimann & Stradner 1960) Bramlette & Wilcoxon 1967 (Pl. 4.5, fig. 11)

Sphenolithus predistentus Bramlette & Wilcoxon 1967 (Pl. 4.5, figs 12-13)

Sphenolithus tribulosus Roth 1970 (Pl. 4.5, figs 14-15)

5. NANNOFOSSIL ASSEMBLAGE CHANGES THROUGH THE EOCENE-OLIGOCENE BOUNDARY AT ST STEPHENS QUARRY, ALABAMA

5.1 Introduction

The former Lone Star Cement quarry at St Stephens, Alabama (Figure 5.1), is historically, one of the classic global reference sections for the Eocene-Oligocene Boundary, with almost 30 years of intensive study focusing on the sequence stratigraphy (Baum & Vail 1988; Loutit *et al.* 1988), planktonic foraminiferal (Mancini & Tew 1991; Tew 1992) and calcareous nannofossil biostratigraphy (Bybell 1982) and stable isotope stratigraphy (Keigwin & Corliss 1986) of the quarry outcrops. In 1987 the ARCO Oil and Gas Company cored the entire EOT succession immediately adjacent to the quarry sections. Subsequent studies of this cored material have produced both an integrated magneto- and strontium-isotope stratigraphy (Miller *et al.* 1993) and more recently an integrated biomagnetostratigraphy and sequence stratigraphy for the upper Eocene - lower Oligocene sediments (Miller *et al.* 2008).

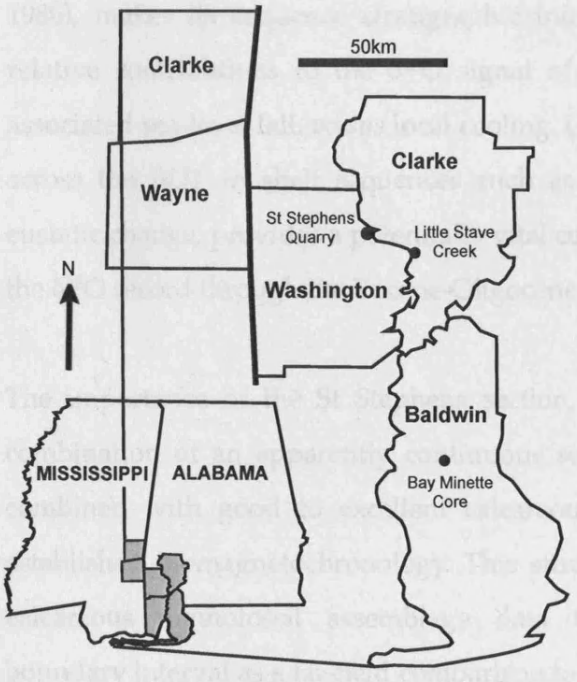

Figure 5.1 Location of St Stephens Quarry, Washington County, Alabama. Also shown are Little Stave Creek and Bay Minette Borehole, two other key Paleogene reference sections.

The predominant focus of previous studies of the Eocene-Oligocene succession at St Stephens, and similar sections elsewhere in Alabama and Mississippi, has been the production of a sequence stratigraphic framework and its relation to the proposed global sea level curves of Vail *et al.* (1977) and Haq *et al.* (1987). There is a general consensus between these studies in both their lithostratigraphic framework and its sequence stratigraphic interpretation. However, there is an

important divergence of opinion over the presence or absence of an earliest Oligocene sequence boundary at the contact between the 1Shubuta and Bumpnose formations. Some interpret this contact, both at St Stephens and elsewhere in Alabama and Mississippi, as a Maximum Flooding Surface (MFS) (Baum & Vail 1988; Echols *et al.* 2003; Jaramillo & Oboh-Ikuenobe 1999; Loutit *et al.* 1988; Mancini & Tew 1991; Tew 1992), whilst others interpret it as a sequence boundary (Dockery III 1982) associated with an increase in $\delta^{18}O$ (Keigwin & Corliss 1986) and a widespread sea-level fall (Miller *et al.* 1993). Part of this confusion may be due to the disconformity (sequence boundary) at the top of the Shubuta being directly overlain by a deep-water blue clay, representing the early highstand systems tract of the following sequence. If this is the case, then the sequence boundary and maximum flooding surface (MFS) of the overlying sequence are adjacent, with no intervening transgressive systems tract making the sequence boundary difficult to recognize (Miller *et al.* 1993).

The correlation of the Shubuta-Bumpnose contact with the earliest Oligocene ~1‰ increase in benthic foraminiferal $\delta^{18}O$ at the start of the EOGM (Keigwin & Corliss 1986), makes its sequence stratigraphic interpretation important in unraveling the relative contributions to the $\delta^{18}O$ signal of an increase in global ice volume, and associated sea-level fall, *versus* local cooling. Quantifying the extent of sea-level change across the EOT in shelf sequences such as this, which are inherently sensitive to eustatic change, provides a potentially vital constraint on the varying interpretations of the $\delta^{18}O$ record through the Eocene-Oligocene transition (Miller *et al.* 2008).

The importance of the St Stephens section, and its relevance to this study, is the combination of an apparently continuous sedimentary succession through the EOT combined with good to excellent calcareous microfossil preservation and a well-established biomagnetochronology. This study presents high-resolution, quantitative calcareous nannofossil assemblage data through the critical Eocene-Oligocene boundary interval as a far-field comparison to the Tanzanian sites.

5.2 Materials and Methods

The St Stephens Quarry (SSQ) core was drilled by the ARCO Oil and Gas Company in 1987, near the highest point on the southwest rim of the former Lone Star Cement Company quarry (Washington County, Alabama; 31° 33'N latitude, 88° 02' W longitude) (Miller *et al.* 1993). The core recovered all of the upper Eocene-lower Oligocene units exposed in the classic outcrop sections of the quarry and penetrated down into the underlying Eocene and upper Paleocene strata (Tew 1992). The upper Eocene to lower Oligocene interval of interest consists of sediments of the Gulf Coast Jackson (~upper Eocene consisting of North Twistwood Creek Clay and Yazoo Formations) and Vicksburg Stages (~lower Oligocene consisting of Bumpnose, Red Bluff, Mint Spring and Marianna Limestone Formations) (Figure 5.2) (Miller et al. 1993). In Alabama the upper Eocene Yazoo Formation is sub-divided into three members, the Cocoa Sand, Pachuta Marl and Shubuta Clay. This study focuses on the cored interval between 165.5ft (50.44m) and 150ft (45.72m), which includes the upper Pachuta Marl and entire Shubuta Clay of the Yazoo Formation and the lower part of the Bumpnose Formation (Figure 5.2). This interval encompasses late Eocene pre-EOT sediments, the "precursor" $\delta^{18}O$ increase (step 1), the Eocene-Oligocene Boundary, the second $\delta^{18}O$ step into the EOGM and the debated Shubuta-Bumpnose contact and span planktonic foraminiferal zones E15 to O1 (Miller *et al.* 2008) and calcareous nannofossil zone NP21 (this study). The lithology of this interval varies from the light grey glauconitic sandy marls of the upper Pachuta Marl to the cream white marls of the Shubuta Clay (Miller *et al.* 2008).

The benthic foraminiferal biofacies of the study interval is dominated by middle to outer shelf *Uvigerina* assemblages (~125m water depth) except for a short interval at the top of the Shubuta Clay (154.6-154.1ft; 47.12-46.97m) where assemblages rapidly shift to a shallower-water (~75m) *Hanzawaia* biofacies before a sharp return to the *Uvigerina* biofacies across the Shubuta-Bumpnose contact (154.1ft; 46.97m). The presence of abundant and diverse calcareous nannofossil assemblages throughout this interval support this paleoenvironmental interpretation of middle to outer shelf, fully-marine conditions.

Figure 5.2 Quantitative lithology, paleobathymetry (benthic foraminifera facies analysis), sequence stratigraphy, benthic foraminifera stable isotopes, magnetostratigraphy and age-depth model for the St Stephens Core. Modified from Miller *et al.* (in press). The interval of interest for this study is shown on the right hand side.

The age model used for this study follows that of Miller *et al.* (in press) (Figure 5.2). Although rare specimens of *D. saipanensis* are found up to a level of 164.25ft (50.06m) within the Pachuta Marl, they are poorly preserved and are probably reworked from older Eocene sediments, as suggested by Miller *et al.* (in press) and Bybell (1982). The rarity of *D. saipanensis* in shelf environments, such as this one, and the potential for reworking within a broadly regressive regime makes the accurate identification of its last occurrence problematic.

Datum	Age (Ma)	Depth
Base Oi1 (Is)	33.545	152ft (46.32m)
FAD Cassigerinella chipolensis (F)	~EOB	159ft (48.46m)
LAD Hantkenina (F)	33.7	163ft (49.68m)
LAD Turborotalia cerroazulensis (F)	33.765	162ft (49.38m)
LAD Pemma papillatum (N)	-	162.25ft (48.84m)

Table 5.1 Age model data for the St Stephens Core; planktonic foraminifera (F), calcareous nannofossil (N) and stable isotope (Is) events. Foraminiferal and isotope events from Miller *et al.* (in press), nannofossil events from this study, age assignments as in Chapter 2.

The placement of the Eocene-Oligocene boundary is also uncertain in this section. The LO of the planktonic foraminifera genus *Hantkenina* in this section occurs at 163ft (49.68m), below the LO of *T. cerroazulensis*, whose LAD is generally accepted to be the marginally older bioevent (Berggren & Pearson 2005). Specimens of *Hantkenina* are rare within this succession and the recorded LO is almost certainly depressed. Interpolating between the recorded LO of *T. cerroazulensis* and the base of magnetochron C13n, Miller *et al.* (in press) predicted that *Hantkenina* should range to ~157.5ft (48.01m).

After recovery, the St Stephens Core was split with half-cores archived at the Geological Survey of Alabama, Tuscaloosa, Alabama and Rutgers Core Repository (Miller et al., in press). The study of Miller *et al.* (in press) is based upon the Rutgers half-core, whereas this study is based on samples taken in May 2007 from the in-tact half-core stored at the Geological Survey of Alabama. The core was archived in 2ft (0.61m) sections, labeled with depth top and bottom, which provides a high degree of confidence in the depth correlation between the two half-cores, however where the

core was fractured or disturbed there may be small inaccuracies in correlation between the two half-cores within each 2ft section (see below).

Sediment samples, approximately $2cm^3$ in volume, were extracted at a frequency of one per 0.25ft (0.08m) between 177 and 144ft (53.95 – 43.89m) and shipped back to UCL for analysis. Simple smear-slides were made in the laboratory at UCL following the method described in Chapter 2. All of the samples appeared homogeneous on the millimetre scale with no sign of laminations. An initial biostratigraphic examination of selected slides revealed a marked change from poorly preserved, moderate to low abundance nannofossil assemblages within a matrix of abundant amorphous carbonate at and below 165.75ft (50.52m), to an abundant, diverse and well-preserved nannofossil assemblage from 165.5ft (50.44m) and above. This change is interpreted as correlating to the sequence boundary identified by Miller *et al.* (in press) at 165.3ft (50.38m), which is marked by a similar change in nannofossil preservation. This implies that the correlation between the two half-cores at this point is in error by between 0.2 and 0.45ft (0.06 – 0.14m). This discrepancy has not been corrected for - all depths for the data presented within this study are as recorded from the Geological Society of Alabama half-core; data from Miller *et al.* (in press) have depths assignments taken from the Rutgers half-core.

A total of 52 slides were examined for calcareous nannofossils, from 165.5ft (50.44m) to 152.0ft (46.33m), using standard light microscope techniques at a magnification of 1250x on an Olympus BX40 microscope. All samples from the studied section contain abundant and diverse well to very well-preserved nannofossil assemblages. All whole, identifiable nannofossil specimens counted within each field of view (FOV), and consecutive FOVs where examined until at least 400 complete, *in situ*, identifiable nannofossils had been counted. Specimens were identified to species level wherever possible, following the taxonomy of Bown (2005b) and Bown & Dunkley Jones (2006). During this count, the number of cubic and framboidal pyrite, glauconite and amorphous carbonate grains were also counted per FOV. Samples and slides are curated at the Department of Earth Sciences, University College London.

A Principal Component Analysis (PCA) was performed, following the same methodology as in Chapter 2, on a reduced set of relative abundance data of 23 species, with the exclusion of species whose standard deviation of their relative abundances was less than 0.25%. Data was additive-log-ratio (ALR) transformed using the small form of *Cyclicargolithus floridanus* (<5μm) as the denominator. Metric Multi-dimensional Scaling (MMDS) was performed on the same ALR transformed, standardized data set following the methodology of Chapter 2.

5.3 Results

Nannofossil abundance, counts of amorphous carbonate and cubic pyrite, Shannon diversity (H) and log species richness (S) are shown in Figure 5.3. Nannofossil abundance is variable but high throughout the studied section (Figure 5.3) - ranging from 1195 to 5595 specimens/mm^2 with a mean value of 3385 specimens/mm^2. The counts of amorphous carbonate grains are distinctly higher at the base of the section, with a mean value of 1177 grains/mm^2 between 165.5 and 163ft (50.44 to 49.68m)

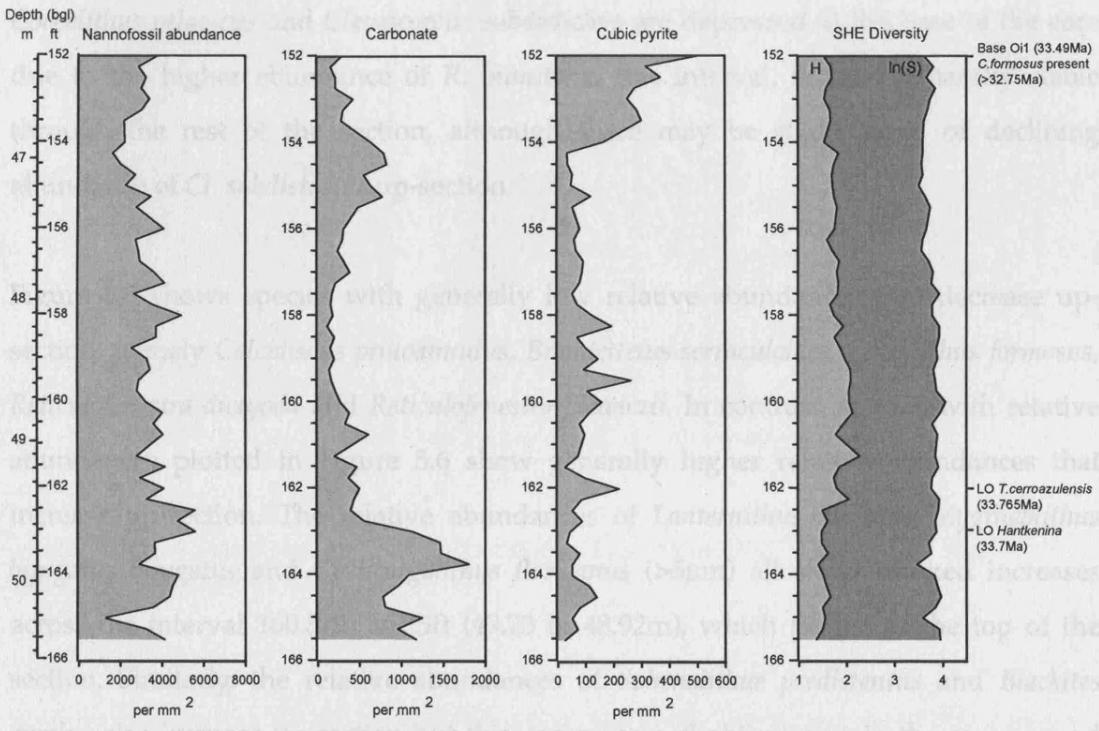

Figure 5.3 Nannofossil, amorphous carbonate and cubic pyrite abundance, Shannon diversity (H) and log species richness (ln(S)) against depth (m/ft bgl).

compared to a mean value of 355 grains/mm^2 between 162.75 and 152ft (49.61 to 46.33m). There is also broad interval of minimum carbonate content between 160 and 156ft (48.77 to 47.55m). Counts of cubic pyrite are fairly constant through much of the core, but increase significantly at 154ft (46.94m) (mean of 88 grains/mm^2 below and 308 grains/mm^2 above), which is the level of the Shubuta-Bumpnose contact. There is no significant shift in species richness through the succession, with a range of 32 to 58 and average of 44 species per sample. The Shannon diversity parameter, H, is somewhat lower at the base of the core, below 162.5ft (49.53m) (mean value 1.52), compared to the section above this level (mean value 1.80).

Plots of the relative abundance for the main species components are shown in Figures 5.4 and 5.5. Figure 5.4 shows the relative abundances of the dominant and sub-dominant species. The small form of *Cyclicargolithus floridanus* (<5μm) is the dominant species through most of the succession, except for the section below 162.25ft (49.45m), which has significantly higher abundances of *Reticulofenestra minuta*, which dominates most of the assemblages in this interval (mean abundance of *R. minuta* from 162.25ft and below is 42%; above is 7.2%). The relative abundance of the sub-dominant taxa *Coccolithus pelagicus* and *Clausicoccus subdistichus* are depressed at the base of the core due to the higher abundance of *R. minuta* in this interval, but are generally stable through the rest of the section, although there may be slight trend of declining abundance of *Cl. subdistichus* up-section.

Figure 5.5 shows species with generally low relative abundances that decrease up-section, namely *Calcidiscus protoannulus, Bramletteius serraculoides, Coccolithus formosus, Reticulofenestra dictyoda* and *Reticulofenestra filewiczii*. In contrast, species with relative abundances plotted in Figure 5.6 show generally higher relative abundances that increase up-section. The relative abundances of *Lanternithus minutus, Zygrhablithus bijugatus bijugatus* and *Cyclicargolithus floridanus* (>5μm) all show marked increases across the interval 160.5 to 161.5ft (49.23 to 48.92m), which persist to the top of the section. Similarly, the relative abundances of *Sphenolithus predistentus* and *Blackites amplus* also increase up-section but this commences slightly lower in the core around 162ft (49.38m). Two low-abundance holococcolith taxa, *Holodiscolithus geisenii* and

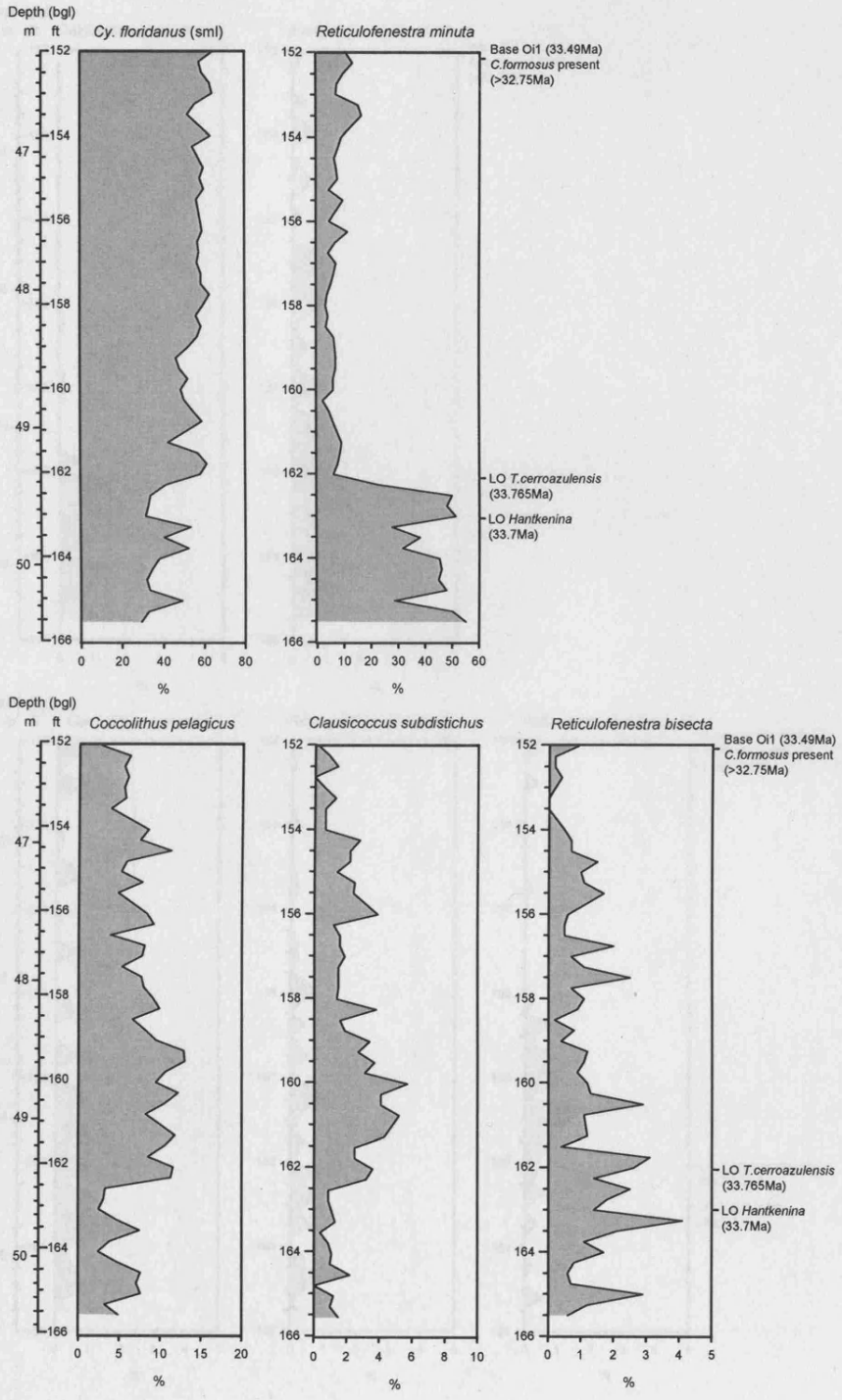

Figure 5.4 Nannofossil species relative abundance data against depth (m/ft bgl) - dominant and sub-dominant taxa.

Holococcolith sp., are nearly absent from the lower part of the section but become more abundant at depths of 157.25ft (47.93m) and 160ft (48.77m) respectively. Although the increases in relative abundances of *Sphenolithus predistentus* and *Blackites amplus*, may

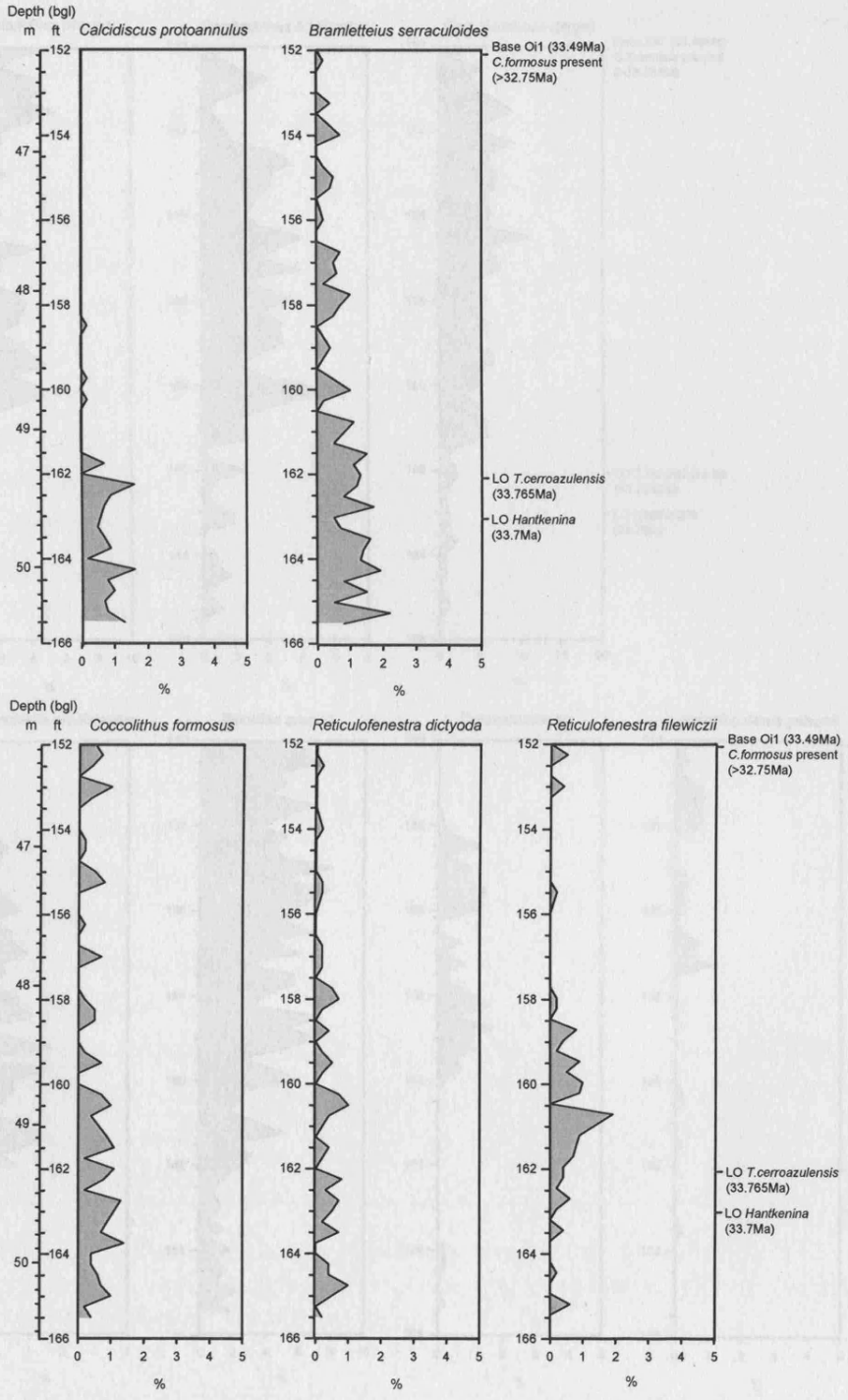

Figure 5.5 Nannofossil species relative abundance data against depth (m/ft bgl) - species with generally declining abundance up-section.

be partially influenced by the drop in abundance of *R. minuta* at around 162ft (49.38m), the increases in the other species in Figure 5.6 are independent of this event.

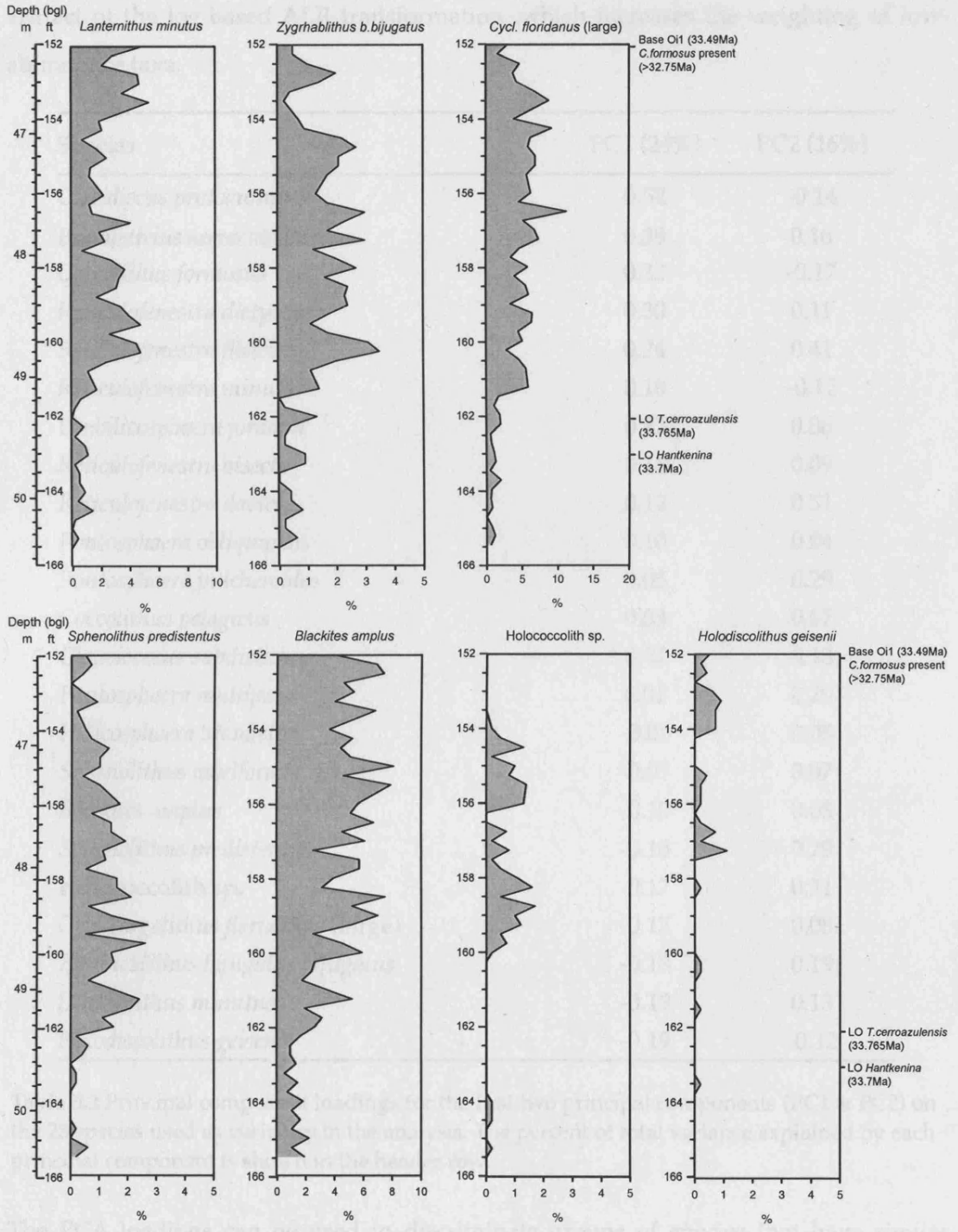

Figure 5.6 Nannofossil species relative abundance data against depth (m/ft bgl) - species with generally increasing abundance up-section.

The loadings of the first two principal components (PC1 and PC2), on the 23 species analyzed, are listed in Table 5.2. PC1 explains 24% of the observed variance in the data, and PC2 16%; these values are lower than might be expected, but this is largely an

artifact of the log-based ALR transformation, which increases the weighting of low-abundance taxa.

Species	PC1 (24%)	PC2 (16%)
Calcidiscus protoannulus	0.52	-0.14
Bramletteius serraculoides	0.39	0.16
Coccolithus formosus	0.33	-0.17
Reticulofenestra dictyoda	0.30	0.11
Reticulofenestra filewiczii	0.24	0.41
Reticulofenestra minuta	0.18	-0.12
Umbilicosphaera jordanii	0.17	0.06
Reticulofenestra bisecta	0.16	0.09
Reticulofenestra daviesii	0.12	0.51
Pontosphaera obliquipons	0.10	0.04
Pontosphaera pulcheroides	0.05	0.29
Coccolithus pelagicus	0.03	0.07
Clausicoccus subdistichus	0.02	0.18
Pontosphaera multipora	0.01	0.29
Helicosphaera bramlettei	-0.05	0.05
Sphenolithus moriformis	-0.05	0.07
Blackites amplus	-0.10	0.05
Sphenolithus predistentus	-0.16	0.29
Holococcolith sp.	-0.17	0.31
Cyclicargolithus floridanus (large)	-0.17	0.08
Zygrhablithus bijugatus bijugatus	-0.18	0.19
Lanternithus minutus	-0.19	0.13
Holodiscolithus geisenii	-0.19	-0.12

Table 5.2 Principal component loadings for the first two principal components (PC1 & PC2) on the 23 species used as variables in the analysis. The percent of total variance explained by each principal component is shown in the header row.

The PCA loadings can be used to discriminate groups of species that have similar loadings in one or both principal components. *Calcidiscus protoannulus, Bramletteius serraculoides, Coccolithus formosus, Reticulofenestra dictyoda,* and *Reticulofenestra filewiczii* (Group 1) have the largest positive loadings on PC1 (0.52 to 0.24) whereas *Holodiscolithus geisenii, Lanternithus minutus, Zygrhablithus bijugatus bijugatus,*

Cyclicargolithus floridanus (large), Holococcolith sp.1, *Sphenolithus predistentus* and *Blackites amplus* (Group 2) have the largest negative loadings on PC1 (-0.10 to –0.19).

The plot of the first two principal component scores (PC1 against PC2) for all the samples analyzed and the plots of these scores with depth (Figure 5.7) reveal a clear

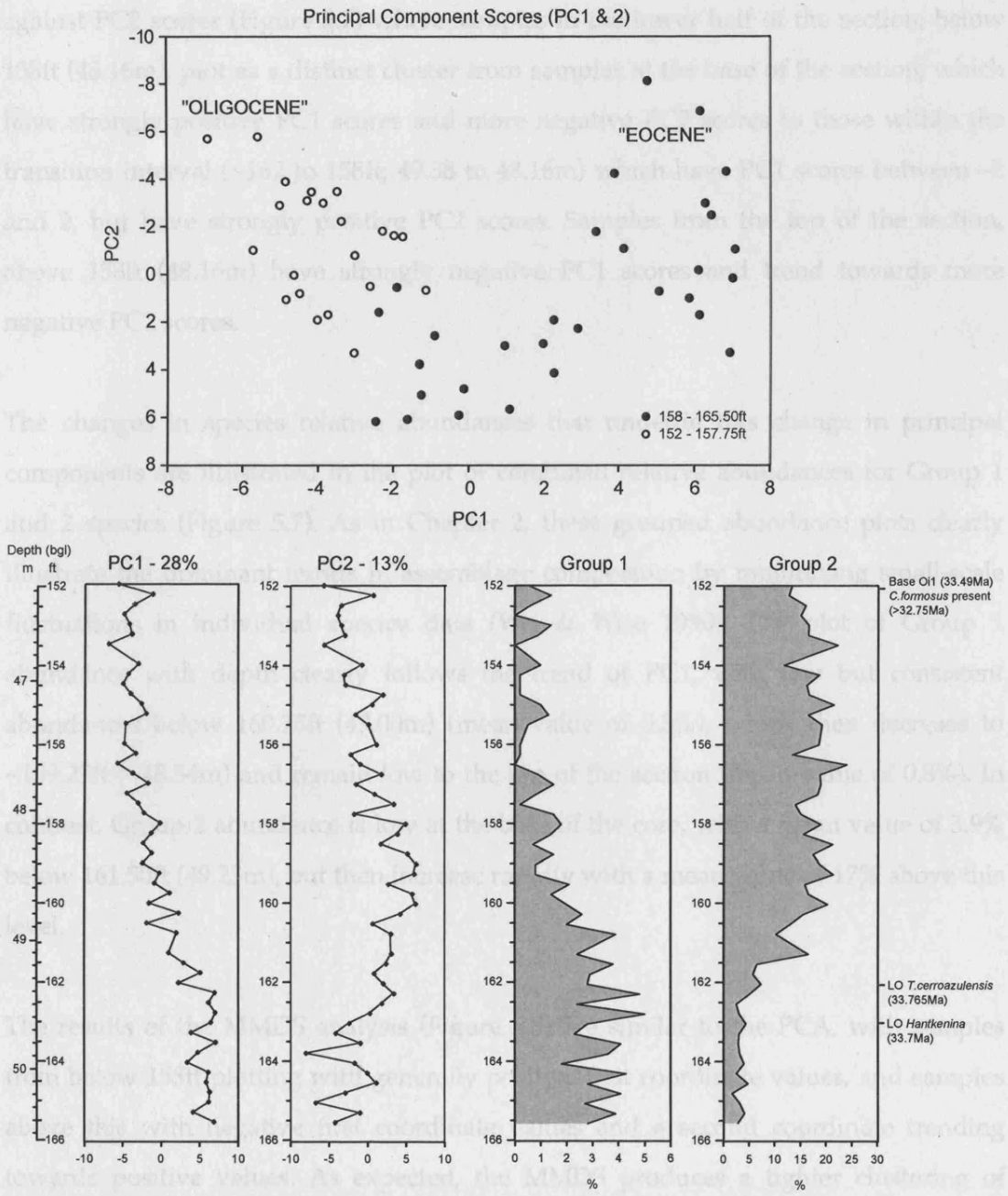

Figure 5.7 Principal component scores for the first two principal components; plotted against each other for all samples (top) and plotted against sample depth (bottom left). In the upper figure, "Eocene" samples are from below 158ft, and "Oligocene" are from above 157.75ft. Also plotted are summed percent relative abundances of Group 1 and 2 species (bottom right).

and marked change in assemblages through the section. The first principal component scores are relatively stable and positive (mean 5.77) at the base of the section, between 165.5 and 162.25ft (48.77 to 49.45m), but then steadily shift to more negative values, up to 156.5ft (47.70m); above this level they are again relatively stable but with consistently negative values (mean –4.1). This trend is clearly visible in the plot of PC1 against PC2 scores (Figure 5.7) where samples in the lower half of the section, below 158ft (48.16m), plot as a distinct cluster from samples at the base of the section, which have strongly positive PC1 scores and more negative PC2 scores to those within the transition interval (~162 to 158ft; 49.38 to 48.16m) which have PC1 scores between –2 and 2, but have strongly positive PC2 scores. Samples from the top of the section, above 158ft (48.16m) have strongly negative PC1 scores and trend towards more negative PC2 scores.

The changes in species relative abundances that underlie this change in principal components are illustrated in the plot of combined relative abundances for Group 1 and 2 species (Figure 5.7). As in Chapter 2, these grouped abundance plots clearly illustrate the dominant trends in assemblage composition by minimizing small-scale fluctuations in individual species data (Wei & Wise 1990). The plot of Group 1 abundance with depth clearly follows the trend of PC1, with low but consistent abundances below 160.75ft (49.00m) (mean value of 3.3%), which then decrease to ~159.25ft (~48.54m) and remain low to the top of the section (mean value of 0.8%). In contrast, Group 2 abundance is low at the base of the core, with a mean value of 3.9% below 161.50ft (49.23m), but then increase rapidly with a mean value of 17% above this level.

The results of the MMDS analysis (Figure 5.8) are similar to the PCA, with samples from below 158ft plotting with generally positive first coordinate values, and samples above this with negative first coordinate values and a second coordinate trending towards positive values. As expected, the MMDS produces a tighter clustering of "adjacent" samples and a greater differentiation between samples from the top and bottom of the section compared to the PCA. The plot of the first coordinate values with

depth closely follows the trend of PC1 scores with depth but again with less variability between adjacent samples, producing a smoother representation of the overall trend.

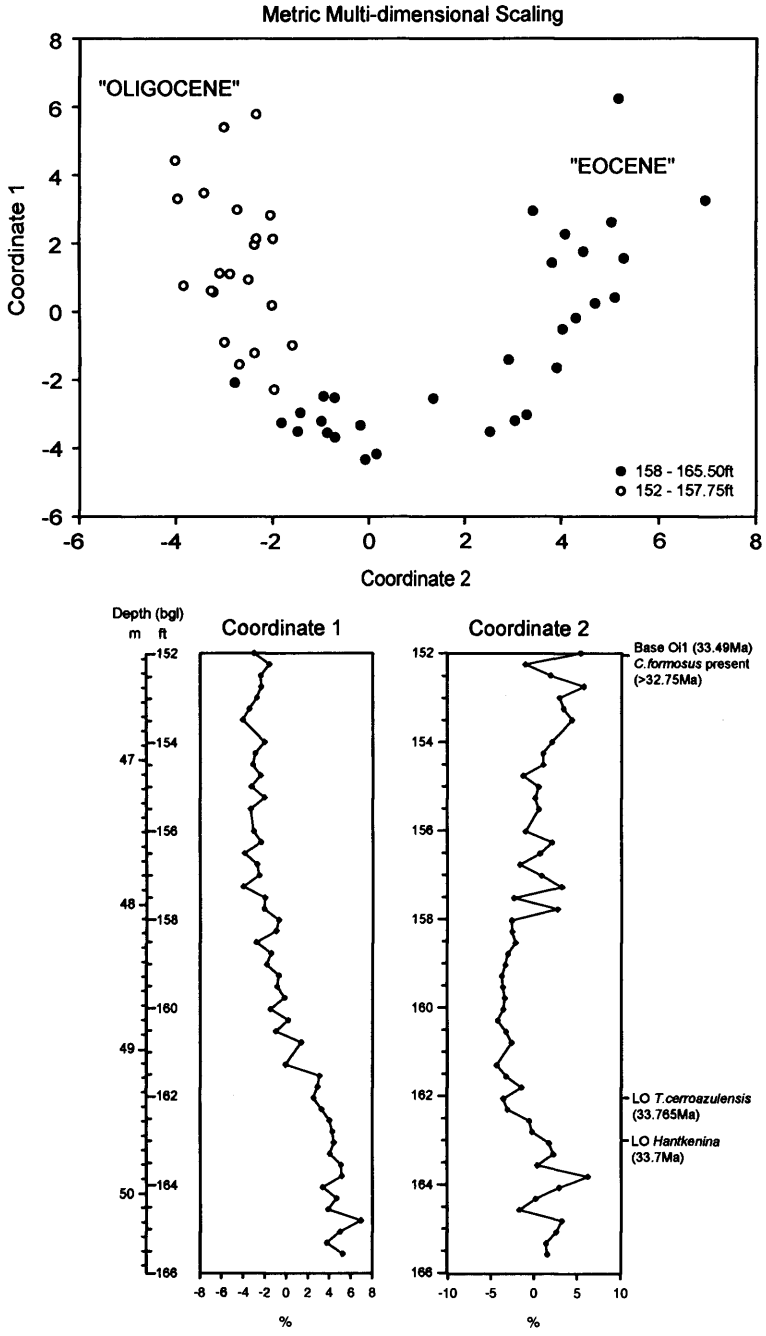

Figure 5.8 Results of the Metric Multi-dimensional Scaling analysis; coordinates 1 and 2 plotted against each other for all samples (top) and plotted against sample depth (bottom). In the upper figure, "Eocene" samples are from below 158ft, and "Oligocene" are from above 157.75ft.

5.4 Discussion

The mineralogical count data presented in this study closely parallel the quantitative lithological results of Miller *et al.* (in press). Counts of amorphous carbonate grains (Figure 5.3) follow an identical trend to the percent carbonate sand (Figure 5.2) with high values at the base of the section, below ~163ft (49.68m), which then decline to a minimum between ~160 and 156ft (48.77 – 47.55m), before increasing slightly above ~155ft (47.24m). This provides confidence that both half-cores are well correlated and that the smear-slide count data accurately reflects the sediment make-up. The sudden increase in cubic pyrite grains from above 154ft (46.94m), correlates directly with the Shubuta-Bumpnose Fm. boundary at 154.1ft (46.97m), with increased pyrite concentrations in the basal blue clay of the Bumpnose Limestone Fm., which again provides confidence in the correlation between the two half-cores.

Calcareous nannofossil assemblages appear to be relatively stable up to 162.25ft (49.45m), when there is a marked drop, of ~30%, in the relative abundance of *R. minuta* (Figure 5.4), which in turn causes an increase in Shannon diversity and probably contributes to the increases in the relative abundances of the sub-dominant taxa *Coccolithus pelagicus* and *Clausicoccus subdistichus* at the same level (Figure 5.4). This almost directly correlates with both the first step in $\delta^{18}O$ of ~0.5‰ and the LO of *T. cerroazulensis* group planktonic foraminifera at 162ft (49.38m). These rapid changes are then closely followed by a marked increase in the abundance of *Lanternithus minutus, Zygrhablithus bijugatus bijugatus, Cyclicargolithus floridanus* (large) and combined Group 2 abundances between ~161.5 and 160.5ft (49.23 – 48.92m) (Figures 5.6 & 5.7). These increases in relative abundances lag, and hence are independent of, the decrease in abundance of *R. minuta*. Above this level there is a broad decline in the combined abundance of Group 1 species between 160.75 and 159.25ft (49.00 – 48.54m) (Figure 5.7).

All of these changes in nannofossil assemblages are reflected in the results of the multivariate analyses, especially the trends in the first principal component of the PCA and coordinate one of the MMDS. These multivariate statistics show a clear pattern of

stability at the base of the section (165.5 to 162.5ft; 50.44 to 49.53m), followed by a steady change from 162.25 to ~156.5ft (49.45 to ~47.70m). The start of these shifts correlates directly with the first step in $\delta^{18}O$ and the LO of *T. cerroazulensis*, however these measures stabilize within the plateau in $\delta^{18}O$ between ~161 - 155ft (49.07 – 47.24m). Above this level it is striking that there is no discernible change in nannofossil assemblages across the second, and larger, shift in $\delta^{18}O$ between 155 and 152ft (47.24 – 46.33m), into the EOGM.

On the basis of their benthic foraminiferal facies analysis, and associated paleodepth interpretations (see Figure 5.2), Miller *et al.* (in press) argue that there is no, or little, sea level fall associated with the first positive step in $\delta^{18}O$ but that there is an estimated ~55m of sea level fall coincident with the second step in $\delta^{18}O$ into the EOGM. This implies that the first step in $\delta^{18}O$, as recorded in the *Cibicidoides* spp. of benthic foraminifera, is almost entirely due to the local cooling of bottom waters, which due to the shallow water depths (~125m pre-EOT) at this site would almost certainly be associated with a cooling of local surface waters. Such a cooling of surface waters has recently been confirmed by coupled measurements of $\delta^{18}O$ and Mg/Ca ratios in planktonic foraminifera at this site (Bridget Wade pers. comm.). The onset of the major shifts in nannofossil assemblages at this site coincident with the first step in $\delta^{18}O$ strongly indicates that these changes are controlled by a cooling of surface waters either directly or via the associated changes in water column stratification and mixing. The extent of the surface water environmental perturbation at this time is indicated by the coincident extinction of the *Turborotalia cerroazulensis* group of planktonic foraminifera. As in the Tanzanian record the major shift in nannofossil assemblages is complete by the time of the second shift in $\delta^{18}O$, which, along with the EOGM, appears to have had little effect on the calcareous plankton.

In terms of the species specific response to the EOT, as in the Tanzanian sites and DSDP Site 242, there is a clear increase in the abundance of the large form of *Cyclicargolithus floridanus* and, to a lesser extent, of *Sphenolithus predistentus* between the two steps in $\delta^{18}O$ (Figure 5.6). Although present at much lower abundances than in the Tanzanian sites, there is a similar decline in the abundance of *Calcidiscus protoannulus*,

to very sporadic occurrences, in the earliest stages of the EOT. The differences in abundance of *C. protoannulus* between the study sites - it occurs in very low abundances in DSDP Site 242 - and its sensitivity to the earliest, cooling-dominated period of the EOT, indicates that this species has a strong warm-water affinity. In contrast to the Tanzanian sites there is an increase in holococcolith abundance, especially of *Lanternithus minutus* and *Zygrhablithus bijugatus bijugatus*, during the EOT. Finally, the largest change in any species is the dramatic decline, from ~40% to ~10%, in the relative abundance of *Reticulofenestra minuta* almost coincident with the LO of *T. cerroazulensis* at the onset of the first $\delta^{18}O$ step.

Although all of these changes are clearly correlated to the EOT transition, especially with the first $\delta^{18}O$ step, taken together it is more difficult to build a coherent picture of the environmental controls on these assemblage changes compared to the Tanzanian record. If the increased abundances of the large form of *Cyclicargolithus floridanus* and *Sphenolithus predistentus* are driven by more eutrophic conditions, it is then difficult to explain the increased abundance of holococcoliths and loss of *Reticulofenestra minuta*, which from its abundance and size is probably an r-selected, bloom-forming taxa. It is possible that *R. minuta* is able to exploit more eutrophic conditions but that it is also strongly temperature controlled, as indicated by its rapid decline at the first $\delta^{18}O$ step. The holococcolith record may be partly explained by an increased quality of preservation above ~162ft (49.38m), which was noted qualitatively during nannofossil counts and correlates with a marked decrease in carbonate contents (Figures 5.2 & 5.3). This improvement in nannofossil preservation is probably due to an increase in the relative clay content of these sediments, which would limit post-depositional diagenetic recrystallization. Although this may have influenced the quality of holococcolith preservation, the consistent presence of moderately well-preserved holococcoliths, especially the more robust *L. minutus* and *Z. b. bijugatus*, throughout the studied interval indicates that a substantial part of the increase in holococcolith abundance is a primary ecological signal.

The most recent estimate of the position of the EOB in the St Stephens section, based on an interpolation between the last occurrence of *T. cerroazulensis* and the base of

magnetochron C13n, places it at 157.5ft (48.01m). This horizon is within the main shift in nannofossil assemblages between 162.25 to ~156.5ft (49.45 to ~47.70m), however, unlike the Tanzanian record there appears to be no sign of accelerated or stepped change at or near to the EOB itself. The complexities of both the taxon-specific changes though the EOT and the limited response to the EOB event at this site, in comparison to the Tanzanian record, may be explained by the different paleoceanographic settings of the two locations. Whereas the Tanzanian site is situated around the shelf-slope break and, based on its nannofossil assemblages, clearly has a strong connection to the open-ocean, the St Stephens section is located on the shelf in shallower water depths (<125m) and is largely sheltered from the open-ocean at the northern margin of the Gulf of Mexico embayment. As a result the environmental and assemblage changes at St Stephens will be influenced by regional/global events, such as widespread cooling, but these will be combined with strong local controls, such as water depth, which at this location roughly halves during the EOT, water-column mixing/stratification, the position of the paleoshoreline and the associated changes in sediment and nutrient supply. A more detailed comparison between the EOT records from the St Stephens section and those of the other study sites will be made in Chapter 6.

5.5 Systematic palaeontology

The taxonomy presented here follows the higher taxonomic rationale and species concepts outlined in Chapter 3. Light microscope images were captured using Scion Image software and macros written by Dr. Jeremy Young (Bown & Young 1998). All light microscope images were captured at the same magnification with a two-micron scale bars shown on each plate (magnification ~x 2180). All sample material and images are stored in the Department of Earth Sciences, University College London.

5.6.1 Placolith coccoliths

Order **ISOCHRYSIDALES** Pascher 1910

Family **NOELAERHABDACEAE** Jerkovic 1970 emend. Young & Bown 1997

Genus ***CYCLICARGOLITHUS*** Bukry 1971

Cyclicargolithus floridanus (Roth & Hay in Hay et al. 1967) Bukry 1971 (Pl. 5.1, figs 1-3)

REMARKS: Specimens informally divided into small (<5μm) and large (>5μm) morphotypes.

Genus ***RETICULOFENESTRA*** Hay, Mohler & Wade 1966

Reticulofenestra dictyoda (Deflandre *in* Deflandre & Fert 1954) Stradner *in* Stradner & Edwards 1968 (Pl. 5.1, figs 4-5)

Reticulofenestra umbilicus (Levin 1965) Martini & Ritzkowski 1968 (Pl. 5.1, fig. 6)

Reticulofenestra minuta Roth 1970 (Pl. 5.1, fig. 7)

Reticulofenestra bisecta (Hay *et al.* 1966) Roth 1970 (Pl. 5.1, fig. 8).

Reticulofenestra stavensis (Levin & Joerger 1967) Varol 1989 (Pl. 5.1, fig. 9)

Reticulofenestra filewiczii Wise & Wiegand *in* Wise 1983 stat. nov. (Pl. 5.1, fig. 10)

Reticulofenestra daviesii (Haq, 1968) Haq, 1971 (Pl. 5.1, figs 11-13)

Reticulofenestra lockeri Müller, 1970 (Pl. 5.1, fig. 14)

Reticulofenestra macmillanii sp. nov. (Pl. 5.1, fig. 15)

REMARKS: See Chapter 3 for description.

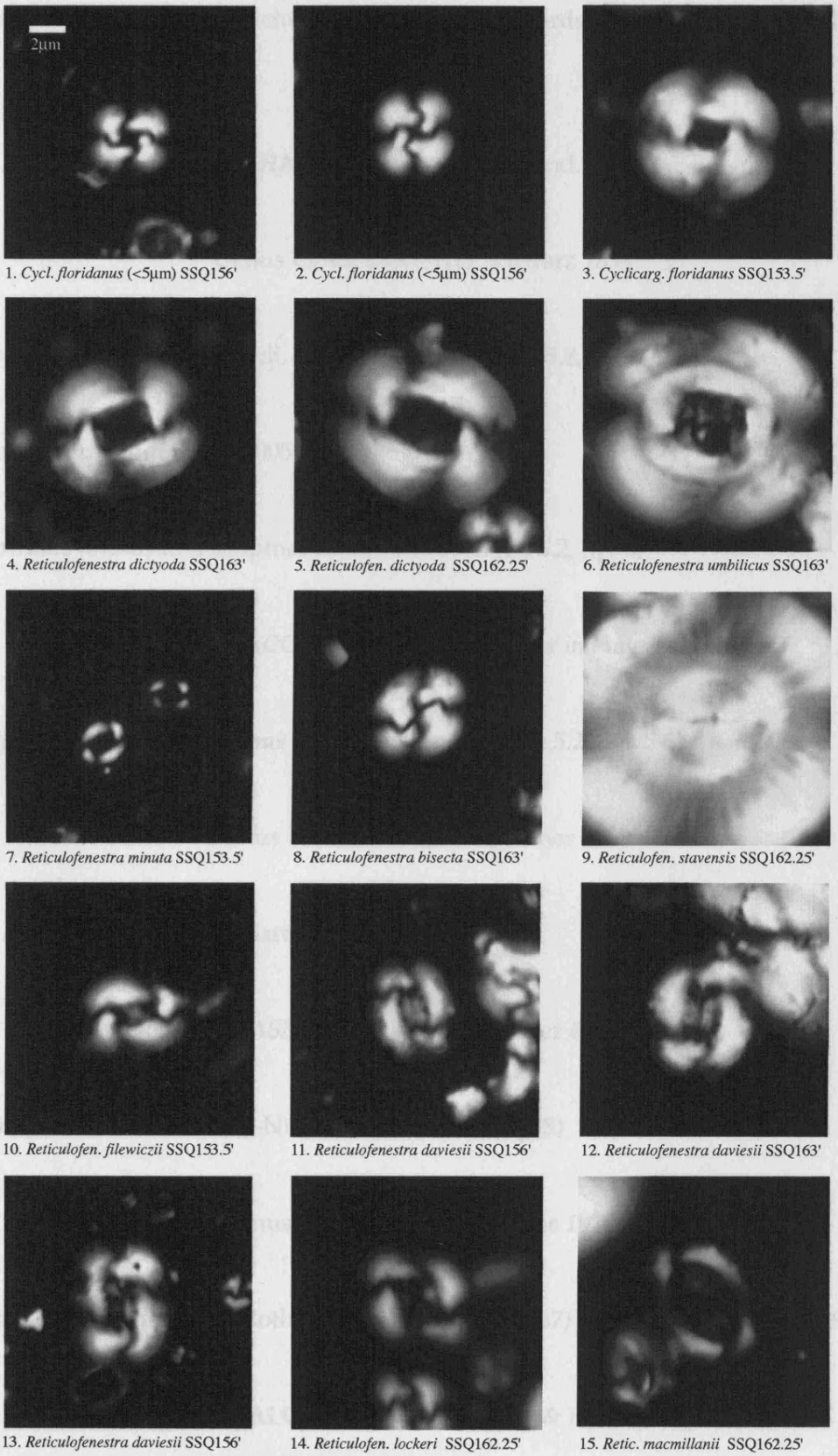

1. *Cycl. floridanus* (<5µm) SSQ156'
2. *Cycl. floridanus* (<5µm) SSQ156'
3. *Cyclicarg. floridanus* SSQ153.5'
4. *Reticulofenestra dictyoda* SSQ163'
5. *Reticulofen. dictyoda* SSQ162.25'
6. *Reticulofenestra umbilicus* SSQ163'
7. *Reticulofenestra minuta* SSQ153.5'
8. *Reticulofenestra bisecta* SSQ163'
9. *Reticulofen. stavensis* SSQ162.25'
10. *Reticulofen. filewiczii* SSQ153.5'
11. *Reticulofenestra daviesii* SSQ156'
12. *Reticulofenestra daviesii* SSQ163'
13. *Reticulofenestra daviesii* SSQ156'
14. *Reticulofen. lockeri* SSQ162.25'
15. *Retic. macmillanii* SSQ162.25'

Plate 5.1 LM images of *Cyclicargolithus* and *Reticulofenestra* placoliths.

Order **COCCOLITHALES** Schwarz 1932 emend. Edvardsen & Eikrem in Edvardsen *et al.* 2000

Family **COCCOLITHACEAE** Poche 1913 emend. Young & Bown 1997

Genus ***COCCOLITHUS*** Schwarz 1894

Coccolithus pelagicus (Wallich, 1877) Schiller 1930 (Pl. 5.2, figs 1-2)

Coccolithus cachaoi Bown 2005 (Pl. 5.2, fig. 3)

Coccolithus formosus (Kamptner 1963) Wise 1973 (Pl. 5.2, fig. 4)

Genus ***CRUCIPLACOLITHUS*** Hay & Mohler *in* Hay *et al.* 1967

Cruciplacolithus* cf. *Cr. primus Perch-Nielsen 1977 (Pl. 5.2, figs 5-6)

Genus ***BRAMLETTEIUS*** Gartner 1969

Bramletteius serraculoides Gartner 1969 (Pl. 5.2, fig. 7)

Genus ***CHIASMOLITHUS*** Hay, Mohler & Wade 1966

Chiasmolithus nitidus Perch-Nielsen 1971 (Pl. 5.2, fig. 8)

Genus ***CLAUSICOCCUS*** Prins 1979

Clausicoccus subdistichus (Roth & Hay *in* Hay *et al.* 1967) Prins 1979 (Pl. 5.2, fig. 9)

Family **CALCIDISCACEAE** Young & Bown 1997

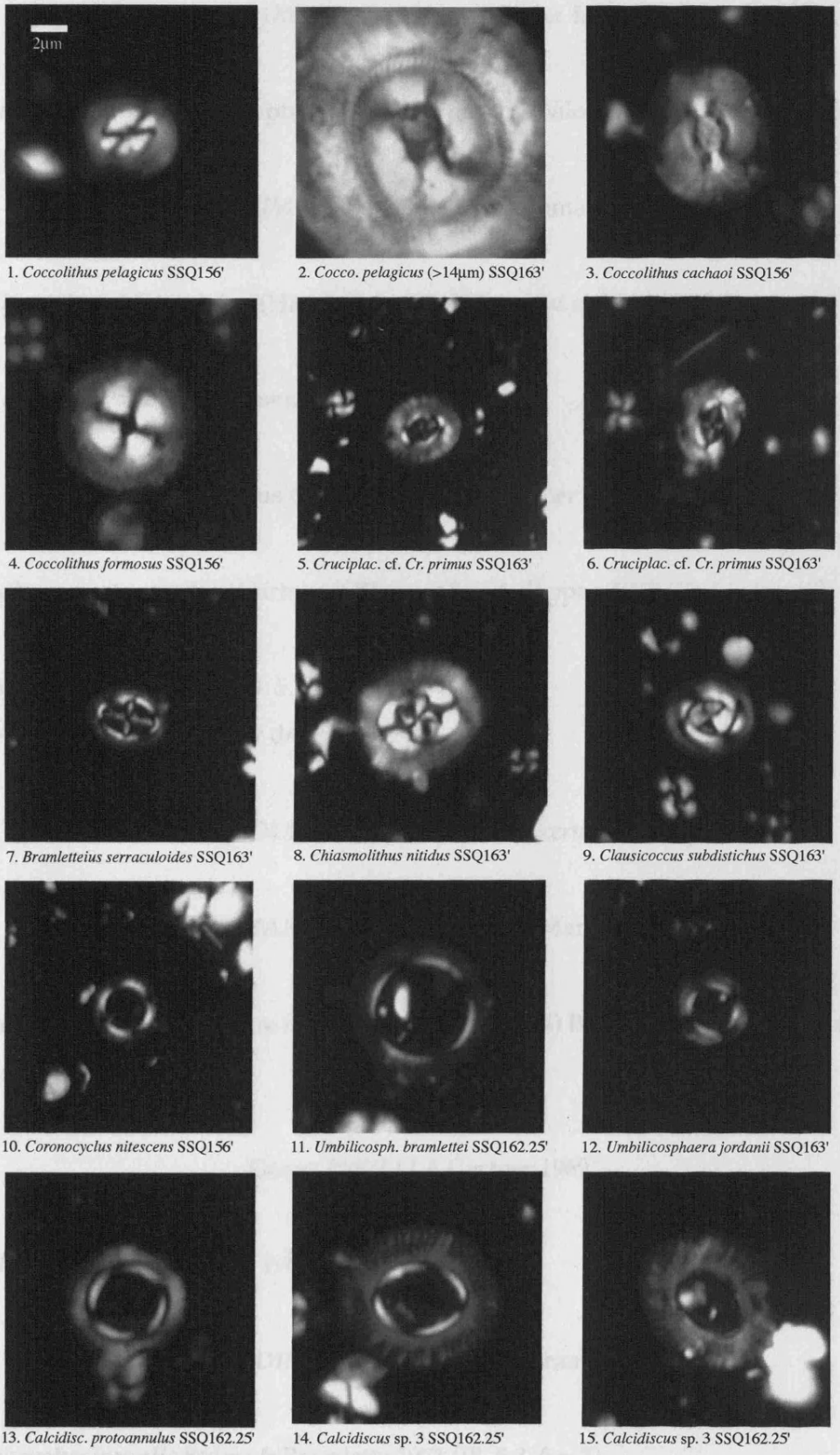

1. *Coccolithus pelagicus* SSQ156'
2. *Cocco. pelagicus* (>14µm) SSQ163'
3. *Coccolithus cachaoi* SSQ156'
4. *Coccolithus formosus* SSQ156'
5. *Cruciplac.* cf. *Cr. primus* SSQ163'
6. *Cruciplac.* cf. *Cr. primus* SSQ163'
7. *Bramletteius serraculoides* SSQ163'
8. *Chiasmolithus nitidus* SSQ163'
9. *Clausicoccus subdistichus* SSQ163'
10. *Coronocyclus nitescens* SSQ156'
11. *Umbilicosph. bramlettei* SSQ162.25'
12. *Umbilicosphaera jordanii* SSQ163'
13. *Calcidisc. protoannulus* SSQ162.25'
14. *Calcidiscus* sp. 3 SSQ162.25'
15. *Calcidiscus* sp. 3 SSQ162.25'

Plate 5.2 LM images of *Coccolithus*, *Cruciplacolithus*, *Bramletteius*, *Chiasmolithus*, *Clausicoccus*, *Coronocyclus*, *Umbilicosphaera* and *Calcidiscus* placoliths.

Genus ***CORONOCYCLUS*** Hay, Mohler & Wade 1966

Coronocyclus nitescens (Kamptner 1963) Bramlette & Wilcoxon 1967 (Pl. 5.2, fig. 10)

Genus ***UMBILICOSPHAERA*** Lohmann 1902

Umbilicosphaera bramlettei (Hay & Towe 1962) Bown *et al.* 2007 (Pl. 5.2, fig. 11)

Umbilicosphaera jordanii Bown 2005 (Pl. 5.2, fig. 12)

Genus ***CALCIDISCUS*** Kamptner 1950

Calcidiscus protoannulus (Gartner 1971) Loeblich & Tappan 1978 (Pl. 5.2, fig. 13)

***Calcidiscus?* sp. 3** sp. nov. (Pl. 5.2, figs 14-15)
REMARKS: See Chapter 3 for description.

PLACOLITH COCCOLITHS *Incertae Sedis*

Genus ***MARKALIUS*** Bramlette & Martini 1964

Markalius inversus (Deflandre *in* Deflandre & Fert 1954) Bramlette & Martini 1964 (Pl. 5.3, fig. 1)

Genus ***HAYELLA*** Gartner 1969

Hayella situliformis Gartner 1969 (Pl. 5.3, fig. 2)

Genus ***PEDINOCYCLUS*** Bukry & Bramlette 1971

Pedinocyclus larvalis Bukry & Bramlette 1971 (Pl. 5.3, fig. 3)

1. *Markalius inversus* SSQ153.5'
2. *Hayella situliformis* SSQ162.25'
3. *Pedinocyclus larvalis* SSQ153.5'
4. *Helicosphaera compacta* SSQ156'
5. *Helicosphaera compacta* SSQ156'
6. *Helicosphaera compacta* SSQ163'
7. *Helicosphaera reticulata* SSQ156'
8.
9. *Helicosphaera seminulum* SSQ163'
10. *Helicosphaera seminulum* SSQ156'
11. *Helicosphaera bramlettei* SSQ163'
12. *Helicosphaera bramlettei* SSQ163'
13. *Helicosphaera euphratis*. SSQ156'
14. *Helicosphaera euphratis* SSQ156'
15. *Helicosphaera euphratis* SSQ156'

Plate 5.3 LM images of *Markalius*, *Hayella* and *Pedinocyclus* placoliths and *Helicosphaera* muroliths.

5.5.2 Murolith Coccoliths

Order **ZYGODISCALES** Young & Bown 1997

Family **HELICOSPHAERACEAE** Black 1971

Genus *HELICOSPHAERA* Kamptner 1954

Helicosphaera compacta Bramlette & Wilcoxon 1967 (Pl. 5.3, figs 4-6)

Helicosphaera reticulata Bramlette & Wilcoxon 1967 (Pl. 5.3, figs 7-8)

Helicosphaera seminulum Bramlette & Sullivan 1961 (Pl. 5.3, figs 9-10)

Helicosphaera bramlettei (Müller 1970) Jafar & Martini 1975 (Pl. 5.3, figs 11-12)

Helicosphaera euphratis Haq 1966 (Pl. 5.3, figs 13-15)

Family **PONTOSPHAERACEAE** Lemmermann 1908

Genus *PONTOSPHAERA* Lohmann 1902

Pontosphaera multipora (Kamptner 1948 *ex* Deflandre 1954) Roth 1970 (Pl. 5.4, fig. 1)

Pontosphaera pectinata (Bramlette & Sullivan 1961) Sherwood 1974 (Pl. 5.4, figs 3-4)

Pontosphaera panarium (Deflandre *in* Deflandre & Fert 1954) Aubry 1986 (Pl. 5.4, fig. 7)

Pontosphaera versa (Bramlette & Sullivan 1961) Sherwood 1974 (Pl. 5.4, fig. 8)

Pontosphaera pulcheroides (Sullivan 1964) Romein 1979 (Pl. 5.4, figs 9-10)

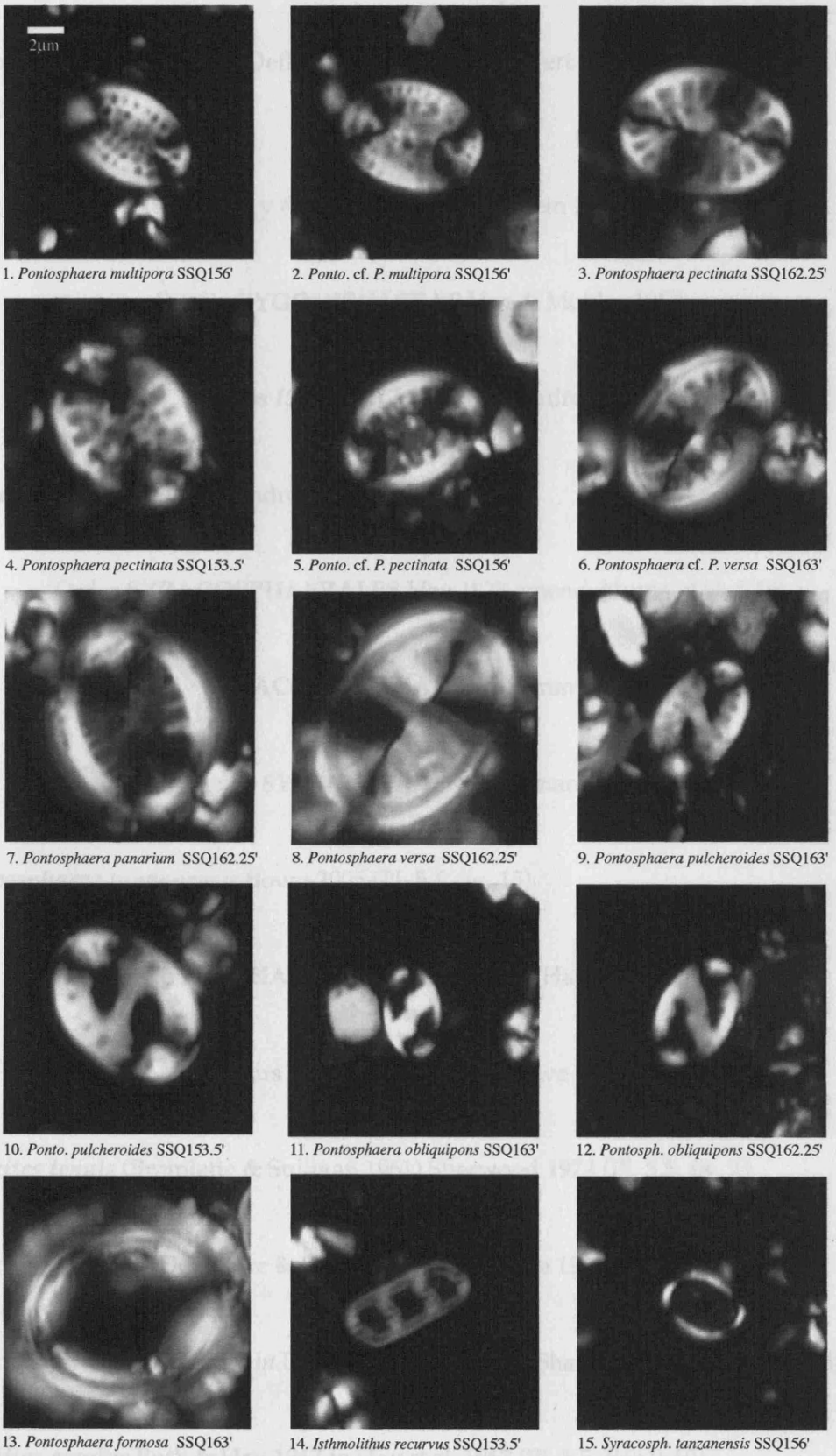

1. *Pontosphaera multipora* SSQ156'
2. *Ponto.* cf. *P. multipora* SSQ156'
3. *Pontosphaera pectinata* SSQ162.25'
4. *Pontosphaera pectinata* SSQ153.5'
5. *Ponto.* cf. *P. pectinata* SSQ156'
6. *Pontosphaera* cf. *P. versa* SSQ163'
7. *Pontosphaera panarium* SSQ162.25'
8. *Pontosphaera versa* SSQ162.25'
9. *Pontosphaera pulcheroides* SSQ163'
10. *Ponto. pulcheroides* SSQ153.5'
11. *Pontosphaera obliquipons* SSQ163'
12. *Pontosph. obliquipons* SSQ162.25'
13. *Pontosphaera formosa* SSQ163'
14. *Isthmolithus recurvus* SSQ153.5'
15. *Syracosph. tanzanensis* SSQ156'

Plate 5.4 LM images of *Pontosphaera, Isthmolithus* and *Syracosphaera* muroliths.

Pontosphaera obliquipons (Deflandre *in* Deflandre & Fert 1954) Romein 1979 (Pl. 5.4, fig. 11-12)

Pontosphaera formosa (Bukry & Bramlette 1968) Romein 1979 (Pl. 5.4, fig. 13)

Family **ZYGODISCACEAE** Hay & Mohler 1967

Genus ***ISTHMOLITHUS*** Deflandre 1954

Isthmolithus recurvus Deflandre 1954 (Pl. 5.4, fig. 14)

Order **SYRACOSPHAERALES** Hay 1977 emend. Young *et al.* 2003

Family **SYRACOSPHAERACEAE** Lemmermann 1908

Genus ***SYRACOSPHAERA*** Lohmann 1902

Syracosphaera tanzanensis Bown 2005 (Pl. 5.4, fig. 15)

Family **RHABDOSPHAERACEAE** Haeckel 1894

Genus ***BLACKITES*** Hay & Towe 1962

Blackites tenuis (Bramlette & Sullivan 1961) Sherwood 1974 (Pl. 5.5, fig. 1)

Blackites spinosus (Deflandre & Fert 1954) Hay & Towe 1962 (Pl. 5.5, figs 2-3)

Blackites vitreus (Deflandre *in* Deflandre & Fert 1954) Shafik 1981 (Pl. 5.5, figs 4-5)

Blackites amplus Roth & Hay 1967 *in* Hay *et al.* 1967 (Pl. 5.5, figs 9-10)

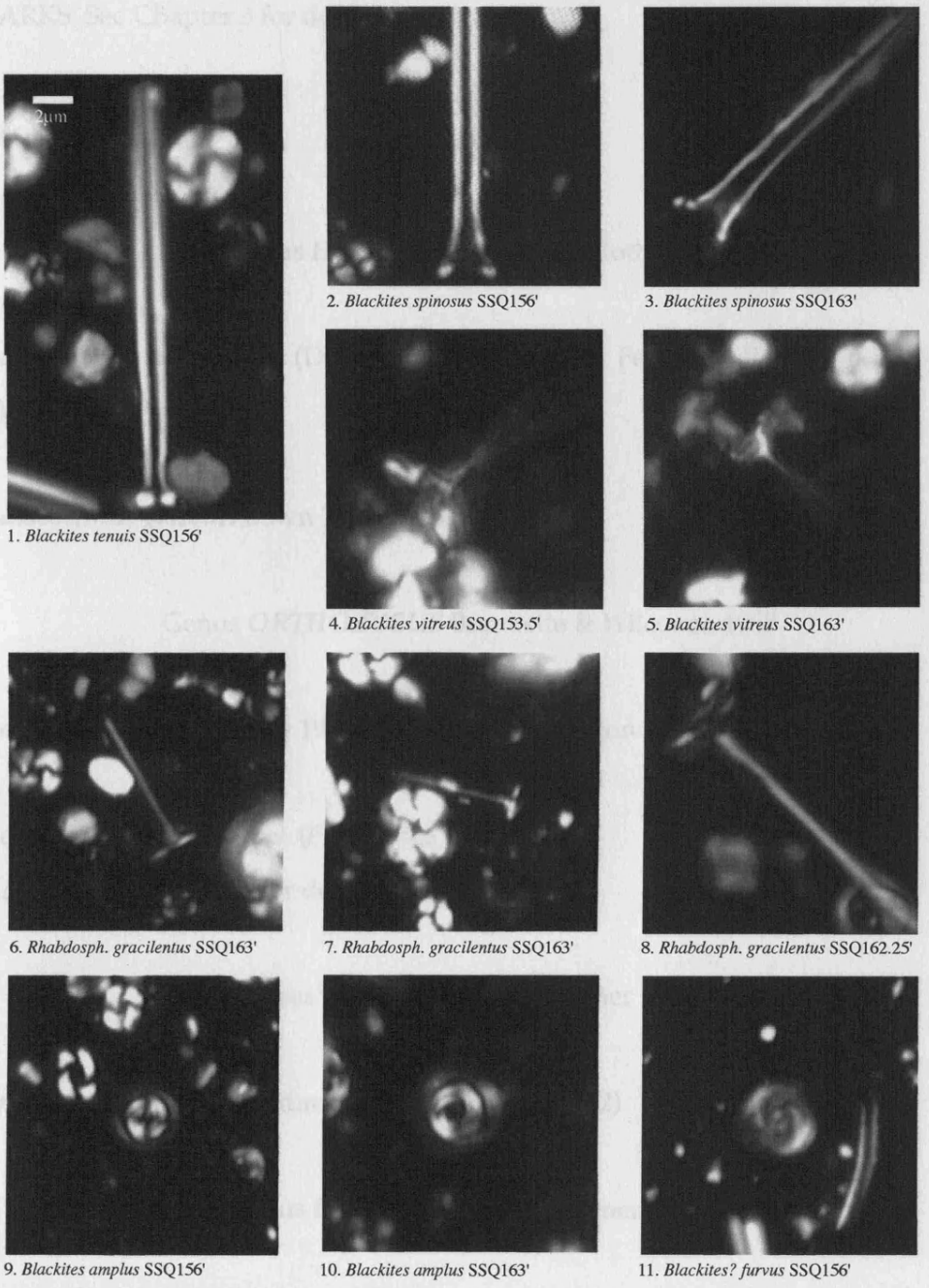

Plate 5.5 LM images of *Blackites* rhabdoliths.

Blackites? furvus Bown & Dunkley Jones 2006 (Pl. 5.5, fig. 11)

Genus ***RHABDOSPHAERA*** Haeckel 1894

Rhabdosphaera gracilentus (Bown & Dunkley Jones 2006) comb. nov. (Pl. 5.5, figs 6-8)

REMARKS: See Chapter 3 for details.

5.5.3 Holococcoliths

Genus ***HOLODISCOLITHUS*** Roth 1970

Holodiscolithus macroporus (Deflandre *in* Deflandre & Fert 1954) Roth 1970 (Pl. 5.6, fig. 1)

Holodiscolithus geisenii Bown 2005 (Pl. 5.6, figs 2-3)

Genus ***ORTHOZYGUS*** Bramlette & Wilcoxon 1967

Orthozygus aureus (Stradner 1962) Bramlette & Wilcoxon 1967 (Pl. 5.6, figs 7-8)

Orthozygus occultus sp. nov. (Pl. 5.6, figs 9-10)
REMARKS: See Chapter 3 for description.

Genus ***CORANNULUS*** Stradner 1962

Corannulus germanicus Stradner 1962 (Pl. 5.6, figs 11-12)

Genus ***LANTERNITHUS*** Stradner 1962

Lanternithus minutus Stradner 1962 (Pl. 5.6, fig. 13)

Genus ***ZYGRHABLITHUS*** Deflandre 1959

Zygrhablithus bijugatus (Deflandre *in* Deflandre & Fert 1954) Deflandre 1959 ***cornutus*** Bown 2005 (Pl. 5.6, fig. 14)

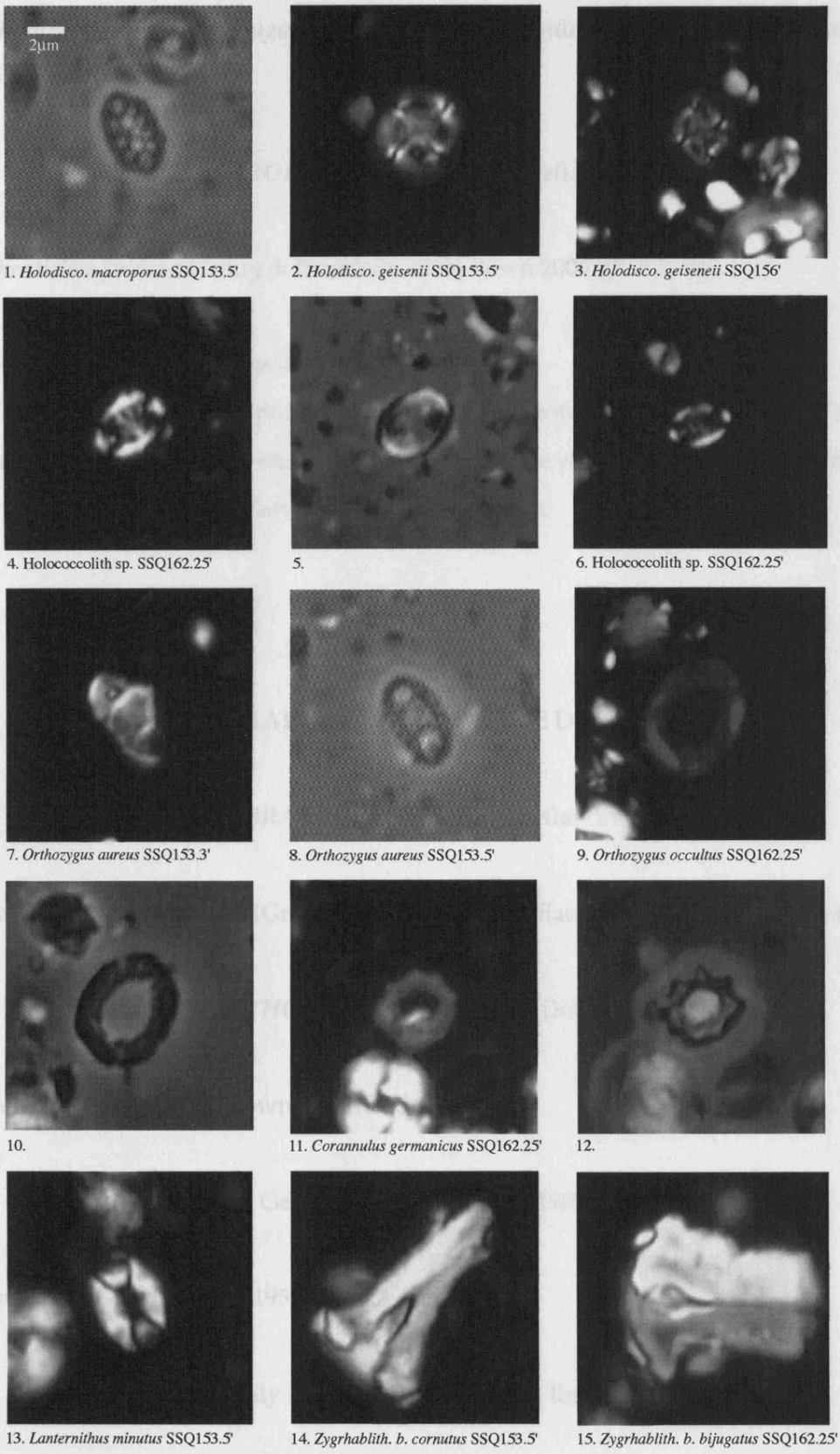

1. *Holodisco. macroporus* SSQ153.5'
2. *Holodisco. geisenii* SSQ153.5'
3. *Holodisco. geiseneii* SSQ156'
4. Holococcolith sp. SSQ162.25'
5.
6. Holococcolith sp. SSQ162.25'
7. *Orthozygus aureus* SSQ153.3'
8. *Orthozygus aureus* SSQ153.5'
9. *Orthozygus occultus* SSQ162.25'
10.
11. *Corannulus germanicus* SSQ162.25'
12.
13. *Lanternithus minutus* SSQ153.5'
14. *Zygrhablith. b. cornutus* SSQ153.5'
15. *Zygrhablith. b. bijugatus* SSQ162.25'

Plate 5.6 LM images of *Holodiscolithus, Orthozygus, Corannulus, Lanternithus* and *Zygrhablithus* holococcoliths.

Zygrhablithus bijugatus bijugatus (Deflandre *in* Deflandre & Fert 1954) Deflandre 1959 (Pl. 5.6, fig. 15)

Genus ***CLATHROLITHUS*** Deflandre *in* Deflandre & Fert 1954

Clathrolithus joidesa (Bukry & Bramlette 1968) Bown 2005 (Pl. 5.7, figs 1-2)

Holococcolith sp. (Pl. 5.6, figs 4-6)
DESCRIPTION: A small, elliptical coccolith with a narrow dark rim (visible in PC) and a complexly-constructed, birefringent central-area plate with bright blocks towards each end. OCCURRENCE: Rare throughout the section.

5.5.4 Nannoliths

Family **BRAARUDOSPHAERACEAE** Deflandre 1947

Genus ***BRAARUDOSPHAERA*** Deflandre 1947

Braarudosphaera bigelowii (Gran & Braarud 1935) Deflandre 1947 (Pl. 5.7, figs 3-4)

Genus ***MICRANTHOLITHUS*** Deflandre *in* Deflandre & Fert 1954

Micrantholithus excelsus Bown 2005 (Pl. 5.7, figs 5-6)

Genus ***PEMMA*** Klumpp 1953

Pemma papillatum Martini 1959 (Pl. 5.7, figs 7-8)

Family **DISCOASTERACEAE** Tan 1927

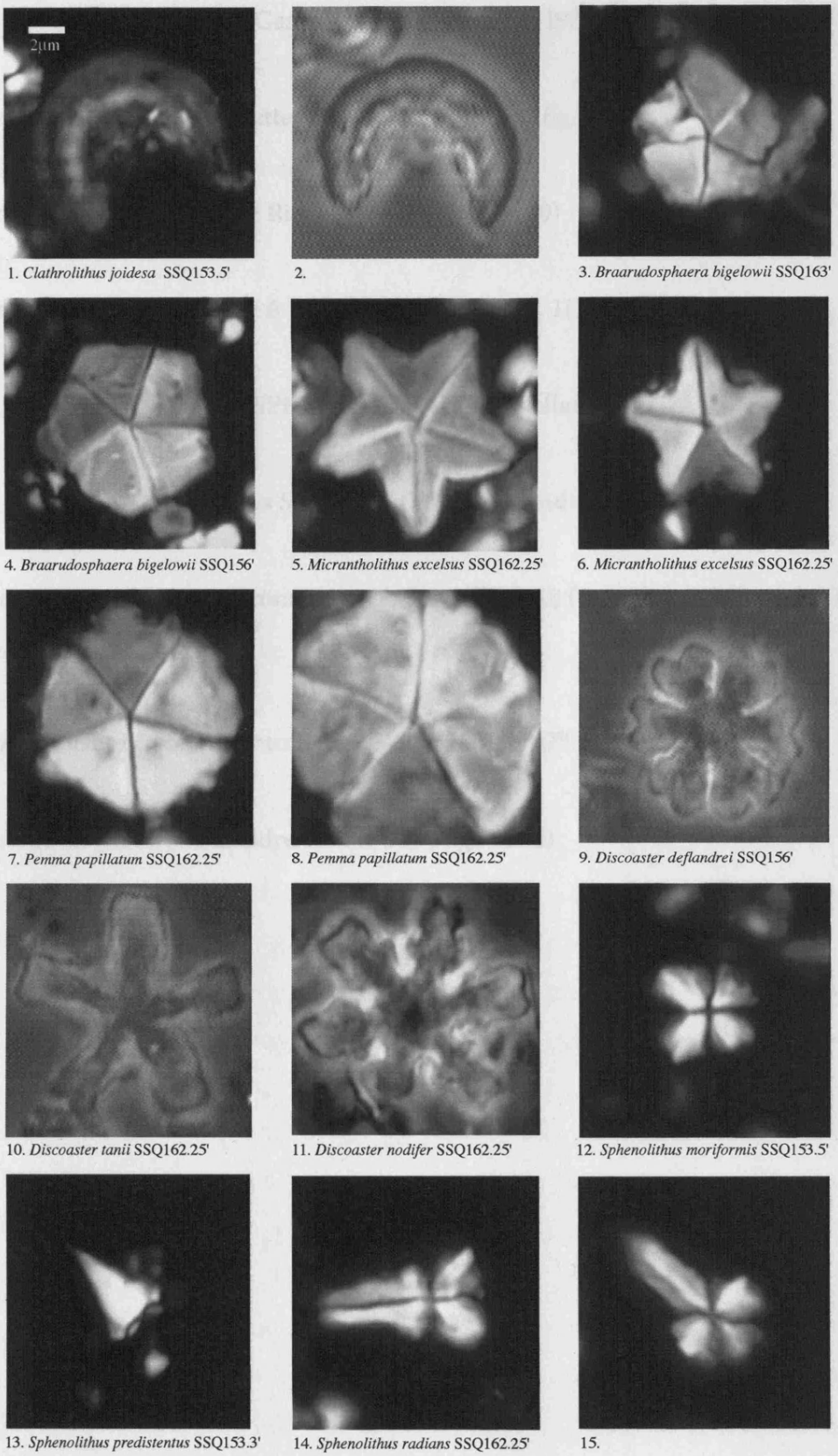

1. *Clathrolithus joidesa* SSQ153.5'
2.
3. *Braarudosphaera bigelowii* SSQ163'
4. *Braarudosphaera bigelowii* SSQ156'
5. *Micrantholithus excelsus* SSQ162.25'
6. *Micrantholithus excelsus* SSQ162.25'
7. *Pemma papillatum* SSQ162.25'
8. *Pemma papillatum* SSQ162.25'
9. *Discoaster deflandrei* SSQ156'
10. *Discoaster tanii* SSQ162.25'
11. *Discoaster nodifer* SSQ162.25'
12. *Sphenolithus moriformis* SSQ153.5'
13. *Sphenolithus predistentus* SSQ153.3'
14. *Sphenolithus radians* SSQ162.25'
15.

Plate 5.7 LM images of *Clathrolithus* holococcoliths and *Braarudosphaera*, *Micrantholithus*, *Pemma*, *Discoaster* and *Sphenolithus* nannoliths.

Genus ***DISCOASTER*** Tan 1927

Discoaster deflandrei Bramlette & Riedel 1954 (Pl. 5.7, fig. 9)

Discoaster tanii Bramlette & Riedel 1954 (Pl. 5.7, fig. 10)

Discoaster nodifer Bramlette & Riedel 1954 (Pl. 5.7, fig. 11)

Family **SPHENOLITHACEAE** Deflandre 1952

Genus ***SPHENOLITHUS*** Deflandre 1952

Sphenolithus moriformis (Brönnimann & Stradner 1960) Bramlette & Wilcoxon 1967 (Pl. 5.7, fig. 12)

Sphenolithus predistentus Bramlette & Wilcoxon 1967 (Pl. 5.7, fig. 13)

Sphenolithus radians Deflandre 1952 (Pl. 5.7, figs 14-15)

6. DISCUSSION: LOW-LATITUDE CALCAREOUS PHYTOPLANKTON AND THE EOCENE-OLIGOCENE TRANSITION

6.1 The Eocene-Oligocene Transition

The primary focus of this discussion is the relationship between the observed changes in calcareous phytoplankton assemblages at the three studied sites and the climatic events through the EOT. In order to compare these sites to one another and with the global record of climatic change through the EOT, the oxygen isotope stratigraphy of the Tanzanian record has been correlated to the deep-sea benthic foraminifera oxygen isotope records of ODP Site 1218 (Coxall *et al.* 2005) and ODP Sites 522 and 744 (Zachos *et al.* 1996). This correlation, and the age model developed from it, then forms the basis for a correlation between the three sites used in this study. These correlations allow for an assessment of the main features of the nannofossil records on a common age model, which in turn are used to integrate and discuss these biotic and climatic records of the EOT.

The initial correlation of the Tanzanian isotope stratigraphy to the deep-sea records of ODP Sites 522, 744 and 1218 was undertaken by Pearson *et al.* (2008) and is shown in Figure 6.1 against the time scale of Berggren *et al.* (1995). The planktonic foraminiferal $\partial^{18}O$ record from the Tanzanian sections has a similar form to the benthic foraminiferal $\partial^{18}O$ record from the deep-sea, with the characteristic two step increase in $\partial^{18}O$ separated by relatively stable $\partial^{18}O$ values but with slightly smaller increases in $\partial^{18}O$ across the two steps; ~0.7per mil across the first step and ~0.4per mil across the second. Also shown are the ranges of larger reef benthic foraminifera - which are a transported allochthonous component present throughout the deeper water TDP sections - as well as the main extinction events within the calcareous plankton (nannofossil and planktonic foraminifera), and an interpretation of the biotic events through the EOT. From the Tanzanian records it is clear that the two classic EOT extinction events within the planktonic foraminifera both fall within the oxygen isotopic shift of the EOT, with that of the *Turborotalia cerroazulensis* group occurring in the middle of the first step in $\partial^{18}O$, and that of the Hantkeninidae after this, within the early part of the plateau in

$\partial^{18}O$. In addition, the last occurrence of the calcareous nannofossil *Pemma papillatum* falls at the base of or just before the first step in oxygen isotopes, and that of *Discoaster saipanensis* is at the base of the whole EOT interval, although the position of this event is difficult to determine accurately due to the low abundances of *D. saipanensis* prior to its last occurrence (Backman 1987) and the clear diachroneity of this event across latitudes (Berggren 1995).

New trace element data from the Tanzanian sections indicate that across the first ~0.7‰ step increase in planktonic $\partial^{18}O$ there was a cooling in both surface and bottom waters of ~2.5°C, as recorded in both planktonic *T. ampliapertura* and benthic *Cibicidoides* Mg/Ca and aragonitic benthic *Epistomina* sp. Sr/Ca ratios (Figure 6.2; Lear et al. submitted). This suggests that ~0.5‰ of the first step can be accounted for by cooling, leaving a change in seawater $\partial^{18}O$ due to ice sheet growth of ~0.2‰, which is equivalent to ~25m of sea level fall. In contrast, across the second step in $\partial^{18}O$ there is no change in planktonic foraminiferal Mg/Ca ratios, suggesting there is no appreciable cooling of surface water temperatures and hence the majority of the ~0.4‰ increase in $\partial^{18}O$ is due to an increase in seawater $\partial^{18}O$ linked to the growth of continental ice sheets and an associated sea level fall of ~50m. Using this data, the estimated increase in ice volume across the entire EOT is between 90 and 120% of the present Antarctic ice sheet, equivalent to a sea level fall of the order of the ~70m (Lear *et al.* submitted), which is in good agreement with independent estimates obtained from sequence stratigraphic studies of the New Jersey Margin (Pekar *et al.* 2002). This is also in agreement with the conclusions of Miller *et al.* (in press), who used benthic foraminiferal facies analysis in the St Stephens core to estimate sea level changes through the EOT and found that most of the sea level fall occurred during the second step in $\partial^{18}O$, implying that the first step in $\partial^{18}O$ is dominated by the cooling effect.

In order to compare nannofossil assemblage data between the Tanzanian sections, DSDP Site 242 and St Stephens Quarry, a correlation between these sites has been made based on the available $\partial^{18}O$ stratigraphy for these locations using the main transitions through the EOT; namely the onset of the first step in oxygen isotopes and then the peak positive $\partial^{18}O$ values of the first and second steps (Figure 6.3). The oxygen isotope

Figure 6.2 Trace element data from TDP cores: a) Oxygen isotope records from benthic foraminifera of ODP Site 1218 and the spliced planktonic foraminiferal record of TDP Sites 12 & 17 (as in Figure 6.1); b) benthic foraminiferal (multispecific *Cibicidoides* and monospecific *Epistomina* sp.) oxygen isotope records and bottom water temperature estimates from Mg/Ca ratios of *Cibicidoides* spp. and Sr/Ca ratios of *Epistomina* sp. from TDP Sites 12 & 17; c) planktonic foraminiferal oxygen isotope record and surface water temperature estimates calculated from *T. ampliapertura* Mg/Ca ratios. Time scale of Cande & Kent (1995). Modified from Lear *et al.* (submitted).

stratigraphy for TDP Sites 12 and 17 is plotted against age, based on the Beggren *et al.* (1995) time scale and the correlation to the deep-sea $\partial^{18}O$ stratigraphy shown in Figure 6.1; this is then linked to the other sites by the correlation lines shown (Figure 6.3). Although the $\partial^{18}O$ records from each of the sites is based on the analysis of different carbonate phases - the TDP data is from the planktonic foraminifera *T. cerroazulensis*, the DSDP Site 242 data is from bulk carbonate analyses and the St Stephens data is from the benthic foraminifera genus *Cibicidoides* - the major global shift of ~1 to 1.5‰

Figure 6.3 Correlation of the Tanzanian oxygen isotope stratigraphy (planktonic *T. ampliapertura*) with those from DSDP Site 242 (bulk carbonate - Bridget Wade pers. comm.) and the St Stephens Quarry Core (*Cibicidoides* spp. - Miller *et al.* 2008).

in $\partial^{18}O$ through the EOT is a sufficiently strong signal to be recognized in all of these records.

The onset of the shift and maxima in steps 1 and 2 have already been identified in the benthic foraminiferal isotope record of St Stephens (Miller *et al.* 2008) and have recently been confirmed by additional high-resolution planktonic and benthic foraminiferal $\partial^{18}O$ (Bridget Wade pers. comm.). This stratigraphy is also consistent with the position of the Chron C13r/C13n boundary at 151ft (46.03m) in the St Stephens core (see Chapter 5 and Miller *et al.* 1991; in press), which is well established as coinciding with the start of the EOGM (Zachos *et al.* 1996; Coxall *et al.* 2005).

The correlation to the DSDP Site 242 bulk rock $\partial^{18}O$ is more problematic. This isotope data was collected as a pilot study prior to future single taxon planktonic and benthic

isotope studies (Bridget Wade pers. comm.). Although a large shift of ~1.5‰ at ~651.70mbsf is relatively unambiguous, it is unclear whether this includes the whole of the EOT isotope shift or is only the first step. A second, slightly more positive peak in $\partial^{18}O$ is reached at ~651.1mbsf, which is separated from the first peak by three data points with $\partial^{18}O$ values ~0.5‰ lower than the peak positive values. This minor reversal is not dissimilar to the Tanzanian record of the "plateau", which also shows a minor reversal in $\partial^{18}O$ values. In the correlation presented here, I have interpreted this second maxima in $\partial^{18}O$ to represent the peak value of the second step in $\partial^{18}O$.

The recognition of the first major transition in $\partial^{18}O$ is key for correlating and interpreting the nannofossil assemblage data between the sites, and this is judged to be a robust tie point between all three locations. This correlation is supported by the last occurrence of the *Turborotalia cerroazulensis* group of planktonic foraminifera in all three sites (Figure 6.4), which consistently falls in the earliest stages of the first $\partial^{18}O$ shift in all three sites. This bioevent is judged to be more reliable than the last occurrence of the Hantkeninidae, which are often poorly preserved in deep-sea sediments and/or subject to both environmental and biogeographic controls on their distribution. Figure 6.4 shows the oxygen isotope curves for the three sites plotted against linearly interpolated ages between and beyond the tie points for DSDP Site 242 and the St Stephens core. Although this correlation needs refinement once high resolution isotope data become available from the last two sites, it is judged to be sufficient to correlate the major changes in nannofossil assemblages within the EOT.

The major shifts in the nannofossil assemblages at each site are best summarized by the first coordinate value of the MMDS multivariate analysis at each location; these are plotted against the new estimated age models along with the oxygen isotope curve for each site in Figure 6.5. As was shown in Chapters 2, 4 and 5, the MMDS1 statistic consistently differentiates pre- and post-EOT/EOB assemblages and summarizes the major shifts in the nannofossil assemblages through time. The spliced records of $\partial^{18}O$ and MMDS1 for the two Tanzanian sites show a remarkable degree of co-variation. In the lower section of these cores, before ~33.9Ma, both measures show slight variations around a stable mean value. At ~33.9Ma, marked as the onset of the $\partial^{18}O$ shift, there is

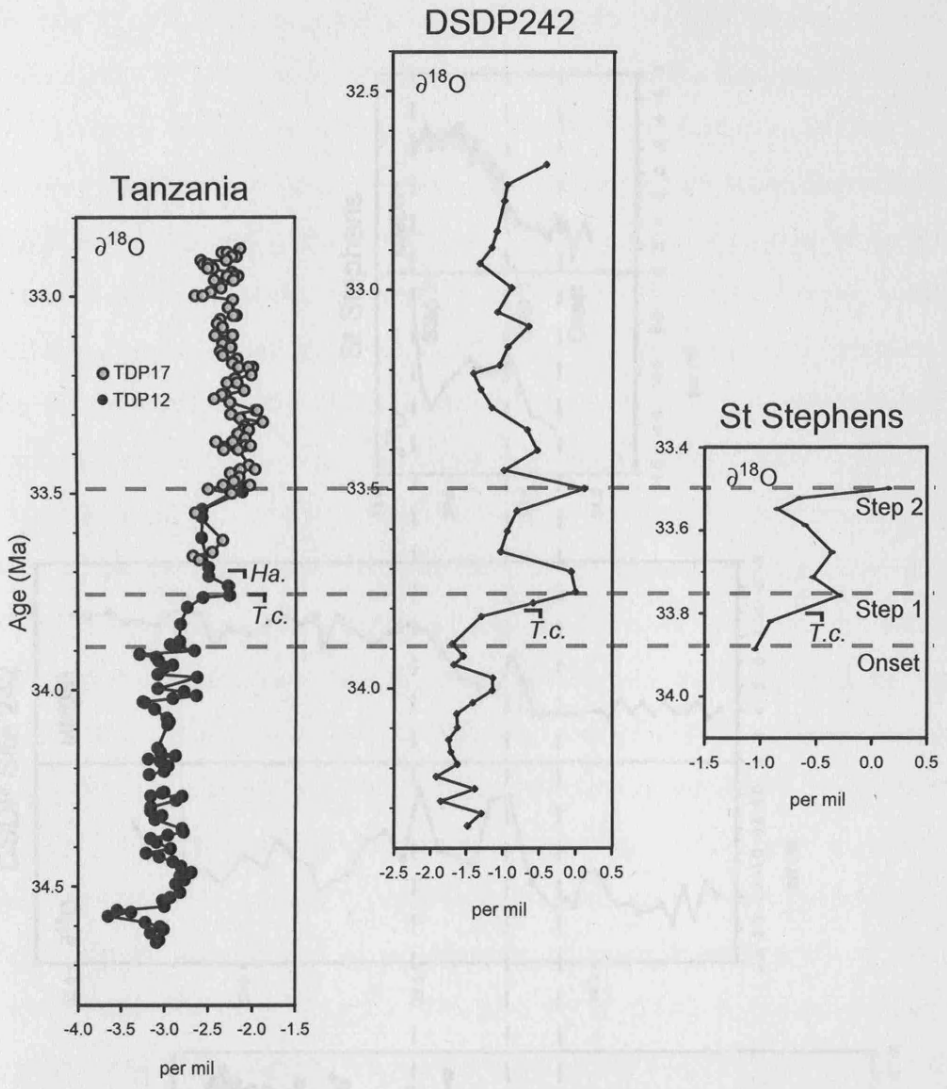

Figure 6.4 Oxygen isotope stratigraphy of all three studied sites plotted against the common time scale of Cande & Kent (1995) based on the correlation lines detailed in Figure 6.3 and shown here as horizontal dashed grey lines. These correlations are supported by the available reliable biostratigraphic data, the last occurrence of the *Turborotalia cerroazulensis* group of planktonic foraminifera; the position of this event in each section is marked as *T.c* and occurs towards the maximum positive $\partial^{18}O$ values of the first step.

a gradual positive trend in $\partial^{18}O$ and a step change to more negative values of MMDS1. This shift in nannofossil assemblages is indicative of a marked change in the local surface water environment and can be directly correlated with the ~2°C cooling of surface waters indicated by the Mg/Ca ratios of *T. ampliapertura*.

As the planktonic $\partial^{18}O$ increases into the positive maxima of the first step, at ~33.75Ma, there is a coincident transient negative maxima in MMDS1, which is also the extinction

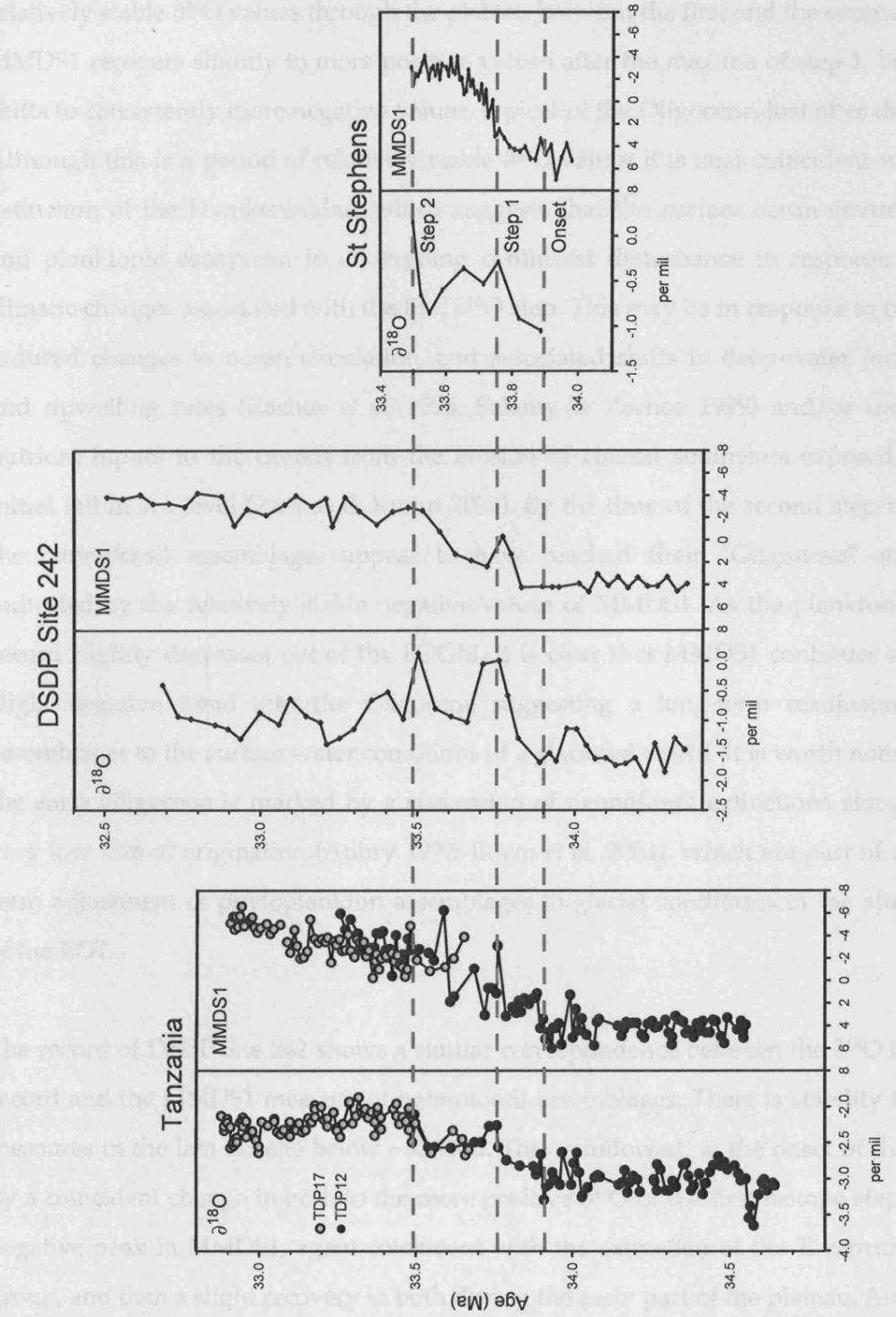

Figure 6.5 The first coordinate of the Metric Multi-dimensional Scaling analyses of nannofossil assemblages plotted against the oxygen isotope records for each study site. Time scale of Cande & Kent (1995).

level of the *T. cerroazulensis* group of planktonic foraminifera. During the interval of relatively stable $\partial^{18}O$ values through the plateau between the first and the second steps, MMDS1 recovers slightly to more positive values after the maxima of step 1, but then shifts to consistently more negative values, typical of the Oligocene, just after the EOB. Although this is a period of relatively stable $\partial^{18}O$ values it is near coincident with the extinction of the Hantkeninidae, which suggests that the surface ocean environment and planktonic ecosystem is undergoing continued disturbance in response to the climatic changes associated with the first $\partial^{18}O$ step. This may be in response to cooling-induced changes in ocean circulation, and associated shifts in deep-water formation and upwelling rates (Zachos *et al.* 1996; Salamy & Zachos 1999) and/or increased nutrient inputs to the oceans from the erosion of coastal sediments exposed by an initial fall in sea level (Zachos & Kump 2005). By the time of the second step in $\partial^{18}O$, the nannofossil assemblages appear to have reached their "Oligocene" state, as indicated by the relatively stable negative values of MMDS1. As the planktonic $\partial^{18}O$ record slightly decreases out of the EOGM, it is clear that MMDS1 continues along a slight negative trend into the Oligocene suggesting a long-term readjustment of assemblages to the surface water conditions of a glaciated world. It is worth noting that the early Oligocene is marked by a succession of nannofossil extinctions alongside a very low rate of origination (Aubry 1992; Bown *et al.* 2004), which are part of a long-term adjustment of phytoplankton assemblages to glacial conditions in the aftermath of the EOT.

The record of DSDP Site 242 shows a similar correspondence between the $\partial^{18}O$ isotope record and the MMDS1 measure of nannofossil assemblages. There is stability in both measures in the late Eocene below ~33.9Ma. This is followed, at the onset of the shift, by a coincident change in both to the more positive $\partial^{18}O$ of the first isotope step and a negative peak in MMDS1, again coincident with the extinction of the *T. cerroazulensis* group, and then a slight recovery in both during the early part of the plateau. Although the resolution of both the isotope and assemblage records is not as good as the Tanzanian record, the next negative shift in MMDS1 again appears to precede the second step in $\partial^{18}O$, occurring in the vicinity of the inferred position of the EOB. As in

Tanzania, MMDS1 has increased to more negative values by the peak of the second step in $\partial^{18}O$ and then stabilizes along a slight negative trend into the early Oligocene.

The record of nannofossil assemblages and $\partial^{18}O$ from St Stephens Quarry lacks much of the more stable, late Eocene, pre-EOT part of the record due to a local unconformity, however the collected nannofossil assemblage data offers a higher resolution view of the EOT itself. As with the other records the assemblages appear to be relatively stable in the pre-onset section but then shift towards negative values in step with the first step in $\partial^{18}O$; again this is coincident with the extinction of the *T. cerroazulensis* group. Unlike the other records there is no temporary stabilization of the MMDS1 values, which instead continue along a negative shift during the first half of the plateau in $\partial^{18}O$, which probably includes the EOB. By the second half of the plateau MMDS1 has stabilized, and although there is not a record above the second $\partial^{18}O$ step, this step itself appears to have little effect on the assemblages. This pattern is consistent with the two other records, suggesting that "Oligocene" assemblages have been established before the peak in the second $\partial^{18}O$ step.

6.2 The nannofossil response to the EOT

The assemblage changes that underlie these shifts in the MMDS1 statistic can be summarized by the grouped abundances of species which have generally decreasing ("Group 1") or increasing ("Group 2") relative abundances up-section. These grouped percentage relative abundances are shown on Figures 6.6 and 6.7; Table 6.1 lists the individual species that form these two group at each site along with the range of their relative abundances for the pre- and post- EOT intervals. It should be noted that these groups contain different species at each site, with individual species even being included in the opposite trending groups at different sites. The general patterns of assemblage change outlined above for the MMDS1 statistic are also clear in the grouped abundance data, namely; 1) relatively stable assemblages before the onset of the isotope shift at ~33.9Ma, 2) a change in assemblages focused around the first positive step in $\partial^{18}O$ and the early part of the plateau and, 3) the development of new,

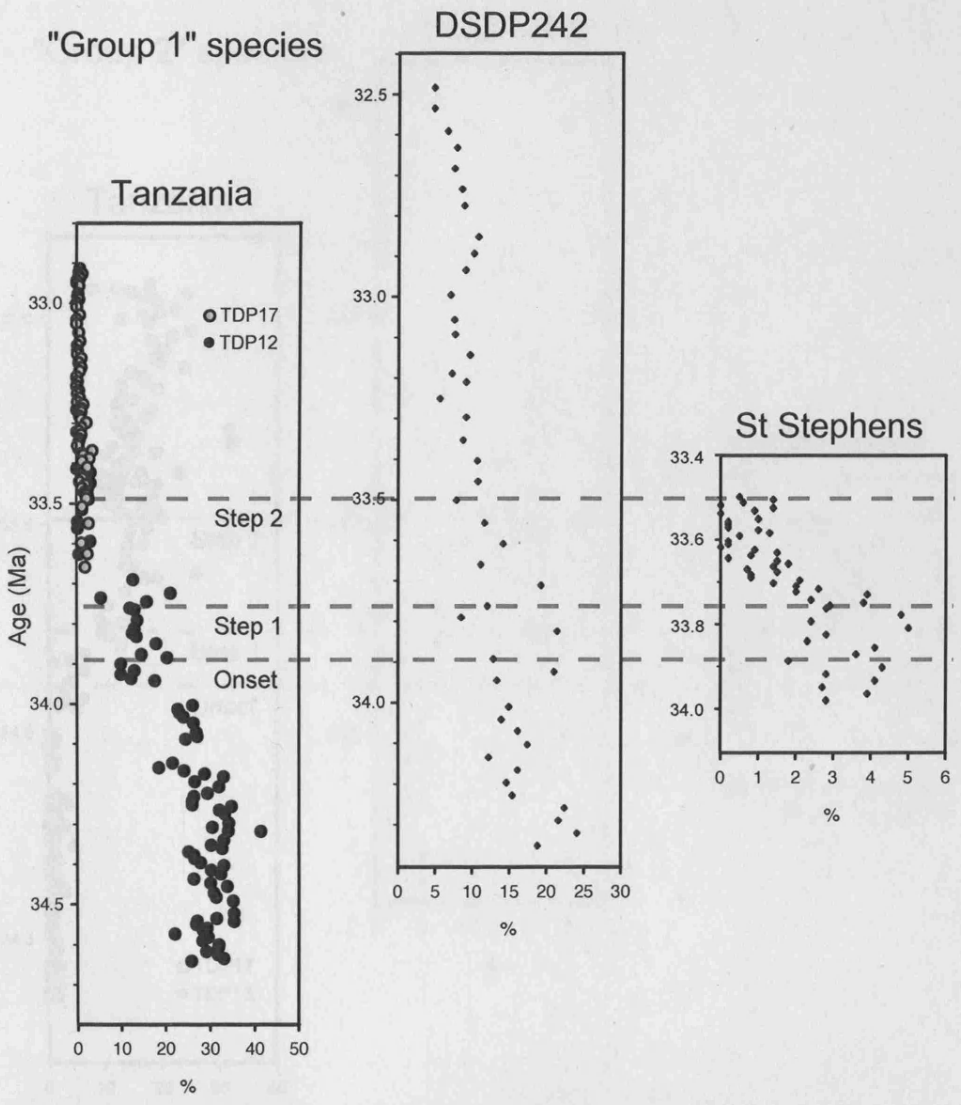

Figure 6.6 Summed percent relative abundances for "Group 1" (generally decreasing abundances up-section) species for the three studied sites. Note that the species composition of this summed data is different at each site - see details in Table 6.1. Time scale of Cande & Kent (1995).

relatively stable, "Oligocene" assemblage before the maxima of the second step in $\partial^{18}O$ and the EOGM. There are some other subtle changes, most notable is the decline in Group 1 species in the Tanzanian sections from ~34.1Ma, suggesting an earlier change in surface water conditions at this site. This correlates to a distinct warming of bottom water temperatures, as determined by trace metal (Sr/Ca and Mg/Ca) ratios of benthic foraminifera, and may indicate a significant change in surface water structure, thermocline depth and stratification (Lear et al. submitted).

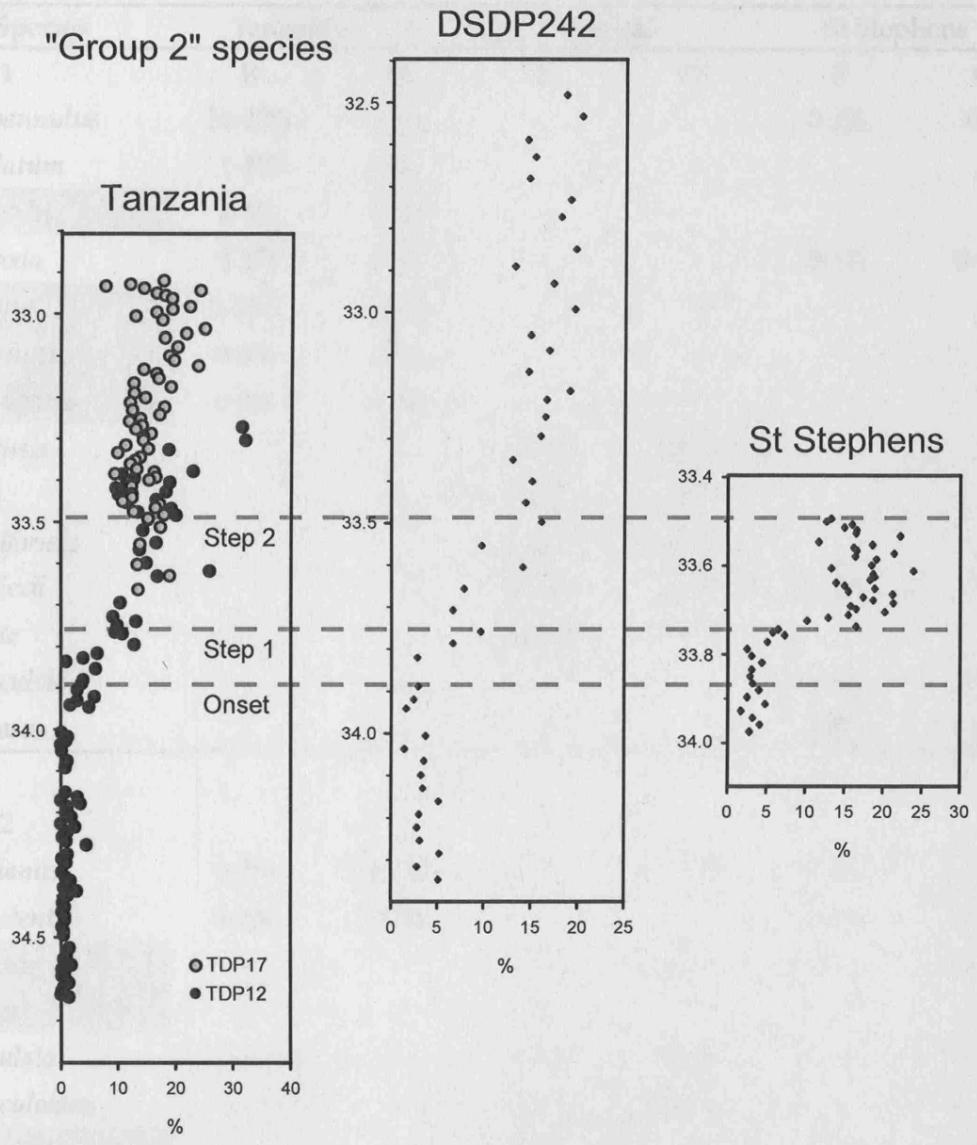

Figure 6.7 Summed percent relative abundances for "Group 2" (generally increasing abundances up-section) species for the three studied sites. Note that the species composition of this summed data is different at each site - see details in Table 6.1. Time scale of Cande & Kent (1995).

These grouped abundance plots also show the relative size of the assemblage shifts at each site and the relative importance of individual species in these trends. The Tanzanian sections clearly have the largest overturn in nannofossil assemblages, with an almost complete loss of Group 1 species, which account for ~30% of the assemblage in the late Eocene and the appearance of Group 2 species, which increase from very low abundances to form ~20% of the Oligocene assemblage. In both DSDP Site 242 and St Stephens, the loss of Group 1 species is far less marked, in Site 242 there is a gentle declining trend in Group 1 species from ~20% to ~10% through the whole section and

Species	Tanzania		DSDP Site 242		St Stephens	
Group 1	E	O	E	O	E	O
C. protoannulus	10-20%	<1%	-	-	0-2%	0%
P. papillatum	1-3%	0%	-	-	-	-
V. macleodii	1-4%	1-2%	-	-	-	-
R. dictyoda	0-2%	<1%	-	-	0-1%	0-1%
L. minutus	5-15%	1-2%	-	-	-	-
Z. b. cornutus	0-5%	<1%	-	-	-	-
Z. b. bijugatus	0-5%	<1%	-	-	-	-
R. stavensis	-	-	2-5%	0-2%	-	-
D. tanii	-	-	1-3%	0-1%	-	-
H. situliformis	-	-	0-1%	0-1%	-	-
R. filewiczii	-	-	0-1%	0-1%	0-1%	<1%
R. bisecta	-	-	10-20%	5-10%	-	-
B. serraculoides	-	-	-	-	1-2%	0-1%
C. formosus	-	-	-	-	0-2%	0-1%
Group 2						
C. floridanus	0-2%	10-15%	0-5%	10-15%	0-2%	5-10%
S. predistentus	0-2%	5-10%	-	-	0-1%	1-3%
L. minutus	-	-	<1%	0-8%	0-2%	2-5%
B. furvus	-	-	0-1%	1-3%	-	-
H. reticulata	-	-	0-1%	0-2%	-	-
B. serraculoides	-	-	0-1%	0-2%	-	-
Z. b. bijugatus	-	-	<1%	0-2%	0-1%	1-3%
S. tanzanensis	-	-	<1%	0-3%	0-1%	0-1%
Cr. cf. *Cr. primus*	-	-	0%	0-1%	-	-
D. deflandrei	-	-	0-1%	0-1%	-	-
H. geisenii	-	-	-	-	<1%	0-1%
Holococcolith sp. 1	-	-	-	-	<1%	0-2%
Bl. amplus	-	-	-	-	0-2%	4-8%

Table 6.1 Species compositions of Groups 1 and 2 (decreasing and increasing relative abundances through the EOT respectively) for each of the studied sites. Percent data refer to the range of relative abundance values for each species at a given site for the period before ("E" ~ Eocene) and after ("O" ~ Oligocene) the main nannofossil shifts of the EOT at each site. These intervals are as follows: Tanzania, E - below 125mbgl, O - above 100m; DSDP Site 242, E - below 652mbsf, O - above 651mbsf; St Stephens core, E - below 162mbgl, O - above 158mbgl. Dissolution susceptible taxa are highlighted in grey.

in St Stephens there is a marked drop in Group 1 abundances at the first isotope step, but this is from a position of relatively low abundances (~3-5%) in the late Eocene. In each of these sites the majority of the assemblage change is due to a marked increase in Group 2 species through the EOT. In Site 242, this is a broad increase from ~5% in the late Eocene to ~20% in the early Oligocene, but is a much sharper increase, coincident with the first isotope step, at St Stephens, with an increase from ~5% to ~15-25%.

An examination of the species components of these changes listed in Table 6.1, makes it clear that the increase in Group 2 species at all sites is dominated by the appearance of the large form of *Cyclicargolithus floridanus* through the EOT, with a lesser contribution from an increased abundance of *Sphenolithus predistentus* in the Tanzanian and St Stephens sections. This is the most consistent signal in individual species abundances between the sites and is probably a widespread signal across low-latitude EOT nannofossil assemblages but may be in response to both cooling and increasingly eutrophic surface water conditions. The pattern of *Calcidiscus protoannulus* abundance between the study sites, with greatest abundance in the Tanzanian sites, followed by St Stephens and then DSDP Site 242, suggest that this is a more low-latitude, warm-water adapted species. This is supported by the observed abundance decline of *C. protoannulus* through the earliest, cooling dominated stages of the EOT in both the Tanzanian sites and St Stephens, which is prior to its final extinction in the earliest Oligocene (Bybell 1982; Bralower & Mutterlose 1995).

The large decline in Group 1 species in Tanzania is largely due to a marked reduction in the abundance of a number of holococcolith taxa. As discussed in Chapter 2, the consistent quality of preservation throughout the Tanzanian sections indicates that this is largely a primary ecological signal, which, based on our current understanding of the ecology of the holococcolith-bearing life cycle stage (Kleijne 1991; Cros *et al.* 2000; Nöel *et al.* 2004; Quintero-Torres *et al.* 2006), is probably related to increasing surface water nutrient levels through the EOT.

Although all three of the study sites are broadly low-latitude (<30°N/S) the coccolithophore biogeographic gradients of the late Eocene and early Oligocene are

strong enough to register some subtle but significant differences in nannofossil assemblages between the sites. First is the total absence of *Isthmolithus recurvus* from the Tanzanian sites compared to its rare but consistent occurrences in the higher latitude St Stephens Core and DSDP Site 242. This is in agreement with biogeographic studies that have showed that *I. recurvus* is a mid- to high-latitude temperate- to cool-water species (Bukry 1978; Wei *et al.* 1992). A similar pattern is observed in the relative abundance of various reticulofenestrid species between the sites. All sites are notably dominated by *Cyclicargolithus floridanus* rather than *Reticulofenestra* species, which is the reverse of contemporaneous assemblages in high-latitude Southern Ocean sites where *C. floridanus* is almost absent (Persico & Villa 2004). There is also a marked difference between the reticulofenestrid assemblages of the Tanzanian sites, which mainly consists of *R. macmillani* and *R. filewiczii,* and the *R. bisecta* and *R. daviesii* dominated assemblages of the higher latitude DSDP Site 242. Again this is consistent with previous work that identified *R. daviesii* as a high-latitude species (Wei & Wise 1990; Wei *et al.* 1992; Persico & Villa 2004) and *R. bisecta* as being dominant in temperate waters (Wei & Wise 1990).

The close correspondence between nannofossil assemblage changes and the oxygen isotope record through the EOT at all three sites requires a coupling of global climatic change and a widespread perturbation in the surface ocean environment. As outlined in Chapter 1 the dominant controls on phytoplankton assemblages are water temperature, nutrient availability and light intensity, which in turn are controlled by the more general climate and changes in ocean circulation, upwelling, mixing and stratification (Balch 2004). Although it is difficult to constrain a particular change in nannofossil assemblages to a particular shift in the physical oceanographic environment or to a assign particular environmental preferences to specific nannofossil taxa, the combination of detailed high resolution nannofossil assemblage data with multi-proxy climate and oceanographic records allows the construction of "best-fit" scenarios, which are consilient with all the available data.

The most striking feature of the nannofossil assemblage data presented above is the initiation of the nannofossil assemblage change around the first shift in $\partial^{18}O$ at all the

study sites. The trace metal data from the Tanzanian sites indicate that this first step is dominated by a cooling of surface waters of ~2°C (Lear et al. submitted). This is consistent with the results of the sequence stratigraphic study of the St Stephens section, which suggests that the majority of eustatic sea level fall occurs over the second step, with the first step in $\partial^{18}O$ being dominated by cooling (Miller *et al.* 2008). The coincidence of this surface water cooling and the first rapid shift in nannofossil assemblages early in the EOT indicates either a direct temperature control on the coccolithophore community and/or via coupled changes in surface water mixing and stratification associated with cooling.

The lack of a significant nannofossil assemblage response to the second step in $\partial^{18}O$ at any of the sites is consistent with this $\partial^{18}O$ signal being largely due to an increase in continental ice volume. In this case the change in seawater $\partial^{18}O$ recorded at all sites is not directly coupled to a change in surface water conditions that impacts the local phytoplankton community. However, between the two $\partial^{18}O$ steps there is a continued change in nannofossil assemblages at all sites that appears to be decoupled from the relatively stable plateau in $\partial^{18}O$. This indicates either a continued perturbation to the surface water environment that is not recorded in $\partial^{18}O$, or it represents a time-lag in the biotic/ecosystem response to the cooling of the first step in $\partial^{18}O$. One possibility is that these biotic events may be related to the purported enhancement of ocean-atmosphere circulation in response to high latitude cooling and the associated changes in mixed layer depth and/or the rates of upwelling (Zachos *et al.* 1996; Salamy & Zachos 1999).

The long-held view that the EOB is not a major extinction event in the calcareous nannoplankton, with greater species loss at the middle/late Eocene boundary and within early Oligocene nannofossil zone NP22 appears to be correct (Corliss *et al.* 1984; Aubry 1992), however, this does not mean that the EOB is not a significant event in the evolutionary history of this group. It is particularly striking that the species which go extinct during early Oligocene zones NP22 and NP23 include *Calcidiscus protoannulus, Reticulofenestra dictyoda, Discoaster nodifer, D. tanii* and *Lanternithus minutus* (Aubry 1992), which all show a dramatic decline in abundance through the EOB of Tanzania. Successive early Oligocene glacial intervals (Pälike *et al.* 2006) may have increasingly

stressed and limited the distribution of these species, eventually leading to their extinction.

6.3 Carbonate production, erosion and the CCD

The record of reworked Cretaceous nannofossils in the Tanzanian sections (Figure 6.8) provides a semi-quantitative record of the erosion and transport of Cretaceous sediments, most likely from sub-aerially exposed Cretaceous claystones of the Kilwa Group. The main features of the reworking record are the absence of significant reworking in the late Eocene (pre ~34.0Ma) interval and the initiation of peak reworking exactly coincident with the second step in $\partial^{18}O$, which is largely attributed to ice-sheet growth. This close correspondence between the reworking signal and the $\partial^{18}O$ record indicates that the reworking signal is sensitive to local sea level changes and as a result the more subtle pattern of reworking around the onset of the EOT may provide an insight into the timing, nature and causes of the early stages of EOT glaciation.

In the record of planktonic foraminiferal $\partial^{13}C$ (Figure 6.8) there is a characteristic negative spike at ~34.0Ma, which has also been noted in many of the deep-sea sections and marks the start of the EOT according to Coxall & Pearson (in press). In the deep-sea this is often associated with a transient shoaling of the CCD, for example in ODP Site 1218 this negative spike in $\partial^{13}C$ corresponds to a short interval of zero carbonate accumulation (Coxall *et al.* 2005). It is however surprising that in both TDP Sites 12 and 17 these negative $\partial^{13}C$ values are directly coincident with distinct barren/low nannofossil abundance intervals, implying that the perturbation in $\partial^{13}C$ and oceanic carbonate chemistry is large enough to have effected the relatively shallow waters above the Tanzanian sites. This perturbation is then immediately followed by the first significant interval of Cretaceous reworking in these sections, indicative of an initial sea level fall and associated ice-sheet growth, between ~34.0 and 33.9Ma. It may be possible to generate this reworking signal without a single, unidirectional fall in sea level/growth in ice-volume, but rather by several transient cycles of sea-level fall and

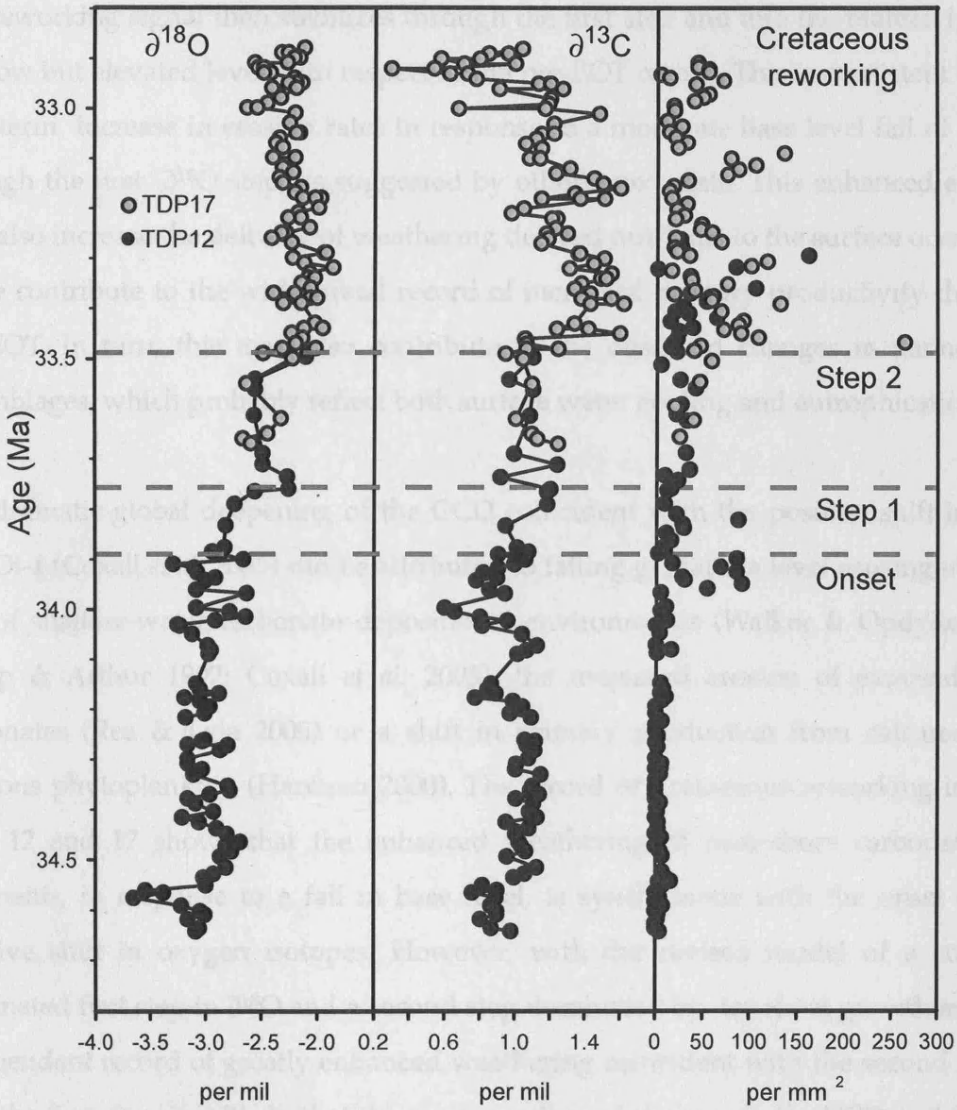

Figure 6.8 Spliced oxygen and carbon isotope records from TDP Sites 12 & 17 (planktonic *T. ampliapertura*) and the record of reworked Cretaceous nannofossils expressed as counts per mm^2 of slide observed.

rise, consistent with the variable $\partial^{18}O$ record though this interval. This observed pattern of negative $\partial^{13}C$ followed by the onset of glaciation is remarkably similar to the results of the EOT carbon cycle model of Zachos & Kump (2005), where glaciation is initiated by a pulse of weathering derived nutrients that simultaneously decreases global $\partial^{13}C$ and stimulates primary productivity, which in turn causes a drawdown in atmospheric carbon dioxide and global cooling.

The reworking signal then stabilizes through the first step and into the plateau in $\partial^{18}O$ at a low but elevated level with respect to the pre-EOT record. This is consistent with a long-term increase in erosion rates in response to a moderate base level fall of ~25m, through the first $\partial^{18}O$ step, as suggested by other proxy data. This enhanced erosion may also increase the delivery of weathering derived nutrients to the surface ocean and hence contribute to the widespread record of increased primary productivity through the EOT. In turn, this may also contribute to the observed changes in nannofossil assemblages, which probably reflect both surface water cooling and eutrophication.

The dramatic global deepening of the CCD coincident with the positive shift in $\partial^{18}O$ into Oi-1 (Coxall *et al.* 2005) can be attributed to falling global sea level causing either a loss of shallow-water carbonate depositional environments (Walker & Opdyke 1995; Kump & Arthur 1997; Coxall *et al.* 2005), the increased erosion of exposed shelf carbonates (Rea & Lyle 2005) or a shift in primary production from calcareous to siliceous phytoplankton (Harrison 2000). The record of Cretaceous reworking in TDP Sites 12 and 17 shows that the enhanced weathering of near-shore carbonate-rich sediments, in response to a fall in base level, is synchronous with the onset of the positive shift in oxygen isotopes. However, with the revised model of a cooling-dominated first step in $\partial^{18}O$ and a second step dominated by ice-sheet growth and the independent record of greatly enhanced weathering coincident with the second rather than the first step, it is likely that the close coupling of changes in the CCD and $\partial^{18}O$ is due to a combination of mechanisms related to both global cooling (decrease in shelf carbonate productivity and/or increase in biosiliceous productivity) and ice-sheet growth/sea level fall (enhanced erosion of shelf carbonates). It should be noted that there is no marked change in nannofossil abundance through the EOT at the three study sites, and although not a direct measure of calcareous phytoplankton productivity, this supports the findings of other studies that find no decrease in calcareous nannofossil productivity through the EOT (Persico & Villa 2004). This supports the hypothesis that the shift in primary production from the calcareous to siliceous phytoplankton was a product of the long-term decline in the calcareous phytoplankton (Aubry 1992; Bown *et al.* 2004) coupled to a rapid increase in siliceous

productivity coincident with global cooling, eutrophication and an increased supply of weathering derived silica to the surface ocean during the EOT (Bown 2005a).

6.4 Preservational controls on nannofossil assemblage data

A comparison of the taxonomic composition of assemblage changes through the EOT from the three study sites suggests that although there is a relatively strong, preservation independent, primary ecological signal - for example the increase in abundance of the large form of *Cyclicargolithus floridanus* in all sections - there may be subtle preservational controls on other aspects of these records. A comparison of species richness data from the three sites (Figure 6.9) shows a clearly divergent trend between the Tanzanian sites and DSDP Site 242. Whereas the Tanzanian sites show a general decline in species richness values above the first step in $\partial^{18}O$, there is a marked increase in the species richness values at DSDP Site 242 between the first and second steps in $\partial^{18}O$. This increase in species richness in DSDP Site 242 is coincident with a general lightening in the sediment colour at this site (Bridget Wade, pers. comm.) indicating that these sediments, in common with other deep-sea locations, show increased carbonate contents through the EOT associated with the global deepening of the CCD. Nannofossil preservation at this site was qualitatively observed to improve up-section with the more frequent observation of dissolution susceptible taxa such as pontosphaerids, *Syracosphaera tanzanensis*, holococcoliths and rhabdoliths. This is supported by assemblage data from this site, which shows clear up-section increases in the abundances of two holococcolith species, *Blackites furvus* and *Syracosphaera tanzanensis*. It is likely that this site was positioned close to the lysocline making the preservational state of its nannofossil assemblages sensitive to the marked drop in CCD through the EOT. The relative preservational states of the three study sites is illustrated by the LM images of selected taxa presented in Plates 6.1 and 6.2, which shows the poor/marginal preservation of *Pontosphaera* species in DSDP Site 242 and the loss of fine structure through calcite overgrowth in the larger holococcolith species.

The divergence between the species richness records of the Tanzanian sites and DSDP Site 242 is not, however, seen in the record of Shannon diversity (H) through the EOT

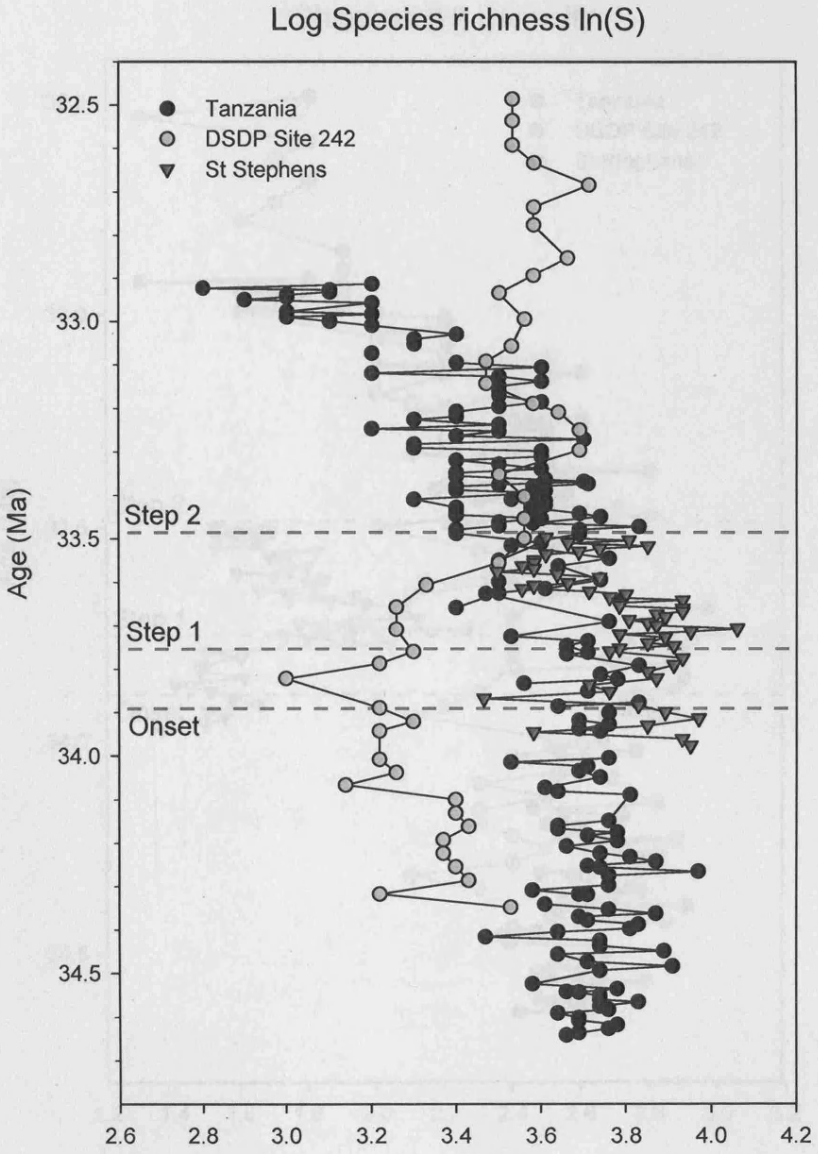

Figure 6.9 Log species richness, ln(S), against age for the three studied sites. The Tanzanian record is a spliced record from TDP Sites 12 and 17. Time scale of Cande & Kent (1995).

(Figure 6.10), which show a parallel trend of declining H values into the early Oligocene of both sites. It is likely that this pattern of declining H diversity is a more faithful to the actual ecological signal of environmental change, and is more independent of preservational quality, because it is controlled by the relative abundances of the dominant and sub-dominant taxa rather than the presence/absence of rare taxa. It is notably that the St Stephens core has markedly lower H diversities than either the Tanzanian sites or DSDP Site 242, most likely due to a genuine

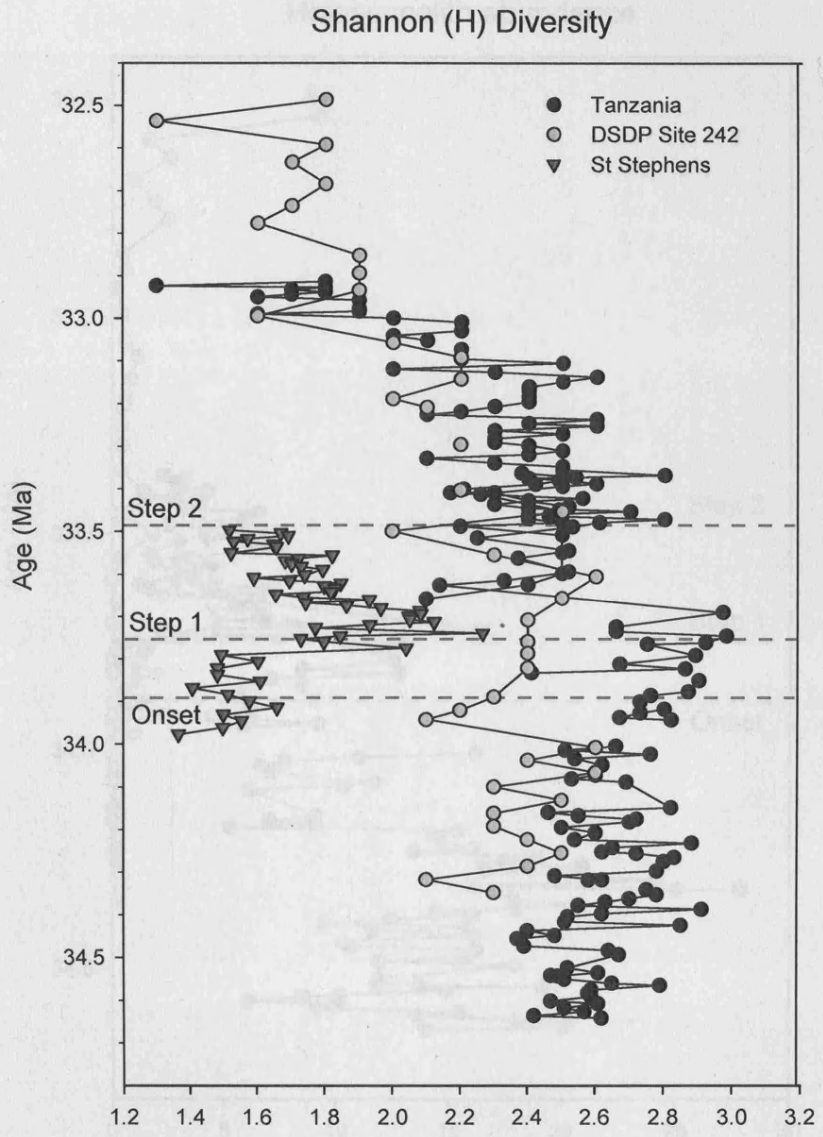

Figure 6.10 Shannon's Diversity (H) against age for the three studied sites. The Tanzanian record is a spliced record from TDP Sites 12 and 17. Time scale of Cande & Kent (1995).

difference between the ecological structure of open-ocean and shallow water coccolithophore assemblages.

Varying preservational state may also control the varying strength of the nannofossil "signal" between the three study sites. It is notable that the Tanzanian sections, which clearly have the highest quality of nannofossil preservation, also have the most marked nannofossil assemblage shifts through the EOT. A consideration of the taxonomic composition of this signal (Table 6.1) shows that the declining Group 1 taxa in the Tanzanian sections has a remarkably large component of highly preservation sensitive

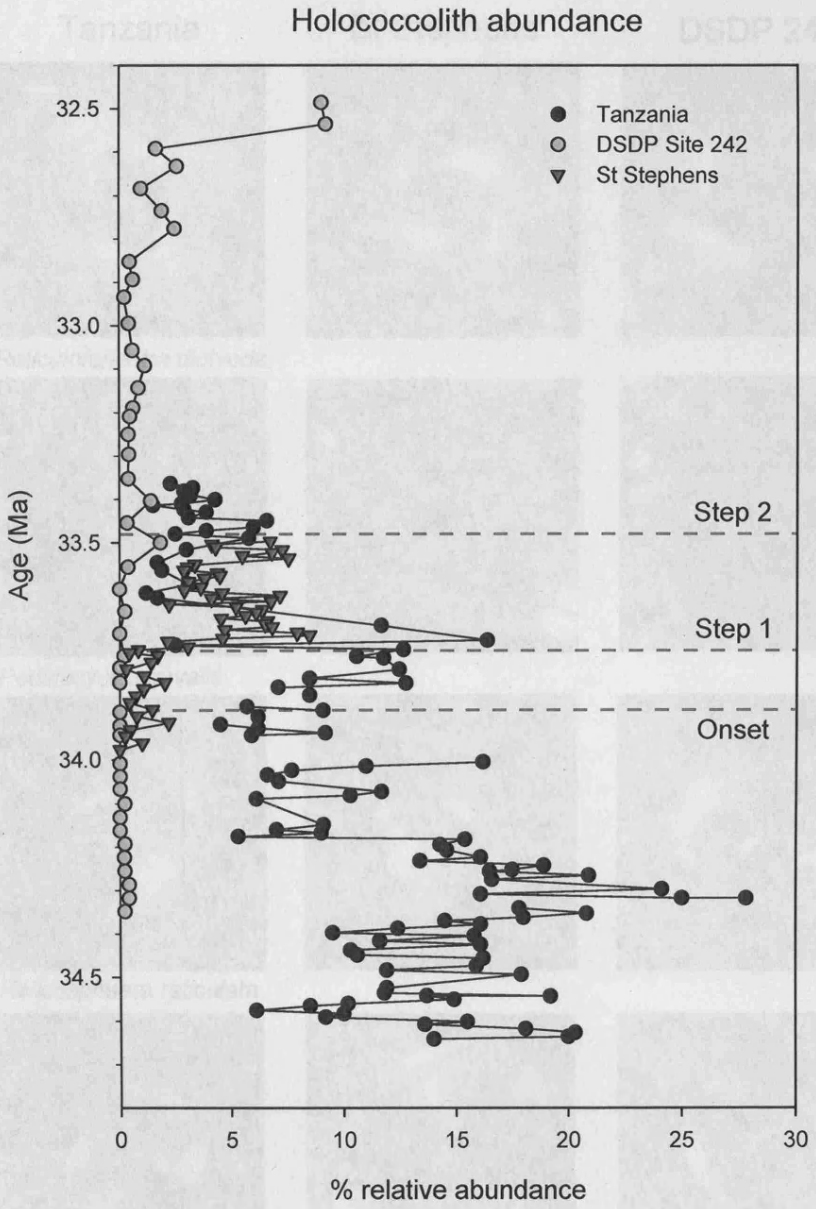

Figure 6.11 Total holococcolith relative abundance against age for the three studied sites. The Tanzanian record is a spliced record from TDP Sites 12 and 17. Time scale of Cande & Kent (1995).

holococcolith taxa (Figure 6.11). As a result this signal, even if it existed in the primary ecological communities above deep-sea sites, such as DSDP Site 242, is either not preserved or is highly attenuated in the sedimentary record. These considerations demonstrate the importance of accurately assessing preservational state when comparing nannofossil records between sites and even within records from a single site when the quality of preservation may vary systematically through the sequence.

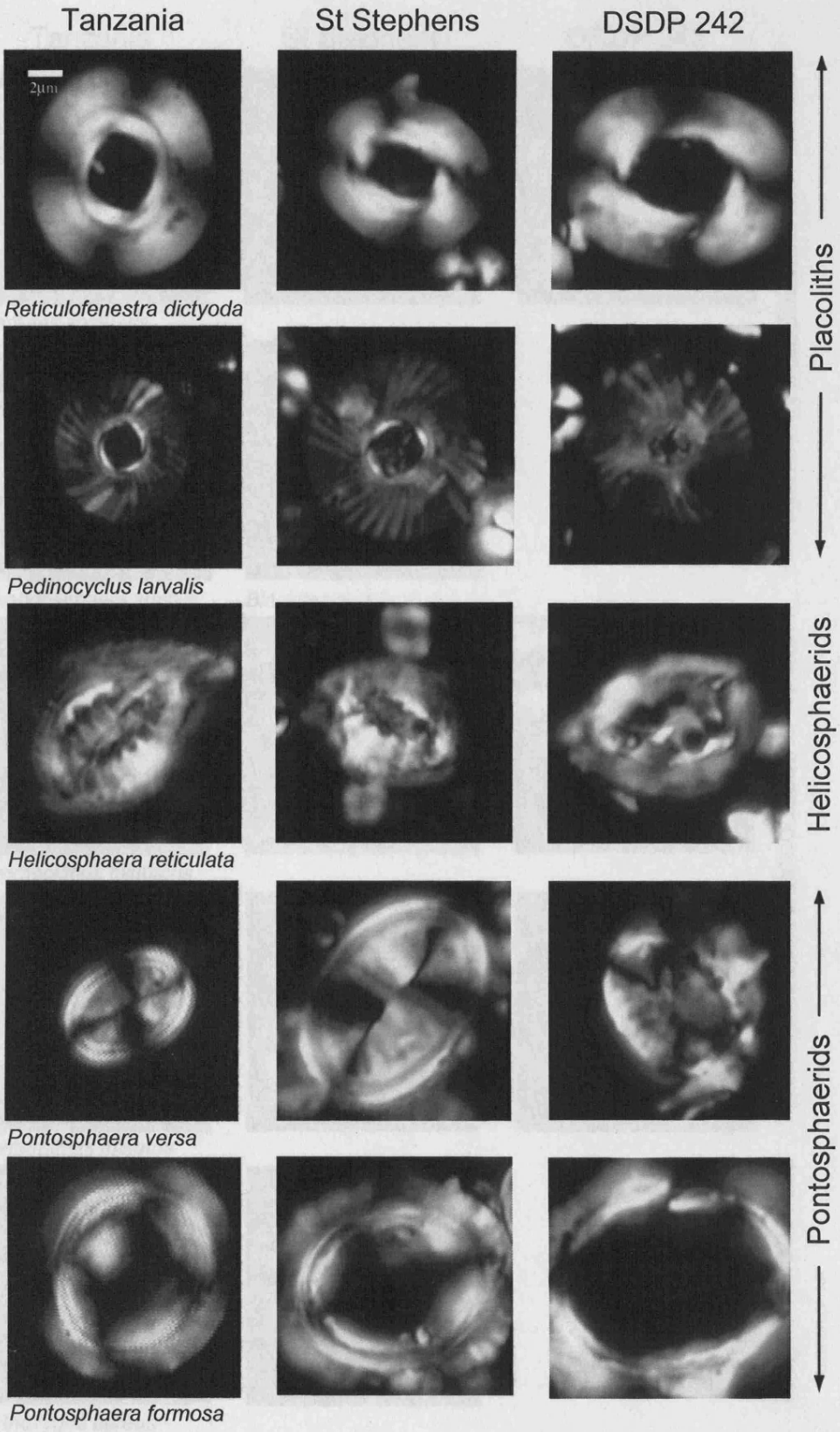

Plate 6.1 Representative light microscope images of selected taxa from the study sites; note general trend of increasing susceptibility to dissolution/recrystallization from top to bottom.

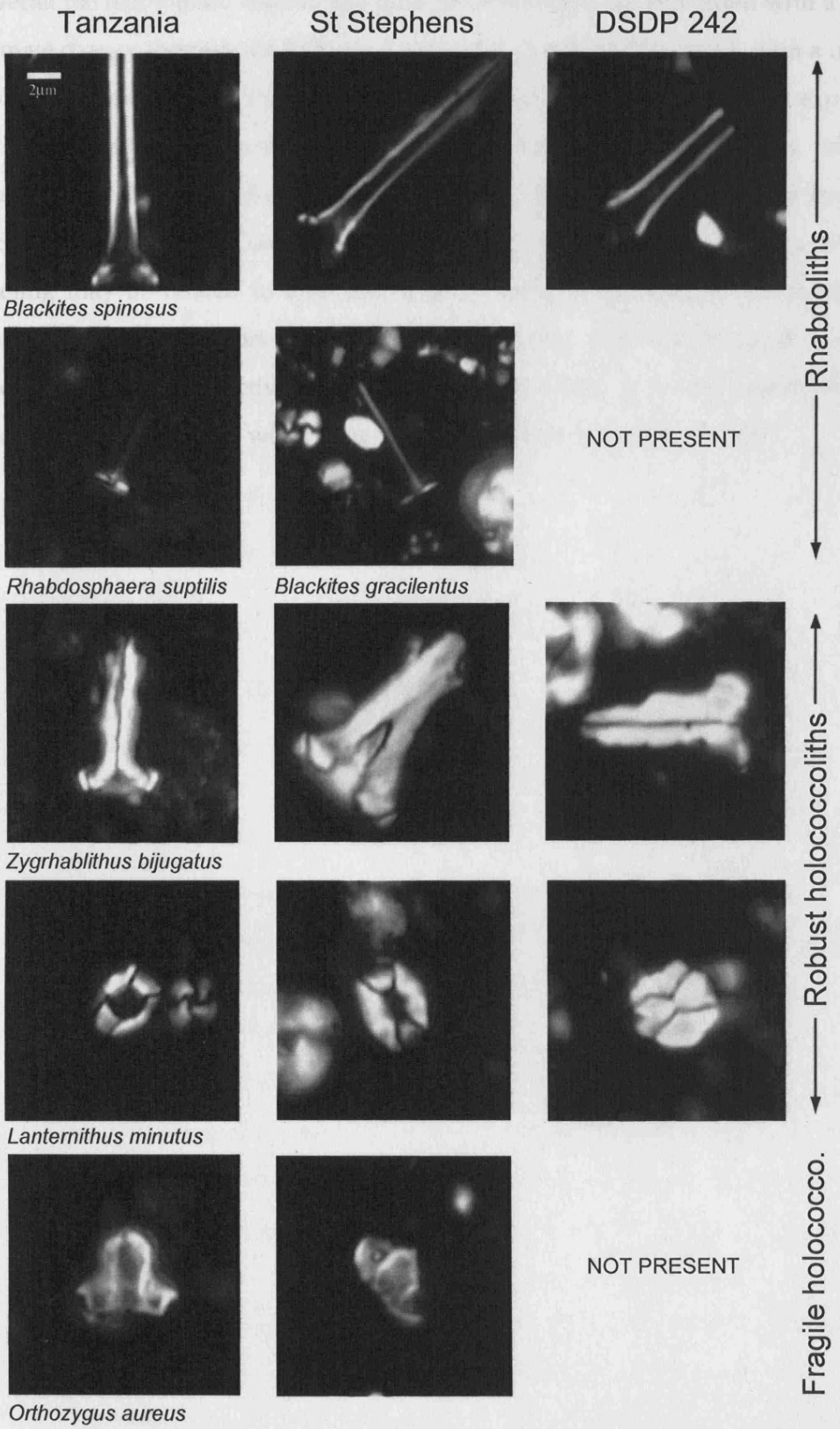

Plate 6.2 Representative light microscope images of selected taxa from the study sites; note general trend of increasing susceptibility to dissolution/recrystallization from top to bottom.

6. Discussion

Overall the nannofossil assemblage data presented here are consistent with a model of climate change through the EOT of; 1) an initial global cooling event, with a minor ice-volume increase during the first step in $\partial^{18}O$ followed by 2) a significant expansion of Antarctic continental ice-sheets during the second step in $\partial^{18}O$. This, in turn, is consistent with a global-cooling mechanism for triggering the onset of major high-latitude glaciation (DeConto & Pollard, 2003a, 2003b; Zachos & Kump, 2005). This cooling may be related to both a long-term trend of declining atmospheric carbon dioxide levels and a short-term carbon cycle trigger, such as a transient increased in oceanic primary productivity (Zachos & Kump, 2005), or a low eccentricity orbital configuration associated with cooler Austral summers (Coxall *et al.* 2005).

7. CONCLUSION

7.1 Exceptional preservation

The record of exceptionally-well preserved calcareous microfossils from the Cretaceous and Paleogene sediments of the Kilwa Group, Tanzania is truly astounding. The level of morphological detail preserved in calcareous and aragonitic benthic and planktonic foraminifera has proved invaluable for recent major taxonomic reviews (Pearson *et al.* 2006), the documentation of new faunas (McMillan *et al.* in prep) and the geochemical analysis of an apparently unaltered carbonate phase (Pearson *et al.* 2001, 2007, in press; Lear *et al.* submitted). It is now clear that this is matched, if not exceeded, by the quality of preservation of calcareous nannofossil assemblages, the study of which has revealed both previously unknown levels of morphological detail and a completely new range of Paleogene diversity (Bown 2005b; Bown & Dunkley Jones 2006; Bown *et al.* 2008). The implications of the late Eocene to early Oligocene calcareous nannofossil assemblages described in this thesis include:

- *Diversity history of coccolithophores:* the most recent global compiled species diversity for the late Eocene zone NP19/20, towards the end of a long-term diversity decline through the middle to late Eocene, was 67 species (Bown 2004). The 114 late Eocene to early Oligocene (zones NP19/20 to NP21) species-equivalent morphotypes described from the Tanzanian sediments in Chapter 3 almost doubles the existing global species diversity for this interval. The effect of these extraordinarily diverse assemblages on the pattern of coccolithophore diversity through time is difficult to assess - the existing global species diversity for the middle Eocene is 106 (zone NP15) (Bown 2004), hence these new assemblages appear to reverse the declining trend in the Paleogene diversity history of the group. Initial investigations of middle Eocene sediments from Tanzania, however, have recorded nannofossil species diversities exceeding 150, which demonstrates both the profound impact that preservational quality can

have on nannofossil records and the extraordinary nature of the Tanzanian assemblages compared to all existing records.

- *Evolution of major groups:* the documentation of a previously unknown Paleogene diversity in a number of major extant taxonomic groups (Syracosphaeraceae, Rhabdosphaeraceae, holococcoliths and deep-photic zone coccolithophores) has greatly extended our understanding of the origins and evolution of these groups. In particular the identification of a number of recognizably modern, specialist deep-photic zone coccolithophores (*Algirosphaera, Gladiolithus*), previously known only from Pleistocene and younger sediments, provides a palaeontological constraint on the timing and evolution of this group.

- *Calcareous microfossil lagerstätte:* the nature of calcareous microfossil preservation within the Cretaceous to Paleogene Kilwa Group of Tanzania clearly justifies its status as a calcareous microfossil lagerstätte (Bown *et al.* 2008). At present the documentation of the calcareous nannofossil floras from these sediments is at an early stage. It is hoped that the taxonomic data presented in Chapter 3 will form the basis for similar descriptions of both the middle Eocene and late Paleocene to early Eocene assemblages already extensively recovered during TDP drilling. The results of these studies will greatly enhance our understanding of Cenozoic coccolithophore evolution and diversity and will spur ongoing and future research into exceptional microfossil preservation at other locations, especially the search for Neogene records that are comparable to the Paleogene of Tanzania.

7.2 The Eocene-Oligocene transition

The Eocene-Oligocene transition is the largest climatic transition of the Cenozoic with the onset of Antarctic glaciation, global cooling, fundamental changes in ocean-atmosphere circulation and ocean chemistry, widespread biotic change resulting in the development of a recognizably modern climate and biota. The details of climatic and biotic change within this transition event itself are, however, still poorly resolved even

though they are crucial to our understanding of cause and effect within the complex interactions and feedbacks between climate and the biosphere. The high-resolution records of biotic change in low-latitude calcareous phytoplankton assemblages through this climate transition presented in this thesis provide some key insights into the timing and relationships between global cooling and biotic change.

- *Global cooling at the first $\partial^{18}O$ step:* the coincident shift in nannofossil assemblages with the first positive step in $\partial^{18}O$ and the last occurrence of the *Turborotalia cerroazulensis* group of planktonic foraminifera at the start of the EOT, which is observed at all three study sites, is evidence for a widespread perturbation in the low-latitude surface water environment. New trace metal (Mg/Ca and Sr/Ca) paleothermometry from the Tanzanian sections (Lear *et al.* submitted) and sequence stratigraphic data from the St Stephens Core (Miler *et al.* in press) indicate that the majority of this first step in $\partial^{18}O$ is due to a widespread, potentially global, cooling of ~2-3°C. This suggests a close coupling between surface water cooling, planktonic foraminifera extinction events and the observed changes in low-latitude calcareous phytoplankton assemblages. A distinct interval of nannofossil dissolution, coincident with a short negative excursion in $\partial^{13}C$, which immediately precedes the first appearance of reworked Cretaceous nannofossils in the Tanzanian sections and the first positive step in $\partial^{18}O$, suggests that the onset of the EOT is related to a transient perturbation in the global carbon cycle closely coupled to the first fall in sea level (and increase in ice-volume) of the EOT. Although the first step appears to be largely related to cooling the record of reworked Cretaceous nannofossils indicates at least some component of ice-sheet growth at the earliest stages of the EOT. Overall this data implies 1) a perturbation to the carbon cycle closely followed by, 2) initial minor ice-sheet growth and sea-level fall, then, 3) widespread global cooling causing, 4) extinctions and assemblage changes in low-latitude surface water ecosystems.

- *Biotic change through the $\partial^{18}O$ plateau:* the placement of the EOB within the period of stable $\partial^{18}O$ values between the first and second $\partial^{18}O$ steps is confirmed by the coincident last occurrences of a number of Hantkeninidae planktonic

foraminifera species in the Tanzanian sections. This is closely coupled to the most rapid (~30kyr) period of nannofossil assemblage change seen in these sections as well as a number of extinctions of larger benthic foraminifera species, indicating a widespread and relatively rapid perturbation to surface water and shelf ecosystems at the EOB *sensu stricto*. The estimated position of the EOB in the St Stephens Core and DSDP Site 242 is coincident with a period of ongoing but more continuous change in nannofossil assemblages, suggesting that the paleoceanographic position of the Tanzanian sites (shelf-slope break) made the calcareous phytoplankton assemblages at this location particularly sensitive to events at the EOB.

- *Major glaciation at the second $\partial^{18}O$ step:* the second step in $\partial^{18}O$ appears to be dominated by a large increase in ice volume, producing a total ice volume increase for the entire EOT of ~70 to 120% of the present Antarctic ice sheet and an associated sea level fall of ~70m (Miller *et al.* 2008; Lear *et al.* submitted). Again this is consistent with the record of nannofossil assemblages at all study sites, which show little response through the second step in $\partial^{18}O$ and hence implying little change in the low-latitude surface water environment. In addition the significant peak in reworked Cretaceous nannofossils coincident with the second step in the Tanzanian sections is supporting evidence for a major sea level fall at this time of greater magnitude than that at the first step.

- *Nannofossil preservation and proxy records;* the relative magnitude of the nannofossil assemblage change through the EOT between the study sites mirrors the relative preservational quality of these assemblages - the Tanzanian assemblages show the largest changes through the EOT and are the best preserved, DSDP Site 242 assemblages show the least change and are the least well preserved. Although this may be coincidence, the importance of fragile nannofossil taxa within the assemblage shifts of the Tanzanian sections implies that increasing nannofossil dissolution/recrystallization can strongly damp a signal of environmental change within nannofossil proxy data. In addition, the systematic increase in preservational quality through the EOT of DSDP Site 242, related to decreased nannofossil dissolution in response to increasing deep-sea

carbonate ion concentrations, may be the dominant nannofossil signal at this site. This indicates the importance of an intelligent and consistent assessment of nannofossil preservational quality both through time at a given site and between locations. At present must rely on detailed images of a representative range of nannofossil taxa and the documentation of abundance changes in dissolution susceptible taxa (e.g. pontosphaerids, rhabdoliths, holococcoliths).

8. REFERENCES

Adams, C. G., Butterlin, J. & Samanta, B. K. 1986. Larger foraminifera and events at the Eocene-Oligocene boundary in the Indo-West Pacific. In: Pomerol, C. & Premoli Silva, I. (Eds.) *Terminal Eocene events*. Elsevier, Amsterdam, pp. 237-252.

Andruleit, H. A., Rogalla, U. & Stäger, S. 2004. From living communities to fossil assemblages: origin and fate of coccolithophores in the northern Arabian Sea. In: Triantaphylou, M. (Ed.) *Advances in the biology, ecology and taxonomy of extant calcareous nannoplankton*. Micropaleontology, pp. 5-21.

Aubry, M. P. 1983. *Corrélations biostratigraphiques entre les formations paléogènes épicontinentales de l'Europe du Nord-Ouest, basées sur la nannoplancton calcaire.* Thèse Université Pierre et Marie Curie, Paris, pp. 208.

Aubry, M. P. 1986. Palaeogene calcareous nannofossil biostratigraphy of northwestern Europe. *Palaeogeography Palaeoclimatology Palaeoecology* **55**: 267-334.

Aubry, M. P. 1988. *Handbook of Cenozoic calcareous nannoplankton, Book 2: Ortholithae (Catinasters, Ceratoliths, Rhabdoliths)*. Micropaleontology Press, American Museum of Natural History, New York.

Aubry, M. P. 1992. Late Paleogene calcareous nannoplankton evolution: a tale of climatic deterioration. In: Prothero, D. R. & Berggren, W. A. (Eds.) *Eocene/ Oligocene Climatic and Biotic Evolution*. Princeton University Press, Princeton, pp. 272-309.

Aubry, M. P. 1999. *Handbook of Cenozoic calcareous nannoplankton, Book 5: Heliolithae (Zygoliths and Rhabdoliths)*. Micropaleontology Press, American Museum of Natural History, New York.

Backman, J. 1987. Quantitative Calcareous Nannofossil Biochronology of Middle Eocene through Early Oligocene Sediment from DSDP Sites 522 and 523. *Abhandlungen der Geologischen Bundesanstalt* **39**: 21-31.

Backman, J. & Hermelin, J. O. R. 1986. Morphometry of the Eocene nannofossil *Reticulofenestra umbilicus* lineage and its biochronological consequences. *Palaeogeography Palaeoclimatology Palaeoecology* **57**: 103-116.

Balch, W. M. 2004. Re-evaluation of the physiological ecology of coccolithophores. In: Thierstein, H. R. & Young, J. R. (Eds.) *Coccolithophores: From Molecular Processes to Global Impact*. Springer-Verlag, Berlin Heidelberg, pp. 165-190.

Barrett, P. J., Hambrey, M. J., Harwood, D. M., Pyne, A. R. & Webb, P. N. 1989. Synthesis. In: Barrett, P. J. (Ed.) *Antarctic Cenozoic history from CIROS-1 drill hole, McMurdo Sound Antarctica*. DSIR Publishing, Wellington, New Zealand, pp. 241-251.

Baum, G. R. & Vail, P. R. 1988. Sequence stratigraphic concepts applied to Paleogene outcrops, Gulf and Atlantic Basins. In: Wilgus, C. K., Hastings, B. S., Kendall, C. G. S. C., Posamentier, H. W., Ross, C. A. & Van Wagoner, J. C. (Eds.) *Sea Level Changes: An Integrated Approach. SEPM (Society for Sedimentary Geology) Special Publication* **42:** 309-327.

Beaufort, L., de Garidel-Thoron, T., Mix, A. C. & Pisias, N. G. 2001. ENSO-like Forcing on Oceanic Primary Production During the Late Pleistocene. *Science* **293**: 2440-2444.

Berger, W. H. & Winterer, E. L. 1974. Plate stratigraphy and the fluctuating carbonate line. In: Hsü, K. J. & Jenkins, H. C. (Eds.) *Pelagic Sediments on Land and Under the Sea, Special Publication of the International Association of Sedimentologists,* **1**: 11-48.

Berggren, W. A., Kent, D. V., Swisher, C. C. & Aubry, M. P. 1995. A Revised Cenozoic

Geochronology and Chronostratigraphy. In: Berggren, W. A., Kent, D. V. & Hardenbol, J. (Eds.) *Geochronology, Time Scales and Global Stratigraphic Correlations: A Unified Temporal Framework for an Historical Geology*. Society of Economic Paleontologists and Mineralogists, Tulsa, Oklahoma, USA, pp. 129-212.

Berggren, W. A. & Pearson, P. N. 2005. A Revised Tropical to Subtropical Paleogene Planktonic Foraminiferal Zonation. *Journal of Foraminiferal Research* **35**: 279-298.

Billard, C. 1994. Life cycles. In: Green, J. C. & Leadbeater, B. S. C. (Eds.) *The Haptophyte Algae*. Clarendon Press, Oxford, pp. 167-186.

Billups, K. & Schrag, D. P. 2003. Application of benthic foraminiferal Mg/Ca ratios to questions of Cenozoic climate change. *Earth and Planetary Science Letters* **209**: 181-195.

Birkenmajer, K. 1996. Tertiary glacial/interglacial palaeoenvironments and sea-level changes, King George Island, West Antarctica. An overview. *Bulletin of the Polish Academy of Sciences, Earth Sciences* **44**: 157-181.

Birkenmajer, K., Gazdzicki, A., Krajewski, K. P., Przybycin, A., Solecki, A., Tatur & Yoon, I., H. 2005. First Cenozoic glaciers in West Antarctica. *Polish Polar Research* **26**: 3-12.

Black, M. 1971. The systematics of coccoliths in relation to the paleontological record. In: Funnel, B. M. & Riedel, W. R. (Eds.) *The Micropaleontology of the Oceans*. Cambridge University Press, Cambridge, pp. 611-624.

Black, M. 1973. British Lower Cretaceous Coccoliths. I - Gault Clay (Part 2). *Palaeontological Society of London (Monograph)* **127**: 49-112.

Boudreaux, J. E. & Hay, W. W. 1969. Calcareous nannoplankton and biostratigraphy of the late Pliocene-Pleistocene-Recent sediments in the Submarex cores. *Revista Española de Micropaleontología* **1**: 249-292.

Bown, P. R. (Ed) 1998. Calcareous Nannofossil Biostratigraphy. Kluwer Academic, London.

Bown, P. R. 2005a. Calcareous nannoplankton evolution: a tale of two oceans. *Micropaleontology* **51**(4): 299-308.

Bown, P. R. 2005b. Paleogene calcareous nannofossils from the Kilwa and Lindi areas of coastal Tanzania (Tanzania Drilling Project 2003-4). *Journal of Nannoplankton Research* **27**: 21-95.

Bown, P. R. & Young, J. R. 1998. Techniques. In: Bown, P. R. (Ed.) *Calcareous Nannofossil Biostratigraphy*. Kluwer Academic, London, pp. 16-28.

Bown, P. R., Lees, J. A. & Young, J. R. 2004. Calcareous nannoplankton evolution and diversity through time. In: Thierstein, H. R. & Young, J. R. (Eds.) *Coccolithophores: From Molecular Processes to Global Impact*. Springer, Berlin, pp. 481-508.

Bown, P. R. & Dunkley Jones, T. 2006. New Paleogene calcareous nannofossil taxa from coastal Tanzania: Tanzania Drilling Project Sites 11 to 14. *Journal of Nannoplankton Research* **28**: 17-34.

Bown, P. R., Dunkley Jones, T. & Young, J. R. 2007. *Umbilicosphaera jordanii* Bown, 2005 from the Paleogene of Tanzania: confirmation of generic assignment and a Palaeocene origination for the family Calcidiscaceae. *Journal of Nannoplankton Research* **29**: 25-30.

Bown, P. R., Dunkley Jones, T., Lees, J. A., Randell, R., Mizzi, J., Pearson, P. N.,

Coxall, H. K., Young, J.R., Nicholas, C.J., Karega, A., Singano, J & Wade, B. S. 2008. The Paleogene Kilwa Group of coastal Tanzania: a calcareous microfossil Konservat-Lagerstätte. *Geological Society of America Bulletin* **120**: 3-12.

Bralower, T. J. 2005. Paleocene-Early Oligocene calcareous nannofossil biostratigraphy, ODP Leg 198 Sites 1209, 1210, and 1211 (Shatsky Rise, Pacific Ocean). *Proceedings of the Ocean Drilling Program, Scientific Results* **198**: [online] http://www-odp.tamu.edu/publications/198_SR/115/115.htm.

Bralower, T. J. & Mutterlose, J. 1995. Calcareous nannofossil biostratigraphy of Site 865, Allison Guyot, Central Pacific Ocean: A tropical Paleogene reference section. *Proceedings of the Ocean Drilling Program, Scientific Results* **143**: 31-74.

Bramlette, M. N. & Riedel, W. R. 1954. Stratigraphic value of discoasters and some other microfossils related to Recent coccolithophores. *Journal of Paleontology* **28**: 385-403.

Bramlette, M. N. & Sullivan, F. R. 1961. Coccolithophorids and related Nannoplankton of the early Tertiary in California. *Micropaleontology* **7**: 129-188.

Bramlette, M. N. & Martini, E. 1964. The great change in calcareous nannoplankton fossils between the Maestrichtian and Danian. *Micropaleontology* **10**: 291-322.

Bramlette, M. N. & Wilcoxon, J. A. 1967. Middle Tertiary calcareous nannoplankton of the Cipero section, Trinidad, W.I. *Tulane Studies in Geology and Paleontology* **5**: 93-131.

Breza, J. R. & Wise, S. W. 1992. Lower Oligocene ice-rafted debris on the Kerguelen Plateau: evidence for East Antarctic continental glaciation. *Proceedings of the Ocean Drilling Program, Scientific Results* **120**: 161-178.

Briggs, D. E. G. 2001. Exceptionally preserved fossils. In Briggs, D. E. G. & Crowther, P.

R. (Eds.) *Palaeobiology*. Blackwell Publishing, pp. 328-332.

Brönnimann, P. & Stradner, H. 1960. Die Foraminiferen und Discoasteridenzonen von Kuba und ihre interkontinentale Korrelation. *Erdoel-Z* **76**: 364-369.

Bukry, D. 1971. Cenozoic calcareous nannofossils from the Pacific Ocean. *San Diego Society of Natural History, Transactions* **16**: 303-327.

Bukry, D. 1978. Biostratigraphy of Cenozoic marine sediments by calcareous nannofossils. *Micropaleontology* **24**: 44-60.

Bukry, D. & Bramlette, M. N. 1968. Stratigraphic significance of two genera of Tertiary calcareous nannofossils. *Tulane Studies in Geology and Paleontology* **6**: 149-155.

Bukry, D. & Bramlette, M. N. 1971. Validation of *Pedinocyclus* and *Guinquerhabdus* new calcareous nannoplankton genera. *Tulane Studies in Geology and Paleontology* **8**: 122.

Bukry, D. & Percival, S. F. 1971. New Tertiary calcareous nannofossils. *Tulane Studies in Geology and Paleontology* **8**: 123-146.

Bybell, L. M. 1982. Late Eocene to Early Oligocene Calcareous Nannofossils in Alabama and Mississippi. *AAPG Bulletin* **66**: 1426-1426.

Cande, S. C. & Kent, D. V. 1995. Revised calibration of the geomagnetic polarity time scale for the Late Cretaceous and Cenozoic. *Journal of Geophysical Research* **100**: 6093-6095.

Cervato, C. & Burckle, L. 2003. Pattern of first and last appearance in diatoms: Oceanic circulation and the position of polar fronts during the Cenozoic. *Paleoceanography* **18**: doi:10.1029/2002PA000805.

Chapman, M. & Chepstow-Lusty, A. 1997. Late Pliocene climatic change and the global extinction of the discoasters: an independent assessment using oxygen isotope records. *Palaeogeography Palaeoclimatology Palaeoecology* **134**: 109-125.

Chepstow-Lusty, A., Backman, J. & Shackleton, N. J. 1989. Comparison of upper Pliocene *Discoaster* abundance variations from North Atlantic sites 522, 607, 658, 659, 662; further evidence for marine plankton responding to orbital forcing. In: Ruddiman, W., Sarnthein, M., *et al.* (Eds.) *Proceedings of the Ocean Drilling Program, Scientific Results* **108**: 121-141.

Chepstow-Lusty, A., Shackleton, N. J. & Backman, J. 1992. Upper Pliocene *Discoaster* abundance variations from the Atlantic, Pacific and Indian Oceans: the significance of productivity pressure at low latitudes. *Memorie di Scienze Geologiche* **44**: 357-373.

Coccioni, R., Monaco, P., Monechi, S., Nocchi, M. & Parisi, G. 1988. Biostratigraphy of the Eocene-Oligocene Boundary at Massignano (Ancona, Italy). In: Premoli Silva, I., Coccioni, R. & Montanari, A. (Eds.) *The Eocene-Oligocene Boundary in the Marche-Umbria Basin (Italy).* International Subcommission on Paleogene Stratigraphy, pp. 59-80.

Coccioni, R. & Galeotti, S. 2003. Deep water benthic foraminiferal events from the Massignano Eocene-Oligocene boundary stratotype, Central Italy. In: Prothero, D. R., Ivany, L. C. & Nesbitt, E. A. (Eds.) *From Greenhouse to Icehouse.* Columbia University Press, pp. 438-452.

Corliss, B. H., Aubry, M. P., Berggren, W. A., Fenner, J. M., Keigwin, L. D. & Keller, G. 1984. The Eocene Oligocene Boundary Event in the Deep-Sea. *Science* **226**: 806-810.

Coxall, H. K., Wilson, P. A., Palike, H., Lear, C. H. & Backman, J. 2005. Rapid stepwise onset of Antarctic glaciation and deeper calcite compensation in the Pacific

Ocean. *Nature* **433**: 53-57.

Coxall, H. K. & Pearson, P. N. in press. The Eocene-Oligocene transition. In: Haywood, A. (Ed.), *Fossils, Proxies and Climate. Geological Society Special Publication.*

Cros, L., Kleijne, A., Zeltner, A., Billard, C. & Young, J. R. 2000. New examples of holococcolith-heterococcolith combination coccospheres and their implications for coccolithophorid biology. *Marine Micropaleontology* **39**: 1-34.

Crudeli, D., Young, J. R., Erba, E., Geisen, M., Ziveri, P., de Lange, G. & Slomp, C. P. 2006. Fossil record of holococcoliths and selected hetero-holococcolith associations from the Mediterranean (Holocene-late Pleistocene): Evaluation of carbonate diagenesis and palaeoecological-palaeoceanographic implications. *Palaeogeography Palaeoclimatology Palaeoecology* **237**: 191-224.

De Conto, R. M. & Pollard, D. 2003a. Rapid Cenozoic glaciation of Antarctica induced by declining atmospheric CO_2. *Nature* **421**: 245-249.

De Conto, R. M. & Pollard, D. 2003b. A coupled climate-ice sheet modeling approach to the Early Cenozoic history of the Antarctic ice sheet. *Palaeogeography, Palaeoclimatology, Palaeoecology* **198**: 39-52.

de Kaenel, E. & Villa, G. 1996. Oligocene-Miocene calcareous nannofossil biostratigraphy and paleoecology from the Iberia Abyssal Plain. *Proceedings of the Ocean Drilling Program, Scientific Results* **149**: 79-145.

Deflandre, G. 1947. *Braarudosphaera* nov. gen., type d'une famille nouvelle de Coccolithophoridés actuels à éléments composites. *Comptes Rendus Hebdomadaires des Séances de l'Académie des Sciences, Paris* **225**: 439-441.

8. References

Deflandre, G. 1952. Classe des Coccolithopridés (Coccolithophoridae Lohmann, 1902). In: Grassé (Ed.) *Traité de zoologie. Anatomie, systématique, biologie, 1, part 1, Phylogenie. Protozoaires: généralités. Flagellés.* Masson and Cie, Paris, pp. 439-470.

Deflandre, G. 1959. Sur les nannofossiles calcaires et leur systématique. *Revue de Micropaleontologie* **2**: 127-152.

Deflandre, G. & Fert, C. 1954. Observations sur les Coccolithophoridés actuels et fossiles en microscopie ordinaire et éléctronique. *Annales de Paléontologie* **40**: 115-176.

Diester-Haass, L. 1995. Late Eocene-Oligocene paleoceanography in the southern Indian Ocean (ODP Site 744). *Marine Geology* **130**: 99-119.

Diester-Haass, L., Robert, C. & Chamley, H. 1996. The Eocene-Oligocene preglacial-glacial transition in the Atlantic sector of the Southern Ocean (ODP Site 690). *Marine Geology* **131**: 123-149.

Diester-Haass, L. & Zahn, R. 1996. Eocene-Oligocene transition in the Southern Ocean: History of water mass circulation and biological productivity. *Geology* **24**: 163-166.

Diester-Haass, L. & Zahn, R. 2001. Paleoproductivity increase at the Eocene-Oligocene climatic transition: ODP/DSDP site 763 and 592. *Palaeogeography, Palaeoclimatology, Palaeoecology* **172**: 153-170.

Diester-Haass, L. & Zachos, J. C. 2003. The Eocene-Oligocene Transition in the Equatorial Atlantic (ODP Site 925): Paleoproductivity increase and positive $\delta^{13}C$ excursion. In: Prothero, D. R., Ivany, L. C. & Nesbitt, E. A. (Eds.) *From greenhouse to icehouse: the marine Eocene-Oligocene transition.* Columbia University Press, New York, pp. 397-416.

Dockery III, D. T. 1982. Lower Oligocene bivalvia of the Vicksburg group in Mississippi. *Mississippi Department of Natural Resources Bureau, Geological Bulletin* **123**: 1-261.

Dockery III, D. T. 1986. Punctuated Succession of Paleogene Mollusks in the Northern Gulf Coastal Plain. *Palaios* **1**(6): 582-589.

Dockery III, D. T., Stover, C. W., Weathersby, P., Stover Jr, W. C. & Ingram, S. L. 1991. A continuous core through the undifferentiated Yazoo Clay (Late Eocene, Jackson Group) of Central Mississippi. *Mississippi Geology* **12**: 23-27.

Dockery III, D. T. & Lozouet, P. 2003. Biotic patterns in Eocene-Oligocene Molluscs of the Atlantic Coastal Plain, USA. In: Prothero, D. R., Ivany, L. C. & Nesbitt, E. A. (Eds.) *From Greenhouse to Icehouse.* Colombia University Press, New York, pp. 303-340.

Dunkley Jones, T. & Bown, P. R. 2007. Post-sampling dissolution and the consistency of nannofossil diversity measures: A case study from freshly cored sediments of coastal Tanzania. *Marine Micropaleontology* **62**: 254-268.

Dupont-Nivet, G., Krijgsman, W., Langereis, C. G., Abels, H. A., Dai, S. & Fang, X. 2007. Tibetan plateau aridification linked to global cooling at the Eocene-Oligocene transition. *Nature* **445**: 635-638.

Echols, R. J., Armentrout, J. M., Root, S. A., Fearn, L. B., Cooke, J. C., Rodgers, B. K. & Thompson, P. R. 2003. Sequence stratigraphy of the Eocene/Oligocene boundary interval: Southeastern Mississippi. In: Prothero, D. R., Ivany, L. C. & Nesbitt, E. A. (Eds.) *From greenhouse to icehouse: The marine Eocene-Oligocene transition.* Columbia University Press, New York, pp. 189-222.

Edvardsen, B., Eikrem, W., Green, J. C., Andersen, R. A., Yeo Moon-Van Der Staay, S. & Medlin, L. K. 2000. Phylogenetic reconstructions of the Haptophyta inferred

from 18S ribosomal DNA sequences and available morphological data. *Phycologia* **39**: 19-35.

Ehrmann, W. U. & Mackensen, A. 1992. Sedimentological evidence for the formation of an east Antarctic ice sheet in Eocene/Oligocene time. *Palaeogeography Palaeoclimatology Palaeoecology* **93**: 85-112.

Eldrett, J. S., Harding, I. C., Wilson, P. A., Butler, E. & Roberts, A. P. 2007. Continental ice in Greenland during the Eocene and Oligocene. *Nature* **446**: 176-179.

Fujiwara, S., Tsuzuki, M., Kawachi, M., Minaka, N. & Inouye, I. 2001. Molecular phylogeny of the haptophyta based on the *rbc*L gene and sequence variation in the spacer region of the RUBISCO operon. *Journal of Phycology* **37**: 121-129.

Funakawa, S., Nishi, H., Moore, T. C. & Nigrini, C. A. 2006. Radiolarian faunal turnover and paleoceanographic change around Eocene/Oligocene boundary in the central equatorial Pacific, ODP Leg 199, Holes 1218A, 1219A, and 1220A. *Palaeogeography Palaeoclimatology Palaeoecology* **230**: 183-203.

Gale, A. S., Huggett, J. M., Pälike, H., Laurie, E., Hailwood, E. A. & Hardenbol, J. 2006. Correlation of Eocene-Oligocene marine and continental records: orbital cyclicity, magnetostratigraphy and sequence stratigraphy of the Solent Group, Isle of Wight, UK. *Journal of the Geological Society, London* **163**: 401-415.

Gartner, S. J. 1969. Two new calcareous nannofossils from the Gulf Coast Eocene. *Micropaleontology* **15**: 31-34.

Gartner, S. J. 1970. Phylogenetic lineages in the Lower Tertiary coccolith genus *Chiasmolithus*. *North American Paleontology Convention Sept. 1969, Proceedings G*: 930-957.

Gartner, S. J. 1971. Calcareous nannofossils from the JOIDES Blake Plateau cores and revision of the Paleogene nannofossil zonation. *Tulane Studies in Geology and Paleontology* **8**: 101-121.

Geisen, M., Billard, C., Broerse, A. T. C., Cros, L., Probert, I. & Young, J. R. 2002. Life-cycle associations involving pairs of holococcolithophorid species: intraspecific variation or cryptic speciation? *European Journal of Phycology* **37**: 531-550.

Gibbs, S., Shackleton, N. J. & Young, J. R. 2004. Orbitally forced climate signals in mid-Pliocene nannofossil assemblages. *Marine Micropaleontology* **51**: 39-56.

Gibbs, S., Bralower, T. J., Bown, P. R., Zachos, J. C. & Bybell, L. M. 2006. Shelf and open-ocean calcareous phytoplankton assemblages across the Paleocene-Eocene Thermal Maximum: Implications for global productivity gradients. *Geology* **34**: 233-236.

Gilbert, R., Domack, E. W. & Camerlenghi, A. 2003. Deglacial history of the Greenpeace Trough: Icesheet to ice shelf transition in the northwestern Weddell Sea. *Antarctic Research Series* **79**: 195-204.

Gran, H. H. 1912. Pelagic plant life. In: Murray, J. & Hjort, J. (Eds.) *The Depths of the Ocean*. Macmillan, London, pp. 307-386.

Gran, H. H. & Braarud, T. 1935. A quantitative study of the phytoplankton in the Bay of Fundy and the Gulf of Maine (including observations on hydrography, chemistry and turbidity). *Journal of the Biological Board of Canada* **1**: 279-467.

Grimes, S. T., Hooker, J. J., Collinson, M. E. & Mattey, D. P. 2005. Summer temperatures of late Eocene to early Oligocene freshwaters. *Geology* **33**: 189-192.

Haeckel, E. 1894. *Systematische Phylogenie der Protisten und Pflanzen*. Reimer, Berlin, 400 pp.

Halldal, P. & Markali, J. 1955. Electron microscope studies on coccolithophorids from the Norwegian Sea, the Gulf Stream and the Mediterranean. *Avhandlinger utgitt av det Norske Videnskapsakademi i Oslo. Mat. - Naturvid. Klasse* **1**: 1-30.

Haq, B. U. 1966. Electron microscope studies on some upper Eocene calcareous nannoplankton from Syria. *Stockholm Contributions in Geology* **15**: 23-37.

Haq, B. U. 1968. Studies on upper Eocene calcareous nannoplankton from NW Germany. *Stockholm Contributions in Geology* **18**: 13-74.

Haq, B. U. 1971. Paleogene calcareous nannoflora. Parts I-IV. *Stockholm Contributions in Geology* **25**: 1-158.

Haq, B. U. & Lohmann, G. P. 1976. Early Cenozoic calcareous nannoplankton biogeography of the Atlantic Ocean. *Marine Micropaleontology* **1**: 119-194.

Haq, B. U., Hardenbol, J. & Vail, P. R. 1987. Chronology of fluctuating sea levels since the Triassic (250 million years ago to present). *Science* **235**: 1156-1167.

Harrison, K. G. 2000. Role of increased marine silica input on paleo-pCO_2 levels. *Paleoceanography* **13**: 292-298.

Hay, W. W. 1977. Calcareous nannofossils. In: Ramsay, A. T. S. (Ed.) *Oceanic Micropalaeontology* 2. Academic Press, London, pp. 1055-1200.

Hay, W. W. 2004. Carbonate fluxes and calcareous nannoplankton. In: Thierstein, H. R. & Young, J. R. (Eds.) *Coccolithophores: From Molecular Processes to Global Impact.* Springer-Verlag, Berlin Heidelberg, pp. 509-528.

Hay, W. W. & Towe, K. M. 1962. Electron microscope examination of some coccoliths from Donzacq (France). *Eclogae geologicae Helvetiae* **55**: 497-517.

Hay, W. W., Mohler, H. & Wade, M. E. 1966. Calcareous Nannofossils from Nal'chik. *Eclogae geologicae Helvetiae* **59**: 379-399.

Hay, W. W., Mohler, H. P., Roth, P. H., Schmidt, R. R. & Boudreaux, J. E. 1967. Calcareous nannoplankton zonation of the Cenozoic of the Gulf Coast and Caribbean-Antillean area, and transoceanic correlation. *Transactions of the Gulf Coast Association of Geological Societies* **17**: 428-480.

Hay, W. W. & Mohler, H. 1967. Calcareous Nannoplankton from Early Tertiary Rocks at Pont Labau, France, and Paleocene-Early Eocene Correlations. *Journal of Paleontology* **41**: 196-206.

Hay, W. W., Flögel, S. & Söding, E. 2005. Is the initiation of glaciation on Antarctica related to a change in the structure of the ocean? *Global and Planetary Change* **45**: 23-33.

Hayek, L.-A. C. & Buzas, M. A. 1997. *Surveying natural populations.* Columbia University Press, New York, 563 pp.

Hickman, C. S. 2003. Evidence for abrupt Eocene-Oligocene molluscan faunal change in the Pacific Northwest. In: Prothero, D. R., Ivany, L. C. & Nesbitt, E. A. (Eds.) *From Greenhouse to Icehouse.* Colombia University Press, New York, pp. 71-87.

Honjo, S. 1976. Coccoliths: production, transportation and sedimentation. *Marine Micropaleontology* **1**: 65-79.

Hsü, J. K. *et al.* 1984. *Initial Reports of the Deep Sea Drilling Project, Volume 73.* U.S. Government Printing Office, Washington D.C., 798 pp.

IPCC. 2007. Summary for Policymakers. In: Solomon, S., Qin, D., Manning, M., Chen, Z., Marquis, M., Averyt, K. B., Tignor, M. & Miller, H. L. (Eds.) *Climate Change*

2007: The Physical Science Basis. Contribution of Working Group I to the Fourth Assessment Report of the Intergovernmental Panel on Climate Change. Cambridge University Press, Cambridge, United Kingdom and New York, NY, USA.

Ivany, L. C., Nesbitt, E. A. & Prothero, D. R. 2003. The Marine Eocene-Oligocene Transition: A synthesis. In: Prothero, D. R., Ivany, L. C. & Nesbitt, E. A. (Eds.) *From greenhouse to icehouse: the marine Eocene-Oligocene transition.* Columbia University Press, New York, pp. 522-534.

Ivany, L. C., Van Simaeys, S., Domack, E. W. & Samson, S. D. 2006. Evidence for an earliest Oligocene ice sheet on the Antarctic Peninsula. *Geology* **34**: 377-380.

Jafar, S. A. & Martini, E. 1975. On the validity of the calcareous nannoplankton genus *Helicosphaera. Senckenbergiana Lethaea* **56**: 381-397.

Jaramillo, C. A. & Oboh-Ikuenobe, F. E. 1999. Sequence stratigraphic interpretations from palynofacies, dinocyst and lithological data of Upper Eocene-Lower Oligocene strata in southern Mississippi and Alabama, U.S. Gulf Coast. *Palaeogeography Palaeoclimatology Palaeoecology* **145**: 259-302.

Jerkovic, L. 1970. *Noelaerhabdus* nov. gen. type d'une nouvelle famille de Coccolithophoridés fossiles. Noelaerhabdaceae du Miocène supérieur de Yougoslavie. *Comptes Rendus (Hebdomadaires des Séances) de l'Académie des Sciences, Paris* **270**: 468-470.

Jordan, R. W. & Chamberlain, A. H. L. 1993. *Vexillarius cancellifer* gen. et sp. nov. and its possible affinities with other living coccolithophorids. In: Hamrsmid, B. & Young, J. R. (Eds.) *INA 1991. Nannoplankton Research, biostratigraphy and paleobiology. Quaternary coccoliths,* pp. 305-325.

Jordan, R. W. & Chamberlain, A. H. L. 1997. Biodiversity among haptophyte algae. *Biodiversity and Conservation* **6**: 131-152.

Jordan, R. W., Cros, L. & Young, J. R. 2004. A revised classification scheme for living haptophytes. *Micropaleontology* **50**: 55-79.

Kamptner, E. 1927. Beitrag zur Kenntnis adriatischer Coccolithophoriden. *Archiv für Protistenkunde* **58**: 173-184.

Kamptner, E. 1948. Coccolithen aus dem Torton des Inneralpinen Wiener Beckens. *Sitzungberichte der Osterreichischen Akademie der Wissenschaften. Mathematisch-Naturwissenschaftliche Klasse* **87**: 152-158.

Kamptner, E. 1950. Uber den submikroskopischen Aufbau der Coccolithen. *Akademie der Wissenschaften in Wien, Mathematisch-Naturwissenschaftliche Klasse* **87**: 152-158.

Kamptner, E. 1954. Untersuchungen uber den Feinbau der Coccolithen. *Archiv für Protistenkunde* **100**: 1-90.

Kamptner, E. 1963. Coccolithineen-Skelettreste aus Tiefseeablagerungen des Pazifischen Ozeans. *Naturhistorischen Museum in Wien, Annalen* **71**: 117-198.

Keigwin, L. D. & Corliss, B. H. 1986. Stable isotopes in late middle Eocene to Oligocene foraminifera. *Geological Society of America Bulletin* **97**: 335-345.

Kiessling, W., Flügel, E. & Golonka, J. 2003. Patterns of Phanerozoic carbonate platform sedimentation. *Lethaia* **36**: 195-225.

Kleijne, A. 1991. Holococcolithophorids from the Indian Ocean, Red Sea, Mediterranean Sea and North Atlantic Ocean. *Marine Micropaleontology* **17**: 1-76.

Kleijne, A. 1992. Extant Rhabdosphaeraceae (coccolithophorids, class Prymnesiophyceae) from the Indian Ocean, Red Sea, Mediterranean Sea and North Atlantic Ocean. *Scripta Geologica* **100**: 1-63.

Klumpp, B. 1953. Beitrag zur Kenntnis der Mikrofossilien des Mittleren und Oberen Eozän. *Palaeontographica* **103A**: 377-406.

Kohn, M. J., Josef, J. A., Madden, R., Vucetich, G. & Carlini, A. A. 2004. Climate stability across the Eocene-Oligocene transition, southern Argentina. *Geology* **23**: 621-624.

Kump, L. R. & Arthur, M. A. 1997. Global chemical erosion during the Cenozoic: weatherability balances the budget. In: Ruddiman, W. F. (Ed.) *Tectonics Uplift and Climate Change*. Plenum Publishing Co, New York and London, pp. 339-426.

Lancelot, Y., Seibold, E., Cepek, P., Dean, W. E., Eremeev, V., Gardner, J., Jansa, L., Johnson, D., Krasheninnikov, V., Pflaumann, U., Rankin, J. G., Trabant, P. & Bukry, D. 1977. Site 366: Sierra Leone Rise. *Initial Reports of the Deep Sea Drilling Project* **41**: 21-162.

Lars Legge, H., Mutterlose, J. & Arz, H. W. 2006. Climatic changes in the northern Red Sea during the last 22,000 years as recorded by calcareous nannofossils. *Paleoceanography* doi:10.1029/2005PA001142.

Lazarus, D. & Caulet, J. P. 1994. Cenozoic Southern Ocean reconstructions from sedimentologic, radiolarian, and other microfossil data. In: Kennett, J. P. & Warnke, D. A. (Eds.) *The Antarctic Paleoenvironment: A perspective on global change. Pt 2, AGU Antarctic Research Series*, **60**: 145-174.

Lear, C. H., Elderfield, H. & Wilson, P. A. 2000. Cenozoic Deep-Sea Temperatures and Global Ice Volumes from Mg/Ca in Benthic Foraminiferal Calcite. *Science* **287**: 269-287.

Lear, C. H., Rosenthal, Y., Coxall, H. K. & Wilson, P. A. 2004. Late Eocene to early Miocene ice sheet dynamics and the global carbon cycle. *Paleoceanography* **19**: doi:10.1029/2004PA00103.

Lear, C. H., Bailey, T. R., Pearson, P. N., Coxall, H. K. & Rosenthal, Y. submitted. Cooling and ice growth across the Eocene-Oligocene transition. *Geology*.

Lees, J. A., Bown, P. R., Young, J. R. & Riding, J. B. 2004. Evidence for annual records of phytoplankton productivity in the Kimmeridge Clay Formation coccolith stone bands (Upper Jurassic, Dorset, UK). *Marine Micropaleontology* **52**: 29-49.

Lemmermann, E. 1908. Flagellatae, Chlorophyceae, Coccosphaerales und Silicoflagellatae. In: Brandt, K. & Apstein, C. (Eds.) *Nordisches Plankton. Botanischer Teil*. Lipsius and Tischer, Kiel and Leipzig, pp. 1-40.

Levin, H. L. 1965. Coccolithophoridae and related microfossils from the Yazoo formation (Eocene) of Mississippi. *Journal of Paleontology* **39**: 265-272.

Levin, H. L. & Joerger, A. P. 1967. Calcareous nannoplankton from the Tertiary of Alabama. *Micropaleontology* **13**: 163-182.

Liu, L. 1996. Eocene calcareous nannofossils from the Iberia Abyssal Plain. *Proceedings of the Ocean Drilling Program, Scientific Results* **149**: 61-78.

Loeblich, A. R. & Tappan, H. 1978. The coccolithophorid genus *Calcidiscus* Kamptner and its synonyms. *Journal of Paleontology* **52**: 1390-1392.

Lohmann, H. 1902. Die Coccolithophoridae, eine Monographie der Coccolithen bildenden Flagellaten, zugleich ein Beitrat zur Kenntnis des Mittelmeerauftriebs. *Archiv für Protistenkunde* **1**: 89-165.

Lohmann, H. 1903. Neue Untersuchungen über den Reichthum des Meeres an Plankton und über die Brauchbarkeit der verschiedenen Fangmethoden. Zugleich auch ein Beitrag zur Kenntnis des Mittelmeerauftriebs. *Wissenschaftliche Meeresuntersuchungen Abteilung Kiel* **7**: 1-87.

Liu, Z., Tou, S., Zhao, Q., Cheng, X. & Huang, W. 2004. Deep-water Earliest Oligocene Glacial Maximum (EOGM) in the South Atlantic. *Chinese Science Bulletin* **49**(20): 2190—2197.

Loutit, T. S., Hardenbol, J., Vail, P. R. & Baum, G. R. 1988. The key to age determination and correlation of continental margin sequences. In: Wilgus, C. K., Hastings, B. S., Kendall, C. G. S. C., Posamentier, H. W., Ross, C. A. & Van Wagoner, J. C. (Eds.) *Sea Level Changes: An Integrated Approach.* SEPM (Society for Sedimentary Geology) Special Publication, pp. 183-213.

Lunt, P. & Sugiatno, H. in press. A review of the Eocene and Oligocene in the Nanggulan area, south central Java. *Bulletin of the Indonesian Geological Survey, Bandung.*

Malin, G. & Steinke, M. 2004. Dimethyl sulfide production: what is the contribution of the coccolithophores? In: Thierstein, H. R. & Young, J. R. (Eds.) *Coccolithophores: From Molecular Processes to Global Impact.* Springer-Verlag, Berlin Heidelberg, pp. 127-164.

Mancini, E. A. & Tew, B. H. 1991. Relationships of Paleogene stages and planktonic foraminiferal zone boundaries to lithostratigraphic and allostratigraphic contacts in the eastern Gulf Coastal Plain. *Journal of Foraminiferal Research* **21**: 48-66.

Marino, M. & Flores, J. A. 2002. Middle Eocene to early Oligocene calcareous nannofossil stratigraphy at Leg 177 Site 1090. *Marine Micropaleontology* **45**: 383-398.

Martini, E. 1958. Discoasteriden und verwandte Formen im NW-deutschen Eozän (Coccolithophorida). 1. Taxonomische Untersuchungen. *Senckenbergiana Lethaea* **39**: 353-388.

Martini, E. 1959. *Pemma angulatum* und *Micrantholithus basquensis,* zwei neue Coccolithophoriden-Arten aus dem Eozän. *Senckenbergiana Lethaea* **40**: 415-21.

Martini, E. 1971. Standard Tertiary and Quaternary calcareous nannoplankton zonation. In: Farinacci, A. (Ed.) *Proceedings of the Second Planktonic Conference, Roma, 1970.* Edizioni Tecnoscienza, Rome, pp. 739-785.

Martini, E. 1976. Cretaceous to Recent calcareous nannoplankton from the Central Pacific Ocean (DSDP Leg 33). *Initial Reports of the Deep Sea Drilling Project* **33**: 383-423.

Martini, E. & Ritzkowski, S. 1968. Die Grenze Eozän/Oligozän in der Typus-Region des Unteroligozäns (Helmstedt-Egeln-Latdorf). *Memoires du Bureau de Recherches Geologiques et Minieres* **69**: 233-7.

McGowran, B., Moss, G. & Beecroft, A. 1992. Late Eocene and early Oligocene in Southern Australia: Local neritic signals of global oceanic changes. In: Prothero, D. R. & Berggren, W. A. (Eds.) *Eocene-Oligocene Climatic and Biotic Evolution.* Princeton University Press, Princeton, NJ, pp. 178-201.

Miller, K. G., Wright, J. D. & Fairbanks, R. G. 1991. Unlocking the Ice House: Oligocene-Miocene Oxygen Isotopes, Eustasy, and Margin Erosion. *Journal of Geophysical Research* **96**: 6829-6848.

Miller, K. G., Thompson, P. R. & Kent, D. V. 1993. Integrated Late Eocene-Oligocene Stratigraphy of the Alabama Coastal-Plain - Correlation of Hiatuses and Stratal Surfaces to Glacioeustatic Lowerings. *Paleoceanography* **8**: 313-331.

Miller, K. G., Browning, J. V., Aubry, M. P., Wade, B. S., Katz, M. E., Kulpecz, A. A. & Wright, J. D. 2008. Eocene-Oligocene global climate and sea-level changes: St Stephens Quarry, Alabama. *Geological Society of America Bulletin* **120**: 34-53.

Milliman, J.D., Troy, P.J., Balch, W.M., Adams, A.K., Li, Y.-H. & Mackenzie, F.T. 1999. Biologically mediated dissolution of calcium carbonate above the chemical lysocline? *Deep-Sea Research I* **46**: 1653-1669.

Monechi, S. 1986. Calcareous nannofossil events around the Eocene-Oligocene boundary in the Umbrian Apennines (Italy). *Palaeogeography Palaeoclimatology Palaeoecology* **57**: 61-69.

Monechi, S., Buccianti, A. & Gardin, S. 2000. Biotic signals from nannoflora across the iridium anomaly in the upper Eocene of the Massignano section: evidence from statistical analysis. *Marine Micropaleontology* **39**: 219-237.

Moore, T. C. J., Rabinowitz, P. D. *et al.* 1984. *Initial Reports of the Deep-sea Drilling Project, Volume 74*. U.S. Government Printing Office, Washington, DC, 894 pp.

Müller, C. 1970. Nannoplankton-Zonen der Unteren-Meeresmolasse Bayerns. *Geologica Bavarica* **63**: 107-118.

Müller, C. 1974. Calcareous Nannoplankton, Leg 25 (Western Indian Ocean). *Initial Reports of the Deep Sea Drilling Project*, **25**: 579-633.

Murray, G. & Blackman, V. H. 1898. On the nature of the Coccospheres and Rhabdospheres. *Philosophical Transactions of the Royal Society of London (B)* **190**: 427-441.

Nebelsick, J. H., Rasser, M. W. & Bassi, D. 2005. Facies dynamics in Eocene to Oligocene circumalpine carbonates. *Facies* **51**: 197-216.

Nesbitt, E. A. 2003. Changes in shallow marine faunas from the Northeaster Pacific margin across the Eocene-Oligocene boundary. In: Prothero, D. R., Ivany, L. C. & Nesbitt, E. A. (Eds.) *From Greenhouse to Icehouse*. Colombia University Press, New York, pp. 57-70.

Nicholas, C. J., Pearson, P. N., Bown, P. R., Dunkley Jones, T., Huber, B. T., Karega, A., Lees, J. A., McMillan, I. K., O'Halloran, A., Singano, J. M. & Wade, B. S. 2006. Stratigraphy and sedimentology of the Upper Cretaceous to Paleogene Kilwa Group, southern coastal Tanzania. *Journal of African Earth Sciences* **45**: 431-466.

Nilsen, E. B., Anderson, L. D. & Delaney, M. L. 2003. Paleoproductivity, nutrient burial, climate change and the carbon cycle in the western equatorial Atlantic across the Eocene/Oligocene boundary. *Paleoceanography* **18**: doi: 10.1029/2002PA000804.

Noël, M.-H., Kawachi, M. & Inouye, I. 2004. Induced dimorphic life cycle of a coccolithophorid, *Calyptrosphaera sphaeroidea* (Prymnesiophyceae, Haptophyta). *Journal of Phycology* **40**: 112-129.

Norris, R. E. 1984. Indian Ocean nanoplankton. I. Rhabdosphaeraceae (Prymnesiophyceae) with a review of extant taxa. *Journal of Phycology* **20**: 27-41.

Oberhansli, H., McKenzie, J., Toumarkine, M. & Weissert, H. 1984. A paleoclimatic and paleoceanographic record of the Paleogene in the central South Atlantic (Leg 73, Sites 522, 523 and 524). *Initial Reports of the Deep Sea Drilling Project* **73**: 737-747.

Okada, H. & Matsuoka, M. 1996. Lower-photic nannoflora as an indicator of the late Quaternary monsoonal paleo-record in the tropical Indian Ocean. In:

Moguilevsky, A. & Whatley, R. (Eds.) *Microfossils and oceanic environments.* University of Wales, Aberystwyth-Press, pp. 231-245.

Olney, M. P., Scherer, R. P., Bohaty, S. M. & Harwood, D. M. 2005. Eocene-Oligocene paleoecology and the diatom genus *Kisseleviella Sheshukova-Poretskaya* from the Victoria Land Basin, Antarctica. *Marine Micropaleontology* **58**: 56-72.

Opdyke, B. N. & Wilkinson, B. H. 1989. Surface area control of shallow cratonic to deep marine carbonate accumulation. *Paleoceanography* **3**: 685-703.

Pascher, A. 1910. Chrysomonaden aus dem Herschberger Grossteiche. *Monographien und Abhandlungen zur Internationale Revue der gasamten Hydrobiologie und Hydrographie* **1**: 1-66.

Pagani, M., Zachos, J. C. & Freeman, K. H. 2002. Eocene/Oligocene alkenone-based CO2 estimates. *Geochimica Et Cosmochimica Acta* **66**: A578-A578.

Pagani, M., Zachos, J. C., Freeman, K. H., Tipple, B. & Bohaty, S. 2005. Marked Decline in Atmospheric Carbon Dioxide Concentrations During the Paleogene. *Science* **309**: 600-603.

Palike, H., Norris, R. D., Herrle, J. O., Wilson, P. A., Coxall, H. K., Lear, C. H., Shackleton, N. J., Tripati, A. & Wade, B. S. 2006. The Heartbeat of the Oligocene Climate System. *Science* **314**: 1894-1898.

Pawlowsky-Glahn, V. & Egozcue, J. J. 2006. Compositional data and their analysis: an introduction. In: Buccianti, A., Mateu-Figueras, G. & Pawlowsky-Glahn, V. (Eds.) *Compositional Data Analysis in the Geosciences: From Theory to Practice.* Geological Society, London, pp. 1-10.

Pearson, P. N. & Palmer, M. R. 2000. Atmospheric carbon dioxide concentrations over the past 60 million years. *Nature* **406**: 695-699.

Pearson, P. N., Ditchfield, P. W., Singano, J., Harcourt-Brown, K. G., Nicholas, C. J., Olsson, R. K., Shackleton, N. J. & Hall, M. A. 2001. Warm tropical sea surface temperatures in the Late Cretaceous and Eocene epochs. *Nature* **413**: 481-487.

Pearson, P. N., Nicholas, C. J., Singano, J., Bown, P. R., Coxall, H. K., van Dongen, B. E., Huber, B. T., Karega, A., Lees, J. A., Msaky, E., Pancost, R. D., Pearson, M. & Roberts, A. P. 2004. Paleogene and Cretaceous sediment cores from the Kilwa and Lindi areas of coastal Tanzania: Tanzania Drilling Project Sites 1-5. *Journal of African Earth Sciences* **39**: 25-62.

Pearson, P. N., Nicholas, C. J., Singano, J. M., Bown, P. R., Coxall, H. K., van Dongen, B. E., Huber, B. T., Karega, A., Lees, J. A., MacLeod, K., McMillan, I. K., Pancost, R. D., Pearson, M. & Msaky, E. 2006. Further Paleogene and Cretaceous sediment cores from the Kilwa area of coastal Tanzania: Tanzania Drilling Project Sites 6-10. *Journal of African Earth Sciences* **45**: 279-317.

Pearson, P. N., Olsson, R. K., Huber, B. T., Hemleben, C. & Berggren, W. A. (Eds.) 2006. *Atlas of Eocene Planktonic Foraminifera.* Cushman Foundation Special Publication No. 41, 514 pp.

Pearson, P. N., van Dongen, B. E., Nicholas, C. J., Pancost, R., Schouten, S., Singano, J. & Wade, B. S. 2007. Stable warm tropical climate through the Eocene Epoch. *Geology* **35**: 211-214.

Pearson, P. N., McMillan, I. K., Wade, B. S., Dunkley Jones, T., Coxall, H. K., Bown, P. R. & Lear, C. H. 2008. Extinction and environmental change across the Eocene-Oligocene boundary in Tanzania. *Geology* **36**: 179-182.

Pekar, S. F., Christie-Blick, N., Kominz, M. A. & Miller, K. G. 2002. Calibration between eustatic estimates from backstipping and oxygen isotopic records for the Oligocene. *Geology* **30**: 903-906.

Perch-Nielsen, K. 1968. Der Feinbau und die klassifikation der Coccolithen aus dem Maastrichtien von Dänemark. *Det Kongelige Danske Videnskabernes Selskab Biologiske Skrifter* **16**: 1-93.

Perch-Nielsen, K. 1969. Die Coccolithen einiger dänischer Maastrichtien- und Danienlokalitäten. *Bulletin of the Geological Society of Denmark* **19**: 51-68.

Perch-Nielsen, K. 1971. Elektronenmikroskopische Untersuchungen an Coccolithen und verwandten Formen aus dem Eozän van Dänemark. *Det Kongelige Danske Videnskabernes Selskab Biologiske Skrifter* **18**: 1-76.

Perch-Nielsen, K. 1977. Albian to Pleistocene calcareous nannofossils from the Western South Atlantic, DSDP Leg 39. *Initial Reports of the Deep Sea Drilling Project* **39**: 699-823.

Perch-Nielsen, K. 1985. Cenozoic Calcareous Nannofossils. In: Bolli, H. M., Saunders, J. B. & Perch-Nielsen, K. (Eds.) *Plankton Stratigraphy*. Cambridge University Press, Cambridge, pp. 329-554.

Persico, D. & Villa, G. 2004. Eocene-Oligocene calcareous nannofossils from Maud Rise and Kerguelen Plateau (Antarctica): paleoecological and paleoceanographic implications. *Marine Micropaleontology* **52**: 153-179.

Peterson, L. C. & Backman, J. 1990. Late Cenozoic carbonate accumulation and the history of the carbonate compensation depth in the western equatorial Indian Ocean. *Proceedings of the Ocean Drilling Program, Scientific Results* **115**: 467-489.

Poche, F. 1913. Das System der Protozoa. *Archiv für Protistenkunde* **30**: 125-321.

Poore, R. Z. 1984. Middle Eocene through Quaternary planktonic foraminifers from the southern Angola Basin: Deep-sea Drilling Project Leg 73. *Initial Reports of the Deep-sea Drilling Project* **73**: 429-448.

Poore, R. Z., Tauxe, L., Percival, S. F. & La Brecque, J. L. 1982. Late Eocene-Oligocene magnetostratigraphy and biostratigraphy at South Atlantic DSDP Site 522. *Geology* **10**: 508-511.

Primoli-Silva, I. & Jenkins, D. G. 1993. Decision on the Eocene-Oligocene boundary stratotype. *Episodes* **16**: 379-381.

Prins, B. 1979. Notes on nannology - 1. *Clausicoccus,* a new genus of fossil coccolithophorids. *INA Newsletter* **1**: N2-N4.

Probert, I., Fresnel, J., Billard, C., Geisen, M. & Young, J. R. 2007. Light and electron microscope observations of *Algirosphaera robusta* (Prymnesiophyceae). *Journal of Phycology* **43**: 319-322.

Prothero, D. R. 1994. The Late Eocene-Oligocene Extinctions. *Annual Review of Earth and Planetary Sciences* **22**: 145-165.

Prothero, D. R. & Heaton, T. H. 1996. Faunal stability during the Early Oligocene climatic crash. *Palaeogeography Palaeoclimatology Palaeoecology* **127**: 257-283.

Quintero-Torres, R., Aragón, J. L., Torres, M., Estrada, M. & Cros, L. 2006. Strong far-field coherent scattering of untraviolet radiation by holococcolithophores. *Physical Review* **74**: doi: 10.1103/PhysRevE.74.032901.

Rea, D. K. & Lyle, M. W. 2005. Paleogene calcite compensation depth in the eastern subtropical Pacific: Answers and Questions. *Paleoceanography* **20**: doi: 10.1029/2004PA001064.

Romein, A. J. T. 1979. Lineages in early Paleogene calcareous nannoplankton. *Utrecht Micropaleontological Bulletins* **22**: 1-230.

Rost, B. & Riebesell, U. 2004. Coccolithophores and the biological pump: responses to environmental changes. In: Thierstein, H. R. & Young, J. R. (Eds.) *Coccolithophores: From Molecular Processes to Global Impact.* Springer-Verlag, Berlin Heidelberg, pp. 99-126.

Roth, P. H. 1970. Oligocene calcareous nannoplankton biostratigraphy. *Eclogae Geologicae Helvetiae* **63**: 799-881.

Sáez, A. G., Probert, I., Geisen, M., Quinn, P., Young, J. R. & Medlin, L. K. 2003. Pseudo-cryptic speciation in coccolithophores. *Proceedings of the National Academy of Sciences of the United States of America* **100**: 7163-7168.

Sáez, A. G., Probert, I., Young, J. R., Edvardsen, B., Eikrem, W. & Medlin, L. K. 2004. A review of the phylogeny of the Haptophyta. In: Thierstein, H. R. & Young, J. R. (Eds.) *Coccolithophores: from molecular processes to global impact.* Springer, Berlin, pp. 251-270.

Salamy, K. A. & Zachos, J. C. 1999. Latest Eocene Early Oligocene climate change and Southern Ocean fertility: inferences from sediment accumulation and stable isotope data. *Palaeogeography Palaeoclimatology Palaeoecology* **145**: 61-77.

Schiller, J. 1913. Vorläufige Ergebnisse der Phtyoplankton-Untersuchungen auf den Fahrten SMS 'Najade' in der Adria 1911/12. I. Die Coccolithophoriden. *Sitzungberichte der Akademie der Wissenschaften in Wien, Mathematisch-Naturwissenschaftliche Klasse* **122**: 597-617.

Schiller, J. 1930. Coccolithineae. In: Rabenhorst, L. (Ed.) *Kryptogamen-Flora von Deutschland, Osterrich und der Schweiz 10. Band, 2 Abt.* Akademische Verlagsgesellschaft, Leipzig, pp. 89-267.

Schlauder, J. 1945. *Recherches sur les flagellés calcaires de la Baie d'Alger.* Université d'Alger, Algiers.

Schwarz, E. H. L. 1894. Coccoliths. *Annals and Magazine of Natural History; ser 6* **14**: 341-346.

Schwarz, E. 1932. Beitrage zur Entwicklungsgeschichte der Protophyten. IX. Der Formwechsel von *Ochrosphaera neapolitana*. *Archiv für Protistenkunde* **77**: 434-462.

Self-Trail, J. M. & Seefelt, E. L. 2005. Rapid dissolution of calcareous nannofossils: a case study from freshly cored sediments of the south-eastern Atlantic Coastal Plain. *Journal of Nannoplankton Research* **27**: 149-159.

Séranne, M. 1999. Early Oligocene stratigraphic turnover on the west Africa continental margin: a signature of the Tertiary greenhouse-to-icehouse transition? *Terra Nova* **11**: 135-140.

Sexton, P. F., Wilson, P. A. & Pearson, P. N. 2006. Microstructural and geochemical perspectives on planktic foraminiferal preservation: "Glassy" versus "Frosty". *Geochemistry Geophysics Geosystems* **7**: doi:10.1029/2006GC001291.

Shafik, S. 1981. Nannofossil biostratigraphy of the *Hantkenina* (foraminiferid) interval in the upper Eocene of southern Australia. *BMR Journal of Australian Geology and Geophysics* **6**: 108-116.

Shafik, S. 1989. Some New Calcareous Nannofossils from Upper Eocene and Lower Oligocene Sediments in the Otway Basin, Southeastern Australia. *Alcheringa* **13**: 69-83.

Sherwood, R. W. 1974. Calcareous nannofossil systematics, paleoecology, and biostratigraphy of the Middle Eocene Weches Formation of Texas. *Tulane Studies in Geology and Paleontology* **11**: 1-79.

Simpson, E. S. W., Schlich, R., Gieskes, J., Girdley, W. A., Leclaire, L., Marshall, B. V., Moore, C., Müller, C., Sigal, J., Vallier, T. L., White, S. M. & Zobel, B. 1974. Site 242. *Initial Reports of the Deep Sea Drilling Project* **25**: 139-176.

Sluijs, A., Brinkhuis, H., Stickley, C. E., Warnaar, J. & Williams, G. L. 2003. Dinoflagellate cysts from the Eocene-Oligocene transition in the Southern Ocean; results from ODP Leg 189. *Proceedings of the Ocean Drilling Program Scientific Results* **189**: doi:10.2973/odp.proc.sr.189.104.2003.

Spencer-Cervato, C. 1999. The Cenozoic Deep Sea Microfossil Record: Explorations of the DSDP/ODP Sample Set Using the Neptune Database. *Palaeontologica Electronica* **2**: art 2.

Squires, R. L. 2003. Turnovers in marine gastropod assemblages in the high-latitude North Pacific. In: Prothero, D. R., Ivany, L. C. & Nesbitt, E. A. (Eds.) *From Greenhouse to Icehouse*. Colombia University Press, New York, pp. 14-35.

Stradner, H. 1962. Über neue und wenig bekannte Nannofossilien aus Kreide und Alttertiär. *Sonderabdruck aus den Verhandlungen der Geologischen Bundesanstalt* **2**: 363-377.

Stradner, H. 1969. The nannofossils of the Eocene flysch in the Hagenbach Valley (northern Vienna Woods), Austria. *Rocznik Polskiego Towarzystwa Geologicznego* **39**: 493-432.

Stradner, H. & Edwards, A. R. 1968. Electron microscope studies on Upper Eocene coccoliths from the Oamaru Diatomite, New Zealand. *Jahrbuch der Geologischen Bundesanstalt Wien, Special Volume* **13**: 1-66.

Sullivan, F. R. 1964. Lower Tertiary nannoplankton from the California Coastal Ranges. I. Paleocene. *University of California Publications in Geological Sciences* **44**: 163-227.

Takahashi, K. & Okada, H. 2000. Environmental control on the biogeography of modern coccolithophores in the southeastern Indian Ocean offshore of Western Australia. *Marine Micropaleontology* **39**: 73-86.

Takano, Y. 2006. Phylogenetic affinities of an enigmatic nannoplankton *Braarudosphaera bigelowii* based on the SSU rDNA sequences. *Marine Micropaleontology* **60**: 145-156.

Tan, S. H. 1927. Discoasteridae incertae sedis. *Koninklijke Akademie van Wetenschappen te Amsterdam Proceedings* **30**: 411-419.

Tew, B. H. 1992. Sequence stratigraphy, lithofacies relationships, and paleogeography of Oligocene strata in southeastern Mississippi and southwestern Alabama. *Geological Survey of Alabama Bulletin* **146**: 1-73.

Theodoridis, S. 1984. Calcareous nannofossil biostratigraphy of the Miocene and revision of the helicoliths and discoasters. *Utrecht Micropaleontological Bulletin* **32**: 1-271.

Thió-Henestrosa, S. & Martín-Fernández, J. A. 2006. Detailed guide to CoDaPack: a freeware compositional software. In: Buccianti, A., Mateu-Figueras, G. & Pawlowsky-Glahn, V. (Eds.) *Compositional Data Analysis in the Geosciences: From Theory to Practice.* Geological Society, London, pp. 101-118.

Thomas, E. 1992. Middle Eocene-late Oligocene bathyal benthic foraminifera (Weddell Sea): faunal changes and implications for ocean circulation. In: Prothero, D. R. & Berggren, W. A. (Eds.) *Eocene-Oligocene climatic and biotic evolution.* Princeton

University Press, Princeton, NY, pp. 245-271.

Thomas, E. & Gooday, A. J. 1996. Cenozoic deep-sea benthic foraminifers: Tracers for changes in oceanic productivity? *Geology* **24**: 355-358.

Trauth, M. H. 2006. *MATLAB Recipes for Earth Sciences*. Springer-Verlag, Berlin Heidelberg, 237pp.

Tripati, A., Backman, J., Elderfield, H. & Ferretti, P. 2005. Eocene bipolar glaciation associated with global carbon cycle changes. *Nature* **436**: 341-346.

Troelsen, J. C. & Quadros, L. P. 1971. Distribuição Biostratigráfica dos Nanofósseis em Sedimentos Marinhos (Aptian-Mioceno) do Brasil. *Annaes da Academia Brasileira de Ciencias* **43**: 577-609.

Vail, P. R., Mitchum Jr, R. M., Todd, R. G., Widmier, J. M., Thompson III, S., Sangree, J. B., Bubb, J. N. & Hatlelid, W. G. 1977. Seismic stratigraphy and global changes of sea level. In: Payton, C. E. (Ed.) *Seismic Stratigraphy - Applications to Hydrocarbon Exploration, American Association of Petroleum Geologists Memoir*, **26**: 49-212.

Van Andel, T. 1975. Mesozoic/Cenozoic calcite compensation depth and the global distribution of calcareous sediments. *Earth and Planetary Science Letters* **26**: 187-194.

Van Mourik, C. A. & Brinkhuis, H. 2005. The Massignano Eocene-Oligocene golden spike section revisited. *Stratigraphy* **2**: 13-30.

Vandenberghe, N., Brinkhuis, H. & Steurbaut, E. 2003. The Eocene-Oligocene boundary in the North Sea Area: a sequence stratigraphic approach. In: Prothero, D. R., Ivany, L. C. & Nesbitt, E. A. (Eds.) *From Greenhouse to Icehouse*. Columbia University Press, New York, pp. 419-438.

Varol, O. 1989. Eocene calcareous nannofossils from Sile (northwest Turkey). *Revista Española de Micropaleontología* **21**: 273-320.

Varol, O. 1991. New Cretaceous and Tertiary calcareous nannofossils. *Neues Jahrbuch fur Geologie und Palaontologie. Abhandlungen* **182**: 211-237.

Varol, O. 1992. *Sullivania* a new genus of Paleogene coccoliths. *Journal of Micropalaeontology* **11**: 141-150.

Varol, O. 1998. Paleogene. In: Bown, P. R. (Ed.) *Calcareous Nannofossil Biostratigraphy*. Kluwer Academic, London, pp. 200-224.

Villa, G. & Persico, D. 2006. Late Oligocene climatic changes: Evidence from calcareous nannofossils at Kerguelen Plateau Site 748 (Southern ocean). *Palaeogeography Palaeoclimatology Palaeoecology* **231**: 110-119.

Wade, B. S. & Palike, H. 2004. Oligocene climate dynamics. *Paleoceanography* **19**: doi: 10.1029/2004PA001042.

Wade, B. S. & Bown, P. R. 2006. Calcareous nannofossils in extreme environments: The Messinian Salinity Crisis, Polemi Basin, Cyprus. *Palaeogeography Palaeoclimatology Palaeoecology* **233**: 271-286.

Wade, B. S. & Pearson, P. N. submitted. Planktonic foraminiferal biotic crisis and diversity fluctuations across the Eocene/Oligocene boundary in Tanzania. *Marine Micropaleontology*.

Walker, J. C. G. & Opdyke, B. C. 1995. Influence of variable rates of neritic carbonate deposition on atmospheric carbon dioxide and pelagic sediments. *Paleoceanography* **10**: 415-427.

Wallich, G. C. 1877. Observations on the coccosphere. *Annals and Magazine of Natural History* **19**: 342-350.

Wei, W. C. & Wise, S. W. 1989. Paleogene Calcareous Nannofossil Magnetobiochronology - Results from South-Atlantic Dsdp-Site-516. *Marine Micropaleontology* **14**: 119-152.

Wei, W. & Wise, S. W. 1990. Biogeographic gradients of middle Eocene-Oligocene calcareous nannoplankton in the South Atlantic Ocean. *Palaeogeography Palaeoclimatology Palaeoecology* **79**: 29-61.

Wei, W., Villa, G. & Wise, S. W. 1992. Paleoceanographic implications of Eocene-Oligocene calcareous nannofossils from Sites 711 and 748 in the Indian Ocean. *Proceedings of the Ocean Drilling Program, Scientific Results* **120**: 979-999.

Whitehead, J. M. 2005. Cenozoic history of Antarctic benthic diatoms. *Alcheringa* **29**: 151-169.

Wise, S. W. 1973. Calcareous nannofossils from cores recovered during Leg 18, Deep Sea Drilling Project: biostratigraphy and observations on diagenesis. *Initial Reports of the Deep Sea Drilling Project* **18**: 569-615.

Wise, S. W. 1983. Mesozoic and Cenozoic calcareous nannofossils recovered by Deep Sea Drilling Project Leg 71 in the Falkland Plateau Region, Southwest Atlantic Ocean. *Initial Reports of the Deep Sea Drilling Project* **71**: 481-550.

Wise, S. W., Breza, J. R., Harwood, D. M. & Wei, W. C. 1991. Paleogene glacial history of Antarctica. In: Mueller, D. W., McKenzie, J. A. & Weissert, H. (Eds.) *Controversies in modern geology: Evolution of geological theories in sedimentology, Earth history and tectonics*. Academic Press, London, United Kingdom, pp. 133-171.

Wise, S. W., Breza, J. R., Harwood, D. M., Wei, W. & Zachos, J. C. 1992. Paleogene glacial history of Antarctica in light of leg 120 drilling results. *Proceedings of the Ocean Drilling Program, Scientific Results* **120**: 1001-1030.

Young, J. R., Didymus, J. M., Bown, P. R., Prins, B. & Mann, S. 1992. Crystal Assembly and Phylogenetic Evolution in Heterococcoliths. *Nature* **356**: 516-518.

Young, J. R. & Bown, P. R. 1997. Cenozoic calcareous nannoplankton classification. *Journal of Nannoplankton Research* **19**: 36-47.

Young, J. R., Bergen, J. A., Bown, P. R., Burnett, J. A., Fiorentino, A., Jordan, R. W., Kleijne, A., Van Niel, B. E., Romein, A. J. T. & Von Salis, K. 1997. Guidelines for Coccolith and Calcareous Nannofossil terminology. *Palaeontology* **40**: 875-912.

Young, J. R., Davis, S. A., Bown, P. R. & Mann, S. 1999. Coccolith ultrastructure and biomineralisation. *Journal of Structural Biology* **126**: 195-215.

Young, J. R., Geisen, M., Cros, L., Kleijne, A., Sprengel, C., Probert, I. & Ostergaard, K. K. 2003. A guide to extant coccolithophore taxonomy. *Journal of Nannoplankton Research, Special Issue* **1**: 125.

Young, J. R., Henriksen, K. & Probert, I. 2004. Structure and morphogenesis of the coccoliths of the CODENET species. In: Thierstein, H. R. & Young, J. R. (Eds.) *Coccolithophores: from molecular process to global impact*. Springer, Berlin, pp. 191-216.

Young, J. R., Geisen, M. & Probert, I. 2005. A review of selected aspects of coccolithophore biology with implications for paleodiversity estimation. *Micropaleontology* **51**: 267-288.

Zachos, J. C., Breza, J. R. & Wise, S. W. 1992. Early Oligocene Ice-Sheet Expansion on

Antarctica - Stable Isotope and Sedimentological Evidence from Kerguelen Plateau, Southern Indian-Ocean. *Geology* **20**: 569-573.

Zachos, J. C., Quinn, T. M. & Salamy, K. A. 1996. High-resolution (10(4) years) deep-sea foraminiferal stable isotope records of the Eocene-Oligocene climate transition. *Paleoceanography* **11**: 251-266.

Zachos, J., Pagani, M., Sloan, L., Thomas, E. & Billups, K. 2001a. Trends, rhythms, and aberrations in global climate 65 Ma to present. *Science* **292**: 686-693.

Zachos, J. C., Shackleton, N. J., Revenaugh, J. S., Palike, H. & Flower, B. P. 2001b. Climate response to orbital forcing across the Oligocene-Miocene boundary. *Science* **292**: 274-278.

Zachos, J. C. & Kump, L. R. 2005. Carbon cycle feedbacks and the initiation of Antarctic glaciation in the earliest Oligocene. *Global and Planetary Change* **47**: 51-66.

Zanazzi, A., Kohn, M. J., MacFadden, B. J. & Terry Jr, D. O. 2007. Large temperature drop across the Eocene-Oligocene transition in central North America. *Nature* **445**: 639-642.

Ziveri, P., Broerse, A. T. C., van Hinte, J. E., Westbroek, P. & Honjo, S. 2000. The fate of coccoliths at 48°N 21°W, Northeastern Atlantic. *Deep-Sea Research* **47**: 1853-1875.